TESE DE DOUTORAMENTO

*Hydrodynamics of NW Iberian Peninsula
under past and future climate conditions*

Marisela Des Villanueva

2020

Mención Internacional

UniversidadeVigo

UniversidadeVigo

Escola Internacional de Doutoramento

Marisela Des Villanueva

TESE DE DOUTORAMENTO

"*Hydrodynamics of NW Iberian Peninsula under past and future climate conditions*"

Dirixida polos doutores:

Mª Teresa de Castro Rodríguez
Ramón Gómez Gesteira
Magda Catarina Ferreira de Sousa

2020

"Mención internacional"

Universidade de Vigo, Campus de Ourense, Departamento de Física Aplicada, Environmental Physics Laboratory (Ephyslab), CIM-Uvigo.

Marisela Des Villanueva (mdes@uvigo.es).

Hydrodynamics of NW Iberian Peninsula under past and future climate conditions. Ourense, marzo de 2020.

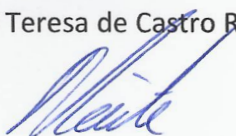# Universida_{de}Vigo

Escola Internacional de Doutoramento

Mª Teresa de Castro Rodríguez, Ramón Gómez Gesteira e Magda catarina Ferreira de Sousa

FAN CONSTAR que o presente traballo, titulado *"Hydrodynamics of NW Iberian Peninsula under past and future climate conditions"*, que presenta Marisela Des Villanueva para a obtención do título de Doutora, foi elaborado baixo a súa dirección no programa de doutoramento *"Marine Sciences, Technology and Management (DO*MAR)"* "interuniversitario das Universidades de Vigo, Santiago de Compostela, A Coruña, Aveiro, Porto, Minho e Tras os Montes e Alto Douro " baixo a modalidade de "Compendio de artigos".

Ourense, 02 de Marzo de 2020.

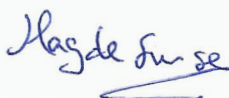O/A/s Director/a/s da tese de doutoramento

Dra. Mª Teresa de Castro Rodríguez   Dr. Ramón Gómez Gesteira

Dra. Magda Catarina Ferreira de Sousa

Agradecementos/Acknowledgments

En primeiro lugar quero agradecerlle ós meus directores de tese todo o traballo e apoio para a realización desta tese, sen eles non sería posible. Especial mención a Maite pola oportunidade que me deu, xa dende que fixen o TFG, para traballar no grupo EPhyslab. Ademais, gracias a Moncho e a Maite por aportarme sensatez en moitos momentos nos que son tozuda e pola súa paciencia infinita. Gracias a Magda por todo o seu tempo e toda a súa axuda, sen ela agora mesmo aínda estaría probando parámetros.

Tamén quero darlle as gracias a Laura, Rubén, Diego, Xurxo, David, Manolo, Ángel, Lucía, Santi, Miki, Susana e Coral pola acollida, por facer o día a día ameno, por escoitarme, polas ceas, os vermús, os xoves de comades e tantas e tantas cousas máis. A Alex, Jose, Orlando, Andrés e a todos os que forman o grupo EPhyslab en maior ou menor medida axudástesme nesta etapa, anque fose cunhas risas.

A xente que me acolleu na estancia en Aveiro e especial mención a Américo, que incluso sufriu a parte final de esta tese.

Gracias á miña familia, os que están e os que non, por aguantarme durante estes anos que é difícil, e por facer que sexa o que son agora. A miña nai e a miña irmá, graciñas e quérovos moito anque volo diga pouco e a meu cuñado David, non me esquezo de ti XD. Graciñas a Erica, Lorena, Aitor, Víctor, basicamente por se non vos dades por aludidos na parte de familia. Especial mención a Víctor por todo, así, en xeral, son demasiadas cousas e ocuparían máis ca memoria da tese. Non podo acabar estes agradecementos sen mencionar a Merchi, os teus tuppers alimentaronme estes últimos meses.

Resumen/Abstract

Los océanos son áreas de una alta productividad primaria que varía geográficamente. En general, las zonas costeras son más productivas y albergan mayor biodiversidad que el océano abierto. Las regiones costeras suelen limitarse a la zona de la plataforma continental y engloban las áreas de afloramiento costero. En estas regiones la circulación oceánica está influenciada principalmente por la topografía y por los vientos costeros. Las zonas costeras al ser altamente productivas concentran un elevado porcentaje de la población mundial por lo que también tienen una importante relevancia socioeconómica. La costa Noroeste de la Península Ibérica (NWIP por sus siglas en inglés) es una de las áreas del mundo con mayor productividad primaria ya que en esta zona confluyen varios factores: (1) se sitúa en el límite Norte del sistema de afloramiento Canario, (2) en ella desembocan gran cantidad de ríos caudalosos que aportan nutrientes y (3) tiene una morfología peculiar con la presencia de las rías gallegas al norte. A lo largo de los años se han realizado numerosas investigaciones científicas en diversos campos para tratar de comprender mejor el comportamiento hidrodinámico de la costa NWIP, pero a pesar de ello aún quedan muchas preguntas sin responder, y más aún si tenemos en cuenta el actual escenario de cambio climático, tanto natural como antropogénico, al que nos estamos enfrentando. El estudio de los efectos del cambio climático en la costa NWIP es una tarea difícil pero necesaria, ya que ayuda a conocer sus vulnerabilidades y permite planificar estrategias de mitigación y adaptación. Los modelos numéricos son herramientas muy útiles para la realización de esta tarea, puesto que nos permiten simular, por ejemplo, la temperatura del agua en el futuro bajo diversos escenarios de cambio climático. Además, los modelos también permiten simular eventos históricos para poder analizarlos en detalle. Por todo lo arriba descrito, el objetivo principal de esta tesis es contribuir al conocimiento oceanográfico de la costa NWIP y ayudar a evaluar el impacto que el cambio climático puede tener en la región. Para ello se utilizó el modelo numérico Delft3D, que permite mejorar la resolución espacial de modelos climáticos globales que abarcan áreas más grandes, para poder resolver procesos regionales e incluso locales de forma más exacta.

La costa NWIP es un sistema complejo en el que la circulación general está modificada por las particularidades morfológicas de la costa, la batimetría, la presencia

de agua dulce proveniente de la descarga de los principales ríos y el régimen de vientos que controla los ciclos de afloramiento y hundimiento. La complejidad del sistema hace que aplicar un modelo numérico como el Delft3D a esta área sea una ardua tarea. En primer lugar, es necesario generar una malla cuya resolución sea la adecuada para reproducir la hidrodinámica de la zona que se desea analizar correctamente. Además, hay que tener en cuenta que las simulaciones requieren un alto coste computacional, por lo que es necesario llegar a una solución de compromiso entre estos factores. Esta tesis se realizó utilizando dos mallas diferentes, una multi-dominio que cubre el NWIP desde 10.20 a 8º W y desde 40 a 43.75º N, y una de dominio único que cubre desde 10.00ºW a 8.33ºW y desde 41.18ºN to 43.50ºN. La malla multi-dominio está compuesta por cinco dominios interconectados y cuya resolución horizontal varía, teniendo mayor resolución los dominios costeros que el dominio oceánico. Este dominio se utilizó para evaluar el efecto del cambio climático en el sistema de afloramiento. La malla de dominio único se utilizó para realizar estudios específicos en el área de las Rías Baixas y el estuario del río Miño.

Una vez que creada la malla es necesario calibrar el modelo. Durante el proceso de calibración se ejecuta el modelo, se comparan los resultados con datos de campo o resultados de otras simulaciones validadas, se modifican los parámetros de la calibración, se vuelve a ejecutar el modelo, se vuelven a comparar con datos de campo o resultados de otras simulaciones validadas y se repite el proceso hasta que los resultados de la simulación son lo suficientemente precisos. En este punto, el modelo está calibrado y puede utilizarse en la zona de estudio. En el caso de esta tesis el modelo se ha calibrado comparando las salidas con datos *in situ* de elevación de la superficie del mar, salinidad, temperatura y velocidad horizontal cerca de la superficie.

La capacidad del modelo para reproducir la dinámica de sistemas costeros, rías y estuarios, costa adyacente y el intercambio de agua entre los sistemas costeros y la costa adyacente, se evaluó estudiando la intrusión de la pluma del río Miño en la Ría de Vigo. El río Miño desemboca aproximadamente 30 km al sur de la Ría de Vigo y estudios previos han observado que, bajo condiciones de vientos del sur, su pluma es capaz de alcanzar las Rías Baixas, entrando en ellas y modificando su patrón de circulación típico. La Ría de Vigo es la ría más al sur de las Rías Baixas y la que está más influenciada por la pluma del río Miño. El patrón de circulación de la Ría de Vigo, al igual que el del resto de rías que conforman las Rías Baixas, es un patrón de circulación estuárico típico, con

agua dulce saliendo por la superficie y agua oceánica salada entrando por las capas profundas. Este patrón se puede revertir bajo la influencia de vientos del sur y por una descarga entre moderada y alta del río Miño ya que los vientos empujan la pluma del río hacia la costa favoreciendo que ésta alcance la ría. Para detectar la intrusión de la pluma del río Miño en la Ría de Vigo se buscaron aquellos días en que la salinidad superficial en la boca sur de la ría fuese inferior a los valores medidos dentro de la ría, este patrón indica intrusión de agua dulce desde la plataforma hacia la ría. Para ello se utilizaron datos semanales de perfiles verticales de salinidad durante el período 2006-2017. Datos de campo mostraron que este patrón de intrusión se detectó varias semanas consecutivas durante los meses de enero y febrero de 2010. Por lo tanto, se seleccionaron estas fechas para realizar las simulaciones numéricas con el objetivo de determinar si se trató de un único evento o varios pulsos consecutivos. Además, se procedió a caracterizar un evento de intrusión completo a partir de secciones transversales y longitudinales de densidad y velocidad horizontal. Este estudio permitió determinar que la pluma del río Miño alcanza la Ría de Vigo unas 12 h después del pico de viento favorable, que los eventos de intrusión tienen una duración típica de 1.5 días y que afectan desde la superficie hasta ~10-15 m de profundidad dentro de la ría. Además, durante el evento de intrusión la influencia del río interior, el Verdugo-Oitavén, en la circulación de la ría es despreciable.

El modelo numérico también fue validado para su utilización cuando las condiciones de frontera provienen de modelos climáticos como los ejecutados en el marco de los proyectos "*Coupled Model Intercomparison*" versión 5 (CMPI5) y "*Coordinated Regional Climate Downscaling Experiment*" (CORDEX). Estos proyectos proporcionan variables climáticas de numerosos modelos ejecutados por diferentes instituciones. Al ser inviable ejecutar Delft3D a partir de las variables obtenidas de todos los modelos que engloban dichos proyectos, se procedió a escoger uno. Para ello se realizó un análisis estadístico para determinar qué modelo de CORDEX reproduce mejor las variables que se utilizan para forzar el modelo Delft3D. La comparación se realizó entre las salidas de los modelos climáticos y los datos de reanálisis de ERA-Interim para el período histórico. De este modo, se determinó que el modelo que mejor reproduce las variables analizadas para el área de estudio es el MOHC-HadGE2-Es y por lo tanto se utilizaron sus salidas para forzar el modelo Delft3D.

Una vez que se validó el modelo y se escogió la fuente de datos para forzar el modelo Delft3D para las proyecciones futuras se procedió a analizar el impacto del

cambio climático en el área de estudio. Las proyecciones futuras se realizaron bajo el escenario de emisión de gases de efecto invernadero RCP8.5 que actualmente, se considera el más probable.

Utilizando la malla multi-dominio se evaluó cómo el cambio climático puede afectar al afloramiento. El objetivo fue reproducir un evento de afloramiento de intenso a extremo característico del periodo histórico y otro para el periodo futuro. Para ello se calculó el índice de afloramiento (UI) durante los meses de julio y agosto, época de afloramiento intenso, en diversos puntos a lo largo de la costa para el período histórico y futuro. Una vez obtenido el UI se escogieron como representativos de eventos entre intensos y extremos los valores comprendidos entre el percentil 75% y el 99%, y se utilizaron para forzar el modelo. Los valores de UI obtenidos son mayores para el futuro que para el periodo histórico. Durante un evento de afloramiento el agua fría rica en nutrientes asciende hacia la superficie, por ello, la eficiencia de un evento de afloramiento puede medirse en términos de la capacidad que tiene para reducir la temperatura de la capa superficial. Así, se calcularon las diferencias en la temperatura superficial (SST) entre el final y el inicio del evento de afloramiento ($\Delta SST = SST_{final} - SST_{inicio}$) y se compararon los resultados obtenidos para el evento histórico y el fututo. Cuanto más negativa sea ΔSST mayor será la capacidad del afloramiento para bombear agua profunda hacia la superficie y, por lo tanto, será más efectivo. Las diferencias en el descenso de SST para los eventos históricos y futuros muestran resultados similares en la mayor parte del dominio, excepto para la región entre 41º 30' N y 42º 15' N. Esta región está dominada por los principales ríos (el Miño, el Douro y el Lima) y cerca de costa los valores oscilan entre un descenso de 2 a 3 ºC en el evento histórico y de 1 a 2 ºC en el futuro. A pesar de que los valores de UI son mayores para el periodo futuro, por lo que cabría esperar que el afloramiento fuese más intenso, las simulaciones sugieren que en el futuro los eventos de afloramiento serán menos efectivos. El análisis de la estratificación de la columna de agua, realizado en términos de frecuencia de Brunt-Väisälä calculada para secciones entre la Ría de Vigo y el estuario del río Miño, indica que va a aumentar en toda la sección para finales de siglo. La termoclina se situará a mayor profundidad y el gradiente será más marcado. De este modo el incremento de la estratificación contrarresta la intensificación de los vientos favorables al afloramiento. Esto podría tener efectos negativos en la producción primaria de la costa NWIP, ya que una reducción de la efectividad del afloramiento implica una reducción de la mezcla vertical y por lo tanto del transporte de

nutrientes y oxígeno a través de la columna de agua. Además, la reducción de la SST debido al ascenso de agua fría está actuando como amortiguador del calentamiento oceánico para muchas especies, las cuales encuentran en las zonas de afloramiento un refugio ante este calentamiento.

Al inicio de este resumen se indicó que las zonas costeras son áreas de gran importancia socioeconómica, en las Rías Baixas concretamente se asientan numerosas empresas ligadas a sectores como la pesca, la acuicultura y el marisqueo. El sector acuícola del mejillón es uno de los más importantes del mundo, en 2018 se produjeron 279000 toneladas de mejillón, lo que representa el 40% de la producción europea y más del 15% de la producción mundial. El cultivo de mejillón se realiza de forma extensiva, encontrándose el mayor número de bateas en la Ría de Arousa. La especie cultivada es *Mytilus galloprovincialis*, y se cultiva en cuerdas cuya longitud suele ser de 12 m. El crecimiento y la mortalidad de los mejillones depende de muchos factores ambientales, como la disponibilidad de oxígeno y fitoplancton, la temperatura del agua, la salinidad y el pH del agua entre otros. La temperatura del agua es el factor más relevante ya que por sí solo es capaz de explicar el 67% de las diferencias en el crecimiento. Estudios previos del *Mytilus galloprovincialis* determinaron que el rango de temperatura óptimo para su crecimiento está entre 14 y 20 ºC. Además, investigaciones sobre la posibilidad de adaptación de los mejillones al esperado incremento de la temperatura del agua indican que, a pesar de que sobreviven en un rango amplio de temperatura, se encuentran cerca de su límite fisiológico de tolerancia térmica, por lo que no se espera que dicho rango óptimo de temperatura varíe significativamente. Por ello, el rango de temperatura óptimo para su crecimiento determinado para la actualidad fue utilizado para determinar el índice de confort tanto en el periodo histórico como para finales de siglo. El índice de confort se definió como el porcentaje de tiempo durante el cual la temperatura del agua permanece dentro del rango de temperatura óptimo para el crecimiento del mejillón. En este caso se ejecutó el modelo utilizando la malla de dominio único para los meses de julio y agosto de 20 años históricos (1999-2018) y futuros (2080-2099). Para calcular el índice de confort se utilizaron los valores de temperatura del agua en la localización de cada uno de los polígonos de batea que hay actualmente distribuidos en las cuatro rías que conforman las Rías Baixas. Puesto que las cuerdas donde se suspenden los mejillones miden como máximo 12 m, se dividió la columna de agua en dos capas, la capa superficial de 0 a 6 m y una capa profunda de 6 a 12 m, y se calculó el índice de confort para cada

una de ellas. Los resultados muestran que para el periodo histórico el índice de confort es de 100% en todos los polígonos, tanto en la capa superficial como en la capa profunda. Esto significa que los mejillones se encuentran el 100% del tiempo bajo condiciones óptimas de temperatura lo que favorece su crecimiento. Por esta razón las Rías Baixas son un lugar idóneo para el cultivo del mejillón tal y como indica la gran producción que sustentan actualmente. Para finales de siglo, las proyecciones indican que en la mayoría de los polígonos de batea el índice de confort en las capas superficiales se reducirá en más de un 60% y entorno a un 30% en las capas profundas. Las zonas más externas de las rías son las menos afectadas, observándose puntos de la capa profunda donde el confort todavía se mantendría en el 100% a finales de siglo. Esto se debe a que son zonas que actualmente se encuentran cerca del límite inferior del rango de temperatura óptima (14 ºC) al estar muy influenciadas por el afloramiento. En estas zonas, aunque en el futuro aumente la temperatura del agua el incremento no será suficiente como para sobrepasar el límite superior (20ºC). La estratificación es otra variable física de gran importancia para la producción del mejillón ya que, como se indicó anteriormente, en una columna de agua muy estratificada el intercambio vertical de nutrientes y oxígeno es limitado. Comparando los valores de la frecuencia de Brunt-Väisälä en cada uno de los puntos de polígonos de bateas para el periodo histórico y para las proyecciones futuras, se observa que para finales de siglo la estratificación aumentará en la mayoría de polígonos de batea. Esta estratificación de la columna de agua solamente se reducirá en la parte más interna de las rías. Esto es debido a que estas áreas están altamente influenciadas por el río interior, produciéndose una estratificación halina. En el futuro, se prevé una reducción del caudal de los ríos del 25% bajo un escenario RCP8.5, por lo que al introducir esta consideración en el modelo se obtiene una reducción en la estratificación de origen halino.

Por último, se evaluó cómo el cambio climático puede afectar a dos especies de macroalgas formadoras de hábitat (*Himantalia elongata* y *Bifurcaria bifurcata*) que actualmente se encuentran en las Rías Baixas. Las macroalgas formadoras de hábitat son especies de gran interés ecológico ya que proporcionan estructura, refugio y alimento para muchas especies acompañantes, conformando comunidades ecológicas. Actualmente se está observando una reducción y una contracción de las poblaciones de estas especies debido al aumento en la temperatura del mar. En las costas de la Península Ibérica se ha observado un decaimiento de las poblaciones en la costa cantábrica. Sin embargo, zonas como las Rías Baixas están actuando como refugios climáticos contemporáneos para estas

especies al ser áreas protegidas de la acción de las olas y puntos donde el afloramiento mantiene el agua más fría que en las zonas costeras adyacentes a la vez que le proporciona gran cantidad de nutrientes. Dada la situación actual, es necesario analizar si en el futuro las rías seguirán actuando como refugio climático o no. Para ello se utilizaron los resultados de temperatura superficial del agua para los meses de julio y agosto del período histórico (1999-2018) y el futuro (2080-2099). Estudios previos determinaron que el umbral térmico de supervivencia de *H. elongata* es 18 ºC y para *B. bifurcata* 24.7 ºC sostenidos, en ambos casos, durante al menos 10 días consecutivos. Se desarrolló un modelo mecanicista de distribución de especies utilizando el umbral térmico de supervivencia de *H. elongata* calibrándolo con datos de campo. Se escogió esta especie porque muestra menos prevalencia en el área de estudio. Este modelo se basa en el porcentaje de tiempo que el alga es capaz de soportar bajo condiciones letales. Una vez calibrado el modelo de distribución de especies se utilizó para realizar los mapas de idoneidad térmica del hábitat para cada una de las macroalgas tanto en la actualidad como para finales de siglo. Actualmente las condiciones térmicas son favorables para la presencia de ambas macoalgas en la mayor parte de las rías. Un análisis en detalle muestra que las rías de Muros y Arousa tienen las condiciones más adecuadas para la presencia de *H. elongata*, aunque en la parte central de la Ría de Arousa son menos favorables cuando se compara con la parte externa. En las Rías de Pontevedra y Vigo las condiciones son menos favorables que en las dos rías más al norte. Los registros de presencias y ausencias de *H. elongata* y otra macroalgas con umbrales similares corroboran estos resultados ya que se observan menos poblaciones en las dos rías del sur. Las proyecciones para finales de siglo indican que las condiciones térmicas serán letales para *H. elongata*, y probablemente para otras macroalagas cuyo umbral térmico sea similar. Sin embargo, el análisis de idoneidad térmica del hábitat para *B. bifurcata*, caracterizada por un umbral térmico de supervivencia superior al de *H. elongata*, muestra que las Rías son térmicamente adecuadas para su presencia y que, de forma general continuarán siéndolo a finales de siglo. Además, debido al afloramiento, las rías seguirán siendo zonas donde la temperatura del agua será inferior a la del océano adyacente, por lo que podrán seguir siendo consideradas refugios térmicos para especies como *B. bifurcata* y aquellas con un umbral térmico similar.

Table of contents

Acronym and abbreviation list

AR5: 5th Assessment Report

CMIP5: Coupled Model Intercomparison Project version 5

CORDEX: Coordinated Regional Climate Downscaling Experiment

EBACWst: ENACW subtropical mode

ECMWF: Center for Medium-range Weather Forecasts

ENACW: Eastern Atlantic Central Water

ENACWsp: ENACW subpolar mode

GCM: Global Climate Models

GEBCO: General Bathymetric Chart of the Oceans

INTECMAR: Instituto Tecnolóxico para o Control do Medio Mariño de Galicia

IPC: Iberian Poleward Current

LSW: Labrador Sea Water

MOHC-HadGEM2-ES: Hadley Centre Global Environment Model–version 2 Earth System

MOW: Mediterranean Overflow Water

NAC: North Atlantic Current

NIP: North Iberian Peninsula

NWIP: Northwest Iberian Peninsula

PC: Portugal Current

PCC: Portugal Coastal Current

PCCC: Portugal Coastal Counter Current

PCUC: Portugal Coast Under Current

PDFs: Probability density functions

RCM: Regional Circulation Model

RCM: Regional Climate Models

RMSW: Root mean square error

SSE: Sea surface elevation

SST: Sea surface temperature

UI: Upwelling index

WIBP: Western Iberian Buoyant Plume

WRF: Weather Research and Forecasting Mode

BODC: British Oceanographic Data Centre

Chapter 1

Introduction

Oceans, and coastal areas in particular, are high productivity systems which arise great interest in the scientific community due to their ecological and economical relevance. The Northwest Iberian Peninsula is one of the most productive systems in the world, e.g. the Rías Baixas support up to 15% of the world aquaculture production of mussels, because it is located on the northern limit of the Eastern North Atlantic Upwelling system and there are several rivers flowing into this area providing high concentrations of nutrients. Currently, this system is facing a climate change scenario which will modify the physical parameters of the region affecting the ecosystems. Therefore, it is necessary to improve knowledge about this area, both its current and future behavior.

This chapter elaborates the motivation to carry out this thesis and presents the objectives to be achieved, as well as detailing the structure of the manuscript.

1.1. Motivation

Climate change is expected to have a significant environmental impact affecting primary production, economy and society. In marine systems, sea-level rise, changes in sea temperature, variations in circulation patterns and frequency, acidification, and severity of extreme events will impact the marine ecosystems. The analysis of the possible and probable vulnerabilities of these systems in a scenario of climate change allows establishing mitigation and adaptation procedures.

The Northwest Iberian Peninsula (NWIP) is located in the northern limit of the Eastern North Atlantic Upwelling system, one of the major coastal upwelling systems. In this area, northerly winds promote upwelling events which pump nutrient-rich Eastern Atlantic Central Water (ENACW) to the surface holding high productivity and biodiversity. The NWIP coast includes three estuarine systems with different morphologies, from south to north: a lagoon-estuarine system (Ria de Aveiro); estuaries connected to the major rivers (Minho, Lima and Douro) and four incised valleys (the Rías Baixas: Ría de Vigo, Ría de Pontevedra, Ría de Arousa and Ría de Muros). From all these systems, the Rías Baixas are of particular interest because they support one of the largest mussel aquaculture industries in the world and they may be acting as contemporary refugia for many species due to their specific oceanographic features (Martínez et al., 2012; Aguiar et al., 2017). Due to their ecological and economic value, it is necessary to study the current behavior and the possible effects that climate change may have on the NWIP coast, and on the Rías Baixas in particular.

Numerical models have shown to be one of the best tools to reproduce reality with enough accuracy and to provide data that would be very difficult to obtain through surveys, or even impossible, such as future projections. However, the databases and regional climate models available have a too coarse spatial resolution to adequately capture regional processes related to topography in the NWIP coast and, even less, inside the Rías Baixas estuaries. For this reason, it is necessary to implement and validate a high spatial resolution numerical model, such as the Delft3D-Flow, to dynamically downscales variables from available databases and climate models to capture the NWIP regional processes accurately.

1.2. Objectives

The main objective of this thesis is to study the possible impact of climate change on the NWIP coast with a particular interest in the Rías Baixas. In order to achieve this goal, it is necessary the implementation of a three-dimensional baroclinic model which allows to simulate the hydrodynamic conditions of the area under study. In particular, this work aims:

- to implement, calibrate and validate the numerical model Delft3D-Flow to the NWIP coast, ensuring that it is capable to reproduce the water exchange between the rias and the adjacent shelf,

- to reproduce and characterize the Minho River plume intrusion into the Rías Baixas analyzing the impact of an intrusion event in the hydrodynamic of the rias.

- to assess the impact of the climate change on upwelling effectivity,

- to evaluate the impact of climate change on water temperature and stratification,

- to investigate how climate change can affect mussel aquaculture in the Rías Baixas,

- to determine changes induced by climate change in geographical distribution of habitat-forming macroalgae inside the Rías Baixas.

1.3. Thesis layout

This is a thesis by published works composed by three articles already published in international peer-reviewed scientific journals and one in the publication process. Thus, this dissertation was structured as follows:

Chapter 1 presents the motivation of the research developed in the present thesis as well as a description of the main objectives to be achieved.

 Chapter 2 presents a detailed description of the area under study.

Chapter 3 presents a description of the database used to perform this research.

Chapter 4 presents a general overview of Delft3D numerical model as well as the setups used.

Chapter 5 includes the articles that compose this thesis.

- *Article 1* details the calibration and validation of the Delft3D numerical model as well as the application of the model to characterize a historical event of Minho River plume intrusion into the Ría de Vigo.

- *Article 2* analyzes the response of the upwelling system to the future climate change under the RCP 8.5 greenhouse gas emission scenario in the Northwest Iberian Peninsula. The effectivity of this coastal upwelling was assessed by numerical simulations of high-extreme upwelling conditions for a historical (1976-2005) and future (2070-2099) period.

- *Article 3* analyzes the future consequences of climate change on mussel productivity in the Rías Baixas. Numerical simulations for historical (1999-2018) and future (2080-2099) periods were performed in order to evaluate changes in the main physical parameters affecting mussel growth (water temperature and stratification).

- *Article 4* analyzes the effects of climate change on the geographical distribution of two habitat-forming macroalgae, *Himanthalia elongata* and *Bifurcaria bifurcata,* in the Rías Baixas. Sea Surface Temperature calculated for historical (1999-2018) and future (2080-2099) periods was used to develop and calibrate a mechanistic geographical distribution model based on the thermal survival threshold of the macroalgae. Then, the distribution model was used to determine and compare de present and future thermal habitat suitability for both macroalgae.

Chapter 6 presents a general discussion about the results obtained and the main conclusions derived from the researches presented in Chapter 5.

Chapter 2

Study area: Northwest coast of the Iberian Peninsula

The study area of the present thesis covers the northwest coast of the Iberian Peninsula (NWIP, Fig. 2.1). The area extends approximately from 40 to 43.75º N and from 8 to 10.20º W, being of particular interest the Rías Baixas and the coastal area under the influence of the Minho River Plume.

In this chapter, the main physiographic, atmospheric and oceanographic characteristics of the NWIP continental shelf, the Rías Baixas, the estuaries of the Minho, Lima and Douro and the Ria de Aveiro are presented.
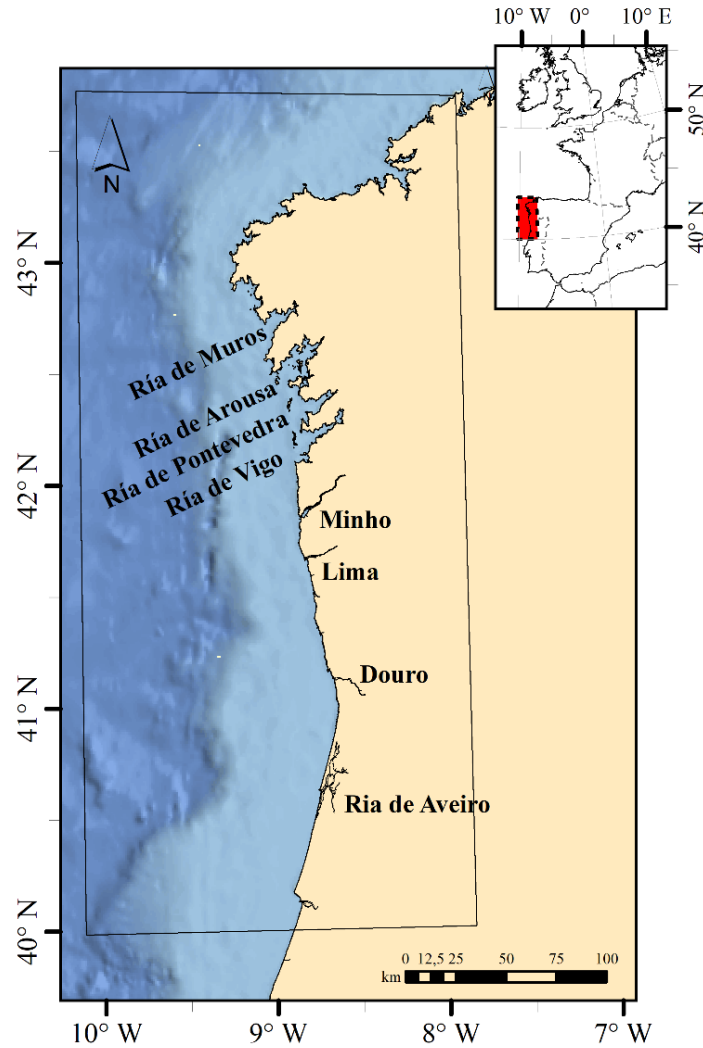
Figure 2.1. Northwestern Iberian Peninsula showing the delimitation of the study area.

2.1. Physiography

The continental shelf off the Northwest Iberian Peninsula coast (NWIP) is narrow, between 30 and 50 km, and the shelf break occurs at depths of 160-180 m (Dias et al., 2002; Lantzsch et al., 2010; Rey et al., 2014). The shelf is dominated by the Ria de Aveiro in the south, the Douro Lima and Minho rivers in the central area and by the Rías Baixas and their feeding rivers in the north. The NWIP continental shelf is a sediment-starved shelf. River discharges provide sediments to the shelf in the southern area while the Galician Rías Baixas usually act as sediment traps. The transition between the two systems occurs at about 42º N, just at the south of the Ría de Vigo (Dias et al., 2002).

2.1.1. Rías Baixas

The rias are usually described as flooded incised valleys (Evans and Prego, 2003), which, according to their hydrodynamic and sedimentological characteristics, are generally divided into three sectors: inner, middle and outer. The outer sector is located in the mouth of the ria where islands and peninsulas usually protect the ria from the direct and energetic influence of the ocean. The middle sector corresponds to the central part of the ria, and the inner sector comprises the shallow head of the ria where the main river usually flows into the ria.

The denomination Rías Baixas is used to refer the set of the southernmost and extensive four rias of the Galician coast. From north to south they are the Muros, Arousa, Pontevedra and Vigo rias. They follow a general SW-NE orientation, almost perpendicular to the main coast, and the depth in their central axes varies from approximately 40-60 m in the outer area to 5-10 m in the head of the ria. The Muros, Pontevedra and Vigo rias have a funnel shape, while the Ría de Arousa is characterized by a more complex physiography. The main characteristics of the Rías Baixas and the fluvial inputs are displayed in Table 2.1.

Rias	Area (km^2)	Volume (km^3)	Main river(s)	Catchment area (km^2)	Mean discharge (m^{3}s^{-1})
Ría de Muros	125	2.1	Tambre	1561	54.10
Ría de Arousa	230	4.5	Ulla	2769	79.30
			Umia	445	16.39
Ría de Pontevedra	141	3.5	Lérez	449	21.21
Ría de Vigo	176	3.1	Verdugo-Oitavén	331	17.00

Table 2.1. Main characteristics of the rias and their fluvial inputs.

2.1.1.1. Ría de Muros

The Ría de Muros is the smallest of the Rías Baixas (Fig. 2.2). It is 12.5 km long following its main axis with a very variable width ranging from 1.3 to 7.9 km. This ria occupies a surface area of 125 km^2 and has a volume of 2.1 km^3. The depth of the ria decreases from 51 m at the mouth to about 5.5 m at the head. In the outer sector a wide central channel, with an average depth of approximately 43 m, is clearly identified. In the middle sector, the ria widens and depth decreases to about 30 m. The inner sector is narrower and shallower, with a mean depth of 15 m. The Tambre River, located in the

innermost part of the ria, is the most significant freshwater input. The main difference between the Ría de Muros and the rest of the Rías Baixas is the absence of islands at its entrance, although a peninsula is present in the northern coast.
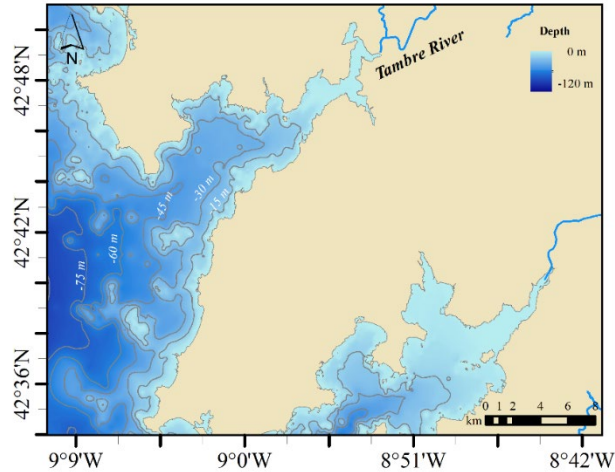

Figure 2.2. Ría de Muros. Bathymetry from nautical charts elaborated by the Spanish Navy Hydrographical Institute.

2.1.1.2. Ría de Arousa

The Ría de Arousa is the larger of the Rías Baixas, both in surface, 230 km^2, and in volume, 4.5 km^3 (Fig. 2.3). Along its main axis, it is 28 km long and the maximum width is 14 km. Its depth varies from 70 m at its southern mouth to 5 m at its head. The north shore is characterized by the presence of many small bays and the south coast by numerous islands of varying dimensions, being the islands of Cortegada and Arousa the most important due to their size. The south shore is also characterized by the presence of a large peninsula, the O Grove peninsula. This ria has to mouths connecting it with the shelf due to the presence of the Salvora Island and several small islands at the entrance of the ria. The southern mouth, between the Sálvora island and the O Grove peninsula, is the main connection. It has a width of 4.5 km and a maximum depth of 70 m. The northern mouth, between the Salvora island and the north shore of the ria, has a width of 3.5 km and is characterized by being shallow: the maximum depth is approximately 10 m. It is also characterized by the presence of several small islands. Two large rivers flow into the Ría de Arousa, the Ulla and Umia rivers. The main runoff is the Ulla River which flows into the ria in its innermost part. The Umia River flows near the O Grove peninsula.
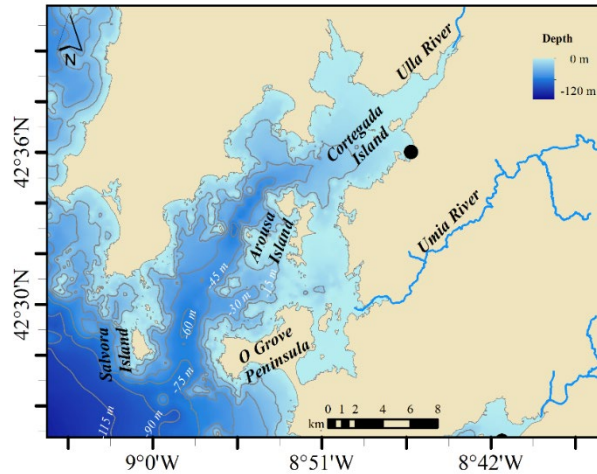
Figure 2.3. Ría de Arousa. Bathymetry from nautical charts elaborated by the Spanish Navy Hydrographical Institute. The black dot indicates the location of the Villagarcia tidal gauge.

2.1.1.3. Ría de Pontevedra

The Ría de Pontevedra occupies an area of 141 km^2 and has a volume of 3.5 km^3 (Fig. 2.4). This ria is 28 km long along its main axis and has a maximum width of 12 km at the mouth decreasing to 2.5 km near the head. The Lerez River flows at the head of the ria. There are three islands in this ria, Tambo in the inner sector and Ons and Onza at the mouth of the ria. Ons and Onza islands integrate the Ons archipelago and divide the ria entrance into two mouths. The southern mouth, between Onza and the south shore of the ria, has a width of 7.3 km and a maximum depth of 60 m. The northern mouth, between the north shore and the Ons island, is narrower (3.6 km) and shallower with depths less than 15 m. There is a deep channel along the main axis of the ria from the south mouth to the inner sector.
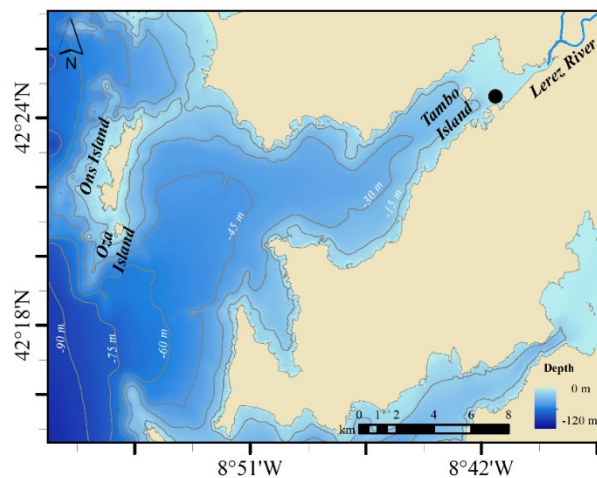
Figure 2.4. Ría de Pontevedra. Bathymetry provided by the General Fishing Secretary. The black dot indicates the location of the Marin tidal gauge.

2.1.1.4. Ría de Vigo

The Ría de Vigo occupies an area of 176 km^2 and a volume of 3.1 km^3 (Fig. 2.5). Its main axis has a length of 30 km and the ria is 13 km wide at the mouth. The Cies archipelago, composed of Monteagudo, Faro and San Martiño islands, is located at the mouth of the ria splitting it into two mouths. The southern mouth, between the San Martiño island and the southern shore of the ria, is 8 km wide and has a maximum depth of 67 m. The northern mouth, between the north shore of the ria and the Monte Agudo island, has a width of 2 km and a maximum depth of 25 m. The ria width and depth decrease from the mouth to the head, although there is a deep channel along the ria from the south mouth to the inner sector. The main input of freshwater into the ria comes from the Verdugo-Oitavén River which flows in the San Simon bay, in the inner sector of the ria. It is the shallowest area of the ria, with an average depth of 7 m. The San Simón bay is connected to the ria through the Rande strait, the narrowest part of the ria, less than 2 km wide.
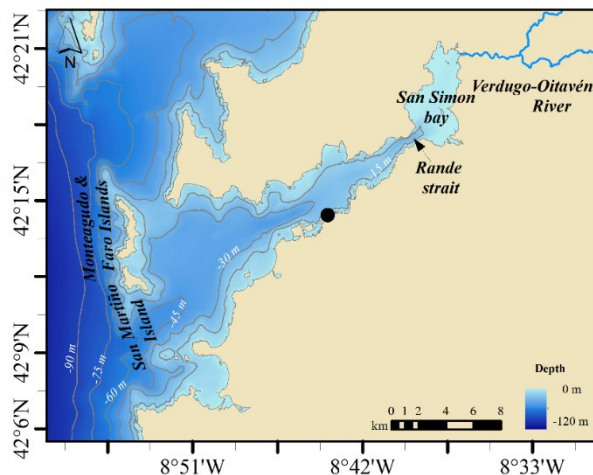

Figure 2.5. Ría de Vigo. Bathymetry provided by the General Fishing Secretary. The black dot indicates the location of the Vigo tidal gauge.

2.1.2. Minho estuary

The Minho River estuary is located 30 km to the south of the Ría de Vigo. The estuary of the Minho River has a NE-SW direction. It is approximately 38 km long and covers an area of 23 km^2 (Fig. 2.6). Its width is highly variable, with a maximum of 2 km near the mouth and a minimum of 100 m at the head. The mean depth of the estuary is 2.6 m with a maximum depth of 4 m near the estuary mouth. The lower estuary is a fine sediment deposits area, leading to the emergence of islands, beaches and extensive sandbanks.

The Minho River acts as a natural border between Spain and Portugal and is one of the most important inputs of freshwater to the West coast of the Iberian Peninsula. Its basin occupies 16275 km^2 and its discharge varies seasonally. Higher discharges occur from December to March and lower from July to September. The mean annual discharge is about 280 m^{3}s^{-1}.
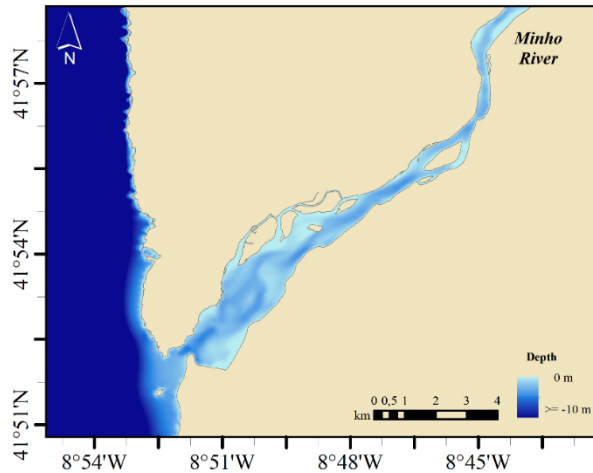

Figure 2.6. Minho estuary. Bathymetry provided by the Portuguese Navy Hydrographic Institute.

2.1.3. Lima estuary

The estuary of the Lima River is located in the northern region of Portugal, 20 km south of the Minho estuary. This estuary has an ENE-WSW direction, is ~ 20 km long and covers an area of 10.4 km^2 (Fig. 2.7). The mean depth is 4 m with a maximum depth of 10 m near the estuary mouth, where it becomes a narrow navigation channel. The estuary is a fine sediment deposits area, leading to the emergence of islands and extensive sandbanks. The mouth of the estuary is partially obstructed by a 2-km-long jetty which deflects the river flow to the south.

The Lima river basin occupies 2446 km^2 and the mean annual river discharge is about 54 m^{3}s^{-1}. The river discharge varies seasonally.
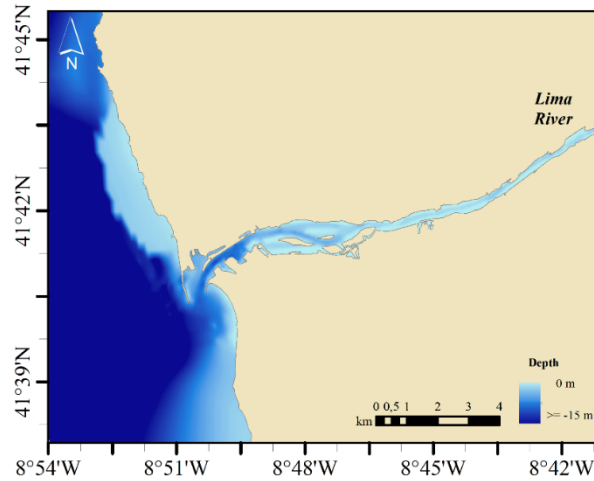
Figure 2.7. Lima estuary. Bathymetry provided by the Portuguese Navy Hydrographic Institute.

2.1.4. Douro estuary

The estuary of the Douro River has a SE-NW direction, is approximately 21 km long and covers an area of 9.8 km^2 (Fig. 2.6). Its width is highly variable, with a maximum of 1.3 km near the mouth and a minimum of 135 m at the head. The depth generally ranges from 0 to 10 m. The mouth is partially obstructed by a ~1000 m long sandbar at ~5 m below the sea surface.

The Douro River, which drains into the Atlantic Ocean at 41º08'N, 8º42'W, is the largest river flowing into the west coast of the Iberian Peninsula. Its basin occupies 98800 km^2 and the mean annual river discharge is about 700 m^{3}s^{-1}.
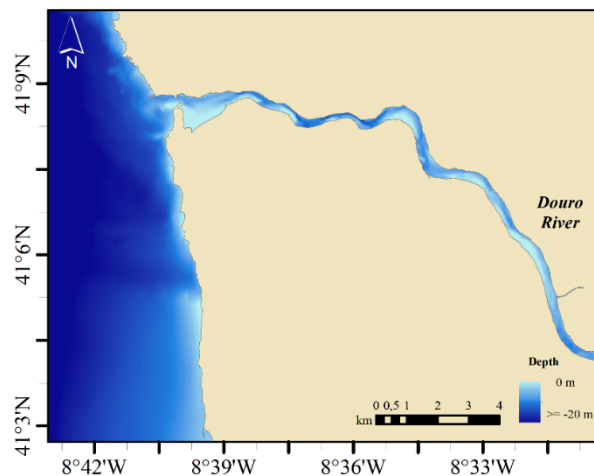
Figure 2.8. Douro estuary. Bathymetry provided by the Portuguese Navy Hydrographic Institute.

2.1.5. Ria de Aveiro

The Ria de Aveiro is a shallow coastal lagoon located at 40º 38' N, 8º 44' W (Fig. 2.9). It occupies an area of 77 km^2. Its maximum length is 45 km and has a width of 10 km. The geometry of the Ria de Aveiro is irregular and characterized by narrow channels and by the presence of several intertidal areas. Despite a sand bar separates the lagoon from the ocean, an artificial channel, that is 1.3 km long, 350 m wide and 20 m deep, connects the lagoon with the ocean.

The Vouga River is the main input of freshwater into the lagoon with a mean annual river discharge about 80 m^{3}s^{-1}.
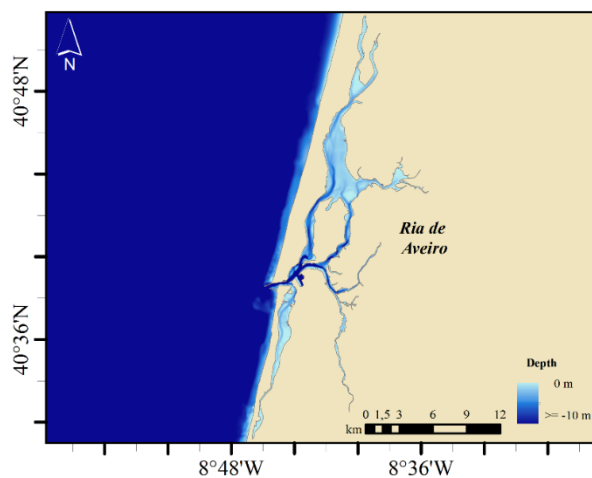
Figure 2.9. Ria de Aveiro. Bathymetry provided by the Aveiro Harbor Administration and Polis Litoral Ria de Aveiro.

2.2. Atmospheric circulation

The atmospheric circulation is mainly governed by the seasonal difference in atmospheric pressure at sea level between Azores High and the Icelandic Low. The Azores High is a permanent high-pressure system located south of 40º N, near the Azores islands, while the Icelandic Low is a low-pressure system located around 60º N, near Iceland. These two systems control the strength and direction of westerly winds and the location of storm tracks across the North Atlantic. During winter, the Azores High moves to its most southern position and the Icelandic Low is reinforced. Pressure differences between these two centers generate steady eastward air-flow. Moreover, the difference between the warm waters of the Gulf Stream and the cold waters of the Labrador Sea

gives rise to a surface weather front, the Polar Front, enhancing the formation of pronounced depressions over the ocean and developing a storm track towards western Europe. From March-April to September-October, the Azores High moves northwestward, a thermal low develops over the Iberian Peninsula, and the Icelandic Low weakens leading to equatorward coastal winds. Due to the coastal orientation of the NWIP, which follows an angle of approximately 90º relative to the equator, these winds, with a prevailing northerly component, are upwelling favorable conditions. Winds with prevailing southerly component, which are predominant during winter, are favorable to downwelling conditions.

2.3. Ocean

2.3.1. Water masses

Several water masses can be found at the NWIP coast differentiated according to their physical properties (salinity, potential temperature and density ranges). These water masses are located at different depths (Fig. 2.10).
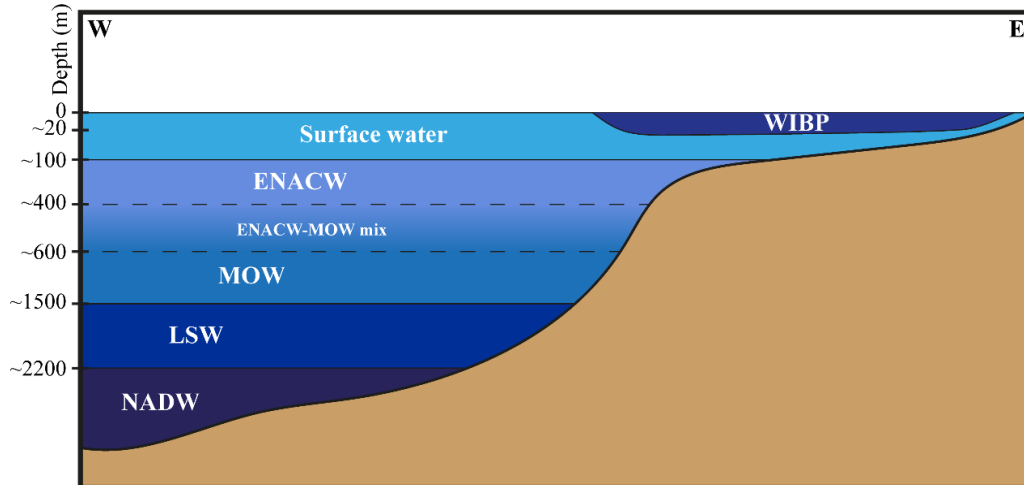

Figure 2.10. Sketch of water masses in the Galician margin.

The surface layer comprises the mixed layer and the seasonal thermocline. The depth of the mixed layer varies along the year from 20 m in summer-early autumn to 125-150 m in winter. The characteristics and thickness of the thermocline are variables depending on the atmosphere-ocean fluxes and runoff seasonality. During summer, thermocline can be found between 10-30 m. In winter, the surface layer is less saline than

in summer and the mixed layer can be found at approximately 100 m of depth (Varela et al., 2005).

The surface layer is influenced by the Western Iberian Buoyant Plume (WIBP), defined by Otero et al. (2008) as a "low-salinity lens formed by river discharge and continental run-off extending along the shelf of the Northwest Iberia". Horizontally, it expands beyond the shelf reaching the 1000 m isobath and occupying the surface layer up to 20 m depth. It is characterized by a salinity lower than 35.7 (Peliz et al., 2002). The main contributors to the WIBP are the Douro and Minho rivers. There is a seasonality related with the river discharge regimes and the WIBP is less developed during the dry season, from July to September, and more developed when higher river discharges occur, from December to March. It is highly influenced by the wind regime, being advected offshore under northerly winds and comprised along the shore under southerly winds (Fernández-Nóvoa et al., 2017; Peliz et al., 2002).

The Eastern North Atlantic Central Water (ENACW) is formed by subduction during winter in a very extensive area eastward of the Mid-Atlantic. The NWIP is affected by ENACW of two different sources: the ENACW subtropical mode (ENACWst) and ENACW subpolar mode (ENACWsp). ENACWst is formed along the Azores Front, at about 35º N and is transported northward by the poleward current. It is lighter, relatively warm and salty and corresponds to a line in the T/S plane between T=13.13 ºC, S=35.80 and T=18.50 ºC, S=36.75. The ENACWsp mode is formed in the eastern North Atlantic, north of 46º N, and is defined by the T/S plane between T=10.00 ºC, S=34.40 and T=12.20 ºC, S=35.66. From April to October, the general southward circulation along the shelf shifts the ENACWsp mode southward. Between 43º N and 44º N, both modes converge and ENACWsp can mix with ENACWst between 26.9 and 27.1 isopycnals (Alvarez et al., 2005). ENACWsp is rich in nutrients and upwelled ENACW water is responsible for the fertility of the coast. The lower limit of the ENACW is located between 300-400 m depth and the position of the upper limit is dependent on the season and meteorological forcings, sometimes even reaching the surface.

The Mediterranean Overflow Water (MOW) is Mediterranean water flowing out through the Strait of Gibraltar. It is characterized by anomalously high salinity (35.1-36.0) and temperature (7-11 ºC). It is centered at a depth of about 1100 m, but after entering the Atlantic, it mixes rapidly with the overlaying ENACW forming an intermediate water mass. Coriolis forces and spreads the dense MOW northward

following the Portuguese shore. Near the area of study, MOW can be distinguished between 800 and 1500 m deep (Liu and Tanhua, 2019; Varela et al., 2005).

The Labrador Sea Water (LSW) is located below the MOW, between 1500 and 2200 m deep. It is characterized by a potential temperature of 3.50 ºC and a salinity of 34.89.

The North Atlantic Deep Water is a complex of several water masses characterized by a potential temperature between 2 and 4 ºC and a salinity ranging from 34.9 to 35.0. This water mass is usually found between 2200 and 4000 m depth.

2.3.2 Ekman transport: the upwelling and downwelling cycle

The NWIP is located at the northernmost limit of the Eastern North Atlantic Upwelling System (Woostern et al., 1976). Coastal upwelling is the result of the joint action of the wind and the rotation of the earth transporting surface water masses seaward of the coast being replaced by water from deeper areas. Despite coastal upwelling is considered a wind-driver process and the variation of upwelling intensity can be explained as the distribution of wind stress, the topography of the area may also affect the upwelling intensity (Alvarez et al., 2008).

A succession of upwelling and downwelling events occur in the study area all year long. Generally, atmospheric regime favors the occurrence of upwelling events from March-April to September-October, although events have also been observed during winter (Alvarez et al., 2009; Álvarez et al., 2003; Prego et al., 2007; Ribeiro et al., 2005). During upwelling events, Ekman transport affects the dynamics of the upper layer (0-200 m) and prevailing upwelling conditions transport significant volumes of water seaward. This water is generally replaced by dense, cold and nutrient-rich deep water known as Eastern North Atlantic Central Water (ENACW). In contrast, downwelling events transport warm and less dense water shoreward. Downwelling events are predominant during winter season when southerly winds at the shore are prevailing.

Regarding the Rías Baixas, upwelling events favor the normal circulation pattern of the rias while downwelling events can revert it, turning them into a system with a negative estuarine circulation (deCastro et al., 2000).

2.3.3. Circulation

The Portugal Coastal Current System or Iberian Coastal Current System (Fig. 2.11) controls the circulation at the ocean side and the continental shelf of the NWIP coast (excluding the Rías Baixas).

The Portugal Current (PC), which is a branch of the North Atlantic Current (NAC), flows in the western boundary of the study area. It is a weak current, about 3 Sv, and flows southwards all year from 45-50º N and 10-20º W (Arístegui et al., 2005).

Closer to coast, the circulation pattern shows a marked seasonality defined by the coastal wind regime. From approximately March-April to September-October, Spring-Summer conditions (Fig. 2.11a), the northeasterly predominant winds promote a southward current, the Portugal Coastal Current (PCC). PCC is a surface current with depths less than 100 m. At the slope, the Iberian Poleward Current (IPC), also called Portugal Coast Under Current (PCUC), flows with a northward direction, at ~200 m depth, with a width between 25 to 40 km (deCastro et al., 2011). During Autumn-Winter conditions (Fig. 2.11b), the IPC intensifies (Peliz, 2003) and the Portugal Coastal Counter Current (PCCC) flows northward from the surface to 1500 m depth, including the MOW (Arístegui et al., 2005).
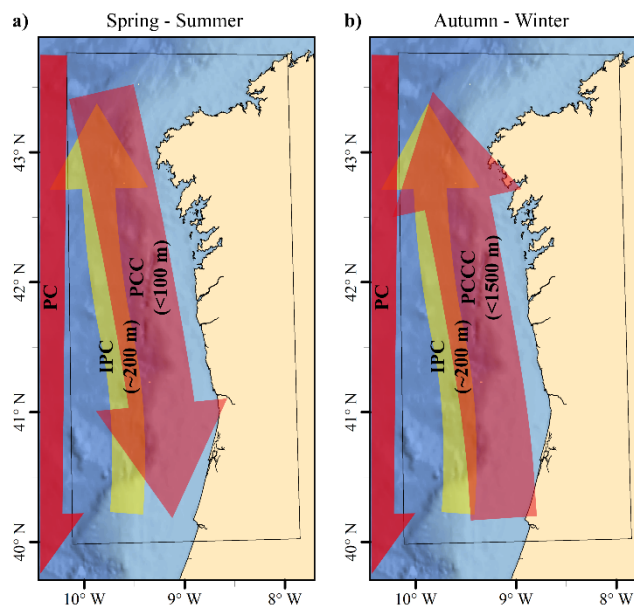

Figure 2.11. Sketch of the Portugal Coastal Current System on the study area in Spring-Summer (a) and Autumn-Winter (b) conditions.

2.4. Rias circulation

The rias are partially mixed estuaries with a partially stratified estuarine circulation: the lower layers are saltier than the upper ones (Taboada et al., 1998). Their typical residual circulation pattern is a positive estuarine circulation with freshwater flowing out through surface layers and oceanic saline water entering through depth layers.

The rias circulation is highly dependent on wind regime, northerly winds at shelf enhance the typical pattern, but southerly winds can reverse the normal circulation pattern, turning it into a negative estuarine circulation.

The circulation in the rias of Arousa, Pontevedra and Vigo is conditioned by the islands located at their mouths. The islands split the entrance in two mouths, the southern and the northern mouths. Barton et al. (2015) have described the general circulation of the Ría de Vigo under upwelling and downwelling conditions. Under upwelling conditions, water enters through bottom layers across both, north and south mouths and flow out through the surface layer across the south mouth due to the action of a cyclonic eddy located in the outer sector of the ria (Figure 2.12a). Under downwelling conditions, water flows into the ria trough the surface layers across the south mouth and flow out through bottom layers across both, north and south mouths (Figure 2.12b). The lateral circulation of the ria is more remarkable on the outer sector and weakens towards the internal part due to the narrowness of the basin.
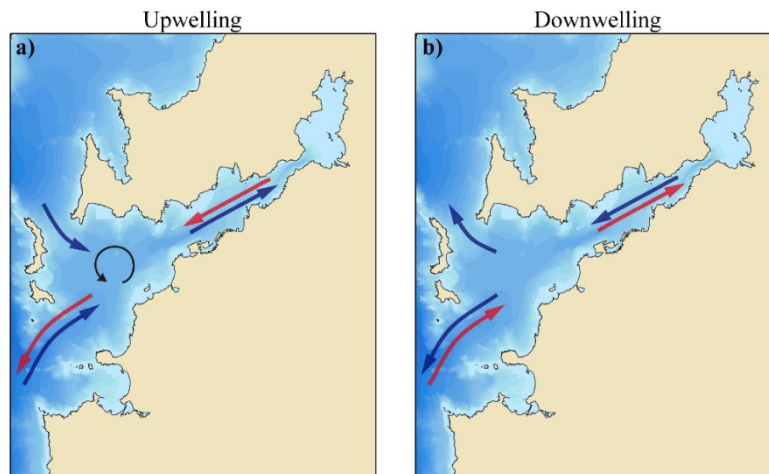

Figure 2.12. Sketch of the circulation of the Ría de Vigo under upwelling (a) and downwelling (b) conditions based on Barton et al. (2015). Red arrows represent surface currents. Blue arrows represent deep currents. The black arrow represents the cyclonic eddy.

The described pattern of circulation for the Ría de Vigo can be extrapolated to the Ría de Pontevedra due to its physiographic similarity with the Ría de Vigo. However, the situation in the Ría de Arousa is slightly different, due to its different and complex physiography, being the southern mouth of the ria of considerable width compare to the north, which is also partially blocked by several smaller islands and structural highs. The exchange of water between the Ría de Arousa and de ocean takes place mainly through the south mouth and corresponds to a typical estuarine circulation. The same circulation pattern can be also described for the Ría de Muros. Under upwelling events, water flows into these rias through deep layers and leaves it through the surface. Conversely, under downwelling events, water flows into these rias through surface layers and outflows through the deep ones.

2.5. Tides and waves

Tides are semi-diurnal and mesotidal, characterized by a period of about 12.25 h and a tidal amplitude varying between 2 m during neap tides and 4 m during spring tides (Sousa et al., 2014). The tidal wave propagates from south to north as Kelvin waves, with amplitude increasing towards the coast. The highest diurnal and semidiurnal harmonics are M_2 (principal lunar), S_2 (principal solar), K_1 (luni-solar semidiurnal) and O_1 (principal lunar diurnal). Amplitude and phase for M_2, S_2, K_1 and O_1 from Villagarcia (Fig. 2.3), Marín (Fig. 2.4) and Vigo (Fig. 2.5) tidal gauge are shown in Table 2.2.

Typical tidal current velocities are 5 cm s^{-1} for deep and 2 cm s^{-1} for shallow waters (Fanjul et al., 1997).

The wave climate regime is also controlled by the seasonal variability of wind, which are highly seasonal. During summer, waves show relative low energy, whilst in winter, waves regime is more energetic with a predominant significant wave height between 1 and 3 m, although it can reach up to 10 m during strong storms. Statistically, northeast to northwest winds are prevailing. Thus, waves arrive roughly from a northwest direction (Oberle et al., 2014).

		Tidal gauge		
		Vigo	**Marín**	**Villagarcia**
M₂	Amplitude (m)	1.11	1.10	1.14
	Phase (°)	75.94	77.15	78.73
S₂	Amplitude (m)	0.46	0.46	0.47
	Phase (°)	120.00	121.09	123.15
O₁	Amplitude (m)	0.07	0.07	0.07
	Phase (°)	323.90	325.80	325.47
K₁	Amplitude (m)	0.08	0.07	0.08
	Phase (°)	85.68	79.28	81.58

Table 2.2. Amplitude and phase of the main tidal constituents in the Vigo, Marín and Villagarcia tidal gauges.

Chapter 3

Data sources

Data from different databases were used to conduct this thesis' research. This chapter presents the main features of all of them. Each database has been chosen depending on the purpose of each study in order to get the best fit between the observed and modeled data and trying to best simulate real conditions with the most adequate spatial and temporal resolution. As a consequence, one single variable may proceed from different databases.

3.1. Bathymetry

The bathymetry used for numerical simulations was elaborated from different sources. The bathymetries for the rias of Arousa, Muros and the adjacent shelf area were digitalized from nautical charts elaborated by the Spanish Navy Hydrographical Institute. The multibeam-sourced bathymetries of the rias of Vigo and Pontevedra were provided by the General Fishing Secretary, dependent on the Spanish Ministry of Agriculture, Fisheries and Food. These multibeam-sourced bathymetries have a horizontal resolution of 5 m. Portuguese Navy Hydrographic Institute provided the bathymetry of the Minho, Lima and Douro estuary. The bathymetries for the Ria de Aveiro was generated from data provided by the Aveiro Harbor Administration and Polis Litoral Ria de Aveiro.

Bathymetry gaps were covered using data from the General Bathymetric Chart of the Oceans (GEBCO, https://www.gebco.net/). This grid is created by the compilation of data from different sources and has a spatial resolution of 30 arc seconds.

3.2. Tide

Thirteen main tidal harmonic constants (M_2, S_2, N_2, K_2, K_1, O_1, P_1, Q_1, M_F, M_M, M_4, MS_4, MN_4) were obtained from 7.2 TOPEX/Poseidon Altimetry http://volkov.oce.orst.edu/tides/global.html) and were imposed to the model as boundary condition. TOPEX/Poseidon Altimetry assimilate data from various altimetric data (Topex Poseidon, Topex Tandem, ERS, GFO) and other datasets (e.g. tide gauges) and has a horizontal resolution of 1/4º.

Harmonic constants from tidal gauges located at Villagarcia (Fig. 2.3), Marin (Fig. 2.4) and Vigo (Fig. 2.5) obtained from Puertos del Estado web portal (http://www.puertos.es), were used to verify the model accuracy in reproducing the main tidal constituents for the Rías Baixas. Puertos del Estado is a Spanish State company responsible for managing the state-own ports.

3.3. Hydrographic variables

Weekly vertical salinity and temperature profiles from 2006 to 2018 were download from the Instituto Tecnolóxico para o Control do Medio Mariño de Galicia

(INTECMAR, www.intecmar.gal) portal. These data were used to evaluate the capability of the model to reproduce thermohaline variables within the rias and to detect days of potential intrusion of Minho River into the Rías Baixas. INTECMAR is a regional agency in charge of controlling the quality of the marine environment and applying the legal provisions regarding the technical-sanitary control of seafood products. They carry out weekly sea surveys collecting sonde data using an SBE25 CTD at 38 field stations (8 at the Ría de Muros, 11 at the Ría de Arousa, 11 at the Ría de Pontevedra and 8 at the Ría de Vigo, Fig. 3.1).
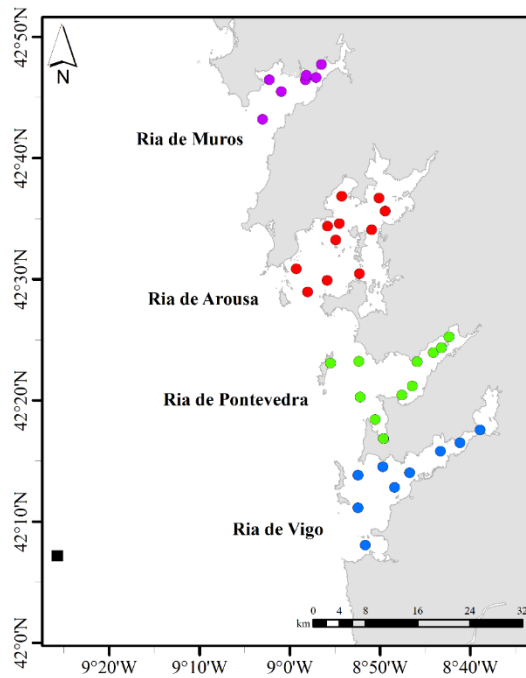
Fig. 3.1. Location of INTECMAR field stations, black points, and Cabo Silleiro boy, black square.

Temperature data for August 2012 was also measured using 19 TidbiT data loggers (9 at the Ría de Muros and 10 at the Ría de Arousa, Fig. 3.2), located in shallow waters. The data loggers were placed on rocks of the intertidal area exposed during most of the tidal cycle, therefore, only data recorded during the high tide was used. These data were used to evaluate the capability of the model to reproduce thermohaline variables in shallow areas of the rias.
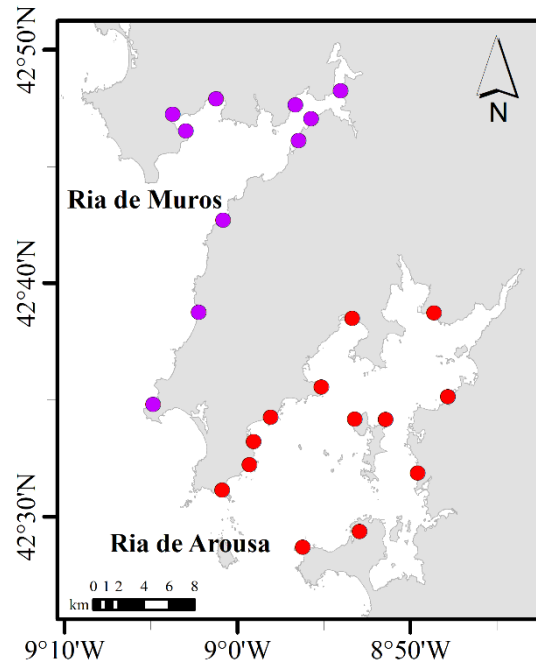
Fig. 3.2. Location of TidbiT field stations.

Hourly water temperature, salinity, and horizontal velocity at 3 m depth for Cape Silleiro buoy (Fig. 3.1.) were provided by Puertos del Estado for the period 1998-2018. These data were used to evaluate the model accuracy in reproducing transport conditions near the open boundary. Besides, these data were also compared with historical climatological data.

Daily salinity and temperature data from Atlantic-Iberian Biscay Irish-Ocean Physics Reanalysis (ibi-reanalysis-phys-005-002-daily) product were download form de project database website (http://marine.copernicus.eu) for the period 2009 to 2018. These data were imposed to the model as transport boundary conditions in realistic experiments. These data are generated through a reanalysis called IBIRYS, developed by Mercator Ocean in collaboration with Puertos del Estado. It is based on NEMO v3.6 ocean general circulation model and the assimilation of altimeter data, *in situ* temperature and vertical profiles and satellite sea surface temperature. Data cover the area from 26º N to 56º N and from 19º W to 5º E with a horizontal resolution of 1/12º, and a vertical resolution of 50 sigma coordinates levels. A remarkable characteristic of the NEMO v3.6 ocean general circulation model is the assimilation of river discharge from 35 rivers. Additional data information can be found in Baladrón et al. (2019).

Seawater potential temperature and seawater salinity from the Hadley Centre Global Environment Model–version 2 Earth System (MOHC-HadGEM2-ES) were used to imposed to the model as transport boundary conditions in climatological experiments. Monthly data from MOHC-HadGEM2-ES Global Circulation Model (GCM) were downloaded for historical (1970 to2005) and future (2006-2099) periods under the RCP8.5 scenario (rpc85 experiment). This model has a horizontal resolution of 1º, increasing to 1/3º at the equator, and a vertical resolution of 40 levels and run under de global project Coupled Model Intercomparison Project version 5 (CMIP5, https://www.wcrp-climate.org/wgcm-cmip/wgcm-cmip5). Among the models provided by the CMIP5 project database, MOHC-HadGEM2-ES model has been chosen because it is the model which better reproduces historical climate conditions in the area under study.

The main characteristics of the hydrographic variables described in this section are summarized in Table 3.1.

Source	Variable	Temporal resolution	Horizontal resolution	Vertical resolution
SBE25 CTD	T and S	Weekly (2006-2018)	38 field stations	variable
TidbiT data loggers	T and S	August (high tide) 2012	19 field stations	Surface
Ibi reanalysis	T and S	Daily (2009-2018)	1/12º	50 σ-layers
RCM MOHC-HadGEM2-ES	T and S	Monthly (1970-2099)	1º	40 levels
Cape Silleiro buoy	T, S and v_x	Hourly (1998-2018)	1 field station	3 m depth

Table 3.1. Hydrographic variables summary. T = water temperature; S= salinity; v_x = horizontal velocity.

3.4. Atmospheric variables

Hourly zonal and meridional wind components, sea level pressure, surface air temperature, relative humidity and solar radiation components from the Weather Research and Forecasting Model (WRF) by the Galician regional meteorological agency (MeteoGalicia) were downloaded for the period of 2009-2018 from the MeteoGalicia

website (www.meteogalicia.gal). Since 2008, MeteoGalicia runs WRF in an operational way twice a day, at 00UTC and 12UTC. Three nested domains are configured for 36, 12 and 4 km resolution. The 4 km resolution domain covering from 40.42 to 45.23 ºN and from 11.26 to 5.11 ºW was chosen. These data were imposed to the model as surface boundary conditions in realistic experiments.

For the climatological experiments, air temperature, sea level pressure, cloudiness, relative humidity and solar radiation components, with a 3 h temporal resolution, and wind components with a 6 h temporal resolution from the Regional Climate Model (RCM) MOHC-HadGEM2-ES-RCA4 were downloaded for historical (1970 to2005) and future (2006-2099) rpc85 experiment from the Coordinated Regional Climate Downscaling Experiment (CORDEX) website (https://www.cordex.org). These data are a dynamical downscaling of the GCMs, thereby, GCMs outputs are used to force RCMs for smaller areas with higher resolution. Thus, MOHC-HadGEM2-ES-RCA4 RCM is the downscaling of MOHC-HadGEM2-ES GCM using the RCA4 model. The EURO-11 domain of CORDEX with a horizontal resolution of 0.11º was chosen. These data were imposed to the model as surface boundary conditions in climatological experiments.

ERA-Interim Version 2.0 dew point temperature, surface temperature, surface pressure, surface thermal radiation, cloud cover, surface net solar radiation and wind components with a temporal resolution of 3 h were downloaded for the period 1978-2018 from the Center for Medium-range Weather Forecasts (ECMWF, https://www.ecmwf.int) database. ERA-Interim is a global atmospheric reanalysis from 1979 to 31 August 2019. Data has a spatial resolution of 60 vertical levels from surface up to 0.1 hPa, T255 spherical-harmonic representation for the basic dynamical fields and a reduced Gaussian grid with approximately uniform 79 km spacing surface. Additional information on ERA-Interim can be found in Berrisford et al. (2011). These data were used to compare ERA-Interim dataset with the historical dataset from MOHC-HadGE2-Es-RCA4 RCM.

The main characteristics of the atmospheric variables described in this section are summarized in Table 3.2.

Source	Variable	Temporal resolution	Horizontal resolution	Vertical resolution
WRF	slp, sr	Hourly (2008-2018)	4 km	surface
WRF	ta, rh	Hourly (2008-2018)	4 km	2 m
WRF	w	Hourly (2008-2018)	4 km	10 m
RCM MOHC-HadGEM2-ES-RCA4	slp, ta, cl, rh and sr	3 h (1970-2099)	0.11°	surface
RCM MOHC-HadGEM2-ES-RCA4	w	6 h (1970-2099)	0.11°	surface
ERA-Interim V 2.0	slp, sr	3 h (1978-2018)	79 km	surface
ERA-Interim V 2.0	Ta, dh	3 h (1978-2018)	79 km	2 m
ERA-Interim V 2.0	cl	3 h (1978-2018)	79 km	-
ERA-Interim V 2.0	w	3 h (1978-2018)	79 km	10 m

Table 3.2. Atmospheric variable summary. w = wind components; slp = sea level pressure; ta = air temperature; cl=cloudiness; rh = relative humidity; sr = solar radiation components, dh = dew point temperature.

3.5. River discharge

Daily data for the Minho river discharge at the Frieira dam and the Tea river flow at Ponteareas station for the period 2009-2018 were provided by the Confederación Hidrográfica Minho-Sil (http://saih.chminosil.es). Confederación Hidrográfica Minho-Sil is an interregional organism dedicated to manage the river basin of the Minho River. This agency collects information about several variables, such as river level, flow, pH, temperature, oxygen and turbidity, at various stations to control the state of the Minho-Sil basin.

In addition, daily river discharge data for the main fluvial inputs into the Rías Baixas are available at the Galician regional meteorological agency website (MeteoGalicia, www.meteogalicia.gal). Data were downloaded at the measuring station

nearest to the mouth of the river for the period 2009-2018. The discharges of the different rivers were obtained as follows:

- Tambre River: sum of the flow of Tambre in Oroso and its main tributaries after the measure station (Barcala, Dubra and Lenguelle rivers).

- Ulla River: sum of Ulla flow at Teo village plus Sar flow at Brión village.

- Umia River: flow at Baixo Umia measured station (Ribadumia).

- Lérez: flow at Pontevedra city.

- Verdugo-Oitavén: sum of Verdugo flow at Pontecaldelas village and Oitavén flow at Soutomaior village.

These *in situ* measured river discharges were imposed to the model as discharge boundary conditions in realistic experiments

Daily simulated river discharges for Tambre, Umia, Ulla, Lérez, Verdugo-Oitavén, Minho, Lima, Douro river and for the major tributaries in the Ria de Aveiro from the Hype model were downloaded from the Hype webpage (https://hypeweb.smhi.se) for the entire period available (1981 to 2010). Hype model is developed by the Hydrological Research Unit at the Swedish Meteorological and Hydrological Institute (SMHI). Hype model is run on a large-scale in operational mode calculating water volume and fluxes over large geographical areas. Simulated river discharges were used to create a river discharge climatology and to impose it to the model as the discharge boundary conditions in climatological experiments.

Chapter 4

Numerical model: DELFT3D-Flow

The Delft3D package is an open-source fully integrated computer software suite developed by WL|Delft Hydraulics in cooperation with Delft University of Technology. It consists of various integrated process modules which interact with each other allowing to perform the simulation of hydrodynamic flow, sediment transport, waves, water quality, morphological developments and ecology. Delft3D is a computer tool designed for coastal, river and estuarine simulations in 2D or 3D with a multi-disciplinary approach.

Delft3D-Flow module performs the simulation of the hydrodynamic flow and the transport of salinity and heat that results from tidal and meteorological forcing on a rectilinear or a curvilinear grid. A sigma coordinate is defined as the vertical grid approach in 3D simulations.

4.1. The hydrodynamic model

This thesis was mainly performed using the hydrodynamic module of the numerical model Delft3D (Delft3D-Flow research version 4.04.01). The Flow module simulates a large number of processes as wind shear, wave forces, tidal forces, density-driven flows and stratification due to salinity or temperature gradients, atmospheric pressure changes, drying and flooding of intertidal flats, etc. It aims to simulate flow phenomena of which the horizontal length and time scales are significantly larger than the vertical scales (Deltares, 2014).

Delft3D solves the horizontal equations of motion, the continuity equation, and the transport equations for conservative constituents. These equations are formulated in orthogonal curvilinear or spherical coordinates. For this thesis, spherical coordinates were chosen which means that the reference plane for surface level and bathymetry follows the Earth's curvature. The Delft3D-Flow numerical method is based on finite differences.

As the vertical scale is much smaller than the horizontal scale, Delft3D-Flow performs simulations of hydrodynamic flow under the shallow water assumption to solve both the 2D and 3D shallow water equations. The shallow water equations are a simplification of the Navier-Stokes equations under the Boussinesq assumption. For more detailed information about Delft3D-Flow see Deltares (2014).

4.1.1. Mesh and bathymetry

To discretize the shallow water equations, the area to be modeled has to be covered by a curvilinear grid which is assumed to be orthogonal and well-structured. Then, this grid, which is defined in the physical space, is discretized on the computational grid and the variables are arranged using the Arakawa G-grid system (Deltares, 2014). The water level and density are defined in the center of a cell while velocity components are perpendicular to the grid cell (Fig. 4.1a). In the vertical direction, where a sigma coordinate is used, the grid is boundary-fitted, the number of layers is constant and the relative layer thickness is usually non-uniform (Fig. 4.1b).
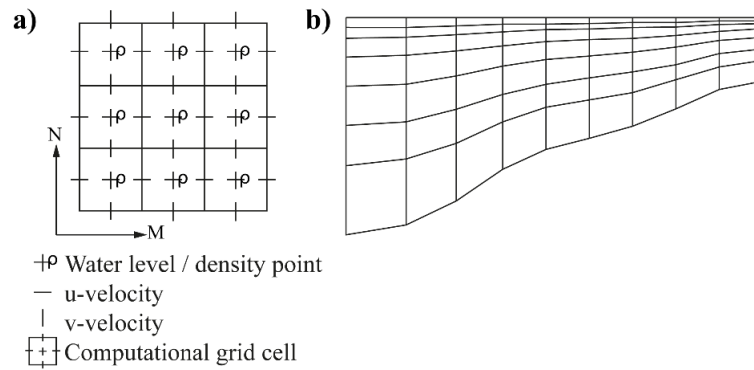
Fig. 4.1. Schematized horizontal (a) and vertical (b) grid of Delft3D-Flow.

Delft3D allows using two different approaches of grid design: unique-domain and multi-domain. Unique-domain is preferable because it avoids numerical discrepancies at the domain decomposition frontiers but it has the disadvantage that does not allow a significant variation of the resolution and, therefore, can be time-consuming. The advantage of using multi-domain is that it allows varying the resolution both vertically and horizontally in each of the domains. This is very useful when the study area is large and there are regions that require a local refinement in order to properly solve hydrodynamic processes. This work was carried out using both approaches: i) a multi-domain was used to assess the impact of climate change on upwelling in the NWIP, which is a large area ($\sim$ 49000 km^2) where the oceanic region requires less resolution than the estuaries; and ii) a single-domain was used to perform specific researches in the area of the Rías Baixas and the Minho estuary.

The multi-domain covers an area from 8 to 10.20º W and from 40 to 43.75º N, dividing the area into five domains connected between them (Fig. 4.2a). The horizontal resolution is different for each domain: ~1500 m for the oceanic domain, ~250 m for the Rías Baixas, ~60 m for the Minho and Lima estuaries, from 45 to 80 m for the Douro estuary and from 45 to 80 m for the Ria de Aveiro. The vertical grid is composed by 13 sigma layers with top layers refined to improve the ability of the model to solve vertical mixing (1st layer 1%, 2nd layer 2%, 3rd layer 3%, 4th layer 4%, 5th layer 5%, 6th layer 6%; 7th layer 8%; 8th layer 11% and from 9th to 13th layers 12% each). A time step of 0.5 min was chosen based on the Courant-Friedrichs-Lewy number.
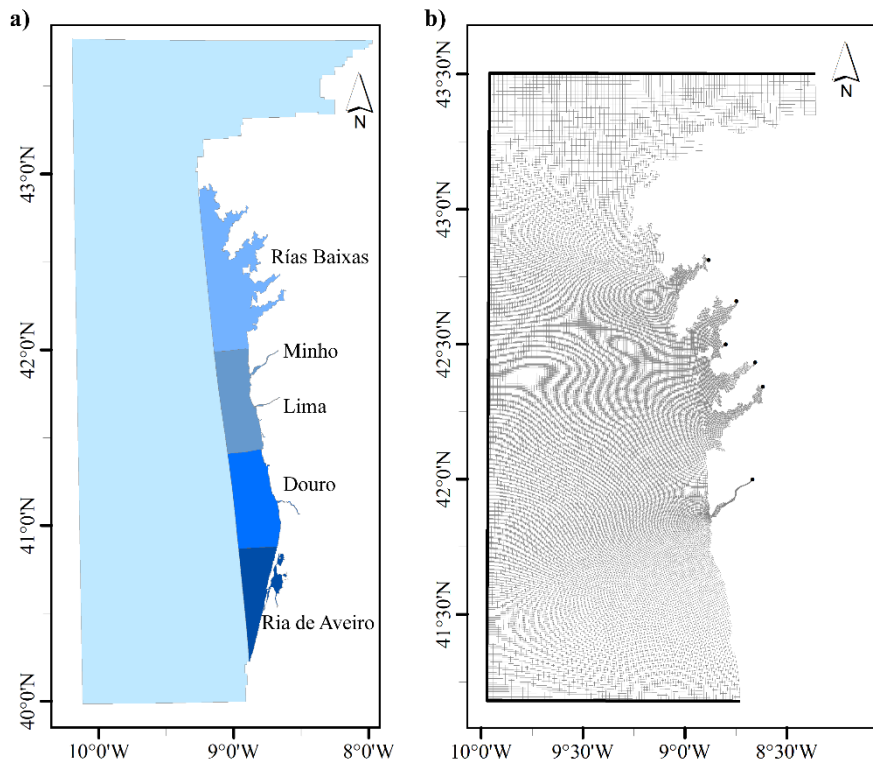
Fig. 4.2. Five domains adopted in the multi-domain approach of the NWIP (a). Morphological grid used to model the Rías Baixas and the adjacent area (b). Thick black lines show the open boundary. Black dots indicate the cells where river discharges were imposed.

The horizontal grid used in the unique-domain approach is shown in figure 4.2b. The domain covers from 10.00ºW to 8.33ºW and from 41.18ºN to 43.50ºN. The number of grid cells is 452 in the M-direction and 446 in the N-direction (see Fig. 4.1a) with a total number of 53603 grid elements. The horizontal resolution increases gradually from 2200 m × 800 m on the West boundary to 220 m × 140 m in the rias and 50 m × 77 m in the Minho estuary. A time step of 0.5 min was chosen based on the Courant-Friedrichs-Lewy number.

The bathymetry used for model simulations was created by the compilation of the bathymetries of: the rias of Arousa and Muros obtained from the nautical charts of the Spanish Navy Hydrographical Institute, the rias of Vigo and Pontevedra from the General Fishing Secretary, the Minho, Lima and Douro estuaries from the Portuguese Navy Hydrographic Institute, the Ria de Aveiro from the Aveiro Harbor Administration and Polis Litoral Ria de Aveiro and finally, the adjacent shelf area and from the General Bathymetry Chart of the Oceans.

4.1.2. Initial and boundary conditions

Delft3D-Flow requires initial conditions of water level, flow velocity components, salinity and water temperature variables to start computation.

To drive a simulation, it is necessary to impose flow and transport boundary conditions at the open boundaries (Fig. 4.2, thick black lines). These conditions represent the influence of the non-modelled area surrounding the modeled area and can be provided as a uniform value for the whole area or as a spatially variable value. For this thesis, the open boundary was divided into 127 sections and the imposed conditions were prescribed for each section. The type of open boundary chosen was water level because is the only variable known with relative accuracy. Hydrodynamic forcing was imposed as astronomic components. Transport conditions, salinity and temperature, were specified per layer. Finally, rivers discharge was prescribed as boundary condition of type discharge per cell (Fig. 4.2, black dots).

A smoothing time of 60 minutes was established at the beginning of simulations to avoid discrepancies between initial and boundary conditions.

4.1.3. Physical parameters

The bottom stress is used to estimate the average velocity of an open channel flow determining the tidal range variation along the study area. It was computed according to Manning formula; in this formulation the Manning's coefficient depends on the bottom roughness. The bottom roughness is a calibration parameter, so its value must be determined in the calibration process. It was considered uniform with a value of 0.024 in both x and y directions for all areas except for Ria de Aveiro where a spatial variable friction coefficient (Lopes and Dias, 2015) was used due to the shallowness of the lagoon.

The values of the horizontal eddy viscosity and diffusivity, which depend on the flow and the grid size, are calibration parameters. Vertical eddy viscosity and diffusivity are also calibration parameters. The K-ε turbulence model was chosen to determine the vertical turbulent eddy viscosity and diffusivity additional to the background values.

Regarding to the heat flux model, two models were used to simulate the exchange of heat through the free surface depending of the domain approach. The "absolute flux, net solar radiation" model was chosen for the unique-domain simulations since allowing higher accuracy during calibration. This model needs relative humidity, air temperature

and the combined net solar (short wave) and net atmospheric (long wave) radiation. The heat loses due to evaporation and convection are computed by the model (Deltares, 2014). However, for simulations using the multi-domain, the "ocean" model was chosen which is the one recommended when simulating large areas since the "absolute flux, net solar radiation" requires to assume a single point as a representative for the entire domain. The "ocean" model needs relative humidity, air temperature and cloudiness varying spatially. Spatially variable values of wind components and pressure were imposed for the two heat flux models.

4.2. Model implementation

Two numerical experiments were developed in the present thesis. In the first one (Exp#1 from now on), Delft3D was forced with real conditions. In the second experiment (Exp#2 from now on), the model was forced with historical and future climatological data. The main differences between the experiments are the databases used to force the boundaries.

4.2.1. Exp#1

Exp#1 simulates the hydrodynamics of the study area for historical period under realistic conditions.

Salinity and temperature data from the operational Atlantic-Iberian Biscay Irish-Ocean Physics Reanalysis were imposed as ocean boundary conditions.

Air temperature, relative humidity, net solar radiation and wind components obtained from MeteoGalicia Weather Research and Forecasting Model were used as surface boundary conditions.

Minho River discharge data was provided by the Confederación Hidrográfica Minho-Sil, and the Verdugo-Oitavén, Lérez, Ulla, and Umia river discharge data from the MeteoGalicia database.

The horizontal eddy viscosity ranged from 500 m^2 s^{-1} on the west open boundary to 5 m^2 s^{-1} on the east. The horizontal eddy diffusivity was set to be constant, 5 m^2 s^{-1}. The vertical eddy viscosity and the vertical eddy diffusivity were 0 m^2 s^{-1}.

4.2.2. Exp#2

Exp#2 simulates the hydrodynamics of the study area for historical and future periods under climatological conditions. The RCP8.5 greenhouse gas emission scenario was considered for future projections.

Salinity and water temperature data for ocean boundary conditions were retrieved from the GCM MOHC-HadGEM2-Es.

Air temperature, relative humidity, cloudiness, net solar radiation and wind components data obtained from the MOHC-HadGEM2-Es-RCA4 RCM were used as surface boundary conditions.

Climatological river discharge data were obtained from the Hype Web portal. In this setup, a reduction of 25% in river discharges was applied for future projections, following the most pessimistic predictions (https://hypeweb.smhi.se/explore-water/climate-impacts/europe-climate-impacts/).

The horizontal eddy viscosity ranged from 500 m^2 s^{-1} on the west open boundary to 5 m^2 s^{-1} on the east. The horizontal eddy diffusivity was set to be constant, 5 m^2 s^{-1}. The vertical eddy viscosity and the vertical eddy diffusivity were 0.0001 m^2 s^{-1} (Sousa et al., 2018).

4.3. Model calibration

A typical calibration procedure consists of three steps: i) running the model, ii) crosschecking the results against measured data or against results from other simulation and iii) adjusting the parameters of the model. This procedure is repeated until the simulation results are accurate enough. The model calibration was evaluated through a qualitative and quantitative comparison of the temporal evolution of predicted sea surface elevation (SSE), velocity, salinity, water temperature data and the concurrent *in situ* data. The calibration was performed by adjusting the bottom friction coefficient, viscosity, and diffusivity for the entire domain. This section shows the crosschecking for the model configuration using realistic data (Exp#1), and the crosschecking for the model configuration using climatological inputs (Exp#2).

A similar procedure to that proposed by Dias et al. (2009) was used to quantify the model accuracy for the Rías Baixas. First, the harmonic constituents computed from the model predictions were compared with those available from SSE field observations (Fig. 1b, black circles). The harmonic analysis was performed using the T_TIDE analysis package (Pawlowicz et al., 2002) for the period from January 17th to February 15th, 2010. The fit degree was assessed using the metrics described below:

The root mean square error (RMSE) was calculated as

$$RMSE = \left\{ \frac{1}{N} \sum_{i=1}^{N} |X_{obs}(t_i) - X_{mod}(t_i)|^2 \right\}^{1/2} \tag{1}$$

where $X_{obs}(t_i)$ and $X_{mod}(t_i)$ are the SSE values computed by the harmonic synthesis of the data and predicted by the model, respectively, and N is the number of samples.

The relative error, ΔE, was calculated to compare the RMSE with the local tidal amplitude as follows:

$$\Delta E = \frac{RMSE}{\frac{1}{n} \sum_{i=1}^{n} \left(A_{max_{obs}}(c_i) - A_{min_{obs}}(c_i) \right)} \ x \ 100 \tag{2}$$

where $A_{max_{obs}}(c_i)$ and $A_{min_{obs}}(c_i)$ are the maximum and minimum elevations for each tidal cycle, respectively, and n is the number of tidal cycles.

The predictive skill also quantifies the agreement between model predictions and observations and was calculated following Warner et al. (2005):

$$Skill = 1 - \frac{\sum_{i=1}^{N} |X_{mod}(t_i) - X_{obs}(t_i)|^2}{\sum_{i=1}^{N} (|X_{mod}(t_i) - \overline{X_{obs}}(t_i)| + |X_{obs}(t_i) - \overline{X_{obs}}(t_i)|)^2} \tag{3}$$

where the horizontal bars represent a temporal mean.

As described by Dias et al. (2009), a skill value of one means a perfect agreement between model predictions and observations, whereas a value of zero means complete disagreement. Skill values > 0.95 represent excellent agreement between predicted and sampled data. In a similar way, an absolute value of ΔE that is < 5% indicates excellent agreement between model predictions and observations, and when it ranges from 5% to 10%, the agreement should be considered to be very good.

Computed and observed near-surface (3 m deep) horizontal velocity, salinity and water temperature were compared with Cape Silleiro buoy data (Fig. 3.1, black square).

Additionally, salinity and water temperature were also compared at nine stations within the Ría de Vigo (V_1 to V_6, V_s, V_m, and V_i, Fig. 1c). RMSE and bias were also used to measure the model accuracy in reproducing transport properties.

$$Bias = \frac{1}{N}\sum_{i=1}^{N}(X_{mod}(t_i) - X_{obs}(t_i)) \tag{4}$$

where $X_{obs}(t_i)$ and $X_{mod}(t_i)$ are the observed and predicted salinity, water temperature or velocity, respectively, and N is the number of samples (time steps).

4.3.1 Tidal

Exp#1 was used to perform tidal calibration. The comparison between the predicted and observed time series of sea surface elevation for Villagarcia, Marin and Vigo tidal gauge stations are shown in Fig. 4.3. The visual comparison shows that the model properly represents the spring-neap tidal cycle.
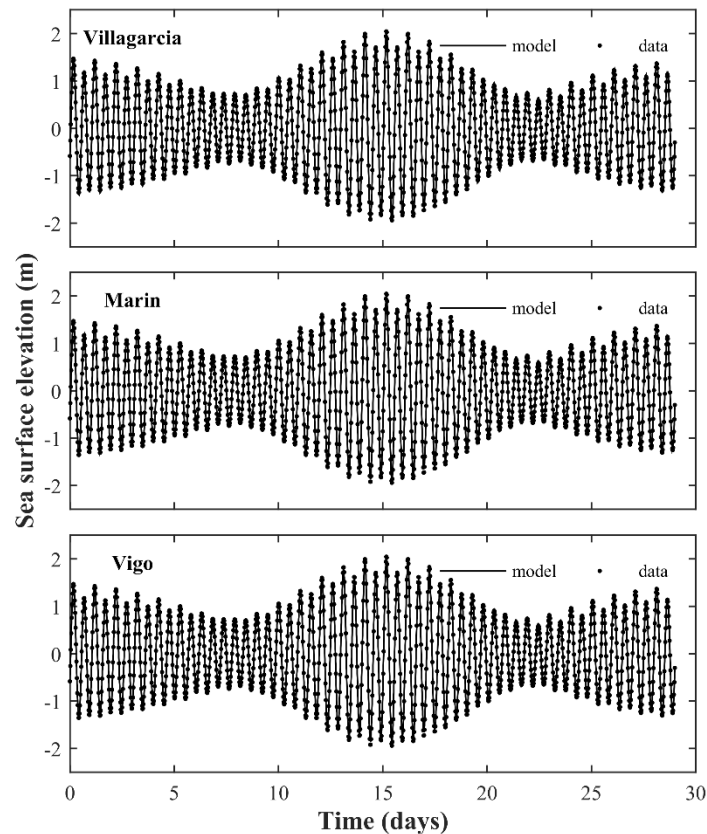
Fig. 4.3. Observed and predicted sea surface elevation time series at Villagarcia, Marin and Vigo tidal gauge stations.

The model accuracy in reproducing the main tidal constituents (M_2, S_2, O_1, and K_1) was analyzed from differences between amplitude and phase of these constituents

determined using predictions and observations (Table 4.1). Accuracy in this study is similar to those obtained by Dias et al. (2009) for the Ria Formosa (Portugal) and by Sousa et al., (2018) for the main estuaries of the NW Iberian Peninsula coast, with good agreement for all constituents, both in amplitude and phase at all harbors. The average difference between observed and predicted semidiurnal tidal constituents (which are the most energetic in the region) was about 2 cm in amplitude and 2º in phase, which means an average delay of 4 min.

	Tide gauge	Amplitude (m)			Phase (°)		
		Data	Model	Difference	Data	Model	Difference
M_2	Vigo	1.11	1.13	0.01	75.94	78.63	2.69
	Marin	1.10	1.13	0.03	77.15	79.16	2.01
	Villagarcia	1.14	1.16	0.02	78.73	80.02	1.29
S_2	Vigo	0.46	0.44	-0.02	120.00	122.14	2.13
	Marin	0.46	0.44	-0.02	121.09	122.76	1.67
	Villagarcia	0.47	0.45	-0.02	123.15	123.85	0.70
O_1	Vigo	0.07	0.06	-0.01	323.90	320.45	-3.45
	Marin	0.07	0.06	-0.01	325.8	320.69	-5.11
	Villagarcia	0.07	0.06	-0.01	325.47	321.12	-4.36
K_1	Vigo	0.08	0.08	0.00	85.68	78.96	-6.72
	Marin	0.07	0.08	0.01	79.28	79.27	-0.01
	Villagarcia	0.08	0.08	0.00	81.58	79.75	-1.84

Table 4.1. Model accuracy in reproducing the main tidal constituents measured at Vigo, Marin, and Villagarcia tidal gauge stations.

Table 4.2 summarizes the model accuracy in reproducing observed SSE. The statistical analysis shows a RMSE of 0.05 m or smaller for all harbors, ΔE of around 2%, and a predictive skill > 0.99. These statistical results indicate an excellent agreement between predicted and observed SSE, following the criteria proposed by Dias et al. (2009).

Tide gauge	RMSE (m)	ΔE (%)	Skill
Vigo	0.05	2.34	0.99
Marin	0.05	2.12	0.99
Villagarcia	0.04	1.74	0.99

Table 4.2. Model accuracy in reproducing observed SSE as characterized by means of the RMSE (m), Relative Error, ΔE (%), and Skill values at Vigo, Marin, and Villagarcia tidal gauge stations.

The subtidal frequency predictions were also evaluated comparing the residual sea level at Vigo, Marin and Villagarcia harbors. The statistical analysis shows a RMSE of 0.006 m and a ΔE of 11.5 % for Vigo, 0.0046 m and 10.3 % for Marin and 0.005 m and 10 % for Villagarcia harbors.

4.3.2 Transport conditions and velocities

Salinity is a natural trace for the calibration of transport processes in estuarine environments. Salinity distribution reflects the combined results of tidal current, freshwater flows, density circulation and turbulent mixing processes (Dias and Lopes, 2006). The heat transport process is highly sensitivity to the heat flux model used. Thus, the calibration parameters and the heat flux model were determined primarily through the crosschecking of the model results against measured salinity and water temperature data or results from other simulations. Several tests were performed adjusting the calibration parameters and the heat flux model until the best fit was achieved.

The accuracy of modeled water temperature and salinity in reproducing thermohaline data inside the Rías Baixas using Exp#1 was investigated by comparing *in situ* vertical profiles from INTECMAR with their corresponding simulated vertical profiles. Two different periods were selected, the first one corresponds to winter conditions (January 1st to February 15th 2010) and the second one, to summer conditions (July 15st to August 31th 2012 and August 2009 to 2018). The bias and RMSE values were calculated for each profile. An example for a particular date is depicted in Figure 4.4 for the Ría de Vigo. This figure shows the salinity (upper row) and water temperature (lower row) vertical profiles, both predicted (black line) and measured (gray line) for February 8th 2010. Predicted and *in situ* profiles follow a similar trend.
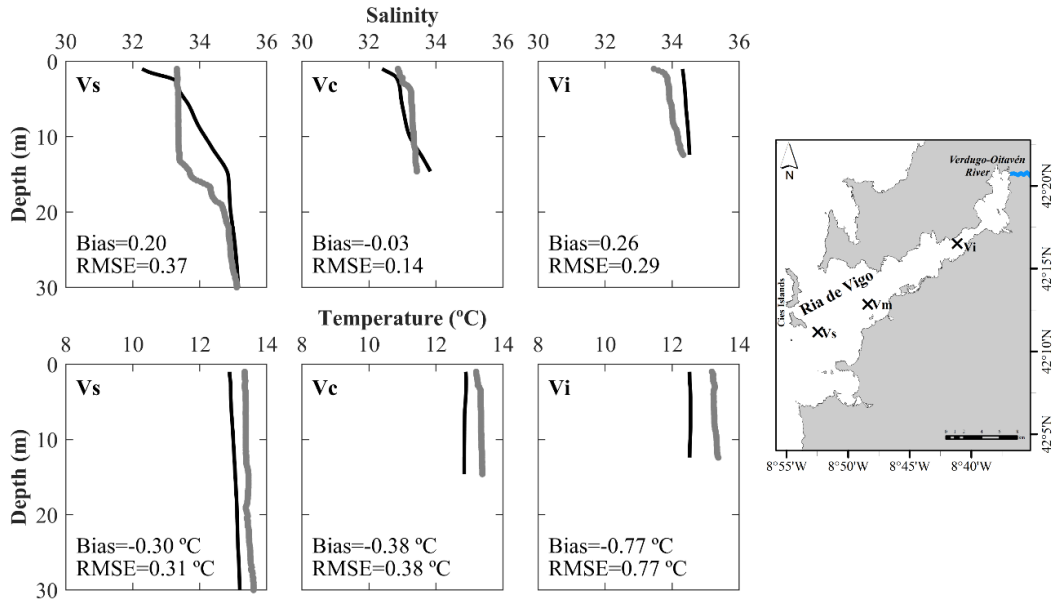
Fig. 4.4. Vertical profiles of salinity (upper row) and water temperature (lower row) obtained using the Delft3D- FLOW model (black line) and measured on February 8th 2010 (gray line) at sampling stations V_s, V_m, and V_i witch location is shown at the map.

Additionally, Fig. 4.5 shows both measured (blue line) and computed (red line) salinity and water temperature vertical profiles for a station located in the middle part of each ria during July and August averaged from 2009 to 2018. Shadows represent measured and numerical standard deviations. These vertical profiles show the accuracy of numerical simulations to reproduce field data.
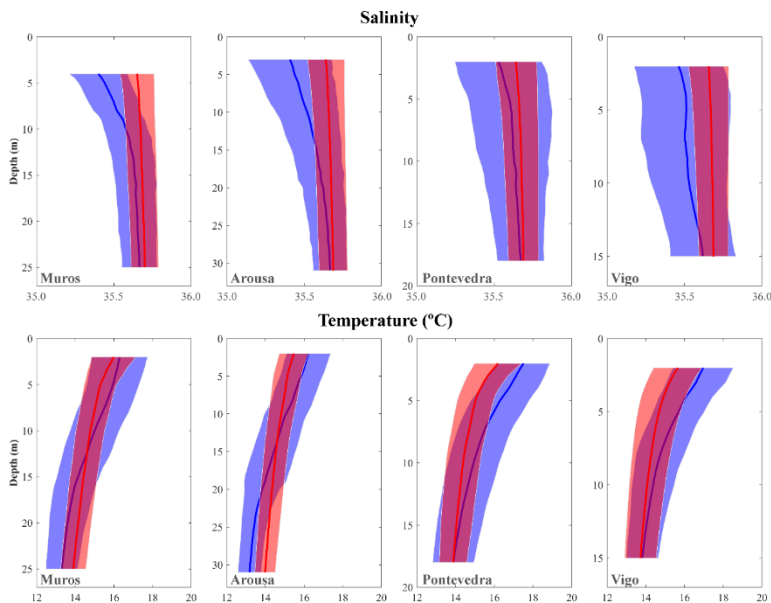
Fig. 4.5. Measured (blue line) and computed (red line) vertical profiles of salinity (upper row) and water temperature (lower row) in a sampling station located in the middle part of the rias of Muros, Arousa, Pontevedra and Vigo during July–August from 2009 to 2018. Shadows represent measured and numerical standard deviations.

The bias and RMSE values calculated for each vertical profile were averaged obtaining a mean value for each station. A positive bias value indicates that model overestimate *in situ* data and conversely negative bias values indicate that model underestimate *in situ* data (Fig. 4.6).
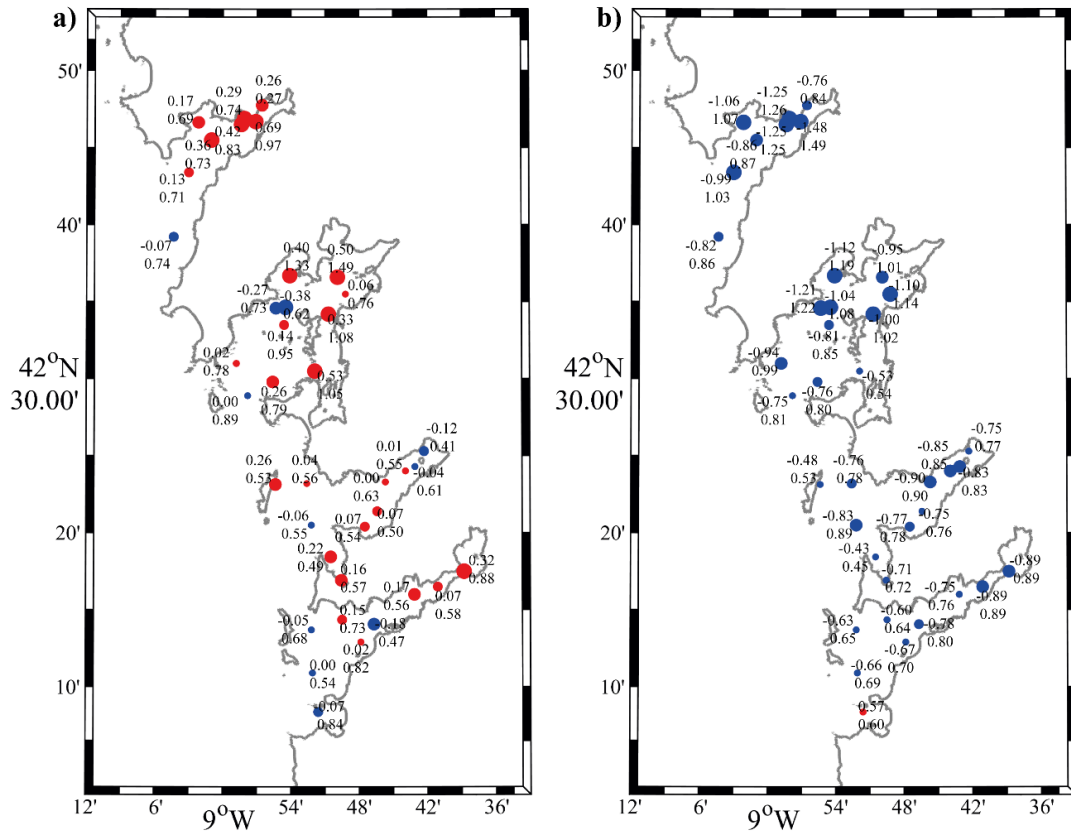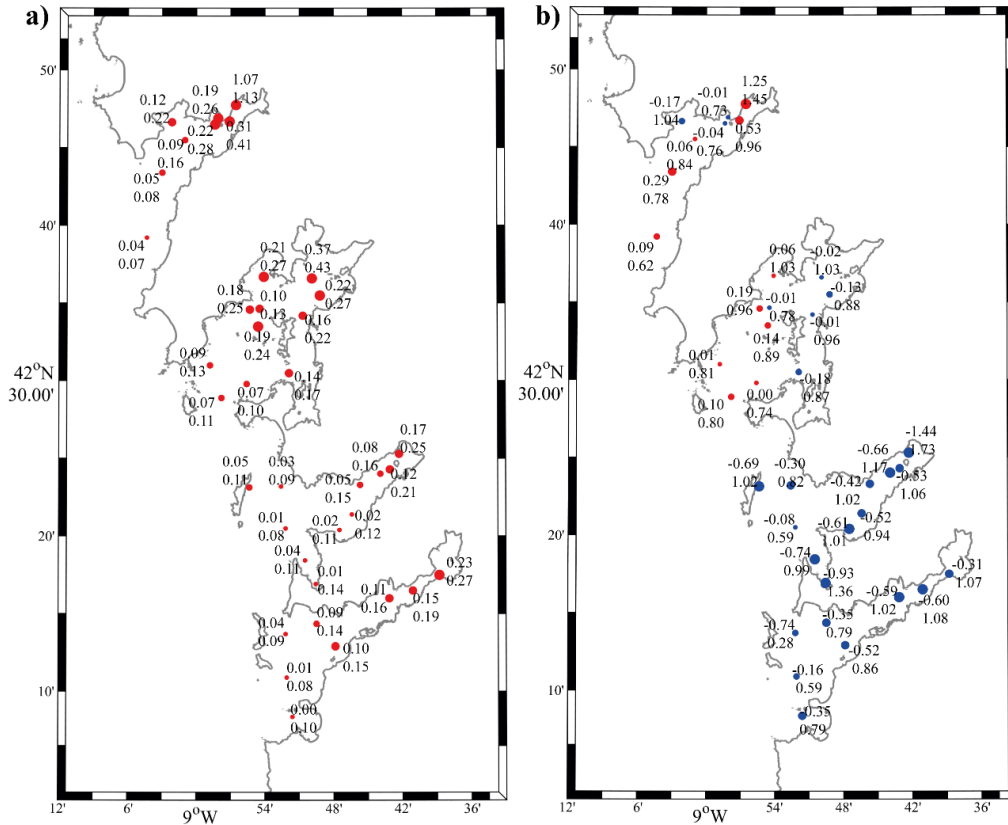

Fig. 4.6. Mean values of bias (upper number) and RMSE (lower number) obtained comparing Delft3D-Flow predicted and measured weekly vertical profiles of salinity (a) and water temperature (b) for January 1st to February 15th 2010. Red dots indicate that the model overestimates *in situ* data, positive bias. Blue dots indicate that the model underestimates *in situ* data, negative bias. Dot size indicates the bias percentile.

Under winter conditions (January 1st to February 15th 2010) the model tends to overestimate *in situ* salinity (Fig. 4.6a) while underestimating *in situ* temperature (Fig. 4.6b) at all stations. Under summer conditions (July 15st to August 31st 2012) the model overestimates *in situ* salinity (Fig. 4.7a) at all stations and *in situ* temperature (Fig. 4.7b) at the rias of Muros and Arousa but there is no clear pattern in the rias of Pontevedra and Vigo.
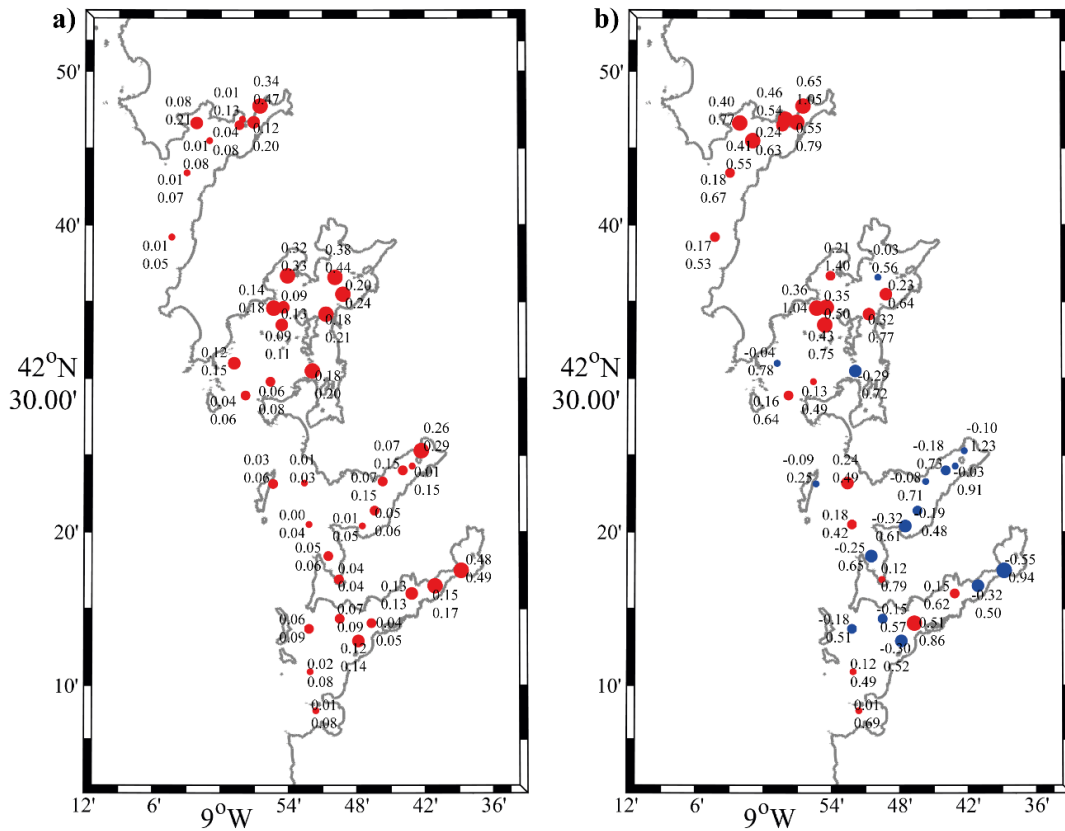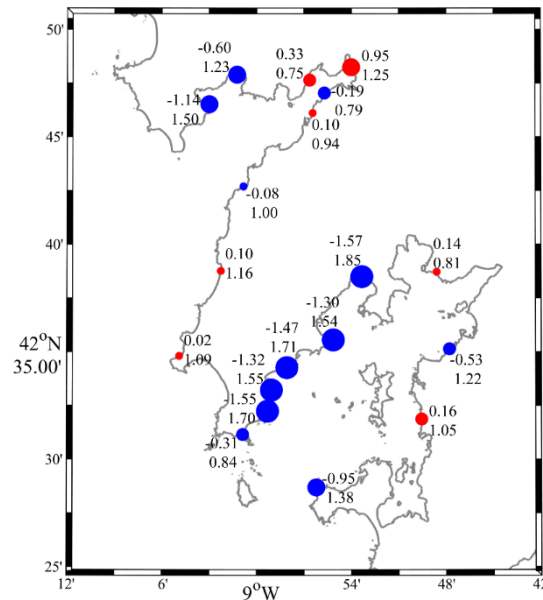
Fig. 4.7. Mean values of bias (upper number) and RMSE (lower number) obtained comparing Delft3D-Flow predicted and measured weekly vertical profiles of salinity (a) and water temperature (b) for July 15st to August 31st 2012. Red dots indicate that the model overestimates *in situ* data, positive bias. Blue dots indicate that the model underestimates *in situ* data, negative bias. Dot size indicates the bias percentile.

The average bias and RMSE for each ria was also calculated and summarized in Table 4.3.

	Salinity				Temperature (ºC)			
Ria	Winter		Summer		Winter		Summer	
	Bias	RMSE	Bias	RMSE	Bias	RMSE	Bias	RMSE
Muros	0.28	0.71	0.08	0.16	-1.06	1.08	0.38	0.69
Arousa	0.15	0.92	0.16	0.19	-0.93	0.97	0.17	0.75
Pontevedra	0.06	0.54	0.05	0.10	-0.73	0.75	-0.06	0.66
Vigo	0.05	0.68	0.12	0.15	-0.71	0.74	-0.08	0.63

Table 4.3. Model accuracy in reproducing *in situ* data of salinity and water temperature in each ria calculated averaging the values for all stations per ria.

Salinity bias is almost zero for the rias of Pontevedra and Vigo under winter conditions and Muros and Pontevedra under summer conditions. Regarding water temperature, the mean bias for the rias of Muros and Arousa are positive, the model overestimates the *in situ* values as it was noted before, while for the rias of Pontevedra and Vigo are close to

zero. To avoid the variability of a particular year, this analysis was carried out for August 2009 to 2018. The bias and RMSE values for each sampling station are depicted in figure 4.8 and the mean values for each ria are shown in Table 4.4.

Fig. 4.8. Mean values of bias (upper number) and RMSE (lower number) obtained comparing Delft3D-Flow predicted and measured weekly vertical profiles of salinity (a) and water temperature (b) for August 2009 to 2018. Red dots indicate that the model overestimates *in situ* data, positive bias. Blue dots indicate that the model underestimates *in situ* data, negative bias. Dot size indicates the bias percentile.

Ria	Salinity		Temperature (ºC)	
	Bias	RMSE	Bias	RMSE
Muros	0.26	0.33	0.25	0.90
Arousa	0.16	0.21	0.01	0.88
Pontevedra	0.06	0.14	-0.63	1.06
Vigo	0.09	0.14	-0.32	0.89

Table 4.4. Model accuracy in reproducing *in situ* data of salinity and water temperature in each ria calculated averaging the values for all stations per ria for August 2009-2018.

The model overestimates *in situ* salinity data for the period 2009- 2018 with bias and RMSE values similar to those obtained for a particular year. Additionally, the model clearly underestimates temperature for the rias of Pontevedra and Vigo and overestimates

it for the rias of Muros and Arousa (Fig 4.8b and Table 4.4). Both RMSE and bias values obtained using Exp#1 were similar to those obtained by Cerralbo et al. (2013) and Sousa et al. (2014) for the same area using ROMS and MOHID models, respectively.

The skill of the numerical model to reproduce water temperature in nearshore shallow areas was evaluated comparing *in situ* water temperature under high tide conditions for August 2012 with the corresponding modeled data. This analysis (Fig. 4.9) shows similar results to that obtained comparing the numerical *vs in situ* INTECMAR data (August 2009 to 2018, Fig. 4.8) although with higher bias and RMSE. These higher errors are probably consequence of the location of sampling points in shallow areas only covered during high tides, so the horizontal resolution of the mesh does not allow a better fit. In spite of this, the adjustment of the model in these points can be considered good.

Fig. 4.9. Mean values of bias (upper number) and RMSE (lower number) obtained comparing Delft3D-Flow predicted and measured the water temperature at 1 m depth for August 2012. Red dots indicate that the model overestimates *in situ* data, positive bias. Blue dots indicate that the model underestimates *in situ* data, negative bias. Dot size indicates the bias percentile.

The model accuracy in reproducing transport conditions near the open boundary was evaluated by comparing near-surface horizontal velocity, salinity and water temperature measured at the Cape Silleiro buoy for January 1st to February 15th 2010 and the corresponding modeled values. The statistical analysis shows a bias and a RMSE of 0.17 and 0.44 for salinity, -0.51 °C and 0.64 °C for water temperature and -0.07 ms^{-1} and 0.12 ms^{-1} for horizontal velocity.

Once the accuracy of the model to reproduce *in situ* data was assessed using the configuration of Exp#1, the calibration of Exp#2 was performed crosschecking the results against Exp#1 simulations. The average temperature field of Exp#1 and Exp#2 for July-August was compared over the period of 2009 to 2018. Top layer temperature outputs for both experiments are depicted in figures 4.10a and 4.10b, respectively. Figure 4.10c shows the difference between these two outputs ($\Delta T = T^{Exp\#2} - T^{Exp\#1}$). The histogram showing in Fig. 4.10d shows that more than 90% of the ΔT values are within the range -1 to 1 ºC. In addition, ΔT tends to be positive, mostly between 0 and 0.75 ºC with an average bias of 0.40 ºC (Fig. 4.10c).
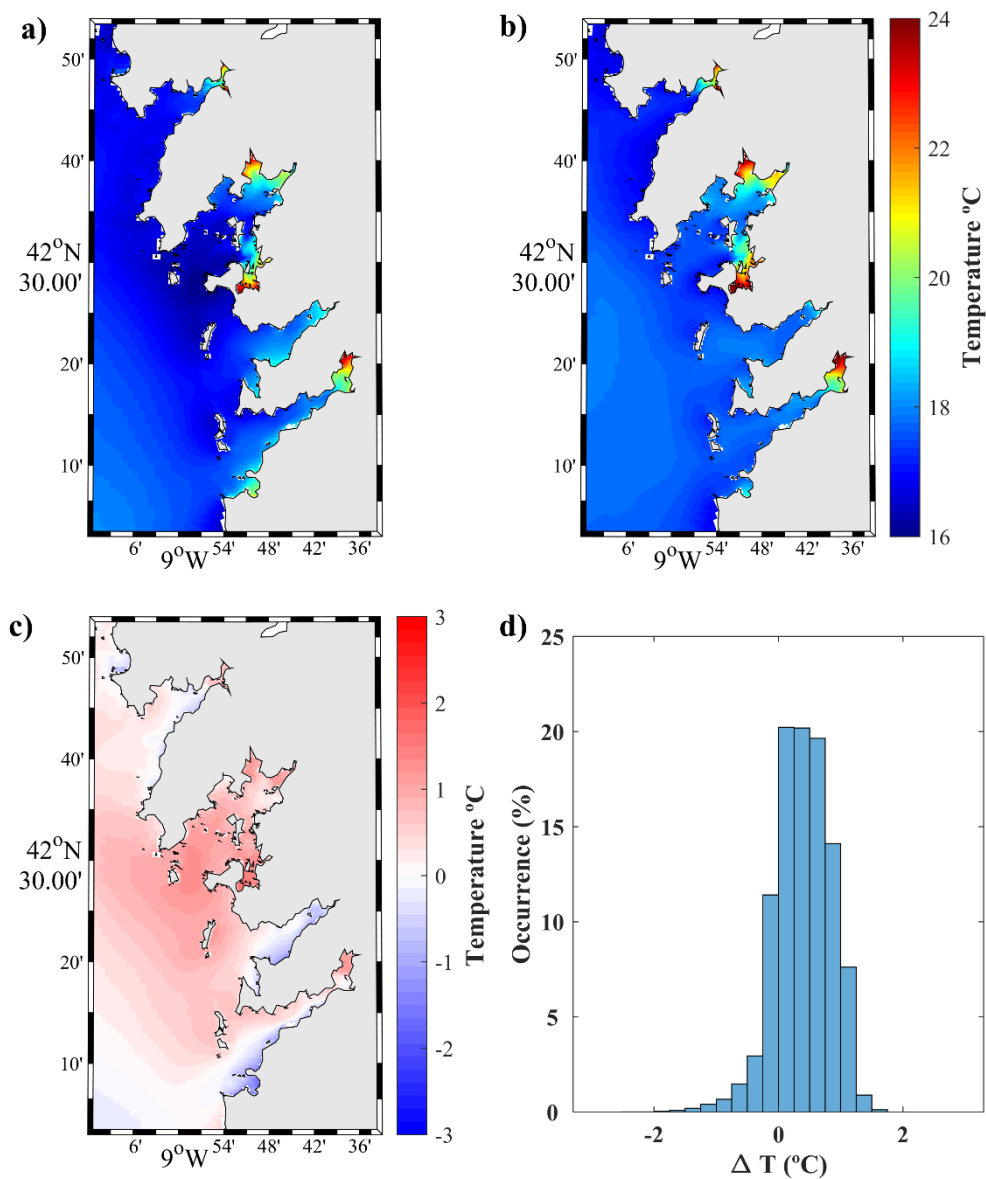
Fig. 4.10. Delft3D-Flow predicted water temperature (upper layer) using Exp#1 (a) and using Exp#2 (b) for July- August over 2009- 2018. Difference between predicted water temperature using Exp#1 and Exp#2 (Exp#2 - Exp#1) (c). Histogram showing the frequency of the temperature differences shown in c (d).

Despite the different nature of data sources used to force the model, both configurations provide, in general, a similar pattern, although numerical results from Exp#2 tend to overestimate the results of Exp#1. The agreement between both setups shows that Delft3D-Flow forced with climatological data can be accurately used to simulate future temperature conditions in the Rías Baixas.

4.3.4 Model limitations

Delft3D-Flow is a numerical model that aims to reproduce natural phenomena. Numerical models are valuable and useful tools to investigate processes occurring in a particular area because they provide a wealth of information that is difficult or even impossible to obtain from other sources. The main limitation of these models is the quality/resolution of the inputs. Thereby, the main sources of error for the numerical simulations carried out during the development of this thesis are the bathymetry, the inputs and the heat flux model.

The study area is a dynamic system in which bathymetry may change over time as sediment is transported, these changes have not been considered and the same bathymetry has been used for all simulations. In addition, the bathymetry used is a composite created by the compilation of different bathymetries obtained at different times and affected by different measurement errors.

The most important source of error is the model inputs. It is important to keep in mind that input errors are propagated by the model, which in turn may influence the obtained results. Oceanic boundary conditions are imposed using data from Ibi reanalysis and the MOHC-HadGEM2-ES GCM, which have a coarse spatial and temporal resolution. Ibi reanalysis provides daily data with a horizontal resolution of 1/12º and a vertical resolution of 50 σ-layers and GCM MOHC-HadGEM2-ES provides monthly data with a horizontal resolution of 1º and a vertical resolution of 40 levels. Delft3D-Flow is used to perform a downscaling of these simulations obtaining a better spatial and temporal resolution and allowing analyzing how events such as river discharge affect the local dynamics. However, these simulations are always influenced by the errors introduced by the input data. River discharge data is also a limiting factor for simulations, and the absence of discharge data at the river mouth is particularly critical.

Regarding the heat model, "absolute flux, net solar radiation", the input of the relative humidity, air temperature and net radiation from a single point are imposed on the entire domain.

Despite the limitations above described, numerical models are, nowadays, the more useful tool to represent reality. In particular, Delft3D-Flow has shown very good results when it was used to simulate real ecosystems (Grunnet et al., 2004; Iglesias and Carballo, 2010, 2009; Sutherland et al., 2004). However, it must be taken into account that, due to natural processes are extraordinarily complex, numerical simulations are only the best approximation of a real system.

4.4. Summary and conclusions

Delft3D-Flow is a numerical model developed by WL|Delft Hydraulics in cooperation with Delft University of Technology. To carry on this thesis, the Delft3D-Flow research version 4.04.01 was used to analyze the hydrodynamics of the NW Iberian Peninsula, with particular interest in the Rías Baixas and the Minho estuary.

This numerical model was used to: i) simulates the hydrodynamics of the study area for historical period under realistic conditions, Exp#1; and ii) simulates the hydrodynamics of the study area for historical and future periods under climatological conditions, Exp#2. The main differences between the experiments are the databases used to force the boundaries.

Model accuracy in reproducing sea surface elevation (SSE) was evaluated by comparing predicted and observed SSE time series for Villagarcia, Marin and Vigo tidal gauge stations. The visual comparison shows that the model is able to properly reproduce the spring-neap tidal cycle. Model accuracy was quantified performing statistical analysis (RMSE, bias and Skill) which indicate excellent agreement between predicted and observed SSE.

The crosschecking of water temperature and salinity vertical profiles simulated by Exp#1 against *in situ* data from INTECMAR database shows that the model is able to reproduce general trends observed in the vertical profiles. The statistical analysis indicates a general overestimation of salinity values, both during winter and summer periods. Trends are not clear for water temperature, under winter conditions simulations

underestimate *in situ* water temperature, however, under summer conditions the bias is positive for the rias of Muros and Arousa and negative for the rias of Pontevedra and Vigo, although absolute values are close to zero. The skill of the numerical model to reproduce water temperature in shallow areas nearshore shows a higher bias and RMSE but the adjustment of the model in these points can be considered good considering the location of sampling points and the horizontal resolution of the mesh. Therefore, Exp#1 was considered to be able to reproduce the transport conditions inside the rias.

Exp#2 was validated under summer conditions. The comparison between surface water temperature outputs from Exp#1 and Exp#2 show a similar pattern. Exp#2 tends to overestimate the results of Exp#1 with an average bias of 0.40 ºC. Considering the different nature of data sources used to force the model the agreement between both setups is good and allows that the model can be used to simulate climatic conditions.

Chapter 5

Set of publications

The first article presented in this thesis is entitled: "*Hydrodynamics of river plume intrusion into an adjacent estuary: The Minho River and Ria de Vigo*" by **M. Des**, M. deCastro, M.C. Sousa, J.M. Dias, and M. Gómez-Gesteira. Published in 2019 in the journal "*Journal of Marine Systems*".

The second article presented in this thesis is entitled: "*NW Iberian Peninsula coastal upwelling future weakening: Competition between wind intensification and surface heating*" by M.C. Sousa, A. Ribeiro, **M. Des**, M. Gomez-Gesteira, M. deCastro, and J.M. Dias. Published in 2020 in the journal "*Science of the Total Environment*".

The third article presented in this thesis is entitled: "*How can ocean warming at the NW Iberian Peninsula affect mussel aquaculture?*" by **M. Des**, M. Gómez-Gesteira, M. deCastro, L. Gómez-Gesteira, and M.C. Sousa. Published in 2020 in the journal "*Science of the Total Environment*".

The fourth article presented in this thesis is entitled: "*The impact of climate change on the geographical distribution of habitat-forming macroalgae in the Rías Baixas*" by **M. Des**, B. Martínez, M. deCastro, R. M. Viejo, M.C. Sousa, and M. Gómez-Gesteira, *in publication process*.

A summary of the main characteristics of each journal is displayed in Table 5.1.

Journal	Category	Rank	Quartile	Impact Factor
Journal of Marine Systems	Marine & Freshwater biology	24/108	Q1	2.539
Science of The Total Environment	Environmental Sciences	27/251	Q1	5.589

Table 5.1. Main characteristics of the journals where the papers of this thesis were published.

Hydrodynamics of river plume intrusion into an adjacent estuary: The Minho River and Ria de Vigo

M. Des[a,*], M. deCastro[a], M.C. Sousa[b], J.M. Dias[b], M. Gómez-Gesteira[a]

[a] EPHYSLAB, Environmental PHYsics LABoratory, Facultad de Ciencias, Universidad de Vigo, 32004 Ourense, Spain
[b] CESAM, Physics Department, University of Aveiro, Aveiro 3810-193, Portugal

ARTICLE INFO

ABSTRACT

Minho River intrusion into the Rias Baixas has a twofold impact on estuaries. On the one hand, freshwater intrusion can modify the water exchange with the shelf affecting the residence time. On the other hand, it can fertilize the area and promote phytoplankton blooms and increase estuarine primary production. For these reasons, it is crucial to understand the frequency, duration, and relaxation of river freshwater intrusions. The frequency of intrusion events into the rias was calculated by means of *in situ* data from 2006 to 2016 using the difference in salinity between the inner part of the estuary and the southern mouth (ΔS) as a proxy. Minho River intrusions, which are characterized by $\Delta S > 0$, were detected in 8.9% of the available measurements in the Ria de Vigo, in 8.4% in the Ria de Pontevedra, and in only 4.5% in the Ria de Arousa. The FLOW module of the Delft3D model, which was previously calibrated and validated for the study area, was used to analyze the hydrodynamics of the intrusion events. The Ria de Vigo, which is the closest one to the Minho Estuary, was chosen to analyze the duration and intensity of the freshwater intrusions. Several consecutive events were detected in early 2010 (January 11th to February 8th) with ΔS values ranging from 0.7 to 2.0. Velocity and density profiles were analyzed in the middle part of the estuary, where seven freshwater intrusions matched the wind peaks favorable to intrusion events with an approximate delay of ~12 h. In general, the duration of the events was on the order of 1.5 days, although in one particular case the event lasted > 3 days. The dynamic behavior of the freshwater intrusions was represented using velocity and density profiles along the main axis of Ria de Vigo. Finally, the phases of an intrusion event were characterized: initial positive estuarine circulation pattern; development of the intrusion; well-developed negative estuarine circulation; relaxation of the intrusion and recovery of the initial positive circulation.

1. Introduction

The Rias Baixas are located on the northwest coast of the Iberian Peninsula at the northern limit of the Eastern North Atlantic Upwelling system. Due to their location, the rias are highly productive and are home to one of the most important marine aquaculture industries in Europe (FAO, 2016; Aguiar et al., 2017). The rias are flooded incised valleys (Evans and Prego, 2003) with a river discharging into their innermost part (Fig. 1). Hydrographically, the rias are partially mixed estuaries with a partially stratified estuarine circulation, and the lower layers are saltier than the upper ones (Taboada et al., 1998). The typical residual circulation corresponds to fresh water flowing out through surface layers and oceanic saline water entering through deeper layers (positive estuarine circulation). This pattern is enhanced by northerly winds that induce upwelling events (Alvarez-Salgado et al., 1993;

Alvarez et al., 2005, 2008a; Gomez-Gesteira et al., 2006; Barton et al., 2015). In contrast, southerly winds at the shelf favor downwelling events (Barton et al., 2015), which have the ability to reverse the usual circulation pattern, turning it into negative estuarine circulation (deCastro et al., 2000). These events are related to the increase of red tides, which negatively affect production and therefore the economy of the area (Tilstone et al., 1994; Blanco et al., 2017). Ria de Vigo (Fig. 1c) is located at the southernmost part of the Rias Baixas. Its entrance is characterized by two mouths separated by the Cies Islands, with cross-section length of ~8 km for the southern mouth and ~2 km for the northern one. The central axis of the estuary lies in the SW-NE direction, with a length of ~30 km from the Cies Islands to the Verdugo-Oitavén River mouth.

Minho River (Fig. 1b) is the main source of freshwater in the immediate vicinity of the Rias Baixas (~30 km south). Near its mouth,

* Corresponding author.
  E-mail address: mdes@uvigo.es (M. Des).
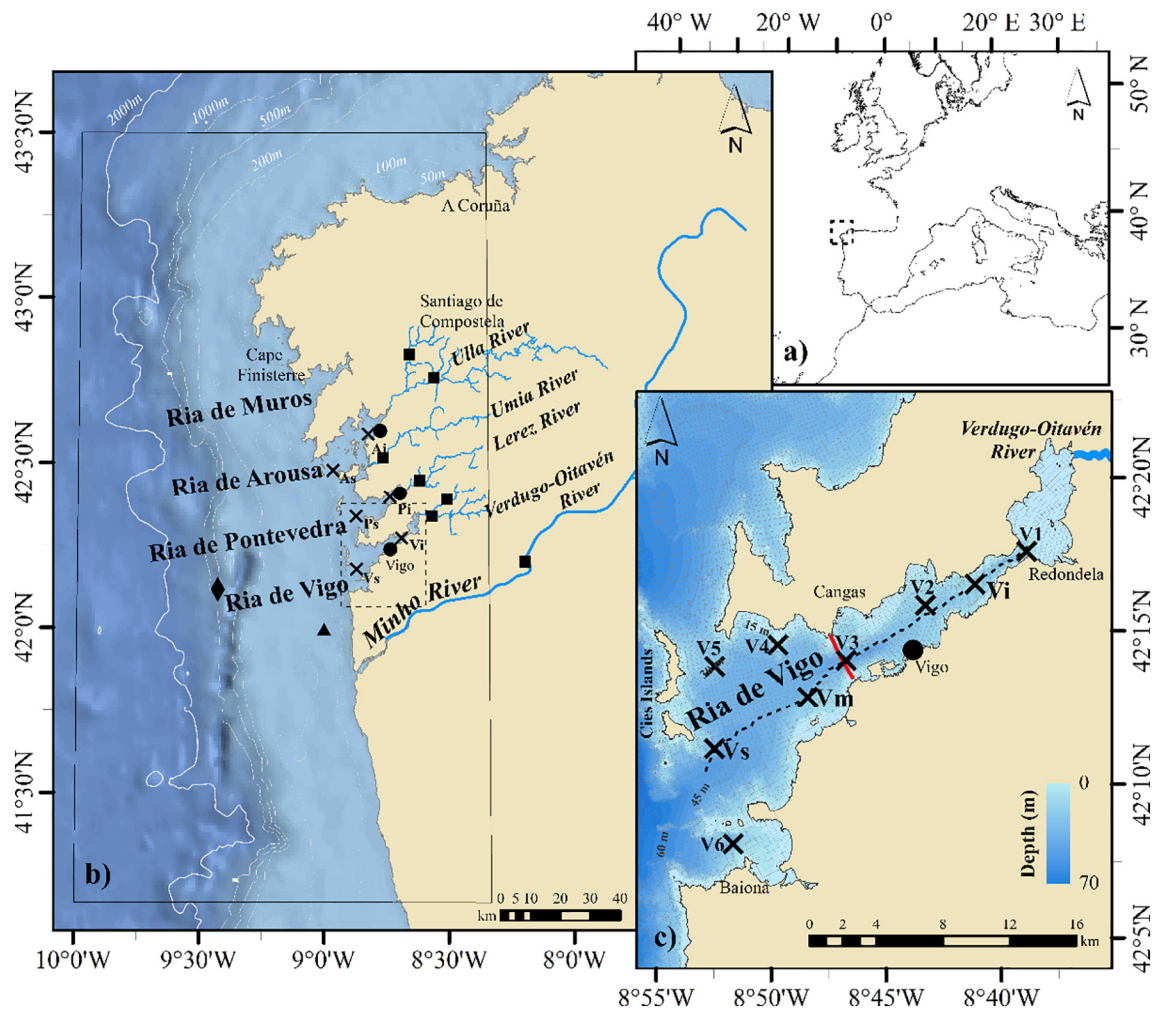
Fig. 1. (a) Location of the study area along the northwestern coast of the Iberian Peninsula. (b) The box indicates the modeled area. Black squares indicate the location of river discharge sampling stations. Black circles indicate the location of the tidal gauges used to calibrate the numerical model. The black triangle indicates the location of the wind data point. The black diamond indicates the location of Cabo Silleiro buoy. Contour bathymetry lines (shown in gray) were elaborated using the General Bathymetric Chart of the Oceans (GEBCO) from the British Oceanographic Data Centre (BODC). (c) A close-up view of the Ria de Vigo is shown with the numerical grid, the position of the salinity and water temperature sampling stations (crosses), the main axis of the estuary is marked with a dashed line and the location of an across-axis transect in the middle of the ria with a red line. (For interpretation of the references to colour in this figure legend, the reader is referred to the web version of this article.)

Minho Valley changes its direction from E-W to N−S and opens to the Atlantic Ocean to become a broad estuary about 40 km long and under tidal influence. Its discharge follows a marked seasonal pattern, with a maximum in winter (January and February) and a minimum in summer (August and September) (deCastro et al., 2006a; Gómez-Gesteira et al., 2011).

The Douro and Minho Rivers are the major contributors to the Western Iberian Buoyant Plume (WIBP) (Otero et al., 2008, 2009). The WIBP is a less dense water mass compared to the surrounding seawater, which is present along the western Iberian coast. It is formed by the combination of high river runoff and downwelling-favorable winds that accumulate water against the coast (Peliz et al., 2002). Recently, Mendes et al. (2016) analyzed the interaction between Douro and Minho plumes and concluded that the Minho River plume has a greater influence on the Rias Baixas. Previous research (deCastro et al., 2004; Alvarez et al., 2006) has shown that the Minho River plume can enter the Rias Baixas, especially Rias de Vigo and Ria de Pontevedra (Alvarez et al., 2006). deCastro et al. (2006b) analyzed the biological implications of these events and concluded that Minho River intrusion can result in two contrasting behaviors. On the one hand, the presence of Minho freshwater at the mouth of the rias can modify the water

exchange with the shelf and fertilize the area, promoting phytoplankton blooms and increasing the primary production (Ware and Thomson, 2005; Dai et al., 2008; Davis et al., 2014).

The intrusion of freshwater along adjacent bays has been previously analyzed from different points of view for several coastal systems located in different parts of the world. The dynamics, frequency and ecological implications of Rhone River plume intrusion into the Bay of Marseille (Mediterranean Sea) were analyzed by Fraysse et al. (2014). In upwelling systems, Shanks et al. (2002) investigated the distribution of larvae of benthic invertebrates off Duck (North Carolina, USA) under an intrusion event of the Chesapeake Bay estuarine plume. Curtis Roegner et al. (2002) described how the Columbia River plume drags a phytoplankton bloom, generated near shore, towards the Willapa Bay (Washington, USA). All these studies concluded that intrusions increase significantly the primary production of the affected area.

In the particular case of Rias Baixas, Sousa et al. (2013, 2014a) analyzed Minho River intrusions using numerical simulations. They showed that an unusually high amount of freshwater can be detected at the mouth of southern Rias Baixas when two conditions are fulfilled: (i) moderate to high Minho River discharge and (ii) the prevalence of northward winds at the shelf.

Despite these studies, the following questions remain unanswered: (i) How often do Minho intrusions occur?; (ii) What is the duration of these events?; (iii) How long is the relaxation period between consecutive events?; and (iv) What is the role of the freshwater input from the river discharging inside the ria (referred to as "inner river" hereafter)? The aim of this study was to answer these questions for the Ria de Vigo, which is the ria closest to the Minho River mouth. First, the frequency of Minho River intrusions into the ria was analyzed using *in situ* salinity data from 2006 to 2016. In addition, this approach was used to identify episodes during which successive events took place in order to analyze both their duration and relaxation. Finally, numerical simulations were performed using the FLOW module of the numerical model Delft3D that was previously calibrated and validated for the study area. These simulations are able to characterize the dynamic behavior of the freshwater intrusions by means of velocity and density profiles along the main axis of Ria de Vigo and to analyze the different phases of an intrusion event: initial positive estuarine circulation pattern; development of the intrusion; well-developed negative estuarine circulation; relaxation of the intrusion and recovery of the initial positive circulation.

2. Data and numerical model

2.1. Field data

Vertical profiles of salinity data measured along the Rias Baixas from late 2006 to the end of 2017 were downloaded from the Instituto Tecnolóxico para o Control do Medio Mariño de Galicia (INTECMAR) website (www.intecmar.gal). These data were collected weekly using a SBE25 CTD. Thirteen field stations were sampled: three were located at the southern mouth (V_s, P_s, A_s) of the rias of Vigo, Pontevedra, and Arousa; three were located in the inner part of those rias (V_i, P_i, A_i), one was located in the middle part of the Ria de Vigo (V_m) and the last six covered the Ria de Vigo (V_1-V_6, Fig. 1b–c, crosses). Statistical methods were used to detect and remove outliers in salinity values (Thompson Tau test, $\alpha = 0.1$). Finally, gaps in salinity data were filled using a cubic interpolation.

Days with near-surface salinity values higher at the inner part of the estuary than at the southern mouth were considered to be days of potential intrusion of the Minho River into the estuary. The salinity difference between outer and inner ria is a better intrusion indicator than salinity in the outer ria because in this outer area salinity values have been reported to be highly variable, also depending on inner river discharge (Alvarez et al., 2005). The weekly sampling and location of the CTD stations may well missed some events, which can last only a few days. Despite of this shortcoming we expect these data will still capture most events intense enough to significantly influence the Ria de Vigo hydrodynamics.

The parameter $\Delta S = S_i - S_s > 0$ was used as a salinity proxy to identify intrusion events. Near-surface values were obtained by averaging salinity data from 2 to 4 m deep. Salinity values in the first two meters were discarded since measurements have not been performed or present high noise in most of the samples. Averaging the near-surface layer from 2 to 4 m showed to be more robust than using only a particular depth.

Daily Minho River discharge data were provided by the Confederación Hidrográfica Miño-Sil (http://saih.chminosil.es). Verdugo-Oitavén River discharge data were downloaded from the website of the regional meteorological agency (MeteoGalicia; www.meteogalicia.gal). River stations are marked with black squares in Fig. 1b.

Harmonic constants from tidal gauges located in the harbors of Vigo, Marin, and Villagarcia (available from Puertos del Estado, (http://www.puertos.es) (Fig. 1b, black circles) and salinity and water temperature data from INTECMAR were used to validate the model for the Rias Baixas.

Hourly salinity, water temperature and horizontal velocity observations collected at 3 m depth from a buoy located at Cape Silleiro were provided by Puertos del Estado (Fig. 1b, diamond).

2.2. Numerical model

Delft3D-FLOW is an open source three-dimensional finite-difference hydrodynamic code developed by WL|Delft Hydraulic in cooperation with Delft University of Technology. The model solves the 3D baroclinic Navier-Stokes and transport equations under the Boussinesq assumption. The FLOW module performs the hydrodynamic computations and calculates heat and salinity transport. A detailed description of this model can be found in Lesser et al. (2004) and Grunnet et al. (2004). The Delft3D-FLOW module was previously used in the Ria de Muros, the northernmost ria of the Rias Baixas, by several authors (Iglesias et al., 2008; Carballo et al., 2009a, 2009b; Iglesias and Carballo, 2009, 2010). The area used for the hydrodynamic computations ranged from 10.00°W to 8.33°W and from 41.18°N to 43.50°N (Fig. 1b, rectangle). This wide domain was implemented because the Rias Baixas comprise several estuaries that cannot be considered to be completely independent (Sousa et al., 2014b).

The Delft3D-Flow platform was set up with a curvilinear irregular grid (452 × 446 cells) with a mean resolution of ~50 m in the Minho River Estuary, ~200 m in the Rias Baixas, and increasing gradually from 800 to 2200 m at the offshore open boundary (Fig. 1b). Sixteen vertical sigma layers with refined surface layers were used because most of the dynamics related to the plumes occur near the surface. The main features of the simulation, including resolution and parameterizations, are summarized in Table 1.

The bathymetry for model simulations was elaborated from different sources. The Minho River bathymetry was obtained from the Portuguese Navy Hydrographic Institute with a spatial resolution of 100 m. The bathymetries of the rias of Vigo and Pontevedra were provided by the General Fishing Secretary with a resolution of 5 m. For rias of Arousa and Muros and the adjacent shelf area, bathymetry data were obtained from nautical charts of the Spanish Navy Hydrographical Institute and from the General Bathymetry Chart of the Oceans (https://www.gebco.net).

Thirteen main tidal harmonic constants (M_2, S_2, N_2, K_2, K_1, O_1, P_1, Q_1, MF, MM, M_4, MS_4, MN_4) obtained from the model TPXO 7.2 TOPEX/Poseidon Altimetry (http://volkov.oce.orst.edu/tides/global.

Table 1
Parameters of the Delft3D numerical simulations.

Parameter	Specification
Domain	10.00°W to 8.33°W
	41.18°N to 43.50°N
Horizontal resolution	Increasing gradually from 2200 m × 800 m on the West boundary to 220 m × 140 m in the Rias and 50 m × 77 m in the Minho River estuary
Vertical resolution	16 sigma layers, top layers refined
Oceanic boundary forcing	Water level with harmonic constituents
Transport conditions	Salinity and water temperature specified per layer
Bottom roughness	Manning's formula.
	Constant Manning's roughness coefficient of 0.024
Horizontal eddy viscosity	500–5 m^2 s^{-1}
Horizontal eddy diffusivity	5 m^2 s^{-1}
Vertical eddy viscosity	0 m^2 s^{-1}
Vertical eddy diffusivity	0 m^2 s^{-1}
Heat flux model	Absolute flux, net solar radiation
Wind	Space varying wind and pressure
Turbulence closure	k-ε
Time step	0.5 min

html) were used as the astronomical forcing at the oceanic open boundary of the model.

Minho, Verdugo-Oitavén, Lérez, Ulla, and Umia river discharge data were retrieved from the MeteoGalicia database (Fig. 1b, black squares). River discharges were entered into the model as fluvial open boundary conditions at the grid cells corresponding to the head of the estuary. The temperature and salinity of river water were considered to be fixed, with typical values for the season for temperature and a fixed value of 0 for the salinity.

Daily thermohaline properties (salinity and water temperature) from the operational Atlantic-Iberian Biscay Irish-Ocean Physics Reanalysis, with a horizontal resolution of $1/12^o$ and a vertical resolution of 50 sigma coordinates levels, were used as boundary conditions. Salinity and water temperature were generated through a re-analysis called IBIRYS that is based on NEMO model application results and was developed by Mercator Ocean in collaboration with Puertos del Estado. Data are available through the Copernicus Marine Service website (http://marine.copernicus.eu).

The surface boundary condition was imposed using hourly meteorological data from MeteoGalicia obtained as means from the Weather Research and Forecasting Model with a resolution of 4 km. A heat model was applied that takes into account air temperature, relative humidity, and net solar radiation to calculate heat losses from convection, evaporation, and black radiation.

2.3. Model calibration

The model calibration was evaluated through a qualitative and quantitative comparison of the temporal evolution of predicted sea surface elevation (SSE), salinity, and water temperature data and concurrent *in situ* data. The calibration was performed by adjusting the bottom friction coefficient, viscosity, and diffusivity for the entire domain. In this study, the best overall adjustment between model results and *in situ* data was achieved with the parametrizations shown in Table 1.

A similar procedure to that proposed by Dias et al. (2009) was used to quantify the model accuracy for the Rias Baixas. First, the harmonic constituents computed from the model predictions were compared with those available from SSE field observations (Fig. 1b, black circles). The harmonic analysis was performed using the T_TIDE analysis package (Pawlowicz et al., 2002) for the period January 17th to February 15th, 2010. The fit degree was assessed using the metrics described below:

The root mean square error (RMSE) was calculated as

$$RMSE = \left\{ \frac{1}{N} \sum_{i=1}^{N} |X_{obs}(t_i) - X_{mod}(t_i)|^2 \right\}^{1/2} \tag{1}$$

where $X_{obs}(t_i)$ and $X_{mod}(t_i)$ are the SSE values computed by harmonic synthesis of the data and predicted by the model, respectively, and N is the number of samples.

The relative error, ΔE, was calculated to compare the RMSE with the local tidal amplitude as follows:

$$\Delta E = \frac{RMSE}{\frac{1}{n} \sum_{i=1}^{n} (A_{max_{obs}}(c_i) - A_{min_{obs}}(c_i))} x\ 100 \tag{2}$$

where $A_{max_{obs}}(c_i)$ and $A_{min_{obs}}(c_i)$ are the maximum and minimum elevations for each tidal cycle, respectively, and n is the number of tidal cycles.

The predictive skill also quantifies the agreement between model predictions and observations and was calculated following Warner et al. (2005):

$$Skill = 1 - \frac{\sum_{i=1}^{N} |X_{mod}(t_i) - X_{obs}(t_i)|^2}{\sum_{i=1}^{N} (|X_{mod}(t_i) - \overline{X_{obs}}(t_i)| + |X_{obs}(t_i) - \overline{X_{obs}}(t_i)|)^2} \tag{3}$$

where the horizontal bars represent a temporal mean.

As described by Dias et al. (2009), a skill value of one means perfect agreement between model predictions and observations, whereas a value of zero means complete disagreement. Skill values > 0.95 represent excellent agreement between predicted and sampled data. In a similar way, an absolute value of ΔE that is < 5% indicates excellent agreement between model predictions and observations, and when it ranges from 5% to 10%, the agreement should be considered to be very good.

Computed and observed near-surface (3 m deep) horizontal velocity, salinity and water temperature were compared at Cape Silleiro buoy (Fig. 1b). Additionally, salinity and water temperature were also compared at nine stations in the Ria de Vigo (V_1 to V_6, V_s, V_m, and V_i, Fig. 1c). RMSE and bias were also used to measure the model accuracy in reproducing transport properties.

$$Bias = \frac{1}{N} \sum_{i=1}^{N} (X_{mod}(t_i) - X_{obs}(t_i)) \tag{4}$$

where $X_{obs}(t_i)$ and $X_{mod}(t_i)$ are the observed and predicted salinity, water temperature or velocity, respectively, and N is the number of samples (time steps).

2.4. Processing of numerical data

The calibrated model was used to assess the frequency, duration, and relaxation of Minho River intrusions into the Ria de Vigo. The simulated period was from December 2009 to February 2010, and the first month was used as the spin-up period. This period was chosen based on the intrusion days detected from salinity *in situ* data.

The procedure previously applied to detect Minho River intrusion into the Ria de Vigo from *in situ* data was replicated with numerical predictions. In this sense, surface salinity data were obtained by averaging salinity predictions between 2 and 4 m deep. Surface salinity values at V_s and V_i (Fig. 1c) stations then were compared, with $\Delta S = S_i - S_s > 0$ indicating a possible Minho River intrusion. Additionally, estuarine along-axis currents were analyzed. Velocities were projected in the direction of the main axis of the estuary following a procedure similar to that described by Míguez et al. (2001). Filtered currents were obtained by removing the tidal component from predicted current velocities by means of a low-pass filter with a cutoff frequency of 34 h (Xie et al., 2017). Numerical density profiles and surface density along the main axis were also used to analyze the thermohaline properties of the estuary.

3. Results and discussion

3.1. Model calibration

The model accuracy in reproducing the main tidal constituents (M_2, S_2, O_1, and K_1) was analyzed from differences between amplitude and phase of these constituents determined from predictions and observations (Table 2). Accuracy in this study was similar to values obtained by Dias et al. (2009) and Sousa et al. (2018) when simulating Ria Formosa (Portugal) and the main estuaries of the NW Iberian Peninsula coast, with good agreement for all constituents, both in amplitude and phase at all harbors. The average difference between observed and predicted semidiurnal tidal constituents (which are the most energetic in the region) was about 2 cm in amplitude and 2° in the phase, which means an average delay of 4 min.

Table 3 summarizes the model accuracy in reproducing observed SSE. The statistical analysis shows a RMSE of 0.05 m or smaller for all harbors, ΔE of around 2%, and a predictive skill > 0.99. These statistical results indicate excellent agreement between predicted and observed SSE, following the criteria proposed by Dias et al. (2009).

The subtidal frequency predictions were also evaluated comparing the residual sea level at Vigo, Marin and Villagarcia harbors, respectively. The statistical analysis shows a RMSE of 0.006 m and an ΔE of

Table 2
Model accuracy in reproducing the main tidal constituents measured at Vigo, Marin, and Villagarcia tidal gauge stations.

	Tide gauge	Amplitude (m)			Phase (°)		
		Data	Model	Difference	Data	Model	Difference
M_2	Vigo	1.11	1.13	0.01	75.94	78.63	2.69
	Marin	1.10	1.13	0.03	77.15	79.16	2.01
	Villagarcia	1.14	1.16	0.02	78.73	80.02	1.29
S_2	Vigo	0.46	0.44	−0.02	120.00	122.14	2.13
	Marin	0.46	0.44	−0.02	121.09	122.76	1.67
	Villagarcia	0.47	0.45	−0.02	123.15	123.85	0.70
O_1	Vigo	0.07	0.06	−0.01	323.90	320.45	−3.45
	Marin	0.07	0.06	−0.01	325.8	320.69	−5.11
	Villagarcia	0.07	0.06	−0.01	325.47	321.12	−4.36
K_1	Vigo	0.08	0.08	0.00	85.68	78.96	−6.72
	Marin	0.07	0.08	0.01	79.28	79.27	−0.01
	Villagarcia	0.08	0.08	0.00	81.58	79.75	−1.84

Table 3
Model accuracy in reproducing observed SSE as characterized by means of the RMSE (m), Relative Error, ΔE (%), and Skill values at Vigo, Marin, and Villagarcia tidal gauge stations.

Tide gauge	RMSE (m)	ΔE (%)	Skill
Vigo	0.05	2.34	0.99
Marin	0.05	2.12	0.99
Villagarcia	0.04	1.74	0.99

11.5% for Vigo, 0.0046 m and 10.3% for Marin and 0.005 m and 10% for Villagarcia harbors.

The model accuracy in reproducing transport conditions near the open boundary was evaluated by comparing near-surface horizontal velocity, salinity and water temperature measured at the Cape Silleiro buoy for the period under study and the corresponding predicted values. The statistical analysis shows a bias and a RMSE of 0.17 and 0.44 for salinity, $-0.51\,°C$ and $0.64\,°C$ for water temperature and $-0.07\,ms^{-1}$ and $0.12\,ms^{-1}$ for horizontal velocity, respectively.

The water temperature and salinity predictions accuracy in reproducing thermohaline data inside the Ria de Vigo was investigated by comparing *in situ* vertical salinity and water temperature profiles collected at nine stations for the period under study (five weekly samples) with their corresponding predicted vertical profiles. The five bias and RMSE values calculated for each station were averaged, obtaining a mean value for each station (Table 4). In general, the model tends to underestimate *in situ* water temperature (negative bias values), with a nearly zero bias for salinity. Both RMSE and bias values were similar to those obtained by Sousa et al. (2014a) and Cerralbo et al. (2013) for the same area using MOHID and ROMS models, respectively.

Table 4
Model accuracy in reproducing measured salinity and water temperature as characterized by the bias and the RMSE calculated at nine sampling stations for the Ria de Vigo.

Sampling station	Salinity		Temperature (°C)	
	Bias	RMSE	Bias	RMSE
V1	0.32	0.88	−0.89	0.89
V2	0.17	0.56	−0.75	0.76
V3	−0.18	0.47	−0.78	0.80
V4	0.15	0.73	−0.60	0.64
V5	−0.05	0.68	−0.63	0.65
V6	−0.07	0.84	−0.57	0.60
Vi	0.07	0.58	−0.89	0.89
Vs	0.02	0.82	−0.67	0.70
Vm	0.00	0.54	−0.66	0.69
Mean	0.05	0.68	−0.71	0.74

Fig. 2 shows the salinity (upper row) and water temperature (lower row) vertical profiles, both predicted (black line) and measured (gray line) for a particular date (February 8th). Predicted and *in situ* profiles follow a similar pattern.

3.2. Frequency of Minho River intrusions into the Rias Baixas

Intrusion of the Minho River plume into the Rias Baixas is characterized by higher surface salinity values inside the ria than at the mouth. According to experimental data, this type of pattern was detected in 8.9% of the available measurements from the Ria de Vigo (48 out of 542 vertical profiles), in 8.4% of the Ria de Pontevedra measurements (46 out of 549), and in only 4.5% of the Ria de Arousa measurements (23 out of 507) over the period 2006–2007. These results complement and quantify the results of previous research in the area. Alvarez et al. (2006) used *in situ* data to analyze an event that took place in the spring of 1998. They observed how the Minho River plume entered the rias of Vigo and Pontevedra without reaching the Ria de Arousa. Sousa et al. (2014b) used a numerical model to perform several experiments regarding Minho River discharge and wind intensity and reported that the Minho River plume reached the Ria de Arousa only under strong winds and high Minho River discharge.

It was commonly accepted that intrusions were isolated in time, however several consecutive intrusions were identified in early 2010 (January 11th and 18th, and February 8th), which constitutes an interesting case to analyze the duration and relaxation of these events. Note that the sampling was carried out weekly, so the presence of this unusual pattern in consecutive samplings does not necessarily assure that the pattern lasted for weeks. Alternatively, it could have been due to short and consecutive pulses.

3.3. Characterization of Minho River intrusions into the Ria de Vigo

The Delft3D model was used to elucidate the duration and intensity of the intrusions covering the period from January 1st, 2009 to February 15th, 2010. Model simulations from January 7th to February 11th show several intrusion events (ΔS > 0 in Fig. 3a). In addition, winds at the shelf that were favorable for Minho River intrusions show seven well-developed peaks (labelled with P in Fig. 3b). According to previous research, southerly winds of at least $3\,ms^{-1}$ are necessary to reverse the normal estuarine circulation of the rias of Vigo and Pontevedra (Sousa et al., 2014b), although the plume of Minho River can reach the ria mouth even without wind forcing (Sousa et al., 2014a). Note that not all of the wind peaks were associated with positive ΔS. Only six salinity difference peaks were found, and they ranged from 0.7 to 2.0. On January 12th and 13th, ΔS was negative and no intrusion was detected under favorable wind conditions (P_2) and with high Minho River discharge. This scenario occurred because the discharge of the inner river (Verdugo-Oitavén) that increased to around 500% during those days (Fig. 3c, gray line) caused a rapid decrease in surface salinity at V_i. Similarly, the peak observed on January 16th and 17th (Fig. 3a) was much lower than the others, even when the wind conditions were very similar. This scenario was also due to the high discharge of the inner river ($\sim90\,m^3\,s^{-1}$ in Fig. 3c, gray line). The positive ΔS peak ultimately was observed due to the previous accumulation of freshwater at the shelf under northeasterly winds (Fernández-Nóvoa et al., 2017). When the wind changed from northerly to southerly, the accumulated freshwater was dragged northward, reaching the external part of the ria and generating salinity values lower than those observed inside the ria, even when the inner river was at its maximum discharge.

The previous analysis showed that even under moderate Minho River discharge and moderate southerly winds at the shelf, a positive ΔS value may not be observed. However, this does not necessarily mean that there was no intrusion. The question that immediately arises is whether high discharges from the inner river can balance the effect of wind and accumulated freshwater at the mouth of the rias and prevent
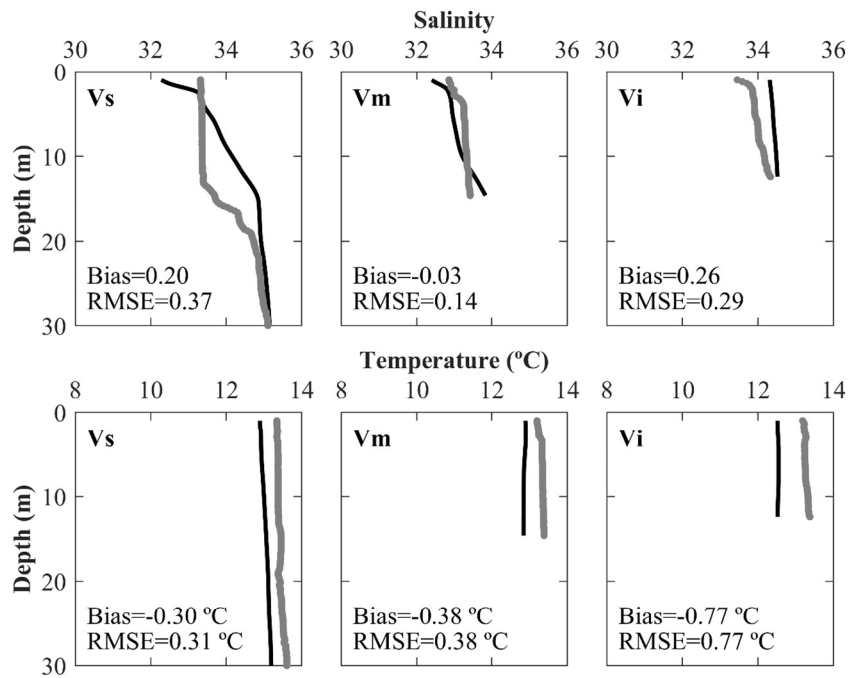
Fig. 2. Vertical profiles of salinity (upper row) and water temperature (lower row) obtained using the Delft3D- FLOW model (black line) and measured on February 8th (gray line) at sampling stations V_s, V_m, and V_i.
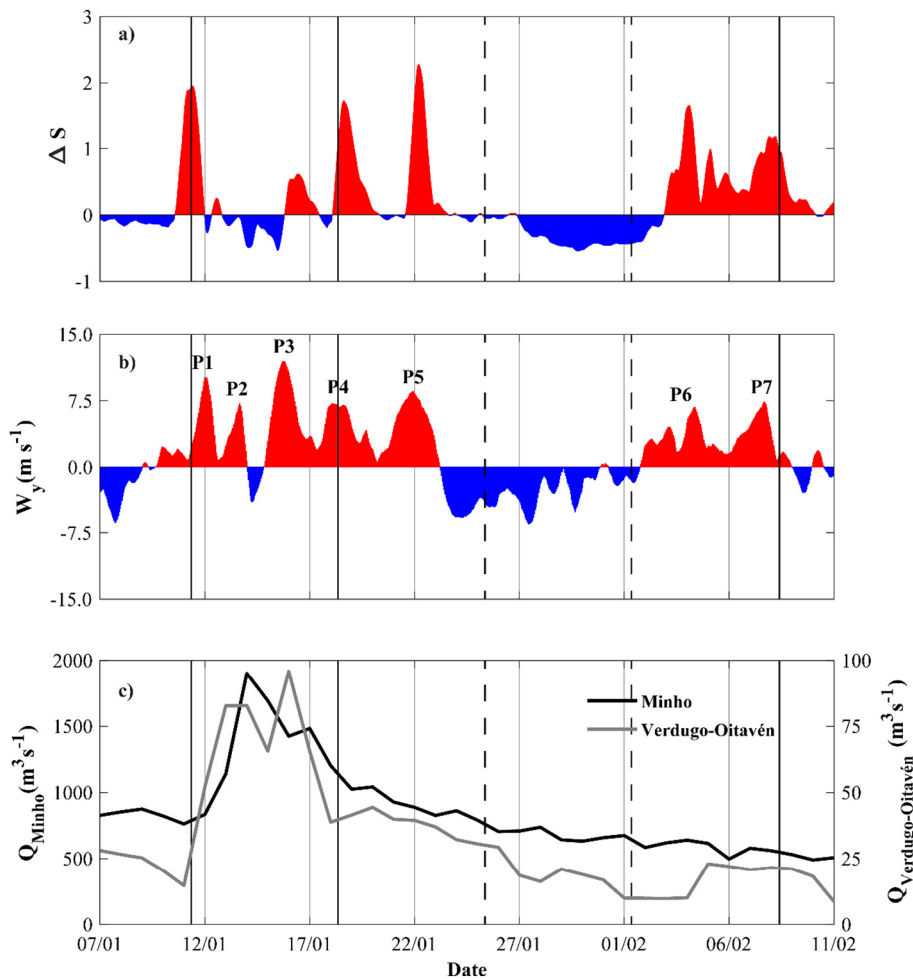

Fig. 3. (a) Simulated surface salinity difference (ΔS) between stations at the inner part and the southern mouth of the Ria de Vigo (V_i and V_s, respectively in Fig. 1c) from January 7th to February 11th, 2010. (b) The meridional wind component (ms^{-1}) at the shelf (black triangle in Fig. 1b). Meridional wind peaks labelled with P represent those winds with a direction and intensity favorable to Minho River intrusion. (c) Discharges of Minho (black line) and Verdugo-Oitavén (gray line) rivers ($m^3 s^{-1}$). Vertical black lines mark the dates of sampling. Solid lines correspond to the dates when intrusion events were detected and dashed lines to the dates when no intrusion was detected.

Fig. 4. (a) Time evolution of the predicted filtered velocity at the middle station of the Ria de Vigo (V_m in Fig. 1c) from January 7th to February 11th, 2010. Red colors indicate water flowing into the ria and blue colors represent water flowing out. The dashed contour line corresponds to $0\,ms^{-1}$. Vertical lines indicate the days when Minho intrusion was detected using *in situ* data. (b) As (a) but only for surface layer (0 m). Velocity peaks labelled with P represent events with positive surface velocity. (For interpretation of the references to colour in this figure legend, the reader is referred to the web version of this article.)

intrusion or is ΔS only a proxy that can be masked under high discharges from the inner river. Thus, a deeper analysis that included water velocity and density was conducted to better identify intrusion events.

3.3.1. Hydrodynamics of Minho River intrusions

Fig. 4a shows vertical profiles of along-axis filtered currents calculated at station V_m from January 7th to February 11th. Horizontal velocities were projected in the direction of the main axis of the estuary following the procedure described in the previous section. Positive values indicate landward currents and negative values indicate seaward currents. Seven positive peaks (red colour) were found to match the wind peaks described in Fig. 3b, with an approximate delay of ~12 h. This time delay coincides with the time that the Minho river plume takes to propagate to the mouth of the Ria de Vigo (Sousa et al., 2014b). This effect was observed from the surface to an approximate depth of 10–15 m depending on the peak. Inflow depths were similar to those reported by Barton et al. (2015) under a comparable wind regime. They observed incoming water flowing at 15 m depth in the middle part of the ria. The analysis of surface velocities (0 m) shows that pulses were relatively short, lasting on the order of 1.5 days (Fig. 4b). However, some peaks lasted longer, such as peak P_1 that lasted > 2 days and peak P_6 that lasted about 3.5 days. On the other hand, peak P_2 was abnormally shorter, lasting ~1 day. In all cases, the duration of the peaks agreed well with the duration of the wind pulses (Fig. 3b). The characteristic circulation of the rias (Taboada et al., 1998), with water entering through bottom layers and leaving through surface layers, was clearly observed when wind conditions were favorable to cessation of intrusion.

The same seven peaks associated with water entering the ria were bserved in the vertical density profile at the middle station (Fig. 5a). During these events, the density decrease affected the entire water column, with values < 1025 kg m^{-3}. The density decrease occurred with a delay relative to wind, as observed for current. All positive surface velocity events (Fig. 4b) were related to an abrupt decrease in
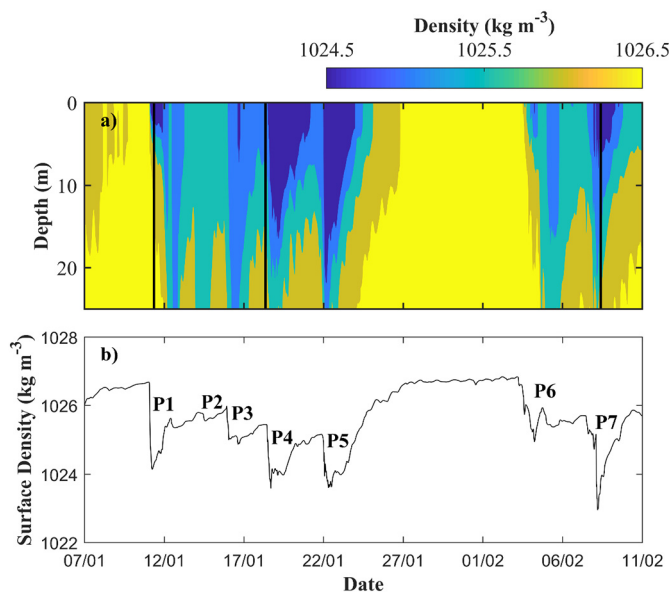
Fig. 5. (a) Time evolution of the predicted density at the middle station of the Ria de Vigo (V_m in Fig. 1c) from January 7th to February 11th, 2010. Vertical lines indicate the days when intrusion was detected using *in situ* data. (b) As (a) but only for surface layer (0 m). Density peaks labelled with P represent those events with an abrupt density decrease in the water column, indicating freshwater input into the estuary.

the surface density, with the exception of P_2 (Fig. 5b). In this case, the outflow previously accumulated in front of the Minho River mouth was partially diluted in the ocean water, thereby increasing its density (Fernández-Nóvoa et al., 2017). Additionally, P_1 and P_2 occurred very close in time, and the density inside the ria had not yet recovered from the P_1 pulse when P_2 entered the area. Density values on the order of 1026 kg m^{-3} were observed throughout the entire water column at the beginning of the study period and between P_5 and P_6 peaks, corresponding to relaxation periods in the estuary.

3.3.2. Development and relaxation of an intrusion event

Vertical profiles of velocity and density along the main axis of the ria and surface density plots of the estuary were used to analyze the dynamics of Minho River intrusion into the Ria de Vigo. In particular, the P_5 intrusion event observed on January 20th–23th was selected and five stages were captured (Fig. 6, rows). Before freshwater intrusion (Fig. 6a–c), the characteristic positive estuarine circulation of the rias (Taboada et al., 1998) was present, with negative velocities near the surface and positive velocities in the bottom layers (Fig. 6a). Additionally, the water column was stratified with low-density layers associated with negative velocities (Fig. 6b). Surface densities ranged from 1024 to 1025.5 and increased from south to north due to the tendency of water to leave the ria through the northern mouth (Taboada et al., 1998; Alvarez et al., 2005).

The beginning of the intrusion event is shown in Fig. 6d–f. The inner and middle part of the ria were dominated by the typical estuarine circulation, and the beginning of the intrusion occurred at the southern mouth, with positive velocities near the surface and negative velocities in deeper layers (Fig. 6d). The density profile (Fig. 6e) was similar to that of the previous stage. The arrival of the Minho River buoyant plume to the Ria de Vigo was marked by the presence of a spot of lighter water near the southern mouth (Fig. 6f).

Fig. 6g–i shows the maximum development of the intrusion event. At this stage, reverse estuarine circulation was present in the ria, with positive velocities at the surface and negative velocities in the bottom layers (Fig. 6g). A similar reverse estuarine circulation was described by deCastro et al. (2004) for the adjacent Ria de Pontevedra. The density
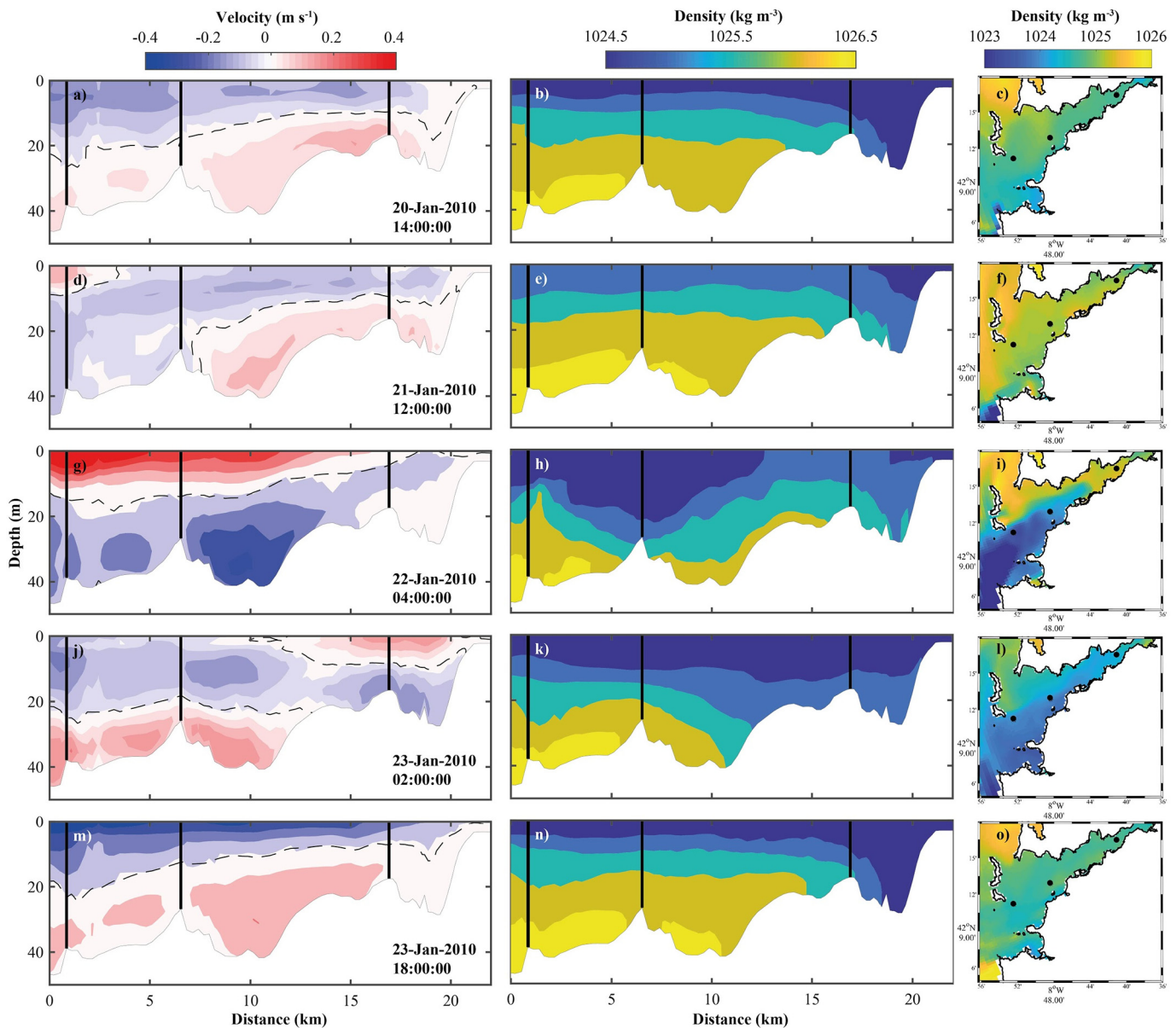
Fig. 6. Hydrodynamic behavior of the Ria de Vigo under a freshwater intrusion simulated using Delft3D. Five stages of the intrusion event corresponding to the P5 wind peak (January 20–23, 2010) are shown (rows). Vertical profiles of velocity (left column) and density (middle column) along the main axis of the ria and surface density plots of the estuary (right column) are plotted. The black dashed line represents null horizontal velocities along the main axis of the estuary. The distance is measured in km from the southern mouth of the estuary.

profile shows that a tongue of light water (density < 1025 kgm^{-3}) entered the ria through surface waters (~20 m) until approximately 12 km from the mouth, where the depth decreases favors vertical mixing (Fig. 6h). As in the previous stage, the influence of the Verdugo-Oitavén River was confined to the inner part of the ria. The surface density plot shows that a freshwater tongue entered the estuary through the southern mouth and flowed along the main axis of the ria, thus density increased gradually from the mouth to the inner part (Fig. 6i). The inflow along the southern shore caused a marked density gradient between the north and south shores. This gradient was previously observed by Barton et al. (2015), who described the exchange of water between the ria and the shelf during a downwelling event. These authors concluded that inflow takes place along the southern shore and outflow occurs at depth along the northern shore, thereby maintaining the north-south density contrast.

Fig. 6j–l illustrates relaxation of the intrusion event. The outer and middle part of the ria recovered the typical estuarine circulation,

whereas the inner part remained under the influence of the freshwater intrusion (Fig. 6j). The incoming oceanic water, which was denser than the ria water, favored estuarine stratification (Fig. 6k). Compared with the maximum development of the intrusion event (previous row), the surface density plot shows increased density in the southern half of the estuary and decreased density in the northern half, thereby reducing the lateral density gradient (Fig. 6l).

Once the intrusion event had finished (Fig. 6m–o), the ria recovered the pattern that was present prior to the intrusion (Fig. 6a–c). The estuary recovered the typical positive estuarine circulation (Fig. 6m), with a stratification pattern characterized by lower density values near the inner river mouth (Fig. 6n). With respect to the previous stage, density increased inside the ria due to the inflow of oceanic water (Fig. 6o). Surface density values were similar to those obtained before the freshwater intrusion (Fig. 6c).
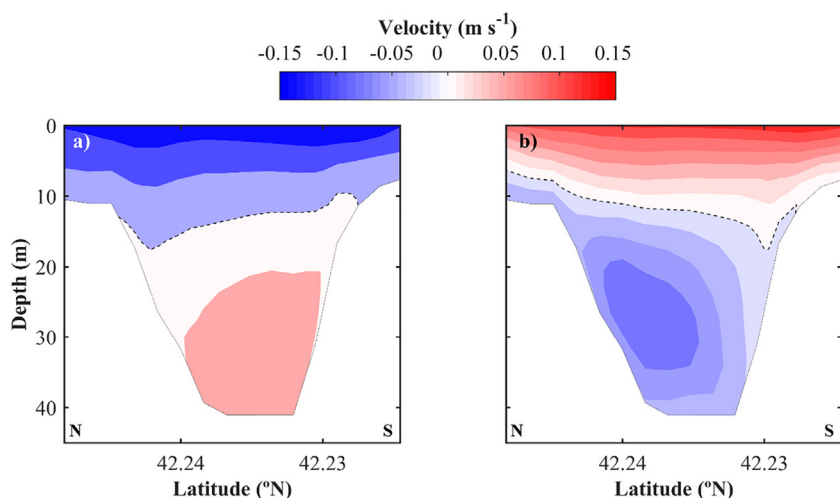
68

Fig. 7. Predicted along axis velocities for the cross-section shown in Fig. 1c (red segment) under (a) upwelling favorable conditions, January 23th to February 1st, 2010 and (b) downwelling favorable conditions with Minho river intrusion, February 2nd to 8th, 2010. Red colors indicate inflowing water and blue colors represent outflowing water. The dashed contour line corresponds to $0\,\mathrm{ms}^{-1}$. (For interpretation of the references to colour in this figure legend, the reader is referred to the web version of this article.)

3.3.3. Impact of intrusions on water exchange

Horizontal velocities along the main axis of the estuary play a key role in the estuarine water exchange. These velocities predicted by the numerical model were analyzed at the cross-section represented in Fig. 1c (red line) under upwelling and downwelling favorable conditions, in order to evaluate the role of Minho intrusion events on estuarine water exchange. Fig. 7(a) represents along axis horizontal velocities during an upwelling event (from the January 23th to February 1st) and Fig. 7(b) during a downwelling event concurrent with Minho River intrusion (from February 2nd to 8th). Positive values indicate landward currents while negative values indicate seaward currents. Under upwelling favorable winds (Fig. 7a) an enhanced double-layer estuarine circulation is observed, with fresher water leaving the estuary through surface layers and saltier water propagating into the estuary through the bottom layers. The water outflow takes place in the first 10 m of the water column, with this layer deepening up to 17 m towards the north shore. The same pattern is observed without wind forcing and considering only the discharge of the inner river, although less intensified. When prevailing winds are favorable to downwelling (Fig. 7b), the inverse situation is observed, with saltier oceanic water propagating into the estuary on the surface layer. Under this wind condition, the offshore oceanic water inflow takes place in the first 7 m, deepening to the south shore up to 18 m. This lateral inhomogeneity was previously observed in the density distribution patterns (Fig. 6).

Predicted density profiles at the cross-section were also obtained under upwelling (Fig. 8a) and downwelling (Fig. 8b) conditions described above. Water is considerably denser during the upwelling

period (Fig. 8a). In addition, isopycnals are tilted in different directions in both cases. Under upwelling wind conditions (Fig. 8a) water is denser at the southern coast for any depth, while under downwelling conditions (Fig. 8b) an inverse pattern is observed.

Although upwelling is markedly seasonal (from April to October) at the NW Iberian Peninsula (Alvarez et al., 2008b), less intense upwelling events may also occur during winter (Ribeiro et al., 2005; deCastro et al., 2006c, 2008). Both along axis horizontal velocities (Fig. 7) and density profiles (Fig. 8) at the cross-section for winter upwelling event show that oceanic water, which is denser and richer in nutrients (Ryther, 1969; Calvert and Price, 1971), enters the estuary through the bottom layers. When oceanic water upwells inside estuaries reaching the photic layers, the primary production increases (Prego et al., 1999; Radi et al., 2007). Additionally, estuarine surface water, which is less dense, leaves the estuary through the surface layers. Prego et al. (2007) did not observe biological implications during a mid-winter upwelling event (January 13 and 27, 1998) in the Ria de Pontevedra, located north of the Ria de Vigo. However, Varela et al. (2008) analyzing a longer period (October 1997 to October 1998) found that winter upwelling events are able to generate phytoplankton blooms, although less intense than those derived from summer upwelling, which can change the spatial distribution of the primary production.

On the other hand, during a downwelling event under Minho River intrusion, less dense oceanic water from the Minho River plume is advected into the ria through the surface layers. The river plume transports land-derived nutrients, enhancing the primary production of the ria, although with a lesser impact than upwelling. Ware and Thomson
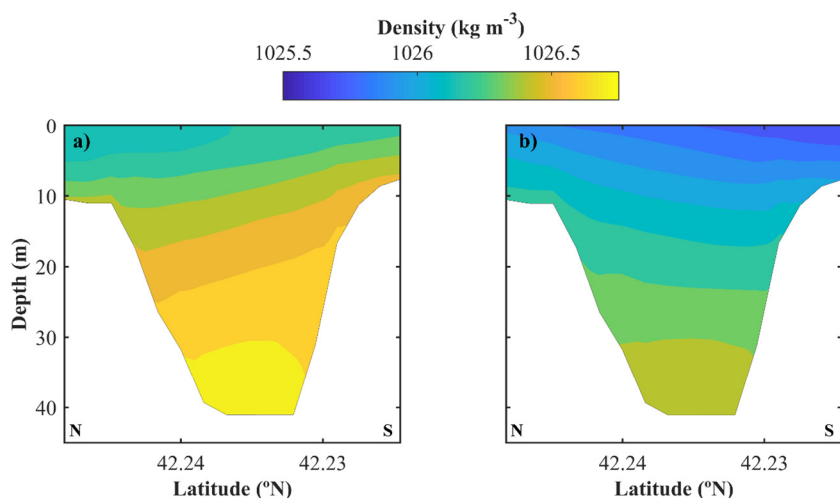
Fig. 8. Predicted density at the cross-section (red segment in Fig. 1c) (a) under upwelling favorable conditions, January 23th to February 1st, 2010 and (b) under downwelling favorable conditions and Minho river intrusion, February 2nd to 8th, 2010. (For interpretation of the references to colour in this figure legend, the reader is referred to the web version of this article.)

69

(2005) studied the bottom-up *versus* top-down ecosystem trophic dynamic in the Northeast Pacific, concluding that coastal upwelling domains are the most productive followed by those downwelling domains where major rivers discharge a large volume of freshwater into coastal areas.

The Minho River intrusion may even favor phytoplankton bloom events, following the case observed by Dai et al. (2008) in the Pearl River estuary and the adjacent coastal region (northern South China Sea) associated with high river discharges. The Minho River plume may modify the spatial distribution of the primary production of the ria and also induce phytoplankton blooms generation on the adjacent shelf into the estuary. This phenomenon was previously observed in the Ria de Pontevedra (deCastro et al., 2006b), as well as in other coastal systems, as for example in the Willapa Bay, which dynamics is driven by the Columbia River (Curtis Roegner et al., 2002).

Finally, the residence time was calculated under both conditions, being approximately 3 days under downwelling conditions and only 18 h under upwelling conditions.

4. Summary

The Delft3D-FLOW model was used to analyze the hydrodynamics of Minho River intrusions into the Ria de Vigo.

Based on *in situ* measurements, freshwater from the Minho River was detected entering the Ria de Vigo in 8.9% of the cases, the Ria de Pontevedra in 8.4% of the cases, and the Ria de Arousa in only 4.5% of the cases. Additionally, several consecutive intrusions were sampled in the Ria de Vigo in early 2010.

Using numerical simulations, seven intrusion events were described in the middle part of the estuary from January 11th to February 8th, 2010. The typical duration of these events was approximately 1.5 days, although one particular case lasted > 3 days. In all cases, each freshwater intrusion matched the peak of wind favorable to intrusion with a delay of ~12 h.

Finally, the dynamic behavior of a freshwater intrusion into the estuary was simulated from January 20th to 23th, 2010, and analyzed in terms of vertical velocity and density profiles along the main axis of the estuary. The simulation allowed analysis of the different phases of intrusion. Starting from a pattern of positive estuarine circulation, the sequence clearly shows three intermediate stages (development, negative circulation, and relaxation) and a final stage with characteristics similar to those of the first one.

In general, the influence of the inner river discharge on the circulation and stratification of the estuary during intrusion events is negligible. Only the external river and the wind field drive the local dynamics.

Acknowledgments

References

Aguiar, E., Piedracoba, S., Alvarez-Salgado, X.A., Labarta, U., 2017. Circulation of water through a mussel raft: clearance area vs. idealized linear flows. Rev. Aquac. 9, 3–22. https://doi.org/10.1111/raq.12099.

Alvarez, I., deCastro, M., Gomez-Gesteira, M., 2005. Inter- and intra-annual analysis of the salinity and temperature evolution in the Galician Rías Baixas–ocean boundary (northwest Spain). J. Geophys. Res. 110. https://doi.org/10.1029/2004JC002504.

Alvarez, I., deCastro, M., Gomez-Gesteira, M., Prego, R., 2006. Hydrographic behavior of the Galician Rias Baixas (NW Spain) under the spring intrusion of the Miño River. J. Mar. Syst. 60, 144–152. https://doi.org/10.1016/j.jmarsys.2005.12.005.

Alvarez, I., Gomez-Gesteira, M., deCastro, M., Novoa, E.M., 2008a. Ekman transport along the Galician Coast (NW, Spain) calculated from QuikSCAT winds. J. Mar. Syst. 72, 101–115. https://doi.org/10.1016/j.jmarsys.2007.01.013.

Alvarez, I., Gomez-Gesteira, M., deCastro, M., Dias, J.M., 2008b. Spatiotemporal evolution of upwelling regime along the western coast of the Iberian Peninsula. J. Geophys. Res. 113. https://doi.org/10.1029/2008JC004744.

Alvarez-Salgado, X.A., Rosón, G., Pérez, F.F., Pazos, Y., 1993. Hydrographic variability off the Rías Baixas (NW Spain) during the upwelling season. J. Geophys. Res. 98, 14447. https://doi.org/10.1029/93JC00458.

Barton, E.D., Largier, J.L., Torres, R., Sheridan, M., Trasviña, A., Souza, A., Pazos, Y., Valle-Levinson, A., 2015. Coastal upwelling and downwelling forcing of circulation in a semi-enclosed bay: Ria de Vigo. Prog. Oceanogr. 134, 173–189. https://doi.org/10.1016/j.pocean.2015.01.014.

Blanco, J., Arévalo, F., Moroño, Á., Correa, J., Muñíz, S., Mariño, C., Martín, H., 2017. Presence of azaspiracids in bivalve molluscs from northern Spain. Toxicon 137, 135–143. https://doi.org/10.1016/j.toxicon.2017.07.025.

Calvert, S.E., Price, N.B., 1971. Upwelling and nutrient regeneration in the Benguela Current, October, 1968. Deep-Sea Res. Oceanogr. Abstr. 18, 505–523. https://doi.org/10.1016/0011-7471(71)90074-X.

Carballo, R., Iglesias, G., Castro, A., 2009a. Numerical model evaluation of tidal stream energy resources in the Ría de Muros (NW Spain). Renew. Energy 34, 1517–1524. https://doi.org/10.1016/j.renene.2008.10.028.

Carballo, R., Iglesias, G., Castro, A., 2009b. Residual circulation in the Ría de Muros (NW Spain): a 3D numerical model study. J. Mar. Syst. 75, 116–130. https://doi.org/10.1016/j.jmarsys.2008.08.004.

Cerralbo, P., Grifoll, M., Espino, M., López, J., 2013. Predictability of currents on a mesotidal estuary (Ria de Vigo, NW Iberia). Ocean Dyn. 63, 131–141. https://doi.org/10.1007/s10236-012-0586-9.

Curtis Roegner, G., Hickey, B.M., Newton, J.A., Shanks, A.L., Armstrong, D.A., 2002. Wind-induced plume and bloom intrusions into Willapa Bay, Washington. Limnol. Oceanogr. 47, 1033–1042.

Dai, M., Zhai, W., Cai, W.-J., Callahan, J., Huang, B., Shang, S., Huang, T., Li, X., Lu, Z., Chen, W., Chen, Z., 2008. Effects of an estuarine plume-associated bloom on the carbonate system in the lower reaches of the Pearl River estuary and the coastal zone of the northern South China Sea. Cont. Shelf Res. 28, 1416–1423. https://doi.org/10.1016/j.csr.2007.04.018.

Davis, K.A., Banas, N.S., Giddings, S.N., Siedlecki, S.A., MacCready, P., Lessard, E.J., Kudela, R.M., Hickey, B.M., 2014. Estuary-enhanced upwelling of marine nutrients fuels coastal productivity in the U.S. Pacific Northwest. J. Geophys. Res. Oceans 119, 8778–8799. https://doi.org/10.1002/2014JC010248.

deCastro, M., Gómez-Gesteira, M., Prego, R., Taboada, J.J., Montero, P., Herbello, P., Pérez-Villar, V., 2000. Wind and tidal influence on water circulation in a Galician Ria (NW Spain). Estuar. Coast. Shelf Sci. 51, 161–176. https://doi.org/10.1006/ecss.2000.0619.

deCastro, M., Gómez-Gesteira, M., Alvarez, I., Prego, R., 2004. Negative estuarine circulation in the Ria of Pontevedra (NW Spain). Estuar. Coast. Shelf Sci. 60, 301–312. https://doi.org/10.1016/j.ecss.2004.01.006.

deCastro, M., Lorenzo, N., Taboada, J.J., Sarmiento, M., Alvarez, I., Gomez-Gesteira, M., 2006a. Influence of teleconnection patterns on precipitation variability and on river flow regimes in the Miño River basin (NW Iberian Peninsula). Clim. Res. 32, 63–73.

deCastro, M., Alvarez, I., Varela, M., Prego, R., Gómez-Gesteira, M., 2006b. Miño River dams discharge on neighbor Galician Rias Baixas (NW Iberian Peninsula): hydrological, chemical and biological changes in water column. Estuar. Coast. Shelf Sci. 70, 52–62. https://doi.org/10.1016/j.ecss.2006.05.035.

deCastro, M., Dale, A.W., Gómez-Gesteira, M., Prego, R., Alvarez, I., 2006c. Hydrographic and atmospheric analysis of an autumnal upwelling event in the Ria of Vigo (NW Iberian Peninsula). Estuar. Coast. Shelf Sci. 68, 529–537. https://doi.org/10.1016/j.ecss.2006.03.004.

deCastro, M., Gómez-Gesteira, M., Alvarez, I., Lorenzo, M., Cabanas, J.M., Prego, R., Crespo, A.J.C., 2008. Characterization of fall–winter upwelling recurrence along the Galician western coast (NW Spain) from 2000 to 2005: dependence on atmospheric forcing. J. Mar. Syst. 72, 145–158. https://doi.org/10.1016/j.jmarsys.2007.04.005.

Dias, J.M., Sousa, M.C., Bertin, X., Fortunato, A.B., Oliveira, A., 2009. Numerical modeling of the impact of the Ancão Inlet relocation (Ria Formosa, Portugal). Environ. Model Softw. 24, 711–725. https://doi.org/10.1016/j.envsoft.2008.10.017.

Evans, G., Prego, R., 2003. Rias, estuaries and incised valleys: is a ria an estuary? Mar. Geol. 196, 171–175. https://doi.org/10.1016/S0025-3227(03)00048-3.

Contributing to food security and nutrition for all. In: FAO (Ed.), The State of World Fisheries and Aquaculture. Rome.

Fernández-Nóvoa, D., deCastro, M., Des, M., Costoya, X., Mendes, R., Gómez-Gesteira, M., 2017. Characterization of Iberian turbid plumes by means of synoptic patterns obtained through MODIS imagery. J. Sea Res. 126, 12–25. https://doi.org/10.1016/j.seares.2017.06.013.

Fraysse, M., Pairaud, I., Ross, O.N., Faure, V.M., Pinazo, C., 2014. Intrusion of Rhone River diluted water into the Bay of Marseille: generation processes and impacts on ecosystem functioning. J. Geophys. Res. Oceans 119, 6535–6556. https://doi.org/10.1002/2014JC010022.

Gomez-Gesteira, M., Moreira, C., Alvarez, I., deCastro, M., 2006. Ekman transport along the Galician coast (northwest Spain) calculated from forecasted winds. J. Geophys. Res. 111. https://doi.org/10.1029/2005JC003331.

Gómez-Gesteira, M., Gimeno, L., deCastro, M., Lorenzo, M., Alvarez, I., Nieto, R., Taboada, J., Crespo, A., Ramos, A., Iglesias, I., Gómez-Gesteira, J., Santo, F.E., Barriopedro, D., Trigo, I.F., 2011. The state of climate in NW Iberia. Clim. Res. 48, 109–144. https://doi.org/10.3354/cr00967.

Grunnet, N.M., Walstra, D.-J.R., Ruessink, B.G., 2004. Process-based modelling of a shoreface nourishment. Coast. Eng. 51, 581–607. https://doi.org/10.1016/j.coastaleng.2004.07.016.

Iglesias, G., Carballo, R., 2009. Seasonality of the circulation in the Ría de Muros (NW Spain). J. Mar. Syst. 78, 94–108. https://doi.org/10.1016/j.jmarsys.2009.04.002.

Iglesias, G., Carballo, R., 2010. Effects of high winds on the circulation of the using a mixed open boundary condition: the Ría de Muros, Spain. Environ. Model Softw. 25, 455–466. https://doi.org/10.1016/j.envsoft.2009.10.013.

Iglesias, G., Carballo, R., Castro, A., 2008. Baroclinic modelling and analysis of tide- and wind-induced circulation in the Ría de Muros (NW Spain). J. Mar. Syst. 74, 475–484. https://doi.org/10.1016/j.jmarsys.2008.03.009.

Lesser, G.R., Roelvink, J.A., van Kester, J.A.T.M., Stelling, G.S., 2004. Development and validation of a three-dimensional morphological model. Coast. Eng. 51, 883–915. https://doi.org/10.1016/j.coastaleng.2004.07.014.

Mendes, R., Sousa, M.C., Decastro, M., Gómez-Gesteira, M., Dias, J.M., 2016. New insights into the Western Iberian Buoyant Plume: interaction between the Douro and Minho River plumes under winter conditions. Prog. Oceanogr. 141, 30–43. https://doi.org/10.1016/j.pocean.2015.11.006.

Míguez, B.M., Pérez, F.F., Souto, C., Fariña-Busto, L., 2001. Flujos residuales de intercambio entre la Ría de Vigo y la plataforma continental. Física de la Tierra 13. pp. 119–137.

Otero, P., Ruiz-Villarreal, M., Peliz, A., 2008. Variability of river plumes off Northwest Iberia in response to wind events. J. Mar. Syst. 72, 238–255. https://doi.org/10.1016/j.jmarsys.2007.05.016.

Otero, P., Ruiz-Villarreal, M., Peliz, A., 2009. River plume fronts off NW Iberia from satellite observations and model data. ICES J. Mar. Sci. 66, 1853–186412. https://doi.org/10.1093/icesjms/fsp156.

Pawlowicz, R., Beardsley, B., Lentz, S., 2002. Classical tidal harmonic analysis including error estimates in MATLAB using T_TIDE. Comput. Geosci. 28, 929–937.

Peliz, Á., Rosa, T.L., Santos, A.M.P., Pissarra, J.L., 2002. Fronts, jets, and counter-flows in the Western Iberian upwelling system. J. Mar. Syst. 35, 61–77. https://doi.org/10.1016/S0924-7963(02)00076-3.

Prego, R., Barciela, M. del C., Varela, M., 1999. Nutrient dynamics in the Galician coastal area (Northwestern Iberian Peninsula): do the Rias Bajas receive more nutrient salts than the Rias Altas? Cont. Shelf Res. 19, 317–334. https://doi.org/10.1016/S0278-4343(98)00099-5.

Prego, R., Guzmán-Zuñiga, D., Varela, M., deCastro, M., Gómez-Gesteira, M., 2007. Consequences of winter upwelling events on biogeochemical and phytoplankton patterns in a western Galician ria (NW Iberian peninsula). Estuar. Coast. Shelf Sci. 73, 409–422. https://doi.org/10.1016/j.ecss.2007.02.004.

Radi, T., Pospelova, V., de Vernal, A., Vaughn Barrie, J., 2007. Dinoflagellate cysts as indicators of water quality and productivity in British Columbia estuarine environments. Mar. Micropaleontol. 62, 269–297. https://doi.org/10.1016/j.marmicro.2006.09.002.

Ribeiro, A.C., Peliz, Á., Santos, A.M.P., 2005. A study of the response of chlorophyll-a biomass to a winter upwelling event off Western Iberia using SeaWiFS and in situ data. J. Mar. Syst. 53, 87–107. https://doi.org/10.1016/j.jmarsys.2004.05.031.

Ryther, J.H., 1969. Photosynthesis and fish production in the sea. Science 166, 72–76.

Shanks, A.L., Largier, J., Brink, L., Brubaker, J., Hooff, R., 2002. Observations on the distribution of meroplankton during a downwelling event and associated intrusion of the Chesapeake Bay estuarine plume. J. Plankton Res. 24, 391–416. https://doi.org/10.4319/lo.2002.47.4.1033.

Sousa, M.C., Vaz, N., Alvarez, I., Dias, J.M., 2013. Effect of Minho estuarine plume on Rias Baixas: numerical modeling approach. J. Coast. Res. 165, 2059–2064. https://doi.org/10.2112/SI65-348.1.

Sousa, M.C., Vaz, N., Alvarez, I., Gomez-Gesteira, M., Dias, J.M., 2014a. Modeling the Minho River plume intrusion into the rias baixas (NW Iberian Peninsula). Cont. Shelf Res. 85, 30–41. https://doi.org/10.1016/j.csr.2014.06.004.

Sousa, M.C., Vaz, N., Alvarez, I., Gomez-Gesteira, M., Dias, J.M., 2014b. Influence of the Minho River plume on the Rias Baixas (NW of the Iberian Peninsula). J. Mar. Syst. 139, 248–260. https://doi.org/10.1016/j.jmarsys.2014.06.012.

Sousa, M.C., Ribeiro, A.S., Des, M., Mendes, R., Alvarez, I., Gomez-Gesteira, M., Dias, J.M., 2018. Integrated high-resolution numerical model for the NW Iberian Peninsula coast and Main estuarine systems. J. Coast. Res. 85, 66–70. https://doi.org/10.2112/SI85-014.1.

Taboada, J.J., Prego, R., Ruiz-Villarreal, M., Gómez-Gesteira, M., Montero, P., Santos, A.P., Pérez-Villar, V., 1998. Evaluation of the seasonal variations in the residual circulation in the Ría of Vigo (NW Spain) by means of a 3D Baroclinic Model taboada et al 1998.pdf. Estuar. Coast. Shelf Sci. 47, 661–670. https://doi.org/10.1006/ecss.1998.0385.

Tilstone, G.H., Figueiras, F.G., Fraga, F., 1994. Upwelling-downwelling sequences in the generation of red tides in a coastal upwelling system. Mar. Ecol. Prog. Ser. 241–253.

Varela, M., Prego, R., Pazos, Y., 2008. Spatial and temporal variability of phytoplankton biomass, primary production and community structure in the Pontevedra Ria (NW Iberian Peninsula): oceanographic periods and possible response to environmental changes. Mar. Biol. 154, 483–499. https://doi.org/10.1007/s00227-008-0943-x.

Ware, D.M., Thomson, R.E., 2005. Bottom-up ecosystem trophic dynamics determine fish production in the Northeast Pacific. Science 308, 1280–1284. https://doi.org/10.1126/science.1109049.

Warner, J.C., Geyer, W.R., Lerczak, J.A., 2005. Numerical modeling of an estuary: a comprehensive skill assessment. J. Geophys. Res. 110. https://doi.org/10.1029/2004JC002691.

Xie, X., Li, M., Boicourt, W.C., 2017. Baroclinic effects on wind-driven lateral circulation in Chesapeake Bay. J. Phys. Oceanogr. 47, 433–445. https://doi.org/10.1175/JPO-D-15-0233.1.

71

NW Iberian Peninsula coastal upwelling future weakening: Competition between wind intensification and surface heating

Magda Catarina Sousa [a,*], Américo Ribeiro [a], Marisela Des [b], Moncho Gomez-Gesteira [b], Maite deCastro [b], João Miguel Dias [a]

[a] CESAM, Departamento de Física, Universidade de Aveiro, 3810-193 Aveiro, Portugal
[b] Environmental Physics Laboratory (EphysLab), CIM-UVIGO, Universidade de Vigo, Edificio Campus da Auga, 32004 Ourense, Spain

HIGHLIGHTS

- Most accurate climate model selection to reproduce past climatic conditions.
- Realistic configuration including interaction between shelf and estuarine processes.
- Coastal upwelling less effective in the future.
- Upwelling weakening due to the future sea surface warming.

GRAPHICAL ABSTRACT
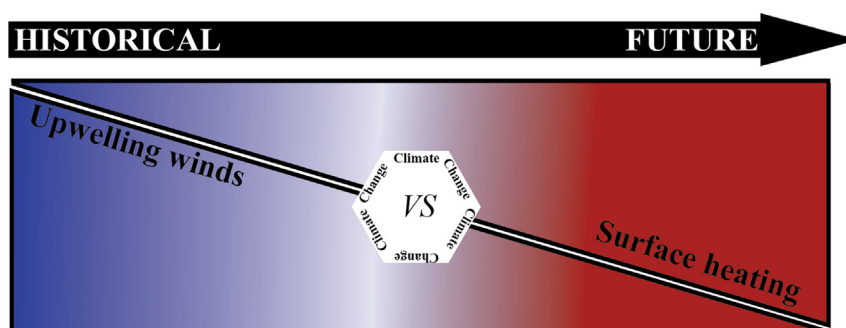
ARTICLE INFO

ABSTRACT

Climate change will modify the oceanographic future properties of the NW Iberian Peninsula due to the projected variations in the meteorological forcing, that will intensify local winds and promote surface heating. The Delft3D-Flow model forced with atmospheric conditions provided within the framework of the CORDEX project under the RCP 8.5 greenhouse emission scenario was used to analyse changes in upwelling. Numerical experiments were conducted under high-extreme upwelling conditions for the historical (1976–2005) and future (2070–2099) period. This study also innovates through the exploitation of a numerical modelling approach that includes both shelf and estuarine processes along the coastal zone. Coastal upwelling will be less effective in the future despite the enhancement of upwelling favorable wind patterns previously predicted for this region. Upwelling weakening is due to the future sea surface warming that will increase the stratification of the upper layers hindering the upward displacement of the underlying water, reducing the surface input of nutrients.

© 2019 Elsevier B.V. All rights reserved.

1. Introduction

There is a worldwide concern about the possible impact of climate change on the circulation and hydrographic patterns of estuarine systems and their adjacent shelf. These changes can affect ecosystems in coastal upwelling areas whose response to surface warming is especially complex. Based on observational wind data, Bakun (1990) hypothesized that global warming could enhance land-sea temperature gradients that would consequently increase upwelling favorable winds. According to recent research, upwelling has increased over the last decades in most of the

* Corresponding author.
  E-mail address: mcsousa@ua.pt (M.C. Sousa).

locations worldwide (Varela et al., 2015) and future projections indicate that upwelling will increase in intensity and duration at high latitudes over the next century (Wang et al., 2015), revealing more noticeable changes in the NW Iberian Peninsula (NWIP) (Sousa et al., 2017). Rykaczewski et al. (2015) and Sousa et al. (2017) showed that this upwelling strengthening is induced by the migration and intensification of the Azores High. On the other hand, the importance of coastal upwelling is twofold since apart from pumping nutrients to the surface, upwelling can also buffer global warming in coastal areas (Santos et al., 2012, 2011; Seabra et al., 2019; Varela et al., 2018). Stratification is also a key process to understand the link between climate change and biology since intensified stratification is negatively correlated with net primary production (Behrenfeld et al., 2006). As a consequence of global warming, the upper ocean has warmed considerably over the last century and projections show that it will keep warming over this one (IPCC, 2013; Levitus et al., 2000). This fact will most likely increase ocean stratification, which can modify the behavior of the upper ocean in different ways. First, temperature anomalies in the upper ocean will penetrate to depth, but at slow rates and remaining confined near surface. Second, enhanced stratification will probably decrease, nutrient exchange through vertical mixing. Thus, increased thermal stratification can render less effective upwelling (García-Reyes et al., 2015; Gruber, 2011).

The NWIP coast is located in the northernmost limit of the Eastern North Atlantic Upwelling System, being characterized by a high primary production (Wooster et al., 1976). Changes in local primary production follow from changes in seawater temperature and salinity that depend on upwelling and freshwater discharge regimes resulting from estuary-near-shelf systems interaction. These drivers are likely to be modified in the future due to climate change. The NWIP coast includes three estuarine systems with different morphologies: high-relief estuaries or drowned river valleys (*Rias Baixas*: Rias de Vigo, Pontevedra, Arousa and Muros); estuaries connected to the major rivers (Minho, Lima and Douro) and a lagoon-estuarine system (*Ria de* Aveiro) (Fig. 1). These estuarine systems are located in the northernmost part of one of the major coastal upwelling systems, being this process the main responsible of the steep-temperature gradient observed between coastal and ocean locations (Santos et al., 2011). On the other hand, the propagation of buoyant plumes, mostly from Douro and Minho rivers, dominates surface layers (Mendes et al., 2016). In summary, both river discharges and winds affect strongly the dynamics of these coupled estuary-near-shelf systems. This fact is especially patent for the *Rias Baixas* (Alvarez et al., 2006; deCastro et al., 2006; Des et al., 2019; Otero et al., 2013; Sousa et al., 2014a, 2014b), where the upwelled water promotes the intense aquaculture (Blanton et al., 1987; Figueiras et al., 2002; Prego et al., 2001). Estuarine circulation and productivity have also been studied for the Minho, Lima, Douro and Ria de Aveiro estuaries (Alvarez et al., 2013; Costa-Dias et al., 2010; Dias and Picado, 2011; Mendes et al., 2013; Queiroga, 2003; Sousa et al., 2011; Vale and Dias, 2011; Vieira and Bordalo, 2000).

As far as we know, there is limited research on future changes in coastal upwelling systems, which can only be identified through the exploitation of fine horizontal and vertical resolution nearshore data. However, that resolution is far from the one provided by the ocean models used in IPCC (2013), which have typical horizontal and vertical resolutions around 1° and on the order of tens of meters, respectively, which are too coarse to reproduce coastal processes. Previous studies based on basin-scale or global circulation models have analyzed the impact of climate change along the coast of Iberian Peninsula (Miranda et al., 2013; Pires et al., 2013, 2015), but were only focused on the shelf. These studies analyzed upwelling changes based on IPCC A2 emission scenario and indicated an increase in coastal upwelling, supporting the idea initially proposed
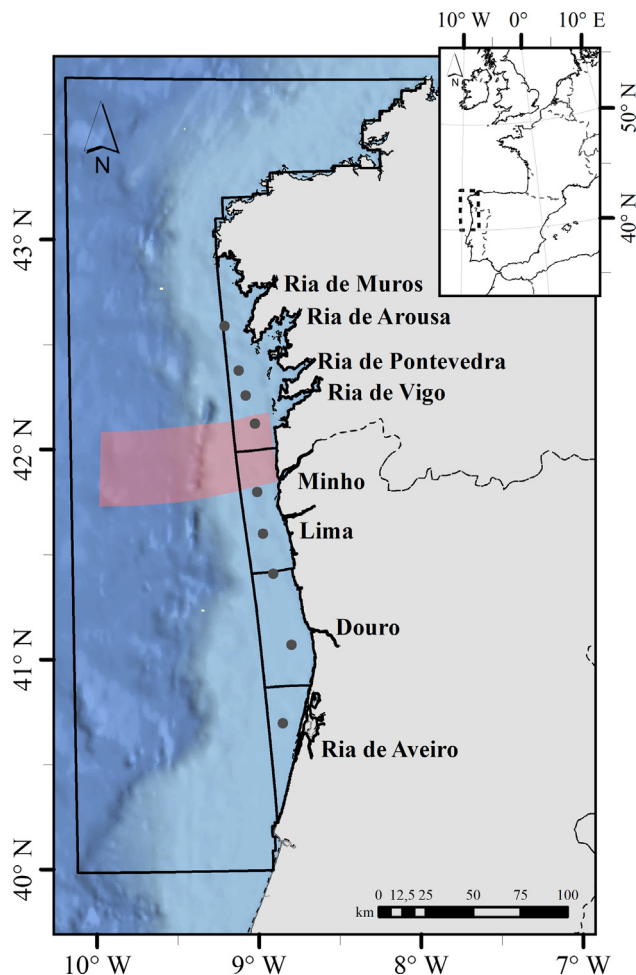
Fig. 1. Location and bathymetry of the study area. Black boxes correspond to the domain decomposition design. Grey dots correspond to the location of control points. The shaded pink area indicates the location of the cross sections used to compute the upwelling index and the Brunt-Väisälä frequency. (For interpretation of the references to colour in this figure legend, the reader is referred to the web version of this article.)

by Bakun (1990). However, a number of limitations contribute to keep the problem of future upwelling changes largely open. As example, most of previous studies based on model applications for NWIP present severe restrictions if used to evaluate climate change impacts, since they were typically implemented under unrealistic conditions neglecting the estuary-near-shelf systems interaction (Pires et al., 2013, 2015) or in the best considering the interaction with a single estuary (Lopes et al., 2017; Mendes et al., 2013). Moreover, simulations were performed using only a single ocean model, and some of the control results were found to be unsatisfactory, with an overestimation of the present climate upwelling mainly attributable to inaccuracies in the wind data associated to the control simulation. In fact, Soares et al. (2012) highlighted the need to use higher resolution atmospheric simulations to represent topographic and coastal processes accurately. Thus, adopting the regional climate models projections from the 5th Assessment Report (AR5) of the IPCC scenarios (IPCC, 2013) to force the oceanographic models seems to be a valuable alternative to achieve the required level of accuracy to describe near-shore processes.

The present work aims at analysing the response of the NWIP coastal waters to future changes projected under the RCP 8.5 greenhouse gas emission scenario. These changes, which are characterized by air and water warming and the increase in upwelling favourable winds will be used to force the Delft3D-Flow model covering both the shelf and the estuaries in order to assess whether

or not future wind and stratification patterns will modify the impact of upwelling in the area.

2. Methodology

2.1. Numerical model

Delft3D-Flow modeling system was used to evaluate the impact of climate change on coastal upwelling along the NWIP coast. Delft3D-Flow is a three-dimensional, finite differences hydrodynamic and transport model. The Navier Stokes shallow water equations are solved with hydrostatic, Boussinesq and f-plane approximations (Deltares, 2014). The model was previously implemented and validated for the area under study by Sousa et al. (2018), which demonstrated its skill and high accuracy in reproducing the local coastal dynamics.

The configuration developed consists in a set of five domains connected by internal domain decomposition boundaries with the capability of two-way communication of water level, currents and hydrographic properties (Fig. 1). These different types of domain discretization recognize the importance of using adaptive resolution meshes. The horizontal resolution of each domain allows reproducing the hydrodynamic of the areas covered, which in many cases have a complex geometry, without a high computational cost. The outer grid includes the continental shelf with a resolution of about ~1500 m. Douro and Ria de Aveiro were covered by two separated domains with a grid resolution varying from 45 to 80 m. Minho and Lima estuaries are combined into a single domain with a ~60 m grid resolution. The Rias Baixas are represented by a single domain with a horizontal resolution of ~250 m and thirteen vertical sigma layers with refined surface layers were used for all domains. The numerical bathymetry of each estuary was obtained from the interpolation of topohydrographic data from several different sources. The bathymetry of ocean, adjacent shelf and the Rias Baixas was generated from data from the General Bathymetry Chart of the Oceans. Minho, Lima and Douro bathymetries were generated from data available at the Portuguese Navy Hydrographic Institute, and the Ria de Aveiro bathymetry was generated from data provided by the Aveiro Harbor Administration and Polis Litoral Ria de Aveiro.

Thirteen main tidal harmonic constants (M_2, S_2, N_2, K_2, K_1, O_1, P_1, Q_1, M_sF, MM, M_4, MS_4 and MN_4) obtained from the model TPXO 7.2 TOPEX/Poseidon Altimetry with a spatial resolution of ~25 km (MacMillan et al., 2004) were prescribed as astronomical forcing at the oceanic open boundary. Transport conditions (salinity and water temperature) were also imposed at this boundary based on monthly global climate models (GCM) from Coupled Model Intercomparison Project Phase 5 (CMIP5). The surface boundary condition was modelled considering daily wind, air temperature, relative humidity and cloudiness provided by CMIP5 atmospheric models. Freshwater discharge for the major tributaries in the Rias Baixas and the Ria de Aveiro and for Minho, Lima and Douro rivers were imposed as fluvial open boundary conditions in each estuary, and were retrieved from the Hype Web portal (http://hypeweb. smhi.se/). A detailed description of the data used as boundary conditions will be described in the next section.

A k-ε model was used for 3D turbulence. A constant manning value of 0.024 was assumed for bottom roughness, except for Ria de Aveiro domain where a spatial variable friction coefficient (Lopes and Dias, 2015) was used due to the shallowness of the lagoon. The vertical eddy viscosity and diffusivity applied was 0.0001 $m^2\,s^{-1}$, whereas a spatially variable horizontal viscosity and diffusivity proportional to the depth was applied, with a value of 5 $m^2\,s^{-1}$ in the inner domains (lowest depth) increasing linearly to 15 $m^2\,s^{-1}$ in the deepest ocean.

Table 1
EURO Cordex simulations. Numbers in brackets correspond to model number shown in Fig. 2.

GCM	RCM		
	RACMO22E	HIRHAM5	RCA4
CNRM-CM5			X[1]
EC-EARTH	X[2]		X[3]
IPSL-CM5A-MR			X[4]
MOHOC-HadGEM2-ES	X[6]	X[5]	X[7]
MPI-ESM-LR			X[8]
NorESM-M		X[9]	

2.2. Climate forcing data

Near surface zonal and meridional wind components, near-surface air temperature, cloud cover, relative humidity and surface air pressure data were obtained from daily Regional Climate Models (RCM) simulations performed within the framework of the CORDEX initiative, with a resolution of 12.5 km. The EURO-CORDEX branch (http://www.euro-cordex.net/) downscales global climate simulations from the CMIP5 long experiments up to the year 2100 (Taylor et al., 2012). For the purposes of this study, the required variables were retrieved from nine RCMs simulations (Table 1) corresponding to the RCP8.5 scenario and assessed for the historical period. These regional simulations were obtained by means of three RCMs forced by six different GCMs (Table 1). A statistical analysis of each atmospheric variable was carried out to determine the most accurate climate model in reproducing past climatic conditions. This analysis compares the dataset obtained from ERA-Interim with the ones provided by RCMs predictions over the historical period (1979–2005). The evaluation is based on the probability density functions (PDFs) and a simple quantitative measure of how efficiently each climate model can capture the observed PDFs for each variable. Thus, a skill score was used to evaluate the PDFs at daily scale:

$$S_{Score} = \sum_{i=1}^{n} minimum\left(Z_m^i, Z_o^i\right) \qquad (1)$$

where Z_m^i and Z_o^i are the predicted and observed probability values of each bin and n is the number of bins. S_{Score} calculates the cumulative minimum value of observed and modeled distributions for each bin, quantifying the overlap between two PDFs (Perkins et al., 2007; Watterson, 2008). Values of S_{Score} equal to one indicate that model simulates the observed conditions perfectly. Hereafter, the mean S_{Score} for each climate simulation was computed, allowing to choose the best model to be used as surface boundary condition in modeling simulations.

The unavailability of ocean data (salinity and water temperature) from RCMs justifies the use of GCM predictions as oceanic boundary conditions. The criterion for selecting the most suitable GCM consists in choosing the same model that forces the best RCM.

2.3. Numerical scenarios

The first step in the definition of the numerical scenarios consists in determining the most suitable wind to force the hydrodynamic model. The protocol, which was used both for the historical (1976–2005) and the future (2070–2099) periods, can be summarized as follows: i) Nine control points located 20 km west from the mouth of each estuary, in order to avoid winds measured on land, were selected; ii) Ekman transport and upwelling index (UI) were calculated at those points following the methodology adopted by Gomez-Gesteira et al. (2006); iii) UI percentiles ranging from 75% to 99% (P7599 from now on) were determined at daily scale

for the most upwelling favorable months (July and August) (Alvarez et al., 2008); (iv) the mean daily zonal and meridional wind corresponding to that interval of percentiles were calculated for each grid point in order to generate a space-varying domain. This procedure was only applied for the most accurate model, which was selected as described in last section. In summary, this approach identifies the wind conditions that characterize future and historical high-extreme upwelling events (percentile 75–99). In order to discard outliers, values higher than 99% were not considered. Space-varying winds were imposed in the simulation event.

A wind statistical analysis was performed considering a Weibull distribution to find the typical wind speed for both climate periods. The Weibull scale parameters are 6.4 and 6.6 m s⁻¹ for historical and future climate periods, respectively. Thus, a constant wind speed of 6 m s⁻¹ and clockwise direction (changing 45° per hour) was imposed for the spin-up both for historical and future periods. As for wind direction, any rotation can be considered (clockwise, counter-clockwise or even random) as far as wind does not blow for a long time (several consecutive hours) from the same direction. The aim of this unusual wind regime is twofold, on the one hand, it allows heat diffusion between the ocean and the atmosphere and, on the other hand, it does not impose a dominant surface-driven circulation pattern (e.g. upwelling and downwelling) due to its continuous change in direction. In summary, at the end of spin-up the initial pattern is characterized by the thermal stratification imposed by the atmosphere in absence of prevailing winds. This allows identifying the supplementary effect of upwelling on that initial configuration.

The transport properties at the oceanic open boundary were determined through the computation of a climatological mean for the favorable months for the historical (1976–2005) and future (2070–2099) periods. The same procedure was carried out for the remaining atmospheric variables (except the wind).

Regarding the river discharges, for the historical period a climatological mean (1981–2010) was also computed (Hundecha et al., 2016). For future simulation, it was found that the most pessimistic prediction anticipated a reduction of 25% in river discharges in this region (https://hypeweb.smhi.se/explore-water/climate-impacts/europe-climate-impacts/), hence, this reduction was considered for the historical climatological values previously obtained. This river discharge reduction is in accordance with the reduction of annual precipitation observed by Collins et al. (2013) and Cardoso Pereira et al. (2019) under the RCP8.5 scenario.

To determine the duration of the simulation, a statistical analysis was performed based on the identification of the high-extreme summer (P7599) upwelling events, revealing that they last from 4 to 6 days. Thus, a 5-day upwelling event preceded by a spin-up period of 3 weeks was simulated under the conditions described above.

3. Results and discussion

3.1. Climate model evaluation

The skill of the climate model to reproduce real data was quantified by means of the S_{Score} for each atmospheric variable (Fig. 2a). The S_{Score} is higher than 0.5 for all models and atmospheric variables. As mentioned above, the score measures the overlap between two PDFs in such way that when it is equal to one the predicted and observed distributions are identical. In addition, the mean S_{Score} for each climate simulation was computed (Fig. 2b) to determine the most accurate climate model in reproducing past climatic conditions. The mean S_{Score} for most RCMs (except models #1 and #4) remains above 0.7, indicating that these models can reproduce accurately the data distribution found in observations. The highest mean S_{Score} (0.81) was found for model #7 (MOHC-HadGE2-Es-RCA4), which showed the best fit between predictions and observations. According to these results, surface and open boundary conditions from the RCM MOHC-HadGEM2-Es-RCA4 and GCM MOHC-HadGEM2-Es, respectively, were used as initial and boundary conditions for the model.
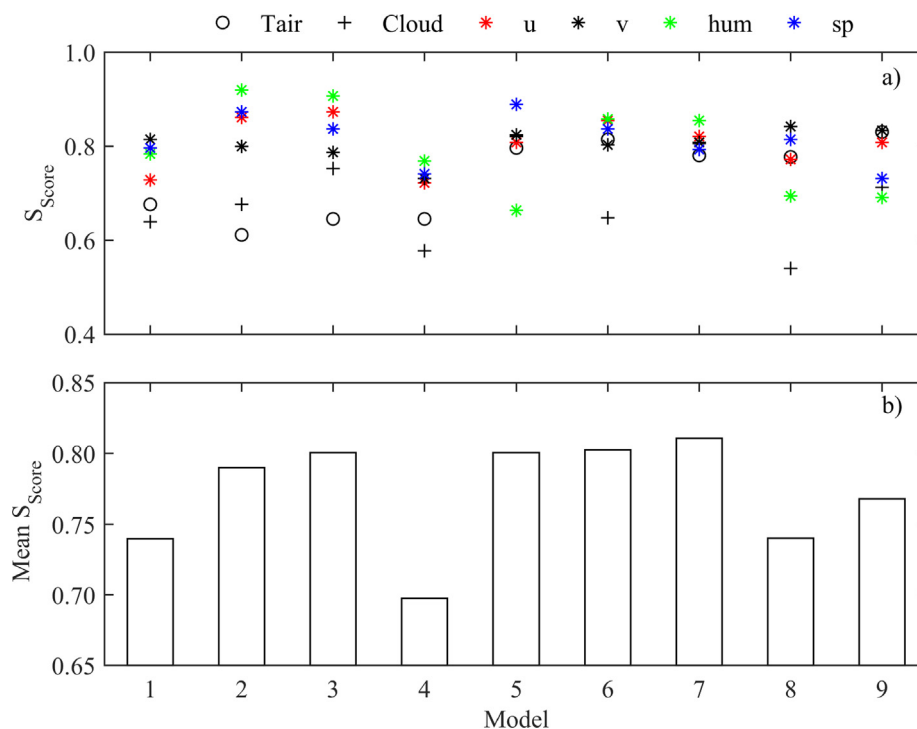
Fig. 2. S_{Score} for air temperature (Tair), air cloudiness (cloud), zonal (u) and meridional (v) components of wind, relative humidity (hum) and surface pressure (sp) for each model (a). Mean S_{Score} of all variables for each model (b).
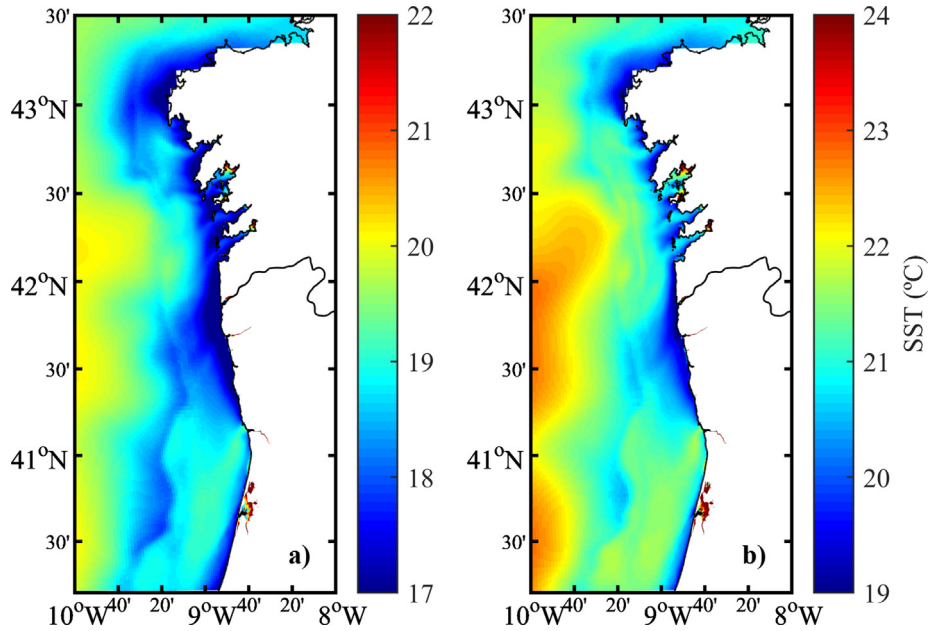
Fig. 3. Mean sea surface temperature under high-extreme upwelling conditions (P7599) for the historical (a) and future (b) periods.

3.2. Climate change impact on coastal upwelling

Predicted sea surface temperature (SST) time-averaged (5 days) was computed for the study region for both climate periods (historical and future) (Fig. 3).

For the historical climate period (Fig. 3a), the mean SST shows the typical coastal upwelling pattern, with a strip of cold water along the NWIP coast, more intense between Douro estuary and north of Cape Finisterre. This was compared with Alvarez et al. (2012) results derived from satellite observations from 1998 to 2007, revealing a very similar pattern, which demonstrates the ability of the model developed. Concerning the future period (Fig. 3b), the SST pattern is similar to the one observed for the his-

torical period (Fig. 3a), although the SST will be significantly higher (>2 °C) in the future. This increase in SST is consistent with the results reported for the same area but using GCMs from CMIP3 (Pires et al., 2015), and in other important upwelling areas such as California (Xiu et al., 2018) and Humboldt Upwelling Systems (Oyarzún and Brierley, 2019) where the most significant warming was observed at the surface of the water column. The increase of the ocean temperatures will lead to changes that can affect ocean ecosystems and biogeochemical processes that are strongly dependent on temperature (Gruber, 2011).

The upwelling imprint between the end and the beginning of the upwelling event ($\Delta SST = SST_{end} - SST_{beginning}$) is quantified in Fig. 4 for both periods. The area adjacent to the NWIP shows a clear
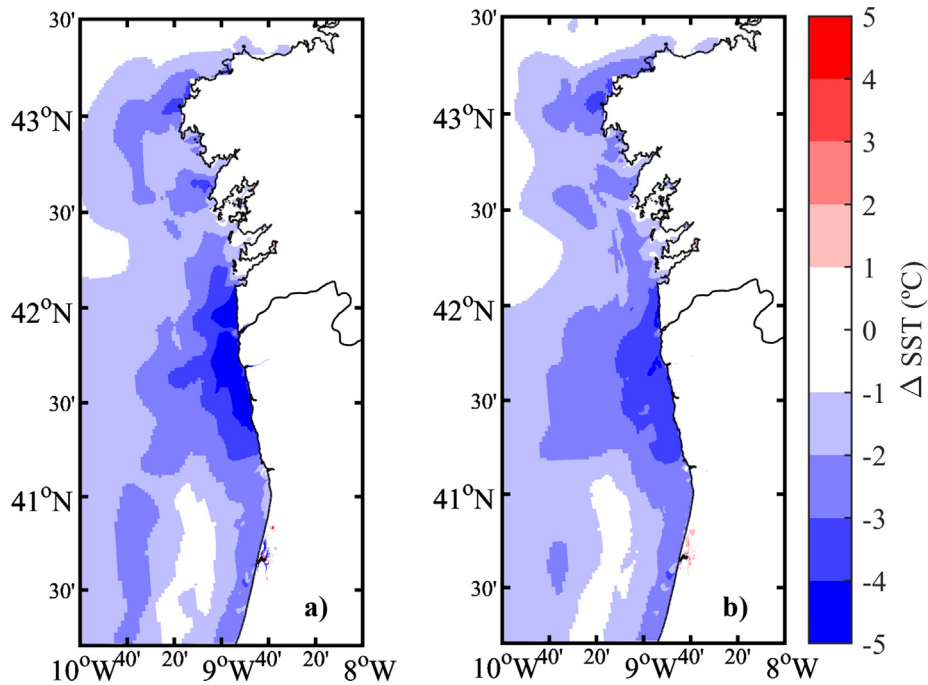
Fig. 4. SST drop between the end and the beginning of the upwelling event ($\Delta SST = SST_{end} - SST_{beginning}$) under high-extreme upwelling conditions (P7599) for the historical (a) and future (b) periods. This increment shows the upwelling imprint under both conditions.

Fig. 5. Difference between historical and future upwelling imprint under high-extreme upwelling conditions (P7599) (calculated subtracting the historical from the future imprint $\Delta SST_{future} - \Delta SST_{historical}$).

and Varela et al. (2018) for most of the world coasts and especially in upwelling systems. Overall, patterns are similar for both climate periods in most of the domain, with the exception of the region between 41° 30′ N and 42° 15′ N, where nearshore values ranging from 2 to 3 °C were observed for the historical period, and from 1 to 2 °C for the future (Fig. 4a and b). Both patterns are a clear proxy of the imprint of high-extreme upwelling events on coastal SST. Thus, the more negative the ΔSST, the more efficient the upwelling mechanism.

Fig. 5 shows the difference between the SST drop for the future and for the historical period, which is positive for most of the coastal domain north of 41° 30′ N and zero for the rest. Positive (red) values indicate that the SST drop is lower for the historical period. This figure shows that despite the strengthening of UI north of 41.5°, which was described by Sousa et al. (2017) using future wind projections, the upward pumping of subsurface water is less effective. These results suggest that other factors apart from wind, like the stratification of the water column prior to the upwelling event should be also considered.

Fig. 6 shows UI and water column stratification, described in terms of the Brunt-Väisälä frequency (N), for the domain between Minho and Ria de Vigo (shaded pink box in Fig. 1). As expected, higher UI values were observed for the future (red line in Fig. 6a). However, water column stratification is higher for the surface mixed layer in the future (Fig. 6c) compared to the historical period (Fig. 6b). Near coast, the highest N values occur between 5 and 15 m depth for the historical period (Fig. 6b) and between 5 and 25 m for the future (Fig. 6c). Thermocline will be deeper and more intense in the future, which will increase the stratification in the whole section. This result is consistent with previous studies derived from numerical models forced with GCMs from CMIP3 (Pires et al., 2015) and CMIP5 (Oerder et al., 2015; Oyarzún and Brierley, 2019) projects. Oyarzún and Brierley (2019) verified that as ocean stratification increases upwelling of

SST drop between the end and the beginning of the upwelling event, as it would be expected due to the cooling of surface water induced by upwelling (Fig. 4). This drop is even more marked near-shore and agrees with the difference between coast and near the adjacent ocean zone observed by Santos et al. (2011) at the NWIP
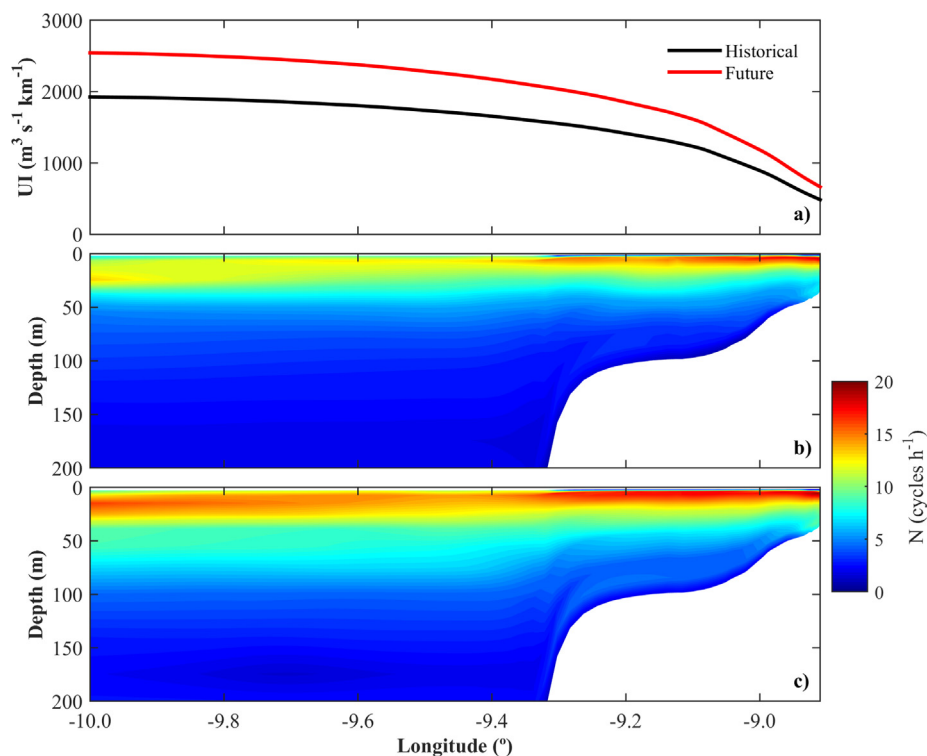
Fig. 6. Upwelling index corresponding to historical and future conditions (a). Brunt-Väisälä frequency (N) prior to the upwelling event for the historical (b) and future (c) periods. Values were calculated for the domain marked with a shaded pink area in Fig. 1.

coastal seawaters sourced from 100 m to at 300 m depth becomes less connected to the wind stress. Thereby, the observed increase in stratification counteracts the intensification of upwelling favourable winds, which results in a decrease of intensity and frequency of upwelling events in the NWIP coast, as observed by Di Lorenzo et al. (2005) for the California Current System. Ocean stratification decreases the upper ocean mixing and transport, which in turns reduces the ability of the oceans to supply the oxygen from the surface into the thermocline (Gruber, 2011). Furthermore, the stratification will limit the subsurface-water upwelled to the sea surface, leading to warmer SST and limiting the nutrient influx. Ocean warming can then have a negative impact on the productivity of the NWIP coast, as described in (Gutierrez et al., 2011), Roemmich and McGowan (1995) for the California Current, where the deepening of the thermocline resulted in the decline of zooplankton production. Additionally, Brochier et al. (2013), using an ocean numerical model, also showed that global warming could reduce the fish capacity in the Humboldt Current system.

4. Conclusions

A realistic configuration of Delft3D-Flow was used to analyse present and future coastal upwelling along the NWIP coast. Firstly, the best atmospheric model to force Delft3D was chosen among the models provided by the CORDEX project. The accuracy of the models to reproduce past climate was assessed in terms of the Perkins analysis, pointing the RCM MOHC-HadGEM2-Es-RCA4 and the GCM MOHC-HadGEM2-Es, as the best candidates to force Delft3D. Numerical experiments were conducted under high-extreme upwelling conditions for two climate periods: a historical period (1976–2005) and a far future period (2070–2099) under the RCP 8.5 greenhouse emission scenario.

Despite wind induced upwelling forcing is projected to intensify during this century, the upwelling imprint, defined in terms of the water-cooling during high-extreme events, will be less intense in the future. This decrease in the effectiveness of upwelling is due to the future increase in the thermal stratification of the water column, which will limit the amount of deeper water that will reach the sea surface in the future. This fact can deeply affect the primary production and, consequently, influence the marine fish stocks.

Declaration of Competing Interest

The authors declare that they have no known competing financial interests or personal relationships that could have appeared to influence the work reported in this paper.

Acknowledgements

References

Alvarez, I., deCastro, M., Gomez-Gesteira, M., Prego, R., 2006. Hydrographic behavior of the Galician Rias Baixas (NW Spain) under the spring intrusion of the Mino River. J. Mar. Syst. 60, 144–152. https://doi.org/10.1016/j.jmarsys.2005.12.005.

Alvarez, I., Gomez-Gesteira, M., Decastro, M., Dias, J.M., 2008. Spatiotemporal evolution of upwelling regime along the western coast of the Iberian Peninsula. J. Geophys. Res. Oceans 113. https://doi.org/10.1029/2008jc004744.

Alvarez, I., Lorenzo, M.N., deCastro, M., 2012. Analysis of chlorophyll a concentration along the Galician coast: seasonal variability and trends. Ices. J. Mar. Sci. 69, 728–738. https://doi.org/10.1093/icesjms/fss045.

Alvarez, I., Dias, J.M., DeCastro, M., Vaz, N., Sousa, M.C., Gómez-Gesteira, M., 2013. Influence of upwelling events on the estuaries of the north-western coast of the Iberian Peninsula. Mar. Freshwater Res. 64. https://doi.org/10.1071/MF12298.

Bakun, A., 1990. Global climate change and intensification of coastal ocean upwelling. Science 247, 198–201. https://doi.org/10.1126/science.247.4939.198.

Behrenfeld, M.J., O'Malley, R.T., Siegel, D.A., McClain, C.R., Sarmiento, J.L., Feldman, G.C., Milligan, A.J., Falkowski, P.G., Letelier, R.M., Boss, E.S., 2006. Climate-driven trends in contemporary ocean productivity. Nature 444, 752–755. https://doi.org/10.1038/nature05317.

Blanton, J.O., Tenore, K.R., Castillejo, F., Atkinson, L.P., Schwing, F.B., Lavin, A., 1987. The relationship of upwelling to mussel production in the rias on the Western Coast of Spain. J. Mar. Res. 45, 497–511.

Brochier, T., Echevin, V., Tam, J., Chaigneau, A., Goubanova, K., Bertrand, A., 2013. Climate change scenarios experiments predict a future reduction in small pelagic fish recruitment in the Humboldt Current system. Glob. Change Biol. 19, 1841–1853. https://doi.org/10.1111/gcb.12184.

Cardoso Pereira, S., Marta-Almeida, M., Carvalho, A.C., Rocha, A., 2019. Extreme precipitation events under climate change in the Iberian Peninsula. Int. J. Climatol. https://doi.org/10.1002/joc.6269.

Collins, M., Knutti, R., Arblaster, J., Dufresne, J.-L., Fichefet, T., Friedlingstein, P., Gao, X., Gutowski, W.J., Johns, T., Krinner, G., Shongwe, M., Tebaldi, C., Weaver, A.J., Wehner, M., 2013. Long-term climate change: projections, commitments and irreversibility. In: Stocker, T.F., Qin, D., Plattner, G.-K., Tignor, M., Allen, S.K., Boschung, J., Nauels, A., Xia, Y., Bex, V., Midgley, P.M. (Eds.), Climate Change 2013: The Physical Science Basis. Contribution of Working Group I to the Fifth Assessment Report of the Intergovernmental Panel on Climate Change, Cambridge University Press, Cambridge, United Kingdom and New York, NY, USA.

Costa-Dias, S., Freitas, V., Sousa, R., Antunes, C., 2010. Factors influencing epibenthic assemblages in the Minho Estuary (NW Iberian Peninsula). Mar. Pollut. Bull. 61, 240–246. https://doi.org/10.1016/j.marpolbul.2010.02.020.

deCastro, M., Alvarez, I., Varela, M., Prego, R., Gomez-Gesteira, M., 2006. Mino River dams discharge on neighbor Galician Rias Baixas (NW Iberian Peninsula): hydrological, chemical and biological changes in water column. Estuarine Coastal and Shelf. Science 70, 52–62. https://doi.org/10.1016/j.ecss.2006.05.035.

Deltares, 2014. Delft3D-FLOW. Simulation of multi-dimensional hydrodynamic flows and transport phenomena, including sediments. User Manual. Hydro-Morphodynamics. Version: 3.15.34158, Delft3D Modeling Suite.

Des, M., deCastro, M., Sousa, M.C., Dias, J.M., Gómez-Gesteira, M., 2019. Hydrodynamics of river plume intrusion into an adjacent estuary: the Minho River and Ria de Vigo. J. Mar. Syst. 189, 87–97. https://doi.org/10.1016/j.jmarsys.2018.10.003.

Di Lorenzo, E., Miller, A.J., Schneider, N., McWilliams, J.C., 2005. The warming of the California current system: dynamics and ecosystem implications. J. Phys. Oceanogr. 35, 336–362. https://doi.org/10.1175/JPO-2690.1.

Dias, J.M., Picado, A., 2011. Impact of morphologic anthropogenic and natural changes in estuarine tidal dynamics. J. Coastal Res. 1490–1494

Figueiras, F.G., Labarta, U., Fernández Reiriz, M.J., 2002. Coastal upwelling, primary production and mussel growth in the Rías Baixas of Galicia. Hydrobiologia, 121–131. https://doi.org/10.1023/A:1021309222459.

García-Reyes, M., Sydeman, W.J., Schoeman, D.S., Rykaczewski, R.R., Black, B.A., Smit, A.J., Bograd, S.J., 2015. Under pressure: climate change, upwelling, and eastern boundary upwelling ecosystems. Front. Mar. Sci. 2. https://doi.org/10.3389/fmars.2015.00109.

Gomez-Gesteira, M., Moreira, C., Alvarez, I., Decastro, M., 2006. Ekman transport along the Galician coast (northwest Spain) calculated from forecasted winds. J. Geophys. Res. Oceans 111. https://doi.org/10.1029/2005jc003331.

Gruber, N., 2011. Warming up, turning sour, losing breath: ocean biogeochemistry under global change. Philos. Trans. R. Soc. A Math. Phys. Eng. Sci. https://doi.org/10.1098/rsta.2011.0003.

Gutierrez, D., Bouloubassi, I., Sifeddine, A., Purca, S., Goubanova, K., Graco, M., Field, D., Mejanelle, L., Velazco, F., Lorre, A., Salvatteci, R., Quispe, D., Vargas, G.,

Dewitte, Ortlieb, L., 1976. Coastal cooling and increased productivity in the main upwelling zone off Peru since the mid-twentieth century. Geophys. Res. Lett. 38. https://doi.org/10.1029/2010gl046324.

Hundecha, Y., Arheimer, B., Donnelly, C., Pechlivanidis, I., 2016. A regional parameter estimation scheme for a pan-European multi-basin model. J. Hydrol.: Reg. Stud. 6, 90–111. https://doi.org/10.1016/j.ejrh.2016.04.002.

IPCC, 2013. Climate Change 2013: The Physical Science Basis.Contribution of Working Group I to the Fifth Assessment Report of the Intergovernmental Panel on Climate Change. In: Stocker, T.F., Qin, D., Plattner, G.-K., Tignor, M., Allen, S.K., Boschung, J., Nauels, A., Xia, Y., Bex, V., Midgley, P.M. (Eds.), Cambridge University Press, Cambridge, United Kingdom and New York, NY, USA.

Levitus, S., Antonov, J.I., Boyer, T.P., Stephens, C., 2000. Warming of the world ocean. Science 287, 2225–2229. https://doi.org/10.1126/science.287.5461.2225.

Lopes, C.L., Alves, F.L., Dias, J.M., 2017. Flood risk assessment in a coastal lagoon under present and future scenarios: Ria de Aveiro case study. Nat. Hazards 89, 1307–1325. https://doi.org/10.1007/s11069-017-3025-x.

Lopes, C.L., Dias, J.M., 2015. Assessment of flood hazard during extreme sea levels in a tidally dominated lagoon. Nat. Hazards 77, 1345–1364. https://doi.org/10.1007/s11069-015-1659-0.

MacMillan, D.S., Beckley, B.D., Fang, P., 2004. Monitoring the TOPEX and Jason-1 microwave radiometers with GPS and VLBI wet zenith path delays. Mar. Geod. 27, 703–716. https://doi.org/10.1080/01490410490904780.

Mendes, Renato, Sousa, M.C., deCastro, M., Gómez-Gesteira, M., Dias, J.M., 2016. New insights into the Western Iberian Buoyant Plume: interaction between the Douro and Minho River plumes under winter conditions. Prog. Oceanogr. 141, 30–43. https://doi.org/10.1016/j.pocean.2015.11.006.

Mendes, R., Vaz, N., Dias, J.M., 2013. Potential impacts of the mean sea level rise on the hydrodynamics of the Douro river estuary. J. Coastal Res. https://doi.org/10.2112/si65-330.1.

Miranda, P.M.A., Alves, J.M.R., Serra, N., 2013. Climate change and upwelling: response of Iberian upwelling to atmospheric forcing in a regional climate scenario. Clim. Dyn. 40, 2813–2824. https://doi.org/10.1007/s00382-012-1442-9.

Oerder, V., Colas, F., Echevin, V., Codron, F., Tam, J., Belmadani, A., 2015. Peru-Chile upwelling dynamics under climate change. J. Geophys. Res. Oceans 120, 1152–1172. https://doi.org/10.1002/2014JC010299.

Otero, P., Ruiz-Villarreal, M., García-García, L., González-Nuevo, G., Cabanas, J.M., 2013. Coastal dynamics off Northwest Iberia during a stormy winter period. Ocean Dyn. 63, 115–129. https://doi.org/10.1007/s10236-012-0585-x.

Oyarzún, D., Brierley, C.M., 2019. The future of coastal upwelling in the Humboldt current from model projections. Clim. Dyn. 52, 599–615. https://doi.org/10.1007/s00382-018-4158-7.

Perkins, S.E., Pitman, A.J., Holbrook, N.J., McAneney, J., 2007. Evaluation of the AR4 climate models' simulated daily maximum temperature, minimum temperature, and precipitation over Australia using probability density functions. J. Clim. 20, 4356–4376. https://doi.org/10.1175/JCLI4253.1.

Pires, A.C., Nolasco, R., Rocha, A., Dubert, J., 2013. Assessing future climate change in the Iberian Upwelling System. J. Coastal Res. 1909–1914. https://doi.org/10.2112/SI65-323.1.

Pires, A.C., Nolasco, R., Rocha, A., Ramos, C., Dubert, J., 2015. Climate change in the Iberian Upwelling System: a numerical study using GCM downscaling. Clim. Dyn., 1–14

Prego, R., Dale, A.W., deCastro, M., Gomez-Gesteira, M., Taboada, J.J., Montero, P., Villareal, M.R., Perez-Villar, V., 2001. Hydrography of the Pontevedra Ria: Intra-annual spatial and temporal variability in a Galician coastal system (NW Spain). J. Geophys. Res. Oceans 106, 19845–19857.

Queiroga, H., 2003. Wind forcing of crab megalopae recruitment to an estuary (ria de aveiro) in the northern portuguese upwelling system. Invertebr. Reprod. Dev. 43, 47–54. https://doi.org/10.1080/07924259.2003.9652521.

Roemmich, D., McGowan, J., 1995. Climatic warming and the decline of zooplankton in the California current. Science 267, 1324–1326. https://doi.org/10.1126/science.267.5202.1324.

Rykaczewski, R.R., Dunne, J.P., Sydeman, W.J., Garcia-Reyes, M., Black, B.A., Bograd, S.J., 2015. Poleward displacement of coastal upwelling-favorable winds in the ocean's eastern boundary currents through the 21st century. Geophys. Res. Lett. 42, 6424–6431. https://doi.org/10.1002/2015GL064694.

Santos, F., Gomez Gesteira, M., deCastro, M., 2011. Coastal and oceanic SST variability along the western Iberian Peninsula. Cont. Shelf Res. 31, 2012–2017. https://doi.org/10.1016/j.csr.2011.10.005.

Santos, F., DeCastro, M., Gómez-Gesteira, M., Allvarez, I., 2012. Differences in coastal and oceanic SST warming rates along the Canary upwelling ecosystem from 1982 to 2010. Cont. Shelf Res. 47, 1–6. https://doi.org/10.1016/j.csr.2012.07.023.

Seabra, R., Varela, R., Santos, A.M., Gómez-Gesteira, M., Meneghesso, C., Wethey, D.S., Lima, F.P., 2019. Reduced nearshore warming associated with Eastern boundary upwelling systems. Front. Mar. Sci. 6. https://doi.org/10.3389/fmars.2019.00104.

Soares, P.M.M., Cardoso, R.M., Miranda, P.M.A., Viterbo, P., Belo-Pereira, M., 2012. Assessment of the ENSEMBLES regional climate models in the representation of precipitation variability and extremes over Portugal. J. Geophys. Res. Atmos. 117. https://doi.org/10.1029/2011jd016768.

Sousa, M.C., Alvarez, I., Vaz, N., Dias, J.M., 2011. Physical forcing of the hydrography of the Ria de Vigo mouth. J. Coastal Res. SI64, 1589–1593.

Sousa, M.C., Vaz, N., Alvarez, I., Gomez-Gesteira, M., Dias, J.M., 2014a. Modeling the Minho River plume intrusion into the Rias Baixas (NW Iberian Peninsula). Cont. Shelf Res. 85, 30–41.

Sousa, M.C., Vaz, N., Alvarez, I., Gomez-Gesteira, M., Dias, J.M., 2014b. Influence of the Minho River plume on the Rias Baixas (NW of the Iberian Peninsula). J. Mar. Syst. 139, 248–260.

Sousa, M.C., deCastro, M., Alvarez, I., Gomez-Gesteira, M., Dias, J.M., 2017. Why coastal upwelling is expected to increase along the western Iberian Peninsula over the next century?. Sci. Total Environ. 592. https://doi.org/10.1016/j.scitotenv.2017.03.046.

Sousa, M.C., Ribeiro, A.S., Des, M., Mendes, R., Alvarez, I., Gomez-Gesteira, M., Dias, J.M., 2018. Integrated high-resolution numerical model for the NW Iberian Peninsula Coast and main estuarine systems. J. Coastal Res. 66–70. https://doi.org/10.2112/SI85-001.1.

Taylor, K.E., Stouffer, R.J., Meehl, G.A., 2012. An overview of Cmip5 and the experiment design. Bull. Am. Meteorol. Soc. 93, 485–498. https://doi.org/10.1175/Bams-D-11-00094.1.

Vale, L.M., Dias, J.M., 2011. The effect of tidal regime and river flow on the hydrodynamics and salinity structure of the Lima Estuary: use of a numerical model to assist on estuary classification. J. Coastal Res., 1604–1608

Varela, R., Alvarez, I., Santos, F., deCastro, M., Gomez-Gesteira, M., 2015. Has upwelling strengthened along worldwide coasts over 1982–2010?. Sci. Rep. 5. https://doi.org/10.1038/Srep10016.

Varela, R., Lima, F.P., Seabra, R., Meneghesso, C., Gómez-Gesteira, M., 2018. Coastal warming and wind-driven upwelling: a global analysis. Sci. Total Environ. 639, 1501–1511. https://doi.org/10.1016/j.scitotenv.2018.05.273.

Vieira, M.E.C., Bordalo, A.A., 2000. The Douro estuary (Portugal): a mesotidal salt wedge. Oceanol. Acta 23, 585–594. https://doi.org/10.1016/S0399-1784(00)01107-5.

Wang, D.W., Gouhier, T.C., Menge, B.A., Ganguly, A.R., 2015. Intensification and spatial homogenization of coastal upwelling under climate change. Nature 518. https://doi.org/10.1038/Nature14235.

Watterson, I.G., 2008. Calculation of probability density functions for temperature and precipitation change under global warming. J. Geophys. Res. Atmos. 113. https://doi.org/10.1029/2007JD009254.

Wooster, W.S., Bakun, A., Mclain, D.R., 1976. Seasonal upwelling cycle along eastern boundary of North-Atlantic. J. Mar. Res. 34, 131–141.

Xiu, P., Chai, F., Curchitser, E.N., Castruccio, F.S., 2018. Future changes in coastal upwelling ecosystems with global warming: the case of the California current system. Sci. Rep. 8. https://doi.org/10.1038/s41598-018-21247-7.

How can ocean warming at the NW Iberian Peninsula affect mussel aquaculture?

M. Des [a,*], M. Gómez-Gesteira [a], M. deCastro [a], L. Gómez-Gesteira [a], M.C. Sousa [b]

[a] Environmental Physics Laboratory (EphysLab), CIM-UVIGO, Universidade de Vigo, Edificio Campus da Auga, 32004 Ourense, Spain
[b] CESAM, Physics Department, University of Aveiro, Aveiro 3810-193, Portugal

HIGHLIGHTS

- Analysis of climate change impact on mussel aquaculture using numerical predictions
- Water temperature and stratification will increase.
- The comfort level of mussels will be reduced, especially in surface layers.
- Changing the mussel raft polygons location may mitigate the climate change impact.

GRAPHICAL ABSTRACT
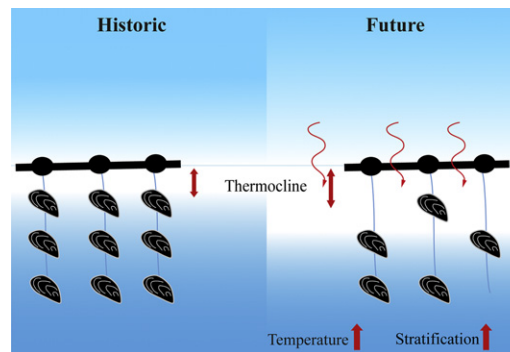
ARTICLE INFO

ABSTRACT

Understanding and forecasting future consequences of climate change in mussel aquaculture industry require the assessment of changes in physical parameters which may affect mussel growth. The FLOW module of Delft3D model forced with climatic data was validated and calibrated for the Rías Baixas (NW Iberian Peninsula), one of the areas with the highest mussel production in the world. This model was used to perform historical (1999–2018) and future (2080–2099) projections. Temperature and stratification water conditions were compared in order to determine at what extent climate change can affect mussel production. Thermal stress will increase in a non-homogeneous throughout the water column and the comfort level of mussels will be reduced by more than 60% in the upper layers and more than 30% in deep layers in most of the mussel raft polygons. Water column stratification will increase ~ 5–10 cycles h^{-1} in most of the polygons reducing the vertical exchange of nutrients and oxygen. Hereby changes in water temperature and stratification at the end of the century will not be favorable for mussel growth.

© 2019 Elsevier B.V. All rights reserved.

1. Introduction

Climate change is expected to have a significant environmental impact affecting primary production, economy and society.

In marine systems, sea-level rise, sea temperature changes, changes in circulation patterns and frequency, acidification, and severity of extreme events will impact the marine ecosystems and therefore, affect fisheries productivity. The analysis of the possible and probable vulnerabilities of these systems in a scenario of climate change allows establishing mitigation and adaptation procedures.

---

 * Corresponding author.
   E-mail address: mdes@uvigo.es (M. Des).

81

The aquaculture sector is growing rapidly and plays a key role in food production to sustain a growing human population. In recent years, capture fisheries have become relatively stable whereas aquaculture production has increased, providing up to 46.8% of the world combined capture and aquaculture production in 2016, of which 35.9% proceeded from marine aquaculture (FAO, 2018). In the coming years, the aquaculture sector will have to face climate-change impacts trough the management of mitigation and adaptation strategies (Duarte et al., 2017; FAO, 2017). Since changes associated with climate change will not be the same everywhere (Cane et al., 1997), the study of the possible effects on specific areas is essential.

This research is focused on the Rías Baixas (Fig. 1), located on the northwest coast of the Iberian Peninsula in the northern limit of the eastern North Atlantic Upwelling system. They are four flooded incised valleys (Evans and Prego, 2003) of high primary productivity, favoured by their location. The economy of the region depends mainly on the fishing, shellfish gathering and aquaculture sectors. This last one is mostly focused on the extensive culture of *Mytilus galloprovincialis* in mussel rafts. Data from the Spanish Ministry of Agriculture, Fisheries and Food show that approximately 279,000 tons of mussels were produced in 2018 in the region of Galicia, most of them within the Rías Baixas (https://www.pescadegalicia.gal), corresponding to up to 40% of the European and up to 15% of the World aquaculture production of mussels (Aguiar et al., 2017).

Growth rate, mortality and production of mussels are dependent on several environmental factors such as oxygen and phytoplankton availability, water temperature, salinity and ocean acidification among others (Pérez Camacho et al., 1995; Anestis et al., 2007; Mesas and Tarifeño, 2015).

Water temperature is one of the most relevant indexes of the quality of aquatic ecosystems due to its importance for biological and chemical processes and species interactions (Zippay and Helmuth, 2012; Gestoso et al., 2016). It is a critical factor in mussel growth, explaining independently 67% of the differences in growth (Kroeker et al., 2014). Biochemical and physiological rates benefit from moderate warming, but only up to an optimal temperature, which is specific for each species (Gillooly et al., 2002; Anestis et al., 2007). Greater warming beyond that optimal range can cause slower growth and reductions in performance and survival (Hrs-Brenko et al., 1977; Anestis et al., 2010).

As mussel aquaculture in the Galician coast depends on the collection of natural seed, both from intertidal rocky shore and collector ropes, most of the studies analyze its distribution and quality (Blanton et al., 1987; Cáceres-Martínez et al., 1993; Cáceres-Martínez and Figueras, 1998; Fuentes et al., 1998). There are numerous studies focused on the mortality of mussels based on the genetics of individuals (Fuentes et al., 1994; López et al., 2001; Fuentes et al., 2002; Diz and Presa, 2009), as well as studies on the factors that can influence mussel productivity, especially in relation with upwelling patterns (Blanton et al., 1987; Figueiras et al., 2002) the proliferation of harmful algae blooms (Álvarez-Salgado et al., 2008; Spyrakos et al., 2011) and the within-raft variability (Fuentes et al., 2000).
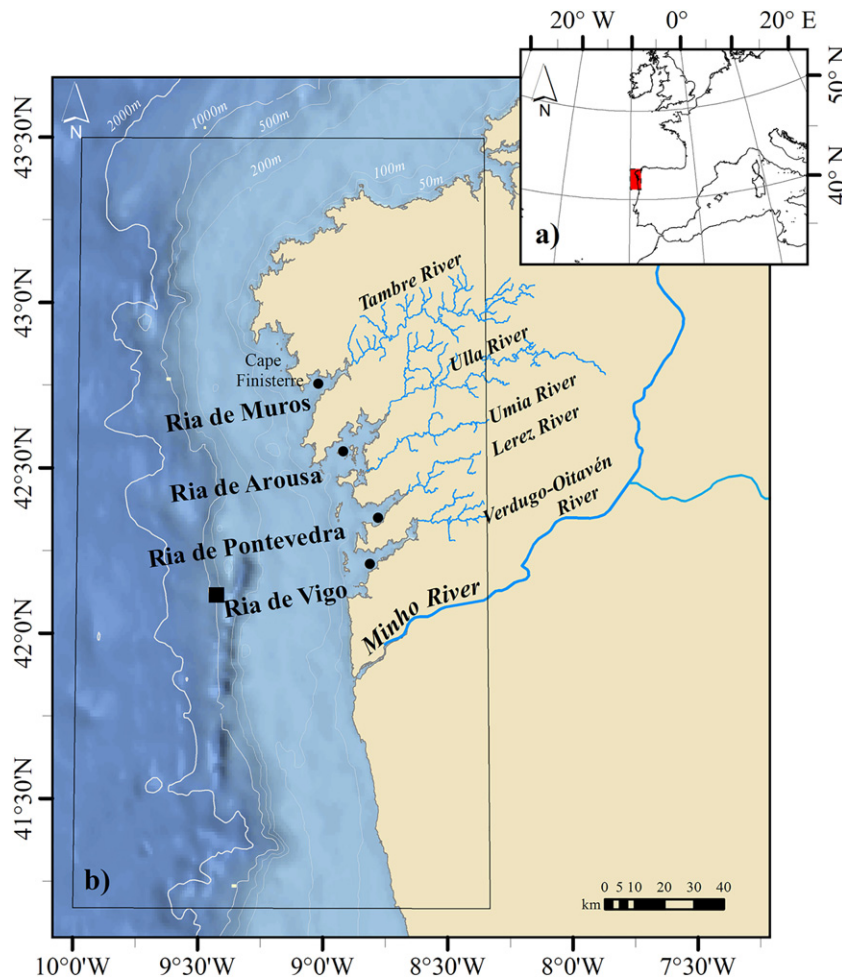
Fig. 1. (a) Location of the study area. (b) The box indicates the modeled area. The black square indicates the location of Cabo Silleiro buoy. The black dots indicate the location of the stations used to perform the vertical profiles. Contour bathymetry lines (shown in gray) were elaborated using the General Bathymetric Chart of the Oceans (GEBCO) from the British Oceanographic Data Centre (BODC).

Most of the studies on the possible impact of climate change on the Rías Baixas investigate the effects on upwelling events (Casabella et al., 2014; Cordeiro Pires et al., 2016; Sousa et al., 2017; Sousa et al., 2020). Few studies have been found that analyze its possible impact on the mussel production, in particular, Pérez Muñuzuri et al. (2009) conclude that if the upwelling weakens under climate change conditions, mussel production would be reduced and Gestoso et al. (2016) analyze the possible competition between the native *Mytilus galloprovincialis* and the invasive mussel *Xenostrobus securis* in a scenario of global ocean warming.

The present study attempts to determine how climate change will affect the Rías Baixas at the end of the century and its possible impact on mussel culture industry. To achieve this goal, numerical simulations using the FLOW module of Delft3D under imposed conditions from projection data were performed for historical and future periods. Firstly, the skill of the Delft3D-Flow to simulate future estuarine conditions was checked. The characterization of future water temperature and stratification obtained from Delft3D-Flow allows improving our knowledgement about how climate change can affect the mussel productivity in the Rías Baixas by the end of the 21st century.

2. Methodology

2.1. Numerical model

Calculations based on climate projections are an arduous task where different sources of error can appear. First, models must be accurate to reproduce *in situ* measurements when forced with real data. In addition,

they must also represent mean conditions when forced with climatic data. Note that the results provided by climatic models for a certain period (*e.g.*, June 2003) do not correspond to the actual conditions for that period, in such a way that a group of years must be averaged to obtain values representative of the climate conditions. Thus, models must be calibrated in two different ways: (i) forcing models with real conditions corresponding to a certain time interval (typically from days to months) and comparing the results with *in situ* data (date-to-date); (ii) forcing models with historical climatic data for longer periods (typically decades) and comparing the mean values with other source at that scale.

The FLOW module of the Delft3D numerical model was used to analyze global warming effects in the Rías Baixas. A detailed description of the numerical model parametrization, implementation and validation for the Galician Rías Baixas can be found in Des et al. (2019).

Two numerical experiments were used in the present manuscript. In the first one (Exp#1 from now on), Delft3D was forced with real conditions and run for the period 2009–2018 to be compared with *in situ* data. This setup was previously used by Des et al. (2019). In the second experiment (Exp#2 from now on), the model was forced with historical climatic data over the period 2009–2018 and values were averaged to be compared with average values provided by Exp#1. Finally, once the accuracy of Delft3D for the area under study was assessed the Exp#2 was extended, comprising the historical (1999–2018) and future (2080–2099) period under climate conditions. The RCP8.5 greenhouse gas emission scenario was considered for future projections.

The model uses a mesh covering an area from 41.18°N to 43.50° N and from 10.00° to 8.33°W (Fig. 1, rectangle). The horizontal resolution increases gradually from 2200 m × 800 m on the oceanic West boundary
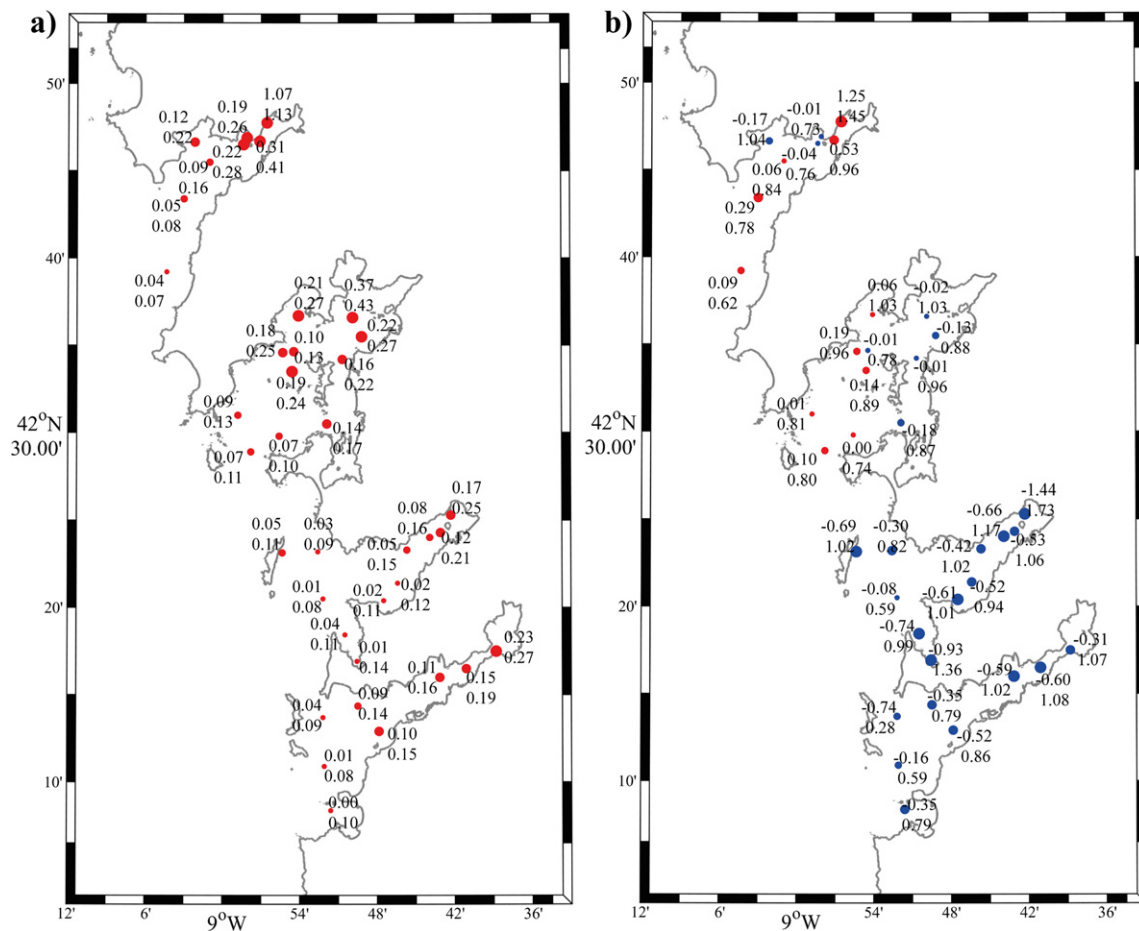
Fig. 2. Mean values of bias (upper number) and RMSE (lower number) obtained comparing Delft3D-Flow predicted and measured weekly vertical profiles of salinity (a) and water temperature (b) for August 2009 to 2018. Red dots indicate that the model overestimates *in situ* data, positive bias. Blue dots indicate that the model underestimates *in situ* data, negative bias. Dot size indicates the bias percentile.

Table 1
Model accuracy in reproducing *in situ* data of salinity and water temperature in each ria calculated averaging the values of all stations per ria.

Ria	Salinity		Temperature (°C)	
	Bias	RMSE	Bias	RMSE
Muros	0.26	0.33	0.25	0.90
Arousa	0.16	0.21	0.01	0.88
Pontevedra	0.06	0.14	−0.63	1.06
Vigo	0.09	0.14	−0.32	0.89

to 220 m × 140 m in the Rías Baixas and to 50 m × 77 m in the Minho River estuary. The vertical resolution is 16 sigma layers with top layers refined.

The bathymetry used for numerical simulations was elaborated by compilation from different sources. The bathymetries for the rias of Arousa, Muros and adjacent shelf area were digitalized from nautical charts elaborated by the Spanish Navy Hydrographical Institute. The multibeam-sourced bathymetries of the rias of Vigo and Pontevedra with a horizontal resolution of 5 m were provided by the General Fishing Secretary, dependent on the Spanish Ministry of Agriculture, Fisheries and Food. Portuguese Navy Hydrographic Institute provided the bathymetry of the Minho estuary. Bathymetry gaps were covered using data from the General Bathymetric Chart of the Oceans (GEBCO, https://www.gebco.net/) which has a spatial resolution of 30 arc sec.

The oceanic boundary was divided into 127 sections and was forced with water level and transport conditions. Thirteen main tidal harmonic constituents obtained from the model TPXO 7.2 TOPEX/Poseidon Altimetry (M_2, S_2, N_2, K_2, K_1, O_1, P_1, Q_1, M_sF, MM, M_4, MS_4, MN_4) were prescribed

as astronomical forcing. Salinity and water temperature (transport conditions, from now on), were specified per layer. Transport conditions for Exp#1 were imposed using daily data from the operational Atlantic-Iberian Biscay Irish-Ocean Physics Reanalysis, with a horizontal resolution of 1/12° and a vertical resolution of 50 sigma coordinate levels. Data are available through the Copernicus Marine Service website (http://marine.copernicus.eu). For the Exp#2, the transport conditions were retrieved from the GCM MOHC-HadGEM2-Es GCM in the framework of phase 5 of the Coupled Model Intercomparison (CMIP5) project.

As surface boundary conditions (air temperature, relative humidity, net solar radiation, surface pressure and wind), Exp#1 used hourly data from MeteoGalicia Weather Research and Forecasting Model, with a resolution of 4 km, Exp #2 were obtained from the MOHC-HadGEM2-Es-RCA4 RCM in the framework of the Coordinated Regional Climate Downscaling Experiment (CORDEX) project. MOHC-HadGEM2-Es-RCA4 is the RCM, which better reproduces historical climate conditions in the area under study, as stated in Sousa et al. (2020).

Freshwater discharges were imposed as fluvial open boundary conditions. Minho River discharge data was provided by the Confederación Hidrográfica Miño-Sil, where the Verdugo-Oitavén, Lérez, Ulla, and Umia river discharge data were retrieved from the MeteoGalicia database for Exp#1. In the Exp#2, the climatologic river discharge data were obtained by accessing to the Hype Web portal. In this setup, a reduction of 25% in river discharges and the RCP8.5 greenhouse gas emission scenario were considered for future projections, following the most pessimistic predictions (https://hypeweb.smhi.se/explore-water/climate-impacts/europe-climate-impacts/).

Both experiments were run for July and August using a spin-up period of two weeks.
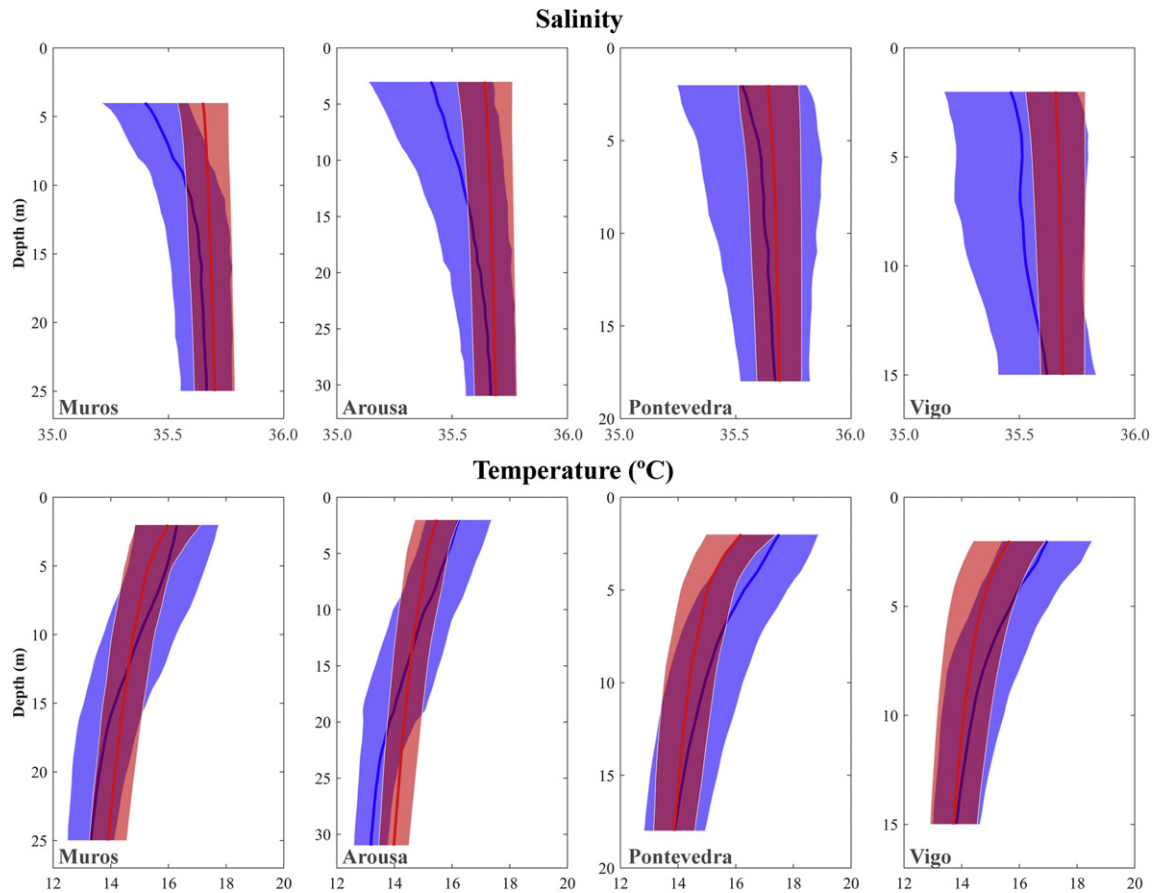
Fig. 3. Measured (blue line) and computed (red line) vertical profiles of salinity (upper row) and water temperature (lower row) in a sampling station located in the middle part of the rias of Muros, Arousa, Pontevedra and Vigo during July–August from 2009 to 2018. Shadows represent measured and numerical standard deviations.

2.2. Processing of numerical data

The skill of numerical simulations carried out using Exp#1 to reproduce thermohaline variables was evaluated through root mean square error (RMSE) and bias indicators. Weekly *in situ* vertical salinity and temperature profiles at 38 sampling stations distributed within the four rias (Fig. 2) were compared with the predicted values date-to-date. These *in situ* data were collected using a SBE25 CTD at 38 field stations (8 at the Ría de Muros, 11 at the Ría de Arousa, 11 at the Ría de Pontevedra and 8 at the Ría de Vigo, Fig. 2) and were downloaded from the Instituto Tecnolóxico para o control do Medio Mariño de Galicia (INTECMAR) website (www.intecmar.gal). Thompson Tau test, with α = 0.1, was used to detect and remove outliers in data. Additionally, gaps were filled using a cubic interpolation.

Statistical analysis over the historical period for each atmospheric and oceanic variable was carried out. Atmospheric dataset from MOHC-HadGE2-Es-RCA4 RCM was compared with ERA-Interim dataset while oceanic data from MOHC-HadGE2-Es GCM were compared with *in situ* data from Cabo Silleiro buoy (Fig. 1). This statistical analysis shows a good agreement for all variables except for the air temperature, for which a bias of 2 °C was observed. Thus, a reduction of 2 °C was applied to predicted air temperature data before entering it into the Delft3D-Flow model.

To assess the impact of the climate change on the aquaculture sector of the Rías Baixas hourly model outputs were used to characterize 44 points located within areas of mussel rafts (referred as mussel raft polygons).

Thermohaline variables were used to analyze the stratification using the Brunt-Väisälä frequency (N). Hourly Brunt-Väisälä frequency was averaged obtaining a representative value for historical ($\overline{N}^H$) and future periods ($\overline{N}^F$).

3. Results and discussion

3.1. Skill of Delft3D-Flow

The capability of the numerical model (Exp#1) to reproduce thermohaline variables in the rias was evaluated by the average of bias and RMSE for each station (Fig. 2). Then, the mean RMSE and bias for each station are averaged for every ria (Table 1). The model overestimates salinity (positive bias values), being the bias for the rias of Pontevedra and Vigo close to zero. Regarding water temperature, the model overestimates *in situ* data for the Ría de Muros and underestimates it in the rias of Pontevedra and Vigo. In the Ría de Arousa, the bias is almost zero. Both bias and RMSE values are similar to those obtained by Des et al. (2019) for the same area using the same numerical model and set up.
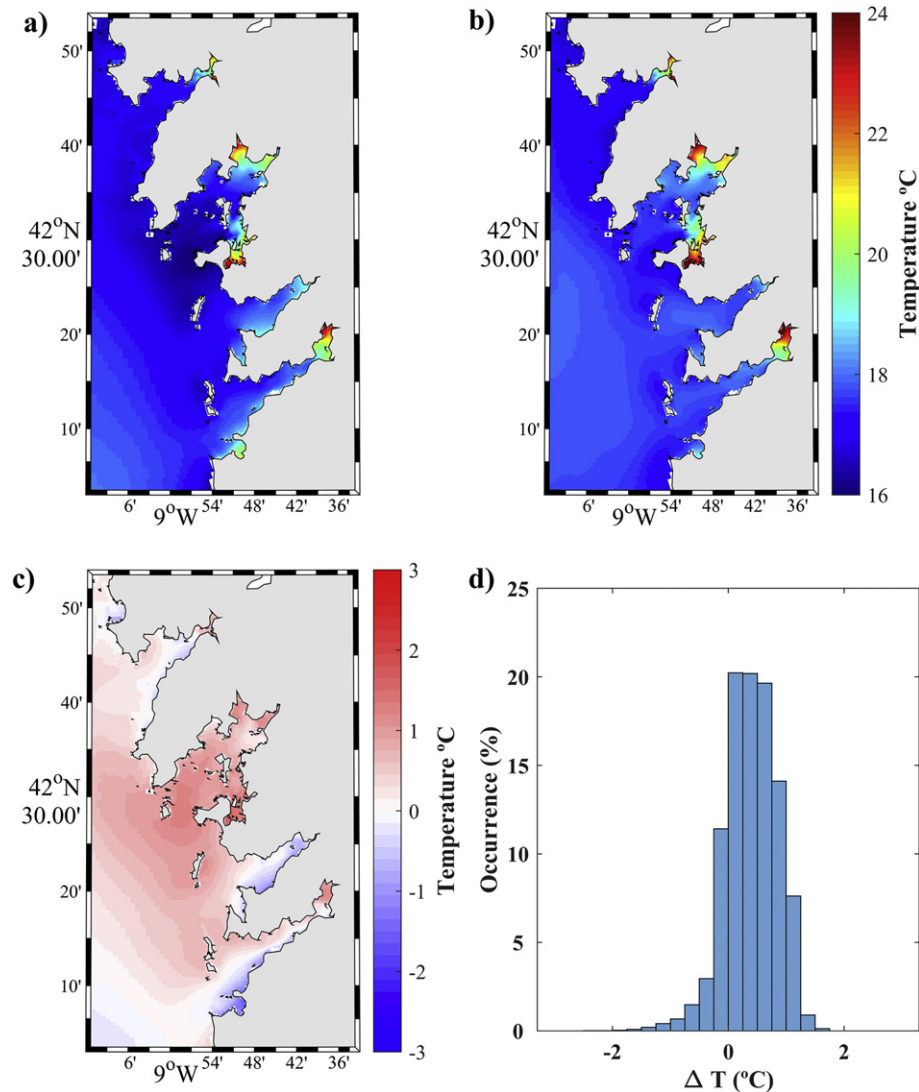
Fig. 4. Delft3D-Flow predicted water temperature (upper layer) using Exp#1 (a) and using Exp#2 (b) for July–August over 2009–2018. Difference between predicted water temperature using Exp#1 and Exp#2 (Exp#2 - Exp#1) (c). Histogram showing the frequency of the temperature differences shown in c (d).

Additionally, Fig. 3 shows both measured (blue line) and computed (red line) salinity and water temperature vertical profiles for a station located in the middle part of each ria during July and August averaged from 2009 to 2018. Shadows represent measured and numerical standard deviations. These vertical profiles show the accuracy of numerical simulations to reproduce field data.

Once the accuracy of the model to reproduce *in situ* data was assessed using the configuration of Exp#1, the average temperature field of Exp#1 and Exp#2 for July–August was compared over the period 2009 to 2018. Top layer temperature outputs for both experiments are depicted in Fig. 4a and Fig. 4b, respectively. Fig. 4c shows the difference between these two outputs ($\Delta T = T^{Exp\#2} - T^{Exp\#1}$). The histogram of Fig. 4d shows that more than 90% of the ΔT values are within the range −1 to 1 °C. In addition, ΔT tends to be positive, mostly between 0 and 0.75 °C with an average bias of 0.40 °C (Fig. 4c). Despite the different nature of data sources used to force the model, both configurations provide, in general, a similar pattern, although numerical results from Exp#2 tend to overestimate the results of Exp#1. The agreement between both setups shows that Delft3D-Flow forced with climatic data can be accurately used to simulate future temperature conditions in the Rías Baixas.

3.2. Physical parameters that can affect mussel production under the future climate warming

Different physical parameters that can change in the future affecting mussel production, like water temperature and stratification, will be analyzed in next subsections. Temperature will be responsible of mussels comfort conditions related to thermal stress while stratification will be a proxy to assess the capability of the water column to allow vertical movements and, hence, the vertical exchange of nutrients and oxygen.

3.2.1. Water temperature

Water temperature is the main physical parameter that affects the mussel productivity of the Rías Baixas. Mussels survive in a wide range of temperature, being able to withstand high temperatures (Gosling, 1992), although the optimal range for mussel growth is narrower. The mechanisms of mussels' adaptation to the water
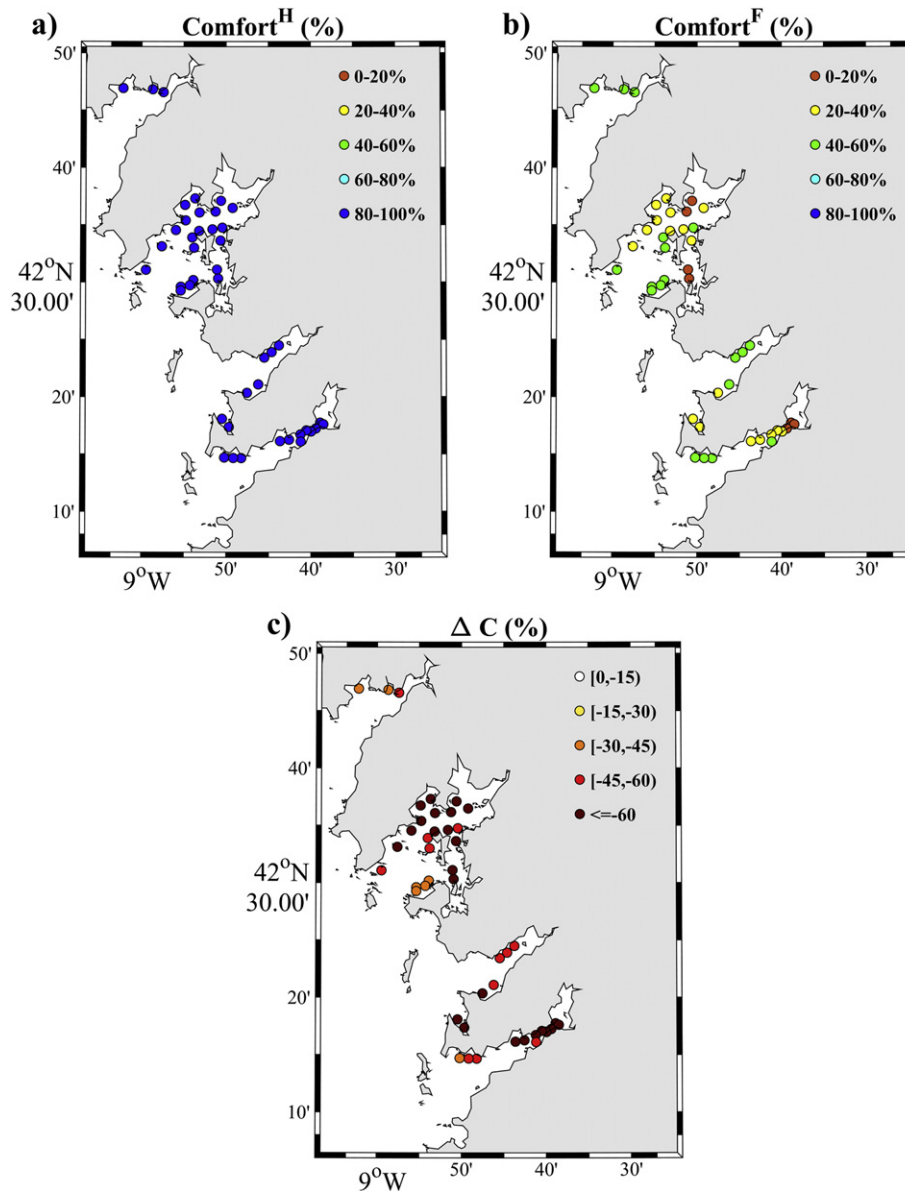
Fig. 5. Percentage of time (July–August) during which mussels are within the comfort temperature range (14–20 °C) for the historical period (a), the future (b) and the difference (Future-Historical, c) considering surface layers [0–6] m.

temperature increase may be limited by their physiological limits. Some studies indicate that mussel has a limited capacity to modify their physiological tolerance limit and that they are experiencing temperatures close to it (Tomanek, 2008; Ioannou et al., 2009). The optimal range for *Mytilus galloprovincialis* growth was determined between 14 and 20 °C following previous research on the effect of water temperature on the growth and mortality of mussels (https://longline.co.uk/meta/List; Hrs-Brenko et al., 1977; Anestis et al., 2007; Peharda et al., 2007; Sánchez-Lazo and Martínez-Pita, 2012; Kroeker et al., 2014). The comfort index was considered as the percentage of time in which water temperature remains within that optimal range. Mussel comfort is 80–100% at the upper layers (0–6 m) for all mussel rafts for the historical period (Fig. 5a). However, comfort at these upper layers will be considerably reduced by the end of the century (Fig. 5b) with a percentage ranging from 40% to 60% in the outer areas of the rias and from 20% to 40% in the middle part, especially near the north shore. The lower values (0–20%) are observed near the mouths of the rivers, possibly due to the shallowness of the zone. Changes in comfort ($\Delta C =$

Comfort^F − Comfort^H in Fig. 5c) will be always negative, reaching values < −60% in most of the points, which results in a remarkable loss in the comfort conditions for the future, which can eventually cause biological stress and reduce mussel growth.

The comfort index at deep layers (6–12 m, Fig. 6) shows a similar pattern than at surface ones. For the historical period, it is in the interval 80–100% (Fig. 6a) for all mussel rafts, equal than previously calculated for surface layers (Fig. 5a), and it is also reduced for the future projections (Fig. 6b). In these future projections the comfort index ranges from 60% to 100% in the outer areas of the rias, from 40% to 80% in the middle part and from 0% to 40% near the mouths of the rivers. These results show that the shallow areas will be more affected by ocean warming. Regarding ΔC (Fig. 6c), values are always negative but only reach < −60% near the river mouths, in general deep layers lose fewer comfort conditions than the upper ones. The locations were lower ΔC are observed correspond to the areas most affected by summer upwelling. The upwelled water, whose current temperature tends to range from 12 to 14 °C
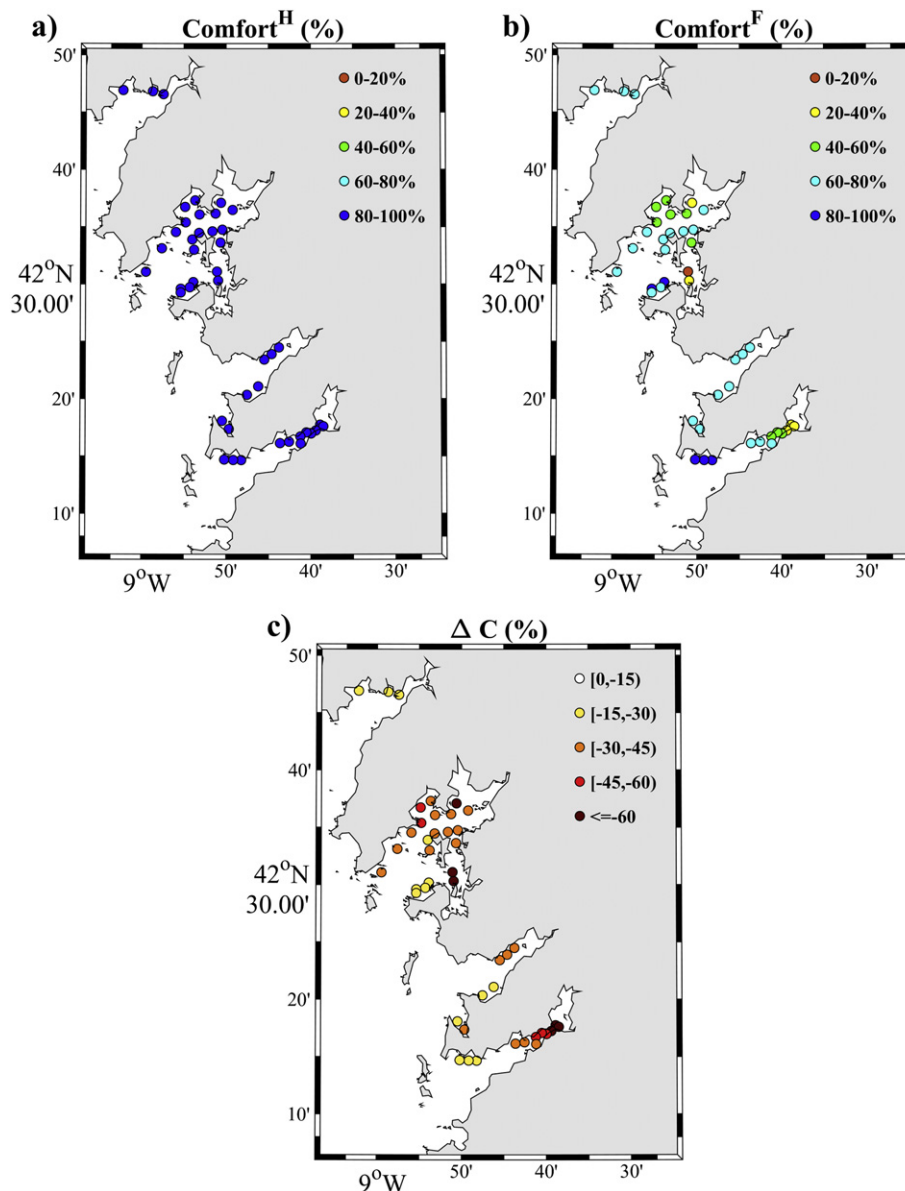
Fig. 6. Percentage of time (July–August) during which mussels are within the comfort temperature range (14–20 °C) for the historical period (a), the future (b) and the difference (Future-Historical, c) considering deep layers [6–12] m.

(Blanton et al., 1987; Prego et al., 2001; Alvarez et al., 2005), mitigate the water temperature rise in deep layers.

As for the future thermal comfort at deep layers (Fig. 6b), in general, it will be higher than at surface layers (Fig. 5b). This fact can have a negative impact on the productivity since, at present, the upper part of the ropes (first meters) tends to be more productive than the lower part (Fuentes et al., 2000; Figueras and Caceres-Martinez, 2007). On the other hand, although all of the locations show negative values, the reduction in future comfort will affects less to the outermost stations (Figs. 5b and 6b) and mainly in the deep layers. In summary, the outermost stations, where productivity is higher at present (Navarro et al., 1991; Pérez Camacho et al., 1995; Figueras and Caceres-Martinez, 2007) will be affected differently by ocean warming depending on the depth. The temperature rise of the deep layers will not have a very significant impact in comfort conditions while temperature will increase at surface layers leading to more stressed conditions for mussel growth.

Finally, it should be noted that this index only refers to thermal comfort not to the concentration of nutrients or oxygen of the upwelled water or to the light conditions.

3.2.2. Water stratification

Water stratification is another important physical parameter to analyze the future survival of mussel aquaculture activities within the Rías Baixas. Water stratification reduces vertical exchange and is usually related to the occurrence of harmful algae blooms (Álvarez-Salgado et al., 2008; Pitcher et al., 2010). The Brunt-Väisälä frequency was calculated and averaged through the water column to determine the stratification of the rias. The Brunt-Väisälä frequency (Fig. 7) shows that the innermost part of the rias is more stratified than the outermost one as it can be observed both for the historical (Fig. 7a) and future (Fig. 7b) period.

The percentage of change in future stratification relative to the historical one is shown in Fig. 7c. This percentage is calculated as $\Delta \overline{N} = 100 \times (\overline{N}^F - \overline{N}^H)/\overline{N}^H$, where the superscripts F and H refer to the future and historical period respectively. An increase in the future stratification is observed in most of the points, being the most significant changes (between 10% and 15%) located in the external part of the south coast of the rias of Pontevedra and Arousa. In general, the percentage of change decreases for the northern shores and, especially, in the areas most influenced by river discharge. Values can even be negative (less stratified
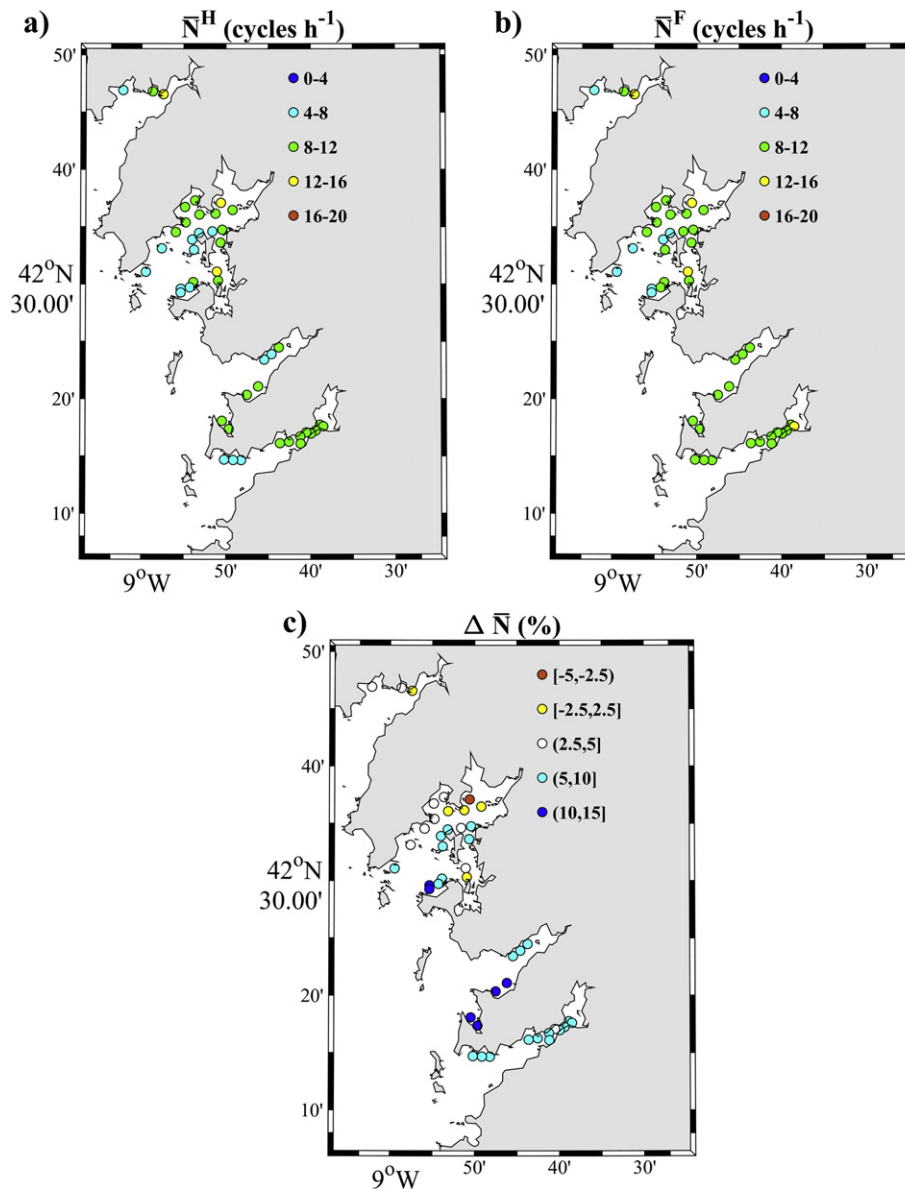
Fig. 7. Predicted mean Brunt-Väisälä frequency for July and August using Exp#2 at mussel raft polygons for (a) historical (1999–2019) period, (b) future (2080–2099) and (c) percentage of change in predicted future Brunt-Väisälä frequency respect to the historical one.

conditions in the future) in the area affected by the Ulla River, the river with the highest runoff in the area and, at a lesser extent, in the areas of influence of Umia River (also in the ria of Arousa) and Tambre River (Ría de Muros) (Fig. 1). The same behaviour was not observed in Vigo and Pontevedra due to the long distance between the mouth of the river and the sampling stations. The pattern is possibly related to the circulation pattern of the rias, where the outer area is more influenced by oceanic conditions while the inner part is controlled by river discharge. It was also observed that the thermocline will be deeper. According to Sousa et al. (2020), the future deepening of the thermocline will counteract the increase in upwelling favorable winds and will induced thermal stratification. The stratification will be more marked in the outer part of the rias while the future reduction in river discharge (https://hypeweb.smhi.se/explore-water/climate-impacts/europe-climate-impacts/) will diminish the haline stratification of the inner part of the rias. The projected increase in stratification, especially at the outer stations (the most productive ones according to Navarro et al. (1991), Pérez Camacho et al. (1995) and Figueras and Caceres-Martinez (2007)) will constitute a clear drawback for mussel exploitation. It will limit the vertical exchange of nutrients and oxygen and will give rise to the probable intensification of harmful algae blooms, increasing the number of days that mussel raft polygons are inactive.

4. Conclusions

Numerical simulations using Delft3D-FLOW under historical and future RCP8.5 conditions were used to analyze how climate change will affect the Rías Baixas at the end of the 21st century and its possible impact on the main physical parameters (water temperature and stratification) that affect mussel aquaculture productivity.

The general rise in water temperature will increase the time during which mussels will be subjected to thermal stress conditions. The impact on the water column will not be homogeneous, upper layers will be more affected than the deep ones. The comfort level of mussels will be reduced by more than 60% in the upper layers in most of the mussel raft polygons. Regarding deeper layers, the mussels comfort conditions will be reduced but less than in the upper layers.

Water column stratification will increase in most of the stations, particularly in the outer areas of the rias. A reduction in stratification is only observed in the areas most affected by river discharge. This increase in water stratification will limit the vertical exchange of nutrients and oxygen and will give rise to less favorable conditions for aquaculture.

The present work helps to improve knowledge about how climate change can affect mussel industry in the Rías Baixas. Analysis of physical parameters shows that changing the location to most suitable areas to ensure aquaculture of mussel raft polygons may help to mitigate the effect of climate change in mussel productivity. The outer areas of the rias seem to be more advisable for new locations.

Declaration of competing interest

The authors declare that they have no known competing financial interests or personal relationships that could have appeared to influence the work reported in this paper.

References

Aguiar, E., Piedracoba, S., Álvarez-Salgado, X.A., Labarta, U., 2017. Circulation of water through a mussel raft: clearance area vs. idealized linear flows. Rev. Aquac. 9, 3–22. https://doi.org/10.1111/raq.12099.

Alvarez, I., deCastro, M., Gomez-Gesteira, M., 2005. Inter- and intra-annual analysis of the salinity and temperature evolution in the Galician Rías Baixas–ocean boundary (northwest Spain). J. Geophys. Res. 110. https://doi.org/10.1029/2004JC002504.

Álvarez-Salgado, X.A., Labarta, U., Fernández-Reiriz, M.J., Figueiras, F.G., Rosón, G., Piedracoba, S., Filgueira, R., Cabanas, J.M., 2008. Renewal time and the impact of harmful algal blooms on the extensive mussel raft culture of the Iberian coastal upwelling system (SW Europe). Harmful Algae 7, 849–855. https://doi.org/10.1016/j.hal.2008.04.007.

Anestis, A., Lazou, A., Pörtner, H.O., Michaelidis, B., 2007. Behavioral, metabolic, and molecular stress responses of marine bivalve *Mytilus galloprovincialis* during long-term acclimation at increasing ambient temperature. Am. J. Phys. Regul. Integr. Comp. Phys. 293, R911–R921. https://doi.org/10.1152/ajpregu.00124.2007.

Anestis, A., Pörtner, H.O., Karagiannis, D., Angelidis, P., Staikou, A., Michaelidis, B., 2010. Response of *Mytilus galloprovincialis* (L.) to increasing seawater temperature and to marteliosis: metabolic and physiological parameters. Comp. Biochem. Physiol. A Mol. Integr. Physiol. 156, 57–66. https://doi.org/10.1016/j.cbpa.2009.12.018.

Blanton, J.O., Tenore, K.R., Castillejo, F., Atkinson, L.P., Schwing, F.B., Lavin, A., 1987. The relationship of upwelling to mussel production in the rias on the western coast of Spain. J. Mar. Res. 45, 497–511.

Cáceres-Martínez, J., Figueras, A., 1998. Distribution and abundance of mussel (*Mytilus galloprovincialis* Lmk) larvae and post-larvae in the Ria de Vigo (NW Spain). J. Exp. Mar. Biol. Ecol. 229, 277–287. https://doi.org/10.1016/S0022-0981(98)00059-8.

Cáceres-Martínez, J., Robledo, J.A.F., Figueras, A., 1993. Settlement of mussels *Mytilus galloprovincialis* on an exposed rocky shore in Ria de Vigo, NW Spain. Mar. Ecol. Prog. Ser. 93, 195–198. https://doi.org/10.3354/meps093195.

Cane, M.A., Clement, A.C., Kaplan, A., Kushnir, Y., Pozdnyakov, D., Seager, R., Zebiak, S.E., Murtugudde, R., 1997. Twentieth-Century sea surface temperature trends. Science 275, 957–960. https://doi.org/10.1126/science.275.5302.957.

Casabella, N., Lorenzo, M.N., Taboada, J.J., 2014. Trends of the Galician upwelling in the context of climate change. J. Sea Res. 93, 23–27. https://doi.org/10.1016/j.seares.2014.01.013.

Cordeiro Pires, A., Nolasco, R., Rocha, A., Ramos, A.M., Dubert, J., 2016. Climate change in the Iberian Upwelling System: a numerical study using GCM downscaling. Clim. Dyn. 47, 451–464. https://doi.org/10.1007/s00382-015-2848-y.

Des, M., deCastro, M., Sousa, M.C., Dias, J.M., Gómez-Gesteira, M., 2019. Hydrodynamics of river plume intrusion into an adjacent estuary: the Minho River and Ria de Vigo. J. Mar. Syst. 189, 87–97. https://doi.org/10.1016/j.jmarsys.2018.10.003.

Diz, A.P., Presa, P., 2009. The genetic diversity pattern of *Mytilus galloprovincialis* in Galician Rías (NW Iberian estuaries). Aquaculture 287, 278–285. https://doi.org/10.1016/j.aquaculture.2008.10.029.

Duarte, C.M., Wu, J., Xiao, X., Bruhn, A., Krause-Jensen, D., 2017. Can seaweed farming play a role in climate change mitigation and adaptation? Front. Mar. Sci. 4, 100. https://doi.org/10.3389/fmars.2017.00100.

Evans, G., Prego, R., 2003. Rias, estuaries and incised valleys: is a ria an estuary? Mar. Geol. 196, 171–175. https://doi.org/10.1016/S0025-3227(03)00048-3.

FAO (Ed.), 2017. Adaptation Strategies of the Aquaculture Sector to the Impacts of Climate Change (Rome).

FAO (Ed.), 2018. Meeting the Sustainable Development Goals, the State of World Fisheries and Aquaculture (Rome).

Figueiras, F.G., Labarta, U., Reiriz, M.F., 2002. Coastal upwelling, primary production and mussel growth in the Rías Baixas of Galicia. Sustainable Increase of Marine Harvesting: Fundamental Mechanisms and New Concepts. Springer, pp. 121–131.

Figueras, A., Caceres-Martinez, J., 2007. Cultivo del mejillón en Galicia. In: Figueras, A. (Ed.), Biología y Cultivo del Mejillón (*Mytilus galloprovincialis*) en Galicia. Consejo Superior de Investigaciones Científicas, Madrid, pp. 19–43.

Fuentes, J., Reyero, I., Zapata, C., Alvarez, G., 1994. Production traits of the mussel *Mytilus galloprovincialis* cultured in Galicia (NW of Spain): relative effects of source of seed and growing environment. Aquaculture 122, 19–31.

Fuentes, J., Molares, J., Villalba, A., 1998. Growth, mortality and parasitization of mussels cultivated in the Ría de Arousa (NW Spain) from two sources of seed: intertidal rocky shore vs. collector ropes. Aquaculture 162, 231–240.

Fuentes, J., Gregorio, V., Giráldez, R., Molares, J., 2000. Within-raft Variability of the Growth Rate of Mussels, *Mytilus galloprovincialis*, Cultivated in the Ría de Arousa (NW Spain). p. 14.

Fuentes, J., López, J.L., Mosquera, E., Vázquez, J., Villalba, A., Álvarez, G., 2002. Growth, mortality, pathological conditions and protein expression of *Mytilus edulis* and *M. galloprovincialis* crosses cultured in the Ría de Arousa (NW of Spain). Aquaculture 213, 233–251. https://doi.org/10.1016/S0044-8486(02)00046-7.

Gestoso, I., Arenas, F., Olabarria, C., 2016. Ecological interactions modulate responses of two intertidal mussel species to changes in temperature and pH. J. Exp. Mar. Biol. Ecol. 474, 116–125. https://doi.org/10.1016/j.jembe.2015.10.006.

Gillooly, J., Charnov, E.L., West, G.B., Savage, V.M., Brown, J.H., 2002. Effects of size and temperature on developmental time. Nature 417, 70–73. https://doi.org/10.1038/417070a.

Gosling, E., 1992. The Mussel Mytilus: Ecology, Physiology, Genetics and Culture. Elsevier, Amsterdam.

Hrs-Brenko, M., Claus, C., Bubic, S., 1977. Synergistic effects of lead, salinity and temperature on embryonic development of the mussel Mytilus galloprovincialis. Mar. Biol. 44, 109–115. https://doi.org/10.1007/BF00386951.

Ioannou, S., Anestis, A., Pörtner, H.O., Michaelidis, B., 2009. Seasonal patterns of metabolism and the heat shock response (HSR) in farmed mussels Mytilus galloprovincialis. J. Exp. Mar. Biol. Ecol. 381, 136–144. https://doi.org/10.1016/j.jembe.2009.09.014.

Kroeker, K.J., Gaylord, B., Hill, T.M., Hosfelt, J.D., Miller, S.H., Sanford, E., 2014. The role of temperature in determining species' vulnerability to ocean acidification: a case study using *Mytilus galloprovincialis*. PLoS One 9, e100353. https://doi.org/10.1371/journal.pone.0100353.

López, J.L., Mosquera, E., Fuentes, J., Marina, A., Vázquez, J., Alvarez, G., 2001. Two-dimensional gel electrophoresis of *Mytilus galloprovincialis*: differences in protein expression between intertidal and cultured mussels. Mar. Ecol. Prog. Ser. 224, 149–156. https://doi.org/10.3354/meps224149.

Mesas, A., Tarifeño, E., 2015. Temperaturas letales superiores para el mejillón, *Mytilus galloprovincialis* (Lamarck, 1819), en la costa de Chile central. Lat. Am. J. Aquat. Res. 11.

Navarro, E., Iglesias, J.I.P., Perez Camacho, A., Labarta, U., Beiras, R., 1991. The physiological energetics of musselsd (*Mytilus galloprovincialis* Lmk) from different cultivation rafts in the Ria de Arosa (Galicia, N.W. Spain). Aquaqulture 94, 197–212.

Peharda, M., Župan, I., Bavčević, L., Frankić, A., Klanjšček, T., 2007. Growth and condition index of mussel *Mytilus galloprovincialis* in experimental integrated aquaculture. Aquaculture Res 38, 1714–1720. https://doi.org/10.1111/j.1365-2109.2007.01840.x.

Pérez Camacho, A., Labarta, U., Beiras, R., 1995. Growth of mussels (*Mytilus edulis galloprovincialis*) on cultivation rafts: influence of seed source, cultivation site and phytoplankton availability. Aquaculture 138, 349–362. https://doi.org/10.1016/0044-8486(95)01139-0.

Pérez Muñuzuri, V., Fernández Cañamero, M., Gómez Gesteira, J.L., 2009. Evidencias e impactos do cambio climático en Galicia. Consellería de Medio Ambiente e Desenvolvemento Sostible, Santiago de Compostela.

Pitcher, G.C., Figueiras, F.G., Hickey, B.M., Moita, M.T., 2010. The physical oceanography of upwelling systems and the development of harmful algal blooms. Prog. Oceanogr. 85, 5–32. https://doi.org/10.1016/j.pocean.2010.02.002.

Prego, R., Dale, A.W., deCastro, M., Gómez-Gesteira, M., Taboada, J.J., Montero, P., Villareal, M.R., Pérez-Villar, V., 2001. Hydrography of the Pontevedra Ria: intra-annual spatial and temporal variability in a Galician coastal system (NW Spain). J. Geophys. Res. 106, 19845–19857. https://doi.org/10.1029/2000JC000775.

Sánchez-Lazo, C., Martínez-Pita, I., 2012. Effect of temperature on survival, growth and development of *Mytilus galloprovincialis* larvae. Aquac. Res. 43, 1127–1133. https://doi.org/10.1111/j.1365-2109.2011.02916.x.

Sousa, M.C., deCastro, M., Alvarez, I., Gomez-Gesteira, M., Dias, J.M., 2017. Why coastal upwelling is expected to increase along the western Iberian Peninsula over the next century? Sci. Total Environ. 592, 243–251. https://doi.org/10.1016/j.scitotenv.2017.03.046.

Sousa, M.C., Ribeiro, A., Des, M., Gomez-Gesteira, M., deCastro, M., Dias, J.M., 2020. NW Iberian Peninsula coastal upwelling future weakening: competition between wind intensification and surface heating. Sci. Total Environ. 703, 134808. https://doi.org/10.1016/j.scitotenv.2019.134808.

Spyrakos, E., González Vilas, L., Torres Palenzuela, J.M., Barton, E.D., 2011. Remote sensing chlorophyll a of optically complex waters (rias Baixas, NW Spain): application of a regionally specific chlorophyll a algorithm for MERIS full resolution data during an upwelling cycle. Remote Sens. Environ. 115, 2471–2485. https://doi.org/10.1016/j.rse.2011.05.008.

Tomanek, L., 2008. The importance of physiological limits in determining biogeographical range shifts due to global climate change: the heat-shock response. Physiol. Biochem. Zool. 81, 709–717. https://doi.org/10.1086/590163.

Zippay, M.L., Helmuth, B., 2012. Effects of temperature change on mussel, *Mytilus*. Integrative Zoology 7, 312–327. https://doi.org/10.1111/j.1749-4877.2012.00310.x.

The impact of climate change on the geographical distribution of habitat-forming macroalgae in the Rías Baixas

M. Des[a]*, B. Martínez[b], M. deCastro[a], R. M. Viejo[b], M.C. Sousa[c] and M. Gómez-Gesteira[a]

[a] Environmental Physics Laboratory (EphysLab), CIM-UVIGO, Universidade de Vigo, Edificio Campus da Auga, 32004 Ourense, Spain.

[b] Departamento de Biología y Geología, Universidad Rey Juan Carlos, E-28933, Móstoles, Madrid, Spain,

[c] CESAM, Physics Department, University of Aveiro, Aveiro 3810-193, Portugal.

* Corresponding author.

E-mail address: mdes@uvigo.es (M. Des).

Abstract

In the current scenario of climate change characterized by a generalized warming, many species are facing local extinctions in areas that are near their thermal tolerance threshold. At present, the southern limit of the geographical distribution of several intertidal seaweeds is located in the Northwest Iberian Peninsula and the Rías Baixas may be acting as contemporary refugia for large habitat-forming macroalgae. Therefore, it is necessary to analyze future changes induced by ocean warming in this area that may induce changes in macroalgae populations. The Delft3D-Flow model forced with climatic data was used to calculate July-August sea surface temperature (SST) for the present (1999-2018) and for the far future (2080-2099). Mean daily SST was used to develop and calibrate a mechanistic geographical distribution model based on the thermal survival threshold of two habitat-forming macroalgaes, *Himanthalia elongata* and *Bifurcaria bifurcata.* Results show that *H. elongata* will become extinct in the Rías Baixas by the end of the century, while *B. bifurcata* and other habitat-forming species of similar thermal tolerance may occupy potential free sites left by the decline in *H. elongata.*

Keywords: climate change; macroalgae; intertidal organisms; species distribution model; Delft3D; CORDEX; CMIP5, RCP8.5

1. Introduction

Ecological systems have to face the modification in environmental conditions that global climate change is causing worldwide (Chen et al., 2011; McMenamin et al., 2008; Parmesan et al., 1999; Poloczanska et al., 2016, 2013). In terrestrial and marine environments, species have to deal with a general increase in warming conditions, which are not homogeneous everywhere (Cane et al., 1997). Often it results in local extinctions at the low latitude range limits of the species distributions (Wiens, 2016). This range contraction and local decrease are especially worrying when it affects conspicuous habitat-forming species because they provide structure, shelter and food to many accompanying species that form the ecological community (they are ecosystem engineers *sensu* (Jones et al., 1994). The pattern of climate change and, in particular, warming may be heterogeneous across the latitudinal gradient of a species distribution (Helmuth et al., 2006) and there may be colder favorable spots at this range margin. These cold spots i.e. contemporary climatic refugia (Ashcroft, 2010; Keppel et al., 2012), may favor the persistence of edge populations.

Bakun (1990) hypothesized that global warming could strength coastal upwelling intensity due to the increase in land-ocean thermal contrast. The strengthening of upwelling-favorable winds would result in cooling of the ocean surface. This hypothesis has been tested for different upwelling systems, finding different trends and concluding that each system responds to global warming differently (Sydeman et al., 2014; Varela et al., 2015; Wang et al., 2015). Despite this, coastal upwelling regions show lower warming rates than the adjacent ocean, buffering the ocean warming (Santos et al., 2012; Bakun et al., 2015; Varela et al., 2018; Seabra et al., 2019). In the same way, the areas affected by river plumes usually show lower warming rates than the adjacent ocean water (Costoya

2

et al., 2017, 2016). Thereby, coastal upwelling regions, estuaries and adjacent coastal areas affected by river plumes may represent climatic refugia for many species.

Coastal rocky systems are among the most productive marine areas (Smale and Wernberg, 2013). In temperate latitudes, these environments are dominated by macroalgae which are declining at a global scale (Kumagai et al., 2018). Kelp forests and the large intertidal macroalgae meadows are threatened all over the planet by climate change and other anthropogenic stressors (Strain et al., 2014; Wernberg et al., 2016). The geographical distribution of these species has traditionally been related to water temperature, in addition to other physical factors of regional and local variation, such as marine salinity (reviewed in Lüning, 1990). The southern, lower latitudinal limit of the geographic distribution of several kelps and large intertidal seaweeds is located in the Northwest Iberian Peninsula (NWIP). A marked contraction of the species range in this area has been detected in recent years (reviewed in Casado-Amezúa et al., 2019). This is the case of *Himathalia elongata*, who has disappeared from a coastal strip of approximately 130 km since the start of this century in the North Iberian Peninsula (NIP) (Duarte et al., 2013), due to its restricted thermal tolerance (Martínez et al., 2015). Currently, its distribution is restricted to the NWIP corner, including the presence inside the large embayments of the Galician rias and in areas moderately exposed to waves (Martínez et al., 2012). This species exemplifies the decline response observed in other habitat-forming macroalgae of cold-temperate affinities. By contrast, the degree of resilience to warming of other macroalgae with greater tolerance to thermal stress, such as *Bifurcaria bifurcata*, is still unknown. Recent studies indicate that these species of warm-temperate affinity is also declining in NIP (Méndez-Sandín and Fernández, 2016).

The Rías Baixas are four flooded incised valleys (Evans and Prego, 2003) located on the NWIP, at the northern limit of the eastern North Atlantic Upwelling system. They

3

are the southernmost rias of Galicia (Fig. 1). Due to their location, they are strongly influenced by upwelling events. Upwelling, together with other co-varying factors as the higher water and nutrient supply, protection from wave action or river flow (Duarte and Viejo, 2018) may be responsible for the rias to be acting as contemporary refugia to warming for large, habitat-forming macroalgae (Lourenço et al., 2016). Although it is expected an intensification of upwelling-favorable winds in the NWIP for the future (Rykaczewski et al., 2015; Sousa et al., 2017). Sousa et al. (2020) have recently obtained that coastal upwelling will be less effective due to the increase in the stratification of the upper layer caused by sea surface warming. In fact, Des et al. (2020) determined that the future increase in water temperature and stratification will negatively affect the growth of *Mytilus galloprovincialis*, the specie used for mussel aquaculture in the area. Considering all these results a question arises, will the Rías Baixas act as climatic refugia to warming for large habitat-forming macroalgae in the future?

The aim of this work is to determine how climate change, and SST warming in particular, will affect the geographical distribution of two intertidal macroalgae, *Himanthalia elongata* and *Bifurcaria bifurcata*, within the Rías Baixas. Firstly, SST data, computed by means of Delft3D-Flow numerical model, were used to detect heat waves that may affect each of the species. Then, a mechanistic distribution model based on the thermal survival threshold for adult plants of each species was calibrated and used to determine the thermal habitat suitability for the present (1999-2018) and by the end of the century (2080-2099). Thermal survival thresholds for adult plants were previously determined by Martínez et al. (2015).
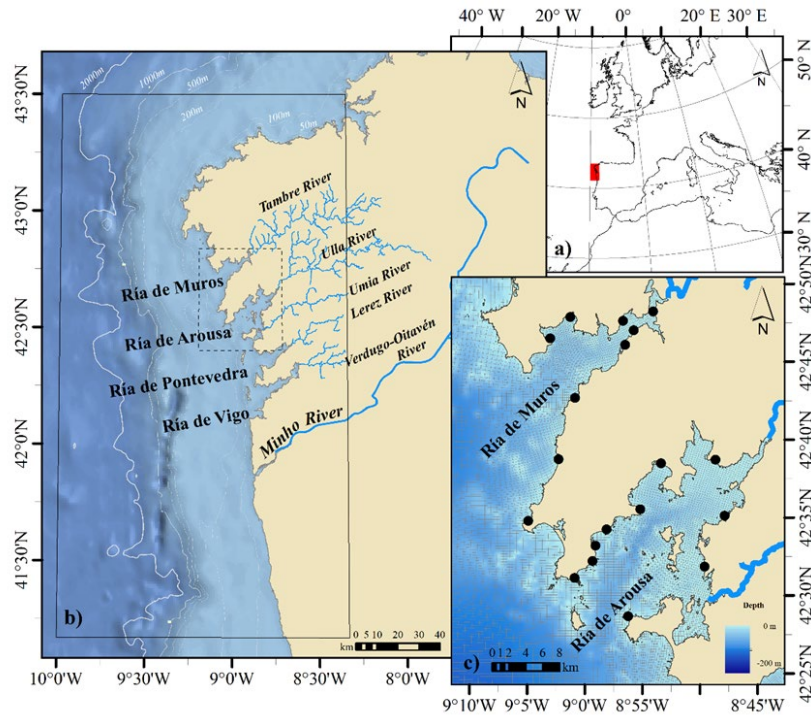
Fig. 1. (a) Location of the study area along the northwestern coast of the Iberian Peninsula. **(b)** The box indicates the modeled area. **(c)** A close-up view of the Ria de Muros and the Ria de Arousa is shown with the numerical grid and the position of TidbiT data loggers sampling stations (black points).

2. Methodology

2.1. Hydrodynamic numerical model

Sea surface temperature (SST) was computed using the hydrodynamic numerical model Delft3D-Flow. Numerical simulations of transport conditions were performed using the mesh, parametrization and implementation previously validated for the Rías Baixas by Des et al. (2019, 2020). These simulations validate de model when it is forced both with data from *in situ* measures and reanalysis and with data from climate models. The main characteristics of the numerical model configuration are described below; however, for a more detailed description of the parametrization see Des et al. (2019, 2020).

The computational grid covers from 8.33ºW to 10.00ºW and from 41.18ºN to 43.50ºN (Fig. 1b, rectangle). A curvilinear irregular grid was adopted with 452 x 446 cells, and a mean resolution of 2200 m × 800 m on the west boundary, gradually increasing towards onshore, allowing higher resolution in the Rias (220 m x 140 m) and the Minho estuary (50 m × 77 m). This high spatial resolution allows Delft3D-Flow to provide, among other variables, SST data in the areas of the Rías Baixas that represent the natural habitats for intertidal macroalgae such as *Himanthalia elongata* and *Bifurcaria bifurcata*. The model uses 16 sigma layers with refined surface layers at the surface, this configuration allows to reproduce the ocean-atmospheric dynamics that characterize the SST.

The bathymetric dataset for model simulations was created compiling data from different sources. Multibeam-sourced bathymetry with a resolution of 5 m for the rias of Vigo and Pontevedra was provided by the General Fishing Secretary. The bathymetry of the Ría de Arousa, the Ría de Muros and the adjacent shelf area was obtained from nautical charts of the Spanish Navy Hydrographical Institute. The Minho estuary bathymetry was provided by the Portuguese Navy Hydrographic Institute. Gaps in the dataset were filled using data from the General Bathymetric Chart of the Oceans with a horizontal resolution of 30 arc seconds (GEBCO, https://www.gebco.net/).

The oceanic boundary was forced with transport conditions (salinity and water temperature) and water level. Tidal harmonic constituents (M_2, S_2, N_2, K_2, K_1, O_1, P_1, Q_1, M_{sF}, MM, M_4, MS_4, MN_4) were obtained from the model TPXO 7.2 TOPEX/Poseidon Altimetry (http://volkov.oce.orst.edu/tides/global.html) and were prescribed as astronomical forcing at the oceanic open boundary. River discharges are imposed as fluvial open boundary condition. The exchange of heat through the free surface was simulated using the "absolute flux, net solar radiation" model. This model requires

6

relative humidity, air temperature and the combined net solar (short wave) and net atmospheric (longwave) radiation. The heat loss due to evaporation and convection is computed by the model (Deltares, 2014). Wind components and pressure values are imposed varying spatially.

Following the procedure described by Des et al. (2020), two numerical experiments were performed. In the first one (Exp#1 from now on), Delft3D was mainly forced with measured and reanalysis data, and the hydrodynamics of the study area were simulated for a historical period. In the second experiment (Exp#2 from now on), the model was mainly forced with historical and future data from the Regional Circulation Models (RCM) driven by General Circulation Models (GCM) executed in the framework of the Coordinated Regional Climate Downscaling Experiment (CORDEX) project (http://www.cordex.org/). Both experiments were run for July and August using a spin-up period of two weeks.

Exp#1 was run for 2012 to be compared with *in situ* coastal temperature data. The thermohaline boundary conditions for Exp#1 were imposed using daily data from the operational Atlantic-Iberian Biscay Irish-Ocean Physics Reanalysis (http://marine.copernicus.eu/). Data from MeteoGalicia Weather Research and Forecasting Model (https://www.meteogalicia.gal),, were used as surface boundary conditions. Minho River discharge data were provided by the Confederación Hidrográfica Miño-Sil (http://saih.chminosil.es), while Verdugo-Oitavén, Lérez, Ulla, and Umia rivers discharge data were retrieved from the MeteoGalicia database.

Exp#2 was run for the historical (1999 - 2018) and future (2080-2099) periods under climatic conditions to perform geographical distribution maps of *Himanthalia elongata* and *Bifurcaria bifurcata* for the present and the future climate periods. Data for ocean boundary conditions were retrieved from the MOHC-HadGEM2-Es GCM outputs

7

(https://esgf-node.ipsl.upmc.fr/projects/esgf-ipsl/). Surface boundary conditions were obtained from the MOHC-HadGEM2-Es-RCA4 RCM outputs (http://www.cordex.org/). Among the available scenarios, the RCP8.5 greenhouse gas emission scenario was considered for future projections. This scenario is quite likely according to the present greenhouse gas emission increase (Brown and Caldeira, 2017). Climatologic river discharge data were obtained from the Hype Web portal (https://hypeweb.smhi.se) and a reduction of 25% in river discharges was considered for future projections (https://hypeweb.smhi.se/explore-water/climate-impacts/europe-climate-impacts/).

2.1.1. Validation of the Hydrodynamic numerical model

As stated above, the capability of the hydrodynamic numerical model to reproduce the hydrodynamic conditions of the Rías Baixas was previously assessed and validated by Des et al. (2019, 2020). Nevertheless, further checking of the skill of the numerical model to reproduce water temperature in shallow coastal areas was carried out using temperature data measured *in situ* using 19 TidbiT data loggers (9 located in the Ría de Muros and 10 in the Ría de Arousa, Fig. 1c). Data loggers recorded the temperature every 30 minutes from January 2012 to September 2013 but only temperatures of August 2012 at the time of high tides were used to validate the model. *In situ* water temperature measurements were compared with simulated temperature data using the root mean square error and bias.

The root mean square error (RMSE) was calculated as

$$RMSE = \left\{ \frac{1}{N} \sum_{i=1}^{N} |X_{obs}(t_i) - X_{mod}(t_i)|^2 \right\}^{1/2} \tag{1}$$

where $X_{obs}(t_i)$ and $X_{mod}(t_i)$ are the measured and Delft3D computed water temperature, respectively, and N is the number of samples.

8

The bias was calculated as

$$Bias = \frac{1}{N}\sum_{i=1}^{N}(X_{mod}(t_i) - X_{obs}(t_i)) \tag{2}$$

where $X_{obs}(t_i)$ and $X_{mod}(t_i)$ are the measured and Delft3D computed water temperature, respectively, and N is the number of samples.

The bias and RMSE were averaged in order to obtain a mean value for each station.

2.2. Mechanistic modeling of the geographic distribution of macroalgae

The distribution models were based on the thermal tolerance threshold for the species survival. The water temperature data obtained from the first layer of the hydrodynamic model was considered as the predictive variable because SST is significantly correlated with the distribution of *H. elongata* and *B. bifurcata,* as it happens in general in seaweeds (Lüning, 1990; Martínez et al., 2012). The number of days (with a minimum number of 10 consecutive days) during which the daily mean SST was higher than the physiological threshold of the algae was calculated for the coastal areas of the Rías Baixas. For a better understanding, the result was expressed as percentage of the time both for historical (July-August 1999 - 2018) and future (July-August 2080-2099) periods. The physiological thresholds considered are based on the lethal conditions determined in tank experiments by Martínez et al. (2015). This lethal conditions occurred when the mean seawater temperature exceeded the specific threshold value of the species, 18 ºC and 24.7 ºC, for *H. elongata* and *B. bifurcata*, respectively, sometime between days 7 and 13 of the experiment (Martínez et al., 2015).

The presence/absence of *H. elongata* and *B. bifurcata* on the shore of the rias of Muros and Arousa was determined from a field survey carried out in 2005 to model the

distribution of these species in the Atlantic Spanish coast (Martínez et al., 2012). A total of 81 rocky locations were visited inside Rías Baixas. The survey was repeated in both rias during low spring tides in 2011. The distributional records of *H. elongata* were used to calibrate the mechanistic distribution model. This species was preferred over *B.bifurcata* because shows less prevalence in the study area. As the presence of a stable population depends on the conditions of several years, the map of percentage of time under lethal conditions for July-August 1999-2011 was used to perform the calibration. A percentage of time of approximately 33% was identified as the threshold for the presence of populations, i.e., none of the present populations was found in grid cells with more than 33% of the days under lethal conditions, which are the periods of at least 10 consecutive days of daily mean SST > 18 ºC (see results). This threshold was used to interpret the current (1999-2018) *H. elongata* maps of thermal habitat suitability, and their future (2080-2099) projections. Areas where the time under lethal conditions exceeds the 33% threshold were interpreted as locations of algae absence. For the remaining areas, three levels of habitat thermal suitability were defined: 1) P1 for values between 0 and 11% ([0, 11] %), representing the conditions farthest from the lethal threshold, 2) P2 for intermediate values ((11, 22] %), and 3) P3 for values between 22 and 33% ((22, 33] %), that may represent sub-lethal temperature conditions. The same criteria were used to interpret the *B. bifurcata* distribution maps (using a thermal survival threshold of 24.7 ºC, see above).

Favorability maps were made to indicate the likelihood of the presence of adequate conditions for *H. elongata* and/or *B. bifurcata* by comparing their maps of thermal habitat suitability. High suitability values (lethal conditions < 33% of the time) in a grid cell implies that *H. elongata* and *B. bifurcata* can be found, then the map will indicate coexistence. If suitability values indicate the absence of *H. elongata* but are

favorable for the presence *B. bifurcata*, then the map will reflect *B. bifurcata*. Finally, if the conditions are unfavorable for both, then the map indicates that this area is not favorable for any of the two algae (none).

3. Results and discussion

3.1. SST validation

Modeled and *in situ* water temperature at 1 m depth for August 2012 were compared by means of the mean bias and RMSE calculated for each TidbiT logger station (Figure 2). The pattern observed is similar in both rias and, in general, the model tends to underestimate *in situ* water temperature along the northern shores of the rias (Fig. 2 blue dots, negative bias). The model tends to overestimate the water temperature in the inner areas (Fig. 2 red dots, positive bias) and the bias is almost zero along the southern shores. The maximum positive, 0.95 ºC, and negative, -1.57 ºC bias observed are quite similar to those obtained by Des et al. (2020), 1.25 ºC and -1.44 ºC, respectively. In general, there are more stations with high bias and RMSE than those observed by Des et al. (2019, 2020) when they compare numerical and *in situ* vertical profiles in deeper sectors of the estuaries. These higher errors are likely due to both the location of the loggers in intertidal coastal areas and the limited horizontal resolution of the mesh due to the complex orography of these estuaries. As the dimensions of a cell within the rias is approximately 220 m × 140 m and the hydrodynamic model calculates the water temperature in the central point of the cell, the water temperature of cells near the coastline is calculated for a point ~100 m away from the data loggers position. Despite limitations, the adjustment of the hydrodynamic model can be considered good.
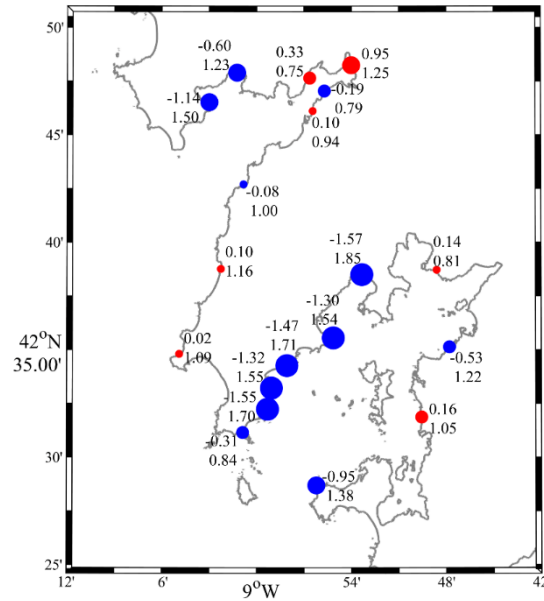
Fig. 2. Mean values of bias (upper number) (ºC) and RMSE (lower number) (ºC) obtained comparing Delft3D-Flow modeled and measured water temperature at 1 m depth for August 2012. Red dots indicate that the model overestimates *in situ* data (positive bias). Blue dots indicate that the model underestimates *in situ* data (negative bias). Dot size indicates the bias percentile.

3.2. Calibration of the species distribution model

The maximum percentage of time under lethal conditions suffered by any stable population of *H. elongata* for the period 1999-2011 (July-August) was 33%. In this study, this value was observed for the northernmost population located in the inner part of the Ría de Muros (Fig. 3, blue dot). When applying this threshold, the mechanistic models properly classify all the presences, however, many absences are still associated with high suitability values (Fig. 3). These absences can be associated to other factors, such as wave action, the presence of muddy and sandy substrates which are unfavorable for the settlement of *H. elongata*, or high atmospheric temperatures during low tide affecting those individuals inhabiting the intertidal (Martínez et al., 2012). Despite the model tending to over-predict the presence of *H. elongata*, it can provide useful information about potential areas of extinction in the future.

12
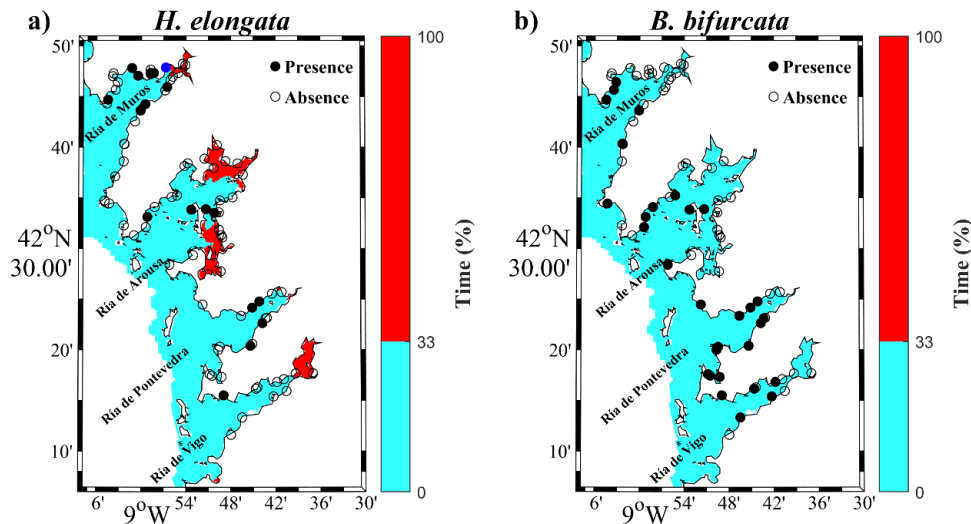
Fig. 3. Percentage of time (July-August 1999-2011) during which lethal conditions for *H. elongata* (a) and for *B. bifurcata* (b). Filled/empty black points indicate the presences/absences recorded in a field survey carried out in 2005 (and re-surveyed in 2011). Filled/empty blue point indicates the location of the presence record which supports lethal conditions for more percentage of time.

When applying the 33% threshold for *B. bifurcata*, taking into account that *B. bifurcata* does not survive in the grid cells when more than 33% of the days are periods of at least 10 consecutive days of daily mean SST > 24.7 ºC, the mechanistic model classifies all the presences properly but not the absences. This is because currently, the Rías Baixas are becoming thermal suitable for *B. bifurcata*, which is expanding within the rias (Martínez et al., 2012).

3.3. Maps of thermal habitat suitability

The potential effect of SST warming on the geographical distribution of *H. elongata* and *B. bifurcata* was estimated comparing the geographical map of thermal habitat suitability for the far future (2080-2099) with the present map (1999-2018).

13

The map of thermal habitat suitability of *H. elongata* for the present (Fig. 4a) shows that the thermal conditions of the Rías Baixas are most favorable to the presence of the algae. Unfavorable thermal conditions have been found in the inner areas of the rias, probably because the influence of the upwelling, which acts reducing water temperature, in these shallow areas is negligible. A more detailed analysis shows that the rias of Muros and Arousa display the most suitable conditions, although the time under lethal conditions increases in the middle part of the Ría de Arousa compared with the outer part. The rias of Pontevedra and Vigo show thermal conditions in the P2 range, indicating that the thermal conditions of these two rias are slightly less favorable than the conditions in the other two northern rias. The records of presence/absence of *H. elongata* and other species of cold-temperate intertidal fucaceae, e.g., *Fucus serratus*, collected during a field survey by Martínez et al. (2012), show a higher number of settlements in the rias of Muros and Arousa than in the rias of Pontevedra and Vigo. These observations support the differences in thermal conditions between the Rias Baixas since a greater number of settlements were registered in the estuaries where thermal conditions are more favorable.

Projections for the far future (Fig. 4b) under the RCP 8.5 greenhouse gas emission scenario indicate that thermal conditions in the Rías Baixas will be lethal for *H. elongata*, which implies that this species is projected to disappear. A range contraction of 21% was already estimated for this species by the reduction in its extent of occurrence in the Cantabrian Sea and Portuguese coast between the periods 1980's-1990's to 2013-2016, as part of a general declining trend observed for many cold-temperate fucoids and kelps at its southern range limit in the Iberian Peninsula (Duarte et al., 2013; Casado-Amezúa et al., 2019). *H. elongata*, together with a list of other species, was suggested to be included in the red list of endangered species of the Spanish government, a decision

14

supported by the results of this study. Currently, the signs of decline inside the rias are less than elsewhere in the open shore, so it can be considered that they are acting as contemporary refugia to warming for several species (Duarte and Viejo, 2018). In the same way, an important habitat-forming species, namely the kelp *Laminaria hyperborea*, with an upper lethal threshold of 23 ºC, has also suffered a decline inside the Galician rias (Casado-Amezúa et al., 2019). The decline of temperate macroalgae does not occur locally or regionally, it is becoming evident as global warming proceeds in areas as far as Australia and South Africa (Wernberg et al., 2016, 2013; IPCC). Therefore, in the case of *H. elongata*, whose tolerance limit (18 ºC) is lower than that of *L. hyperborean* (23 ºC), it can be considered that the Rías Baixas will no longer be refugia for this species by the end of the century.
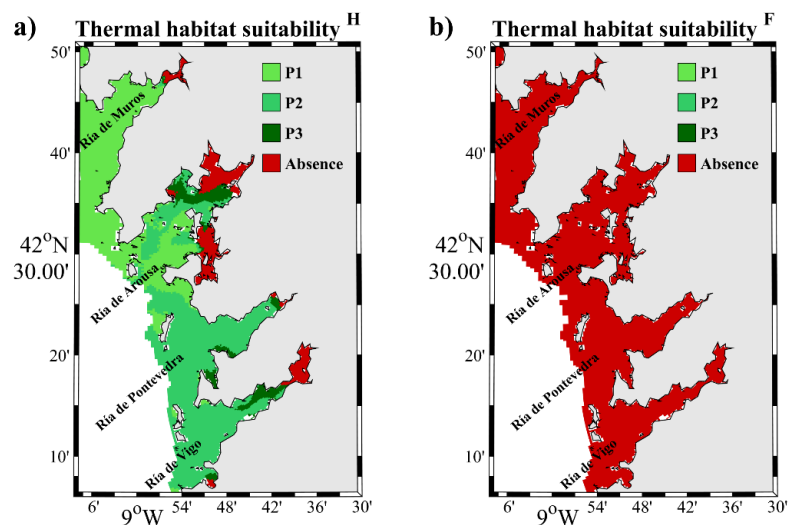
Fig. 4. Thermal habitat suitability for *H. elongata* based on modeled SST for July-August for the present (1999- 2018) (a) and the far future (2080-2099) (b). Green scale represents areas suitable for presence and red for absence. P1 represents the conditions farthest from the lethal ones, P2 intermediate values and P3 sub-lethal SST conditions.

Regarding *B. bifurcata*, whose lethal temperature threshold is higher (24.7°C) than H. *elongata* (18 °C), results for the present (Fig. 5a) show that the thermal conditions of the Rías Baixas are favorable to the presence of the algae. By the end of the century (Fig. 5b), this situation will not

15

vary greatly, and only the innermost part of the rias may turn inappropriate for the algae. As previously stated, the rias are considered contemporary refugia to warming for several species (Duarte and Viejo, 2018) because their tendency towards warming is lower than the trend of adjacent coastal areas. This lower tendency is due to the fact that the rias are located in the northern limit of the eastern North Atlantic Upwelling system which buffers the ocean warming (Santos et al., 2012; Bakun et al., 2015; Varela et al., 2018; Seabra et al., 2019). Thereby, and although the upwelling may be less effective in the future (Sousa et al. 2020), the water temperature within the estuaries will continue to be lower than that of the adjacent coastal areas and, then, they potentially represent climatic refugia for the persistence of *B. bifurcata*, and those of similar thermal tolerance.
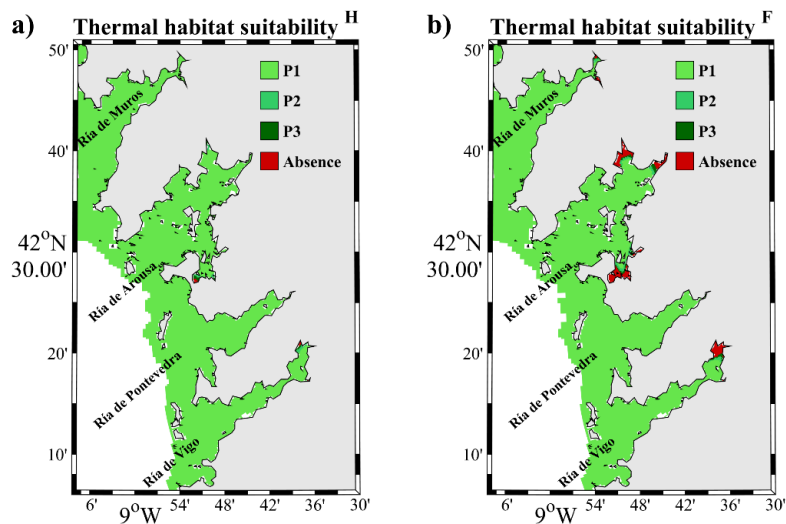
Fig. 5. Thermal habitat suitability for *B. bifurcata* based on modeled SST for July-August for the present (1999- 2018) (a) and the far future (2080-2099) (b). Green scale represents areas suitable for presence and red for absence. P1 represents the conditions farthest from the lethal ones, P2 intermediate values and P3 sub-optimal and sub-lethal SST conditions.

The upper survival thresholds of other habitat-forming macroalgae, which play an important ecological role as foundational species in the southern Atlantic coast, providing habitat and resources, are similar to that of *B. bifurcata*. Large intertidal fucoids, namely *Fucus serratus* and *Ascophyllum nodosum*, showed lethal conditions at about 24 and 25 ºC, respectively. The threatened kelp *Laminaria ochroleuca*, foundation species of the

16

subtidal kelp forest, has been shown to die back at 24.6 ºC (Franco et al., 2018). The abundant annual kelp *Saccorhiza polyschides*, has an upper survival threshold of 24-25ºC (tom Dieck and de Oliveira, 1993). The distributions of these species are suffering a drastic contraction in their extent of occurrence in the Cantabrian Sea and Portuguese coast, as well as local declines in abundance in some populations inside the rias, but most populations currently find refugia inside the rias and persist (Casado-Amezúa et al., 2019). Thus, we may hypothesize that the thermal conditions of the Rías Baixas will be favorable for all these species, as exemplified in this study by *B. bifurcata*.

Favorability maps (Fig. 6) also confirm that by the end of the century (Fig. 6b) the increase in the water temperature of the rias may lead to increased prevalence of *B. bifurcata* or the aforementioned habitat-forming species of similar thermal tolerance if they manage to occupied potential free sites left by the predicted decline of *H. elongata*.
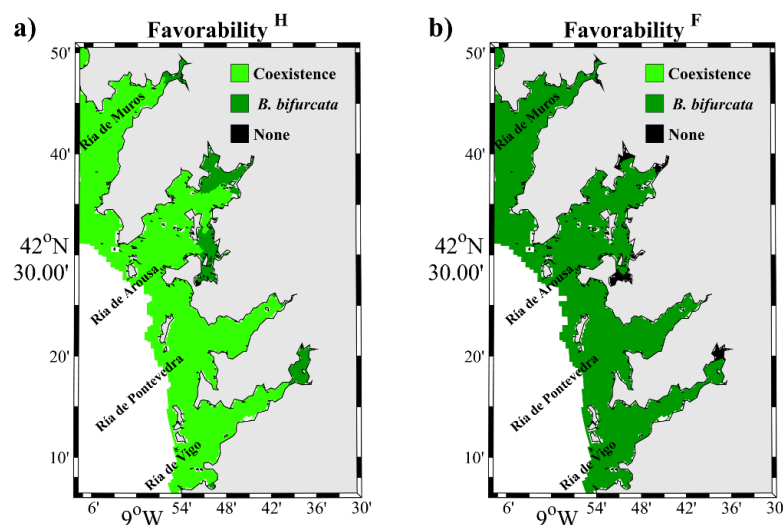
Fig. 6. Favorability maps for *H. elongate* and *B. bifurcata* based on lethal conditions for July-August for the present (1999- 2018) (a) and the far future (2080- 2099) (b). Light green represents the coexistence of both species, dark green the prevalence of B. *bifurcata* and black the absence of both species.

17

4. Summary

The effect of SST warming on the geographical distribution of two intertidal macroalgae, *Himanthalia elongata* and *Bifurcaria bifurcata* was elucidated in the Rías Baixas by the end of the century. The Rias Baixas are the contemporary refugia to warming for these habitat-forming macroalgae. The analysis was carried out using a mechanistic distribution model based on the thermal survival threshold, which used SST computed by Delft3D-Flow hydrodynamic model both at the present and by the end of the century under the RCP8.5 greenhouse gas emission scenario.

Projected SST data for the end of the century shows that the global sea temperature warming will increase the exposure time of macroalgae to heatwaves. This increase may lead to the local extinction of *H. elongata* and those macroalgae of similar thermal tolerance. However, the analysis of thermal habitat suitability for *B. bifurcata*, whose thermal survival threshold is greater than that of *H. elongata*, shows that, by the end of the century, thermal conditions may favor the settlement of these macroalgae and other habitat-forming species with a similar thermal tolerance making that the Rias Baixas remain as refugia for these species.

Acknowledgements

References

Ashcroft, M.B., 2010. Identifying refugia from climate change: Identifying refugia from climate change. J. Biogeogr. 37, 1407-1413. https://doi.org/10.1111/j.1365-2699.2010.02300.x

Bakun, A., 1990. Global climate change and intensification of coastal ocean upwelling. Science 247, 198–201.

Bakun, A., Black, B.A., Bograd, S.J., García-Reyes, M., Miller, A.J., Rykaczewski, R.R., Sydeman, W.J., 2015. Anticipated Effects of Climate Change on Coastal Upwelling Ecosystems. Curr. Clim. Change Rep. 1, 85–93. https://doi.org/10.1007/s40641-015-0008-4

Brown, P.T., Caldeira, K., 2017. Greater future global warming inferred from Earth's recent energy budget. Nature 552, 45–50. https://doi.org/10.1038/nature24672

Cane, M.A., Clement, A.C., Kaplan, A., Kushnir, Y., Pozdnyakov, D., Seager, R., Zebiak, S.E., Murtugudde, R., 1997. Twentieth-Century Sea Surface Temperature Trends. Science 275, 957–960. https://doi.org/10.1126/science.275.5302.957

Casado-Amezúa, P., Araújo, R., Bárbara, I., Bermejo, R., Borja, Á., Díez, I., Fernández, C., Gorostiaga, J.M., Guinda, X., Hernández, I., Juanes, J.A., Peña, V., Peteiro, C., Puente, A., Quintana, I., Tuya, F., Viejo, R.M., Altamirano, M., Gallardo, T., Martínez, B., 2019. Distributional shifts of canopy-forming seaweeds from the Atlantic coast of Southern Europe. Biodivers. Conserv. 28, 1151–1172. https://doi.org/10.1007/s10531-019-01716-9

Chen, I.-C., Hill, J.K., Ohlemuller, R., Roy, D.B., Thomas, C.D., 2011. Rapid Range Shifts of Species Associated with High Levels of Climate Warming. Science 333, 1024–1026. https://doi.org/10.1126/science.1206432

Costoya, X., Fernández-Nóvoa, D., deCastro, M., Gómez-Gesteira, M., 2017. Loire and Gironde turbid plumes: Characterization and influence on thermohaline properties. J. Sea Res. 130, 7–16. https://doi.org/10.1016/j.seares.2017.04.003

Costoya, X., Fernández-Nóvoa, D., deCastro, M., Santos, F., Lazure, P., Gómez-Gesteira, M., 2016. Modulation of sea surface temperature warming in the Bay of Biscay by Loire and Gironde Rivers. J. Geophys. Res. Oceans 121, 966–979. https://doi.org/10.1002/2015JC011157

Des, M., deCastro, M., Sousa, M.C., Dias, J.M., Gómez-Gesteira, M., 2019. Hydrodynamics of river plume intrusion into an adjacent estuary: The Minho River and Ria de Vigo. J. Mar. Syst. 189, 87–97. https://doi.org/10.1016/j.jmarsys.2018.10.003

20

Des, M., Gómez-Gesteira, M., deCastro, M., Gómez-Gesteira, L., Sousa, M.C., 2020. How can ocean warming at the NW Iberian Peninsula affect mussel aquaculture? Sci. Total Environ. 709, 136117. https://doi.org/10.1016/j.scitotenv.2019.136117

Duarte, L., Viejo, R.M., 2018. Environmental and phenotypic heterogeneity of populations at the trailing range-edge of the habitat-forming macroalga Fucus serratus. Mar. Environ. Res. 136, 16–26. https://doi.org/10.1016/j.marenvres.2018.02.004

Duarte, L., Viejo, R.M., Martínez, B., deCastro, M., Gómez-Gesteira, M., Gallardo, T., 2013. Recent and historical range shifts of two canopy-forming seaweeds in North Spain and the link with trends in sea surface temperature. Acta Oecologica 51, 1–10. https://doi.org/10.1016/j.actao.2013.05.002

Evans, G., Prego, R., 2003. Rias, estuaries and incised valleys: is a ria an estuary? Mar. Geol. 196, 171–175. https://doi.org/10.1016/S0025-3227(03)00048-3

Franco, J.N., Tuya, F., Bertocci, I., Rodríguez, L., Martínez, B., Sousa-Pinto, I., Arenas, F., 2018. The 'golden kelp' *Laminaria ochroleuca* under global change: Integrating multiple eco-physiological responses with species distribution models. J. Ecol. 106, 47–58. https://doi.org/10.1111/1365-2745.12810

Helmuth, B., Broitman, B.R., Blanchette, C.A., Gilman, S., Halpin, P., Harley, C.D.G., O'Donnell, M.J., Hofmann, G.E., Menge, B., Strickland, D., 2006. Mosaic patterns of thermal stress in the rocky intertidal zone: implications for climate change. Ecol. Monogr. 76, 461–479. https://doi.org/10.1890/0012-9615(2006)076[0461:MPOTSI]2.0.CO;2

Jones, C.G., Lawton, J.H., Shachak, M., 1994. Organisms as Ecosystem Engineers. Oikos 69, 373. https://doi.org/10.2307/3545850

21

Keppel, G., Van Niel, K.P., Wardell-Johnson, G.W., Yates, C.J., Byrne, M., Mucina, L., Schut, A.G.T., Hopper, S.D., Franklin, S.E., 2012. Refugia: identifying and understanding safe havens for biodiversity under climate change: Identifying and understanding refugia. Glob. Ecol. Biogeogr. 21, 393–404. https://doi.org/10.1111/j.1466-8238.2011.00686.x

Kumagai, N.H., García Molinos, J., Yamano, H., Takao, S., Fujii, M., Yamanaka, Y., 2018. Ocean currents and herbivory drive macroalgae-to-coral community shift under climate warming. Proc. Natl. Acad. Sci. 115, 8990–8995. https://doi.org/10.1073/pnas.1716826115

Lourenço, C.R., Zardi, G.I., McQuaid, C.D., Serrão, E.A., Pearson, G.A., Jacinto, R., Nicastro, K.R., 2016. Upwelling areas as climate change refugia for the distribution and genetic diversity of a marine macroalga. J. Biogeogr. 43, 1595–1607. https://doi.org/10.1111/jbi.12744

Lüning, K., 1990. Seaweeds: their environment, biogeography, and ecophysiology. John Wiley & Sons.

Martínez, B., Arenas, F., Trilla, A., Viejo, R.M., Carreño, F., 2015. Combining physiological threshold knowledge to species distribution models is key to improving forecasts of the future niche for macroalgae. Glob. Change Biol. 21, 1422–1433.

Martínez, B., Viejo, R.M., Carreño, F., Aranda, S.C., 2012. Habitat distribution models for intertidal seaweeds: responses to climatic and non-climatic drivers: Distribution models for intertidal seaweeds in north-western Iberia. J. Biogeogr. 39, 1877–1890. https://doi.org/10.1111/j.1365-2699.2012.02741.x

22

McMenamin, S.K., Hadly, E.A., Wright, C.K., 2008. Climatic change and wetland desiccation cause amphibian decline in Yellowstone National Park. Proc. Natl. Acad. Sci. 105, 16988–16993. https://doi.org/10.1073/pnas.0809090105

Méndez-Sandín, M., Fernández, C., 2016. Changes in the structure and dynamics of marine assemblages dominated by *Bifurcaria bifurcata* and *Cystoseira* species over three decades (1977–2007). Estuar. Coast. Shelf Sci. 175, 46–56. https://doi.org/10.1016/j.ecss.2016.03.015

Parmesan, C., Ryrholm, N., Stefanescu, C., Hill, J.K., Thomas, C.D., Descimon, H., Huntley, B., Kaila, L., Kullberg, J., Tammaru, T., Tennent, W.J., Thomas, J.A., Warren, M., 1999. Poleward shifts in geographical ranges of butterfly species associated with regional warming. Nature 399, 579–583. https://doi.org/10.1038/21181

Poloczanska, E.S., Brown, C.J., Sydeman, W.J., Kiessling, W., Schoeman, D.S., Moore, P.J., Brander, K., Bruno, J.F., Buckley, L.B., Burrows, M.T., Duarte, C.M., Halpern, B.S., Holding, J., Kappel, C.V., O'Connor, M.I., Pandolfi, J.M., Parmesan, C., Schwing, F., Thompson, S.A., Richardson, A.J., 2013. Global imprint of climate change on marine life. Nat. Clim. Change 3, 919–925. https://doi.org/10.1038/nclimate1958

Poloczanska, E.S., Burrows, M.T., Brown, C.J., García Molinos, J., Halpern, B.S., Hoegh-Guldberg, O., Kappel, C.V., Moore, P.J., Richardson, A.J., Schoeman, D.S., Sydeman, W.J., 2016. Responses of Marine Organisms to Climate Change across Oceans. Front. Mar. Sci. 3. https://doi.org/10.3389/fmars.2016.00062

Rykaczewski, R.R., Dunne, J.P., Sydeman, W.J., García-Reyes, M., Black, B.A., Bograd, S.J., 2015. Poleward displacement of coastal upwelling-favorable winds in the

ocean's eastern boundary currents through the 21st century. Geophys. Res. Lett. 42, 6424–6431. https://doi.org/10.1002/2015GL064694

Santos, F., deCastro, M., Gómez-Gesteira, M., Álvarez, I., 2012. Differences in coastal and oceanic SST warming rates along the Canary upwelling ecosystem from 1982 to 2010. Cont. Shelf Res. 47, 1–6. https://doi.org/10.1016/j.csr.2012.07.023

Seabra, R., Varela, R., Santos, A.M., Gómez-Gesteira, M., Meneghesso, C., Wethey, D.S., Lima, F.P., 2019. Reduced Nearshore Warming Associated With Eastern Boundary Upwelling Systems. Front. Mar. Sci. 6, 104. https://doi.org/10.3389/fmars.2019.00104

Smale, D.A., Wernberg, T., 2013. Extreme climatic event drives range contraction of a habitat-forming species. Proc. R. Soc. B Biol. Sci. 280, 20122829. https://doi.org/10.1098/rspb.2012.2829

Sousa, M.C., deCastro, M., Alvarez, I., Gomez-Gesteira, M., Dias, J.M., 2017. Why coastal upwelling is expected to increase along the western Iberian Peninsula over the next century? Sci. Total Environ. 592, 243–251. https://doi.org/10.1016/j.scitotenv.2017.03.046

Sousa, M.C., Ribeiro, A., Des, M., Gomez-Gesteira, M., deCastro, M., Dias, J.M., 2020. NW Iberian Peninsula coastal upwelling future weakening: Competition between wind intensification and surface heating. Sci. Total Environ. 703, 134808. https://doi.org/10.1016/j.scitotenv.2019.134808

Strain, E.M.A., Thomson, R.J., Micheli, F., Mancuso, F.P., Airoldi, L., 2014. Identifying the interacting roles of stressors in driving the global loss of canopy-forming to mat-forming algae in marine ecosystems. Glob. Change Biol. 20, 3300–3312. https://doi.org/10.1111/gcb.12619

Sydeman, W.J., García-Reyes, M., Schoeman, D.S., Rykaczewski, R.R., Thompson, S.A., Black, B.A., Bograd, S.J., 2014. Climate change and wind intensification in coastal upwelling ecosystems. Science 345, 77–80. https://doi.org/10.1126/science.1251635

tom Dieck, I., de Oliveira, E.C., 1993. The section Digitatae of the genus Laminaria (Phaeophyta) in the northern and southern Atlantic: crossing experiments and temperature responses. Mar. Biol. 115, 151–160. https://doi.org/10.1007/BF00349397

Varela, R., Álvarez, I., Santos, F., deCastro, M., Gómez-Gesteira, M., 2015. Has upwelling strengthened along worldwide coasts over 1982-2010? Sci. Rep. 5, 10016. https://doi.org/10.1038/srep10016

Varela, R., Lima, F.P., Seabra, R., Meneghesso, C., Gómez-Gesteira, M., 2018. Coastal warming and wind-driven upwelling: A global analysis. Sci. Total Environ. 639, 1501–1511. https://doi.org/10.1016/j.scitotenv.2018.05.273

Wang, D., Gouhier, T.C., Menge, B.A., Ganguly, A.R., 2015. Intensification and spatial homogenization of coastal upwelling under climate change. Nature 518, 390–394. https://doi.org/10.1038/nature14235

Wernberg, T., Bennett, S., Babcock, R.C., de Bettignies, T., Cure, K., Depczynski, M., Dufois, F., Fromont, J., Fulton, C.J., Hovey, R.K., Harvey, E.S., Holmes, T.H., Kendrick, G.A., Radford, B., Santana-Garcon, J., Saunders, B.J., Smale, D.A., Thomsen, M.S., Tuckett, C.A., Tuya, F., Vanderklift, M.A., Wilson, S., 2016. Climate-driven regime shift of a temperate marine ecosystem. Science 353, 169–172. https://doi.org/10.1126/science.aad8745

Wernberg, T., Smale, D.A., Tuya, F., Thomsen, M.S., Langlois, T.J., de Bettignies, T., Bennett, S., Rousseaux, C.S., 2013. An extreme climatic event alters marine

ecosystem structure in a global biodiversity hotspot. Nat. Clim. Change 3, 78–82.

https://doi.org/10.1038/nclimate1627

Chapter 6

Synthesis

In this chapter, the integrated approach of the articles included in this thesis is developed. Firstly, a general discussion of the results is carried out and then, the main conclusions are presented.

6.1. Discussion

One of the main objectives of this thesis was to implement a hydrodynamic numerical model for the Northwest Iberian Peninsula (NWIP) coast. The NWIP coast is a complex system in which the general ocean circulation is modified by the particular features of the coast, the bathymetry, the discharge of the main rivers, and the wind regimen that release upwelling and downwelling events. Therefore, the numerical model has to be able to reproduce the interaction between all these drivers accurately. An example of a complex process governed by the interaction of all these drivers is the Minho River plume intrusion into the rias. The correct reproduction of this event allows testing the capability of the model to simulate the complex hydrodynamic of the rias and the shelf, as well as investigate in detail the dynamics of river intrusion events inside the rias. The Flow module of Delft3D numerical model was implemented and calibrated for the NWIP coast, the validation of the model was performed through a qualitative and quantitative comparison of the modeled data and concurrent *in situ* data, including sea surface elevation (SSE), salinity, water temperature and near-surface horizontal velocity. Accuracy in this study was similar to values obtained by Dias et al. (2009) and Sousa et al. (2018) for SSE and by Cerralbo et al. (2013) and Sousa et al. (2014b) for transport conditions. In addition, model capability to reproduce the dynamics of the coastal systems (rias and estuaries), the dynamics of the adjacent shelf and the exchange of water between them was analyzed by studying the intrusion of the Minho River plume into the Ría de Vigo. Intrusions of freshwater into adjacent estuaries or bays have been previously analyzed for several coastal systems located worldwide (Curtis Roegner et al., 2002; Shanks et al., 2002; Ware and Thomson, 2005; Dai et al., 2008; Davis et al., 2014; Fraysse et al., 2014). All these studies concluded that intrusion events modify water exchange with the shelf and fertilize the area promoting phytoplankton blooms and significantly increasing primary production. Typically, the Rías Baixas have a positive estuarine circulation which is enhanced by northerly winds (upwelling-favorable winds). However, it can be reverted (negative estuarine circulation) by southerly winds (downwelling-favorable winds). Moreover, prevalent southerly winds at the shelf favor the Minho River plume to reach the mouth of the rias and even to enter into some of them. Starting from a pattern of positive estuarine circulation, the different phases of an intrusion event (the development, negative circulation and relaxation) and a final stage returning to the positive estuarine circulation was described in detail. Before the intrusion event starts and

when it ends the typical positive circulation pattern of the rias described by Taboada et al. (1998) is observed. During the intrusion event, the circulation is reverted, turning into negative estuarine circulation, which follows a pattern similar to that previously described by deCastro et al. (2004) in the Ría de Pontevedra. It was observed that the Minho River plume reaches the mouth of the ria with a delay of ~12h relative to the start of favorable wind conditions, this is in line with the times proposed by Sousa et al. (2014a). The effect of the plume intrusion inside the ria was observed from surface to ~10-15 m of depth; these depths were similar to those reported by Barton et al. (2015) under a comparable wind regime. The typical duration of the intrusion events is ~1.5 days and the main drivers of these events are the discharge of the external river and the wind field, being negligible the influence of the discharge of inner rivers. During intrusion events, less dense oceanic water is advected into the ria through the surface layer transporting land-derived nutrients. These nutrients enhance primary production in the ria, although with less impact than upwelling, and may favor phytoplankton bloom events.

Once the model's capability to reproduce the hydrodynamics of the study area was positively evaluated, it was used to make projections by the end of the century with the aim of assessing the effects of climate change on the NWIP. To perform these simulations, firstly, it was determined which of the models provided by the CORDEX project is the one that best reproduces the historical atmospheric conditions of the NWIP. The Perkins analysis determined that the RCM MOHC-HadGEM2-Es-RCA4 and the GCM MOHC-HadGEM2-Es are the most accurate. Data from these models were used as input for the Delft3D model in order to reproduce two realistic extreme upwelling events, one that represents a historical event and another that represents a future event under the RCP 8.5 greenhouse emission scenario.

Data from the RCM MOHC-HadGEM2-Es-RCA4 model shows an increase in upwelling index (UI), these results are in agreement with recent researches which predict an increase in intensity and duration of upwelling favorable winds (Varela et al., 2015; Wang et al., 2015; Sousa et al., 2017). This increase can buffer the ocean warming in coastal areas (Santos et al., 2012; Varela et al., 2018; Seabra et al., 2019) however, ocean thermal stratification may also increase as ocean warming is not homogeneous through the water column. This increase in thermal stratification can result in a less effective upwelling (Gruber, 2011; García-Reyes et al., 2015) limiting vertical exchange through the water column. The present and future effectivity of high-extreme upwelling events,

i.e. UI ranging from 75% to 99% percentiles, along the NWIP was evaluated using Delft3D-Flow numerical model. Upwelling events pump nutrient-rich cold water to the surface cooling the surface layer. Differences in sea surface temperature (SST) between the end and the beginning of the upwelling event (ΔSST= SSTend - SSTbeginning) were compared both for historical and future events. A SST reduction was observed for both periods with a marked drop in the nearshore area compared with the near ocean area. This pattern is in good agreement with that observed by Santos et al. (2012) and Varela et al. (2018) for most upwelling systems. ΔSST was used as a proxy to evaluate the efficiency of upwelling events: more negative ΔSST implies a higher capacity to pump depth-cold water to the surface and therefore a more effective upwelling. Differences in the SST drop for future and historical periods show a similar cooling capacity for most of the coastal domain, with the exception of the region between 41º 30' N and 42º 15' N. This region is dominated by the major rivers (Minho, Douro and Lima) and nearshore values ranging from 2 to 3 °C were observed for the historical period, and from 1 to 2 °C for the future. Thereby, future projections suggest that future upwelling events will be less effective in this area despite the predicted increase in intensity and duration of upwelling favorable winds. The water column stratification, which was described in terms of the Brunt-Väisälä frequency calculated for sections between the Minho River and the Ría de Vigo, increases in the whole section by the end of the century. The thermocline will be deeper and the gradient will be more marked. As ocean stratification increases, the upwelling of deeper water (100 to 300 m) becomes less connected to the wind stress (Oyarzún and Brierley, 2019). Thereby, the increase in stratification counteracts the intensification of upwelling-favorable winds, which results in a decrease in the effectivity of upwelling events. For the Californian current, Roemmich and McGowan (1995) have observed that the increase in stratification limits the nutrient influx to the surface layer for biological production. Moreover, Gruber (2011) determined that ocean stratification decreases the upper ocean mixing and transport reducing the ability of the oceans to supply the oxygen from the surface into the thermocline. Therefore, the reduction in upwelling effectivity may negatively affect the primary production in the NWIP coast.

The Rías Baixas are characterized by a high primary production and the economy of the region depends mainly on the fishing, shellfish gathering and aquaculture sectors. The extensive culture of *Mytilus galloprovincialis* in mussel rafts is one of the most important industries of the region. As stated above, the ocean warming and the increase

in stratification may reduce primary production in the NWIP coast and hence, in the Rías Baixas. In this sense, the main physical parameters affecting mussel productivity, temperature and stratification, were analyzed in order to determine the possible impact of the climate change. Delft3D-Flow was used to characterize the areas where mussel rafts (mussel raft polygons) are currently located in the Rías Baixas under summer conditions both for historical and future periods. Results show that the water column stratification will increase in most of the mussel rafts polygon areas, especially in the outer areas of the rias where, according to Navarro et al. (1991), are the most productive ones. A reduction in stratification is only observed in the areas most affected by the river discharge. This increase in water stratification will limit the vertical exchange of nutrients and oxygen and it will constitute a clear drawback for mussel exploitation.

Water temperature is also a critical factor in mussel growth, explaining independently the 67% of the differences in growth in laboratory experiments (Kroeker et al., 2014). Each specie is characterized by an optimal range of water temperature in which biochemical and physiological rates are benefited (Kroeker et al., 2014). Water temperatures up to the optimal range can cause a slower growth and reductions in performance and survival (Anestis et al., 2007; Hrs-Brenko et al., 1977). *Mytilus galloprovincialis* survives in a wide range of temperatures, being able to withstand high temperatures (Gosling, 1992), although the optimal range for mussel growth was determined between 14 and 20 °C following previous research (https://longline.co.uk/meta/ List; Hrs-Brenko et al., 1977; Anestis et al., 2007; Peharda et al., 2007; Sánchez-Lazo and Martínez-Pita, 2012; Kroeker et al., 2014). This temperature range was used to determine the mussel comfort index, which was defined as the percentage of time in which water temperature remains within that optimal range. This index was determined both for historical and future periods as the mechanisms of mussels' adaptation to the ocean warming may be limited by their physiological limits (Tomanek, 2008; Ioannou et al., 2009). The general rise in water temperature will increase the time during which mussels will be subjected to thermal stress conditions. The impact on the water column will not be homogeneous, as upper layers will be more affected than the deeper ones. The comfort level of mussels will be reduced by more than 60% in the upper layers in most of the mussel raft polygons. Regarding deeper layers, although mussels comfort conditions will be reduced, the reduction will be lower (30 %) than in the upper layers. The reduction in comfort conditions, and mainly in upper layers, may

have a negative impact on the productivity since the upper part of the ropes (first meters) tends to be more productive at present than the lower part (Fuentes et al., 2000; Figueras and Caceres-Martinez, 2007). On the other hand, although the reduction in comfort conditions is widespread in all polygons, the reduction in future comfort will be lower for the outermost stations and mainly limited to the deeper layers. Results indicate that changing the location of the mussel raft polygons to the outer areas of the rias may help to mitigate the effect of climate change on mussel productivity.

Ocean warming is affecting many species and often results in local extinctions at the low latitude range limits of species distribution (Wiens, 2016; Russell et al., 2013). The contraction and local decrease are especially worrying when it affects conspicuous habitat-forming species because they provide structure, shelter and food to many accompanying species that form the ecological community (they are ecosystem engineers *sensu* Jones et al., 1994). Nowadays, the southern limit of the geographical distribution of several kelps and large intertidal seaweeds is the NWIP. A marked contraction of the species range in this area has been detected in recent years (reviewed in Casado-Amezúa et al., 2019). This is the case of *Himathalia elongata*, who has disappeared from a coastal strip of approximately 130 km since the start of this century in the North Iberian Peninsula (NIP) (Duarte et al., 2013) due to its restricted thermal tolerance (Martínez et al., 2015). On the other hand, warming patterns may be heterogeneous across the latitudinal gradient of species distribution (Helmuth et al., 2006) and there may be colder favorable spots at this range margin, the called climatic refugia (Ashcroft, 2010; Keppel et al., 2012). These climatic refugia may favor the persistence of edge populations. The Rías Baixas are large embayments protected from the wave action and highly influenced by upwelling, which reduces water temperature and provides a high amount of nutrients. These characteristics may be responsible for the rias to be acting as contemporary refugia to warming for large, habitat-forming macroalgae (Lourenço et al. 2016). Climate change and the consequent changes in water temperature, upwelling and stratification may affect the geographical distribution of these macroalgae. The Delft3D-Flow simulation under summer conditions for historical and future periods was used to analyze the effects of climate change on the geographical distribution of two intertidal macroalgae, *Himanthalia elongata* and *Bifurcaria bifurcata*, within the Rías Baixas. Based on the thermal survival thresholds for adult plants previously determined by Martínez et al. (2015), SST data were used to detect heat waves that may affect each of the species. Then, a mechanistic distribution model

based on the thermal survival threshold for adult plants of each species was calibrated and used to determine the thermal habitat suitability for the present and by the end of the century. The mechanistic distribution model was calibrated using the distribution records of *H. elongata* determined from a field survey. This species was preferred over *B.bifurcata* because shows less prevalence in the study area.

At present, thermal conditions of the Rías Baixas are mostly favorable to the presence of both algae. Unfavorable thermal conditions for *H. elongata* have been found in the inner areas of the rias, probably because the influence of the upwelling, which acts reducing water temperature, in these shallow areas is negligible. A more detailed analysis of the thermal habitat suitability for *H. elongata* shows that the rias of Muros and Arousa display the most suitable conditions, although the time under lethal conditions increases in the middle part of the Ría de Arousa compared with the outer part. Thermal conditions of Pontevedra and Vigo are slightly less favorable than the conditions in the other two northern rias. The records of presence/absence of *H. elongata* and other species of cold-temperate intertidal fucaceae, e.g., Fucus serratus, collected during a field survey by Martínez et al. (2012) support the differences in thermal conditions between the Rías Baixas since a greater number of settlements were registered in the estuaries where thermal conditions are more favorable. Projections for the far future indicate that thermal conditions in the Rías Baixas will be lethal for *H. elongata*, which implies that this species is projected to disappear. A contraction for this species and a general declining trend was observed for many cold-temperate fucoids and kelps at its southern range limit in the Iberian Peninsula (Duarte et al., 2013; Casado-Amezúa et al., 2019). However, the analysis of thermal habitat suitability for *B. bifurcata*, whose thermal survival threshold is greater than that of *H. elongata*, shows that thermal conditions may favor the settlement of these macroalgae by the end of the century, as well as for other habitat-forming species with a similar thermal tolerance. As described before, a climatic refugia is an area where the mean temperature is lower than the temperature of the adjacent area and, currently, the rias are considered climatic refugia due to the upwelling influence. Effectivity of upwelling will be, in general, less effective in the shelf area outside the rias, however, inside the rias, the capability of the upwelling to cool the water will remain similar to present day, with the exception of the Ría de Arousa where it will be slightly reduced. Therefore, the rias will potentially represent climatic refugia for the persistence of *B. bifurcata* and other macroalgae of similar thermal tolerance.

6.2. Conclusions

The general objective of this dissertation was to study the possible impacts of climate change, under the RCP 8.5 greenhouse emission scenario, on the NWIP coast, with a particular interest in the Rías Baixas, by applying a numerical model capable of simulating coastal and estuarine processes. To achieve this, Delft3D numerical model was chosen to perform the hydrodynamic numerical simulations. Two configurations of the model were used, one based on five domains, covering the NWIP coast from the Ría de Aveiro to the Rías Baixas connected by internal domain decomposition boundaries, and another one based on a unique domain covering from the Minho estuary to the Rías Baixas. The main conclusions to be drawn from the work performed using this numerical model can be summarized as follows:

- The use of an adaptive resolution mesh allows to properly reproduce the hydrodynamics of the NWIP coast without a high computational cost.

- Intrusion events of the Minho River plume are more common in the Ría de Vigo than in the others Rías Baixas. These events are related to southerly winds and show a delay of ~12h relative to the favorable wind peak. The duration of an intrusion event is ~1.5 days. During an intrusion event, inner river influence on circulation and stratification is negligible.

- Hydrodynamic simulations of the NWIP show that upwelling will be less effective in the future. Future increases in water temperature will lead to an increase in the thermal stratification which will counteract the effects of the intensification of the upwelling-favorable winds. The stratification increase will limit the vertical exchange of water and consequently, the vertical transport of nutrient-rich cold water and oxygen through the water column. This fact may have a negative impact on the productivity of the area and in the key socio-economic sectors.

- The general rise in water temperature will increase the time during which mussels will be subjected to thermal stress conditions. The impact on the water column will not be homogeneous and upper layers will be more affected than the deep ones. In most of the mussel raft polygons analyzed, the comfort level of mussels will be reduced by more than 60% in the upper layers and more than 30% in deep

layers. In addition, water column stratification will increase approximately 5–10 cycles h^{-1} reducing the vertical exchange of nutrients and oxygen. Hereby, changes in water temperature and stratification by the end of the century will not be favorable to mussel growth and consequently may decrease productivity of the mussel rafts.

- At present, the Rías Baixas are, in general, thermally suitable for the presence of two relevant habitat-forming macroalgae, *Himanthalia elongata* and *Bifurcaria bifurcata*. In contrast, by the end of the century the rise in sea surface temperature will increase the exposure time of macroalgae to heatwaves, and may lead to the local extinction of *H. elongata* and those macroalgae of similar thermal tolerance. However, projected thermal conditions may favor the settlement of *B. bifurcata* and other habitat-forming species with a similar thermal tolerance making the Rías Baixas climatic refugia for these species.

References

Aguiar, E., Piedracoba, S., Álvarez-Salgado, X.A., Labarta, U., 2017. Circulation of water through a mussel raft: clearance area vs. idealized linear flows. Rev. Aquac. 9, 3–22. https://doi.org/10.1111/raq.12099

Alvarez, I., deCastro, M., Gomez-Gesteira, M., 2005. Inter- and intra-annual analysis of the salinity and temperature evolution in the Galician Rías Baixas–ocean boundary (northwest Spain). J. Geophys. Res. 110. https://doi.org/10.1029/2004JC002504

Álvarez, I., deCastro, M., Prego, R., Gómez-Gesteira, M., 2003. Hydrographic characterization of a winter-upwelling event in the Ria of Pontevedra (NW Spain). Estuar. Coast. Shelf Sci. 56, 869–876. https://doi.org/10.1016/S0272-7714(02)00309-8

Alvarez, I., deCastro, M., Gomez-Gesteira, M., Prego, R., 2006. Hydrographic behavior of the Galician Rias Baixas (NW Spain) under the spring intrusion of the Miño River. J. Mar. Syst. 60, 144–152. https://doi.org/10.1016/j.jmarsys.2005.12.005

Alvarez, I., Gomez-Gesteira, M., deCastro, M., Dias, J.M., 2008a. Spatiotemporal evolution of upwelling regime along the western coast of the Iberian Peninsula. J. Geophys. Res. 113. https://doi.org/10.1029/2008JC004744

Alvarez, I., Gomez-Gesteira, M., deCastro, M., Novoa, E.M., 2008b. Ekman transport along the Galician Coast (NW, Spain) calculated from QuikSCAT winds. J. Mar. Syst. 72, 101–115. https://doi.org/10.1016/j.jmarsys.2007.01.013

Alvarez, I., Ospina-Alvarez, N., Pazos, Y., deCastro, M., Bernardez, P., Campos, M.J., Gomez-Gesteira, J.L., Alvarez-Ossorio, M.T., Varela, M., Gomez-Gesteira, M., Prego, R., 2009. A winter upwelling event in the Northern Galician Rias: Frequency and oceanographic implications. Estuar. Coast. Shelf Sci. 82, 573–582. https://doi.org/10.1016/j.ecss.2009.02.023

Alvarez, I., Lorenzo, M.N., deCastro, M., 2012. Analysis of chlorophyll a concentration along the Galician coast: seasonal variability and trends. ICES J. Mar. Sci. 69, 728–738. https://doi.org/DOI 10.1093/icesjms/fss045

Alvarez, I., Dias, J.M., DeCastro, M., Vaz, N., Sousa, M.C., Gómez-Gesteira, M., 2013. Influence of upwelling events on the estuaries of the north-western coast of the Iberian Peninsula. Mar. Freshw. Res. 64. https://doi.org/10.1071/MF12298

Alvarez-Salgado, X.A., Rosón, G., Pérez, F.F., Pazos, Y., 1993. Hydrographic variability off the Rías Baixas (NW Spain) during the upwelling season. J. Geophys. Res. 98, 14447. https://doi.org/10.1029/93JC00458

Álvarez-Salgado, X.A., Labarta, U., Fernández-Reiriz, M.J., Figueiras, F.G., Rosón, G., Piedracoba, S., Filgueira, R., Cabanas, J.M., 2008. Renewal time and the impact of harmful algal blooms on the extensive mussel raft culture of the Iberian coastal upwelling system (SW Europe). Harmful Algae 7, 849–855. https://doi.org/10.1016/j.hal.2008.04.007

Anestis, A., Lazou, A., Pörtner, H.O., Michaelidis, B., 2007. Behavioral, metabolic, and molecular stress responses of marine bivalve *Mytilus galloprovincialis* during long-term acclimation at increasing ambient temperature. Am. J. Physiol.-Regul. Integr. Comp. Physiol. 293, R911–R921. https://doi.org/10.1152/ajpregu.00124.2007

Anestis, A., Pörtner, H.O., Karagiannis, D., Angelidis, P., Staikou, A., Michaelidis, B., 2010. Response of *Mytilus galloprovincialis* (L.) to increasing seawater temperature and to marteliosis: Metabolic and physiological parameters. Comp. Biochem. Physiol. A. Mol. Integr. Physiol. 156, 57–66. https://doi.org/10.1016/j.cbpa.2009.12.018

Arístegui, J., Álvarez-Salgado, X.A., Barton, E.D., Figueiras, F.G., Hernández-León, S., Roy, C., Santos, A.M.P., 2004 Chapter 23. Oceanography and fisheries of the Canary current / Iberian region of the eastern North Atlantic (18a,E). In: The Sea, The Global Coastal Ocean: Interdisciplinary Regional Studies and Syntheses, Volume 14, A.R. Robinson, K.H. Brink (Eds.), Harvard University Press, Cambridge, MA, pp. 877-931.

Ashcroft, M.B., 2010. Identifying refugia from climate change: Identifying refugia from climate change. J. Biogeogr. 37, 1407-1413. https://doi.org/10.1111/j.1365-2699.2010.02300.x

Bakun, A., 1990. Global Climate Change and Intensification of Coastal Ocean Upwelling. Sci. 247, 198–201. https://doi.org/DOI 10.1126/science.247.4939.198

Barton, E.D., Largier, J.L., Torres, R., Sheridan, M., Trasviña, A., Souza, A., Pazos, Y., Valle-Levinson, A., 2015. Coastal upwelling and downwelling forcing of circulation in a semi-enclosed bay: Ria de Vigo. Prog. Oceanogr. 134, 173–189. https://doi.org/10.1016/j.pocean.2015.01.014

Behrenfeld, M.J., O'Malley, R.T., Siegel, D.A., McClain, C.R., Sarmiento, J.L., Feldman, G.C., Milligan, A.J., Falkowski, P.G., Letelier, R.M., Boss, E.S., 2006. Climate-driven trends in contemporary ocean productivity. Nature 444, 752–755. https://doi.org/10.1038/nature05317

Blanco, J., Arévalo, F., Moroño, Á., Correa, J., Muñíz, S., Mariño, C., Martín, H., 2017. Presence of azaspiracids in bivalve molluscs from Northern Spain. Toxicon 137, 135–143. https://doi.org/10.1016/j.toxicon.2017.07.025

Blanton, J.O., Tenore, K.R., Castillejo, F., Atkinson, L.P., Schwing, F.B., Lavin, A., 1987. The relationship of upwelling to mussel production in the Rias on the Western Coast of Spain. J. Mar. Res. 45, 497–511.

Brochier, T., Echevin, V., Tam, J., Chaigneau, A., Goubanova, K., Bertrand, A., 2013. Climate change scenarios experiments predict a future reduction in small pelagic fish recruitment in the Humboldt Current system. Glob. Change Biol. 19, 1841–1853. https://doi.org/10.1111/gcb.12184

Cáceres-Martínez, J., Robledo, J.A.F., Figueras, A., 1993. Settlement of mussels *Mytilus galloprovincialis* on an exposed rocky shore in Ria de Vigo, NW Spain. Mar. Ecol. Prog. Ser. 93, 195–198. https://doi.org/10.3354/meps093195

Cáceres-Martínez, J., Figueras, A., 1998. Distribution and abundance of mussel (*Mytilus galloprovincialis* Lmk) larvae and post-larvae in the Ria de Vigo (NW Spain). J. Exp. Mar. Biol. Ecol. 229, 277–287. https://doi.org/10.1016/S0022-0981(98)00059-8

Cane, M.A., Clement, A.C., Kaplan, A., Kushnir, Y., Pozdnyakov, D., Seager, R., Zebiak, S.E., Murtugudde, R., 1997. Twentieth-Century Sea Surface Temperature Trends. Science 275, 957–960. https://doi.org/10.1126/science.275.5302.957

Carballo, R., Iglesias, G., Castro, A., 2009a. Numerical model evaluation of tidal stream energy resources in the Ría de Muros (NW Spain). Renew. Energy 34, 1517–1524. https://doi.org/10.1016/j.renene.2008.10.028

Carballo, R., Iglesias, G., Castro, A., 2009b. Residual circulation in the Ría de Muros (NW Spain): A 3D numerical model study. J. Mar. Syst. 75, 116–130. https://doi.org/10.1016/j.jmarsys.2008.08.004

Cardoso Pereira, S., Marta-Almeida, M., Carvalho, A.C., Rocha, A., 2019. Extreme Precipitation Events under Climate Change in the Iberian Peninsula. INT J CLIMATOL joc.6269. https://doi.org/10.1002/joc.6269

Casabella, N., Lorenzo, M.N., Taboada, J.J., 2014. Trends of the Galician upwelling in the context of climate change. J. Sea Res. 93, 23–27. https://doi.org/10.1016/j.seares.2014.01.013

Casado-Amezúa, P., Araújo, R., Bárbara, I., Bermejo, R., Borja, Á., Díez, I., Fernández, C., Gorostiaga, J.M., Guinda, X., Hernández, I., Juanes, J.A., Peña, V., Peteiro, C., Puente, A., Quintana, I., Tuya, F., Viejo, R.M., Altamirano, M., Gallardo, T., Martínez, B., 2019. Distributional shifts of canopy-forming seaweeds from the Atlantic coast of Southern Europe. Biodivers. Conserv. 28, 1151–1172. https://doi.org/10.1007/s10531-019-01716-9

Cerralbo, P., Grifoll, M., Espino, M., López, J., 2013. Predictability of currents on a mesotidal estuary (Ria de Vigo, NW Iberia). Ocean Dyn. 63, 131–141. https://doi.org/10.1007/s10236-012-0586-9

Collins, M., R. Knutti, J. Arblaster, J.-L. Dufresne, T. Fichefet, P. Friedlingstein, X. Gao, W.J. Gutowski, T. Johns, G. Krinner, M. Shongwe, C. Tebaldi, A.J. Weaver and M. Wehner, 2013: Long-term Climate Change: Projections, Com - mitments and Irreversibility. In: Climate Change 2013: The Physical Science Basis. Contribution of Working Group I to the Fifth Assessment Report of the Intergovernmental Panel on Climate Change [Stocker, T.F., D. Qin, G.-K. Plattner, M. Tignor, S.K. Allen, J. Boschung, A. Nauels, Y. Xia, V. Bex and P.M. Midgley (eds.)]. Cambridge University Press, Cambridge, United Kingdom and New York, NY, USA.

Cordeiro Pires, A., Nolasco, R., Rocha, A., Ramos, A.M., Dubert, J., 2016. Climate change in the Iberian Upwelling System: a numerical study using GCM downscaling. Clim. Dyn. 47, 451–464. https://doi.org/10.1007/s00382-015-2848-y

Costa-Dias, S., Freitas, V., Sousa, R., Antunes, C., 2010. Factors influencing epibenthic assemblages in the Minho Estuary (NW Iberian Peninsula). Mar. 61, 240–246. https://doi.org/DOI 10.1016/j.marpolbul.2010.02.020

Curtis Roegner, G., Hickey, B.M., Newton, J.A., Shanks, A.L., Armstrong, D.A., 2002. Wind-induced plume and bloom intrusions into Willapa Bay, Washington. Limnol. Oceanogr. 47, 1033–1042.

Dai, M., Zhai, W., Cai, W.-J., Callahan, J., Huang, B., Shang, S., Huang, T., Li, X., Lu, Z., Chen, W., Chen, Z., 2008. Effects of an estuarine plume-associated bloom on the carbonate system in the lower reaches of the Pearl River estuary and the coastal zone of the northern South China Sea. Cont. Shelf Res. 28, 1416–1423. https://doi.org/10.1016/j.csr.2007.04.018

Davis, K.A., Banas, N.S., Giddings, S.N., Siedlecki, S.A., MacCready, P., Lessard, E.J., Kudela, R.M., Hickey, B.M., 2014. Estuary-enhanced upwelling of marine nutrients fuels coastal productivity in the U.S. Pacific Northwest. J. Geophys. Res. Oceans 119, 8778–8799. https://doi.org/10.1002/2014JC010248

deCastro, M., Gómez-Gesteira, M., Alvarez, I., Prego, R., 2004. Negative estuarine circulation in the Ria of Pontevedra (NW Spain). Estuar. Coast. Shelf Sci. 60, 301–312. https://doi.org/10.1016/j.ecss.2004.01.006

deCastro, M., Gómez-Gesteira, M., Prego, R., Taboada, J.J., Montero, P., Herbello, P., Pérez-Villar, V., 2000. Wind and Tidal Influence on Water Circulation in a Galician Ria (NW Spain). Estuar. Coast. Shelf Sci. 51, 161–176. https://doi.org/10.1006/ecss.2000.0619

deCastro, M., Alvarez, I., Varela, M., Prego, R., Gómez-Gesteira, M., 2006a. Miño River dams discharge on neighbor Galician Rias Baixas (NW Iberian Peninsula): Hydrological, chemical and biological changes in water column. Estuar. Coast. Shelf Sci. 70, 52–62. https://doi.org/10.1016/j.ecss.2006.05.035

deCastro, M., Lorenzo, N., Taboada, J.J., Sarmiento, M., Alvarez, I., Gomez-Gesteira, M., 2006b. Influence of teleconnection patterns on precipitation variability and on river flow regimes in the Miño River basin (NW Iberian Peninsula). Clim. Res. 32, 63–73.

deCastro, M., Gómez-Gesteira, M., Álvarez, I., Crespo, A.J.C., 2011. Atmospheric modes influence on Iberian Poleward Current variability. Cont. Shelf Res. 31, 425–432. https://doi.org/10.1016/j.csr.2010.03.004

Deltares, 2014. Delft3D-FLOW. Simulation of multi-dimensional hydrodynamic flows and transport phenomena, including sediments. User Manual. Hydro-Morphodynamics. Version: 3.15.34158, Delft3D Modeling Suite.

Des, M., deCastro, M., Sousa, M.C., Dias, J.M., Gómez-Gesteira, M., 2019. Hydrodynamics of river plume intrusion into an adjacent estuary: The Minho River and Ria de Vigo. J. Mar. Syst. 189, 87–97. https://doi.org/10.1016/j.jmarsys.2018.10.003

Di Lorenzo, E., Miller, A.J., Schneider, N., McWilliams, J.C., 2005. The Warming of the California Current System: Dynamics and Ecosystem Implications. J. Phys. Oceanogr. 35, 336–362. https://doi.org/10.1175/JPO-2690.1

Dias, J.M.A., Gonzalez, R., Garcia, C., Diaz-del-Rio, V., 2002. Sediment distribution patterns on the Galicia-Minho continental shelf. Prog. Oceanogr. 52, 215–231. https://doi.org/10.1016/S0079-6611(02)00007-1

Dias, J.M., Lopes, J.F., 2006. Implementation and assessment of hydrodynamic, salt and heat transport models: The case of Ria de Aveiro Lagoon (Portugal). Environ. Model. Softw. 21, 1–15. https://doi.org/10.1016/j.envsoft.2004.09.002

Dias, J.M., Sousa, M.C., Bertin, X., Fortunato, A.B., Oliveira, A., 2009. Numerical modeling of the impact of the Ancão Inlet relocation (Ria Formosa, Portugal). Environ. Model. Softw. 24, 711–725. https://doi.org/10.1016/j.envsoft.2008.10.017

Dias, J.M., Picado, A., 2011. Impact of morphologic anthropogenic and natural changes in estuarine tidal dynamics. Journal of Coastal Research 1490–1494.

Diz, A.P., Presa, P., 2009. The genetic diversity pattern of *Mytilus galloprovincialis* in Galician Rías (NW Iberian estuaries). Aquaculture 287, 278–285. https://doi.org/10.1016/j.aquaculture.2008.10.029

Duarte, L., Viejo, R.M., Martínez, B., deCastro, M., Gómez-Gesteira, M., Gallardo, T., 2013. Recent and historical range shifts of two canopy-forming seaweeds in North Spain and the link with trends in sea surface temperature. Acta Oecologica 51, 1–10. https://doi.org/10.1016/j.actao.2013.05.002

Duarte, C.M., Wu, J., Xiao, X., Bruhn, A., Krause-Jensen, D., 2017. Can Seaweed Farming Play a Role in Climate Change Mitigation and Adaptation? Front. Mar. Sci. 4:100. https://doi.org/10.3389/fmars.2017.00100

Evans, G., Prego, R., 2003. Rias, estuaries and incised valleys: is a ria an estuary? Mar. Geol. 196, 171–175. https://doi.org/10.1016/S0025-3227(03)00048-3

Fanjul, E.A., Gómez, B.P., Sánchez-Arévalo, I.R., 1997. A description of the tides in the Eastern North Atlantic. Prog. Oceanogr. 40, 217–244. https://doi.org/10.1016/S0079-6611(98)00003-2

FAO (Ed.), 2016. Contributing to food security and nutrition for all, The state of world fisheries and aquaculture. Rome.

FAO (Ed.), 2017. Adaptation strategies of the aquaculture sector to the impacts of climate change. Rome.

FAO (Ed.), 2018. Meeting the sustainable development goals, The state of world fisheries and aquaculture. Rome.

Fernández-Nóvoa, D., deCastro, M., Des, M., Costoya, X., Mendes, R., Gómez-Gesteira, M., 2017. Characterization of Iberian turbid plumes by means of synoptic patterns obtained through MODIS imagery. J. Sea Res. 126, 12–25. https://doi.org/10.1016/j.seares.2017.06.013

Figueiras, F.G., Labarta, U., Reiriz, M.F., 2002. Coastal upwelling, primary production and mussel growth in the Rías Baixas of Galicia, in: Sustainable Increase of Marine Harvesting: Fundamental Mechanisms and New Concepts. Springer, pp. 121–131. https://doi.org/10.1023/A:1021309222459

Fraysse, M., Pairaud, I., Ross, O.N., Faure, V.M., Pinazo, C., 2014. Intrusion of Rhone River diluted water into the Bay of Marseille: Generation processes and impacts on ecosystem functioning. J. Geophys. Res. Oceans 119, 6535–6556. https://doi.org/10.1002/2014JC010022

Fuentes, J., Reyero, I., Zapata, C., Alvarez, G., 1994. Production traits of the mussel *Mytilus galloprovincialis* cultured in Galicia (NW of Spain): relative effects of source of seed and growing environment. Aquaculture 122, 19–31.

Fuentes, J., Molares, J., Villalba, A., 1998. Growth, mortality and parasitization of mussels cultivated in the Ría de Arousa (NW Spain) from two sources of seed: intertidal rocky shore vs. collector ropes. Aquaculture 162, 231–240.

Fuentes, José, Gregorio, V., Giráldez, R., Molares, J., 2000. Within-raft variability of the growth rate of mussels, *Mytilus galloprovincialis*, cultivated in the Ría de Arousa (NW Spain) 14.

Fuentes, J., López, J.L., Mosquera, E., Vázquez, J., Villalba, A., Álvarez, G., 2002. Growth, mortality, pathological conditions and protein expression of *Mytilus edulis* and *M. galloprovincialis* crosses cultured in the Ría de Arousa (NW of Spain). Aquaculture 213, 233–251. https://doi.org/10.1016/S0044-8486(02)00046-7

García-Reyes, M., Sydeman, W.J., Schoeman, D.S., Rykaczewski, R.R., Black, B.A., Smit, A.J., Bograd, S.J., 2015. Under Pressure: Climate Change, Upwelling, and Eastern Boundary Upwelling Ecosystems. Front. Mar. Sci. 2, 109. https://doi.org/10.3389/fmars.2015.00109

Gestoso, I., Arenas, F., Olabarria, C., 2016. Ecological interactions modulate responses of two intertidal mussel species to changes in temperature and pH. J. Exp. Mar. Biol. Ecol. 474, 116–125. https://doi.org/10.1016/j.jembe.2015.10.006

Gillooly, James.F., Charnov, E.L., West, G.B., Savage, V.M., Brown, J.H., 2002. Effects of size and temperature on developmental time. Nature 417, 70–73. https://doi.org/10.1038/417070a

Gomez-Gesteira, M., Moreira, C., Alvarez, I., deCastro, M., 2006. Ekman transport along the Galician coast (northwest Spain) calculated from forecasted winds. J. Geophys. Res. 111. https://doi.org/10.1029/2005JC003331

Gómez-Gesteira, M., Gimeno, L., deCastro, M., Lorenzo, N., Alvarez, I., Nieto, R., Taboada, J., Crespo, A., Ramos, A., Iglesias, I., Gómez-Gesteira, J.L., Santo, F., Barriopedro, D., Trigo, I., 2011. The state of climate in NW Iberia. Clim. Res. 48, 109–144. https://doi.org/10.3354/cr00967

Gruber, N., 2011. Warming up, turning sour, losing breath: ocean biogeochemistry under global change. Philos. Trans. R. Soc. Math. Phys. Eng. Sci. 369, 1980–1996. https://doi.org/10.1098/rsta.2011.0003

Grunnet, N.M., Walstra, D.-J.R., Ruessink, B.G., 2004. Process-based modelling of a shoreface nourishment. Coast. Eng. 51, 581–607. https://doi.org/10.1016/j.coastaleng.2004.07.016

Gutierrez, D., Bouloubassi, I., Sifeddine, A., Purca, S., Goubanova, K., Graco, M., Field, D., Mejanelle, L., Velazco, F., Lorre, A., Salvatteci, R., Quispe, D., Vargas, G., Dewitte, B., Ortlieb, L., 2011. Coastal cooling and increased productivity in the main upwelling zone off Peru since the mid-twentieth century. Geophys. Res. Lett. 38. https://doi.org/Artn L07603Doi 10.1029/2010gl046324

Helmuth, B., Broitman, B.R., Blanchette, C.A., Gilman, S., Halpin, P., Harley, C.D.G., O'Donnell, M.J., Hofmann, G.E., Menge, B., Strickland, D., 2006. Mosaic patterns of thermal stress in the rocky intertidal zone: implications for climate change. Ecol. Monogr. 76, 461–479. https://doi.org/10.1890/0012-9615(2006)076[0461:MPOTSI]2.0.CO;2

Hrs-Brenko, M., Claus, C., Bubic, S., 1977. Synergistic effects of lead, salinity and temperature on embryonic development of the mussel *Mytilus galloprovincialis*. Mar. Biol. 44, 109–115. https://doi.org/10.1007/BF00386951

Hundecha, Y., Arheimer, B., Donnelly, C., Pechlivanidis, I., 2016. A regional parameter estimation scheme for a pan-European multi-basin model. Journal of Hydrology: Regional Studies 6, 90–111. https://doi.org/10.1016/j.ejrh.2016.04.002

Iglesias, G., Carballo, R., Castro, A., 2008. Baroclinic modelling and analysis of tide- and wind-induced circulation in the Ría de Muros (NW Spain). J. Mar. Syst. 74, 475–484. https://doi.org/10.1016/j.jmarsys.2008.03.009

Iglesias, G., Carballo, R., 2009. Seasonality of the circulation in the Ría de Muros (NW Spain). J. Mar. Syst. 78, 94–108. https://doi.org/10.1016/j.jmarsys.2009.04.002

Iglesias, G., Carballo, R., 2010a. Wave energy and nearshore hot spots: The case of the SE Bay of Biscay. Renew. Energy 35, 2490–2500. https://doi.org/10.1016/j.renene.2010.03.016

Iglesias, G., Carballo, R., 2010b. Effects of high winds on the circulation of the using a mixed open boundary condition: the Ría de Muros, Spain. Environ. Model. Softw. 25, 455–466. https://doi.org/10.1016/j.envsoft.2009.10.013

Ioannou, S., Anestis, A., Pörtner, H.O., Michaelidis, B., 2009. Seasonal patterns of metabolism and the heat shock response (HSR) in farmed mussels Mytilus galloprovincialis. J. Exp. Mar. Biol. Ecol. 381, 136–144. https://doi.org/10.1016/j.jembe.2009.09.014

IPCC, 2013. Climate Change 2013: The Physical Science Basis.Contribution of Working Group I to the Fifth Assessment Report of the Intergovernmental Panel on Climate Change, Stocker, T.F., D. Qin, G.-K. Plattner, M. Tignor, S.K. Allen, J. Boschung, A. Nauels, Y. Xia, V. Bex and P.M. Midgley (eds.). Cambridge University Press, Cambridge, United Kingdom and New York, NY, USA.

Jones, C.G., Lawton, J.H., Shachak, M., 1994. Organisms as Ecosystem Engineers. Oikos 69, 373. https://doi.org/10.2307/3545850

Keppel, G., Van Niel, K.P., Wardell-Johnson, G.W., Yates, C.J., Byrne, M., Mucina, L., Schut, A.G.T., Hopper, S.D., Franklin, S.E., 2012. Refugia: identifying and understanding safe havens for biodiversity under climate change: Identifying and understanding refugia. Glob. Ecol. Biogeogr. 21, 393–404. https://doi.org/10.1111/j.1466-8238.2011.00686.x

Kroeker, K.J., Gaylord, B., Hill, T.M., Hosfelt, J.D., Miller, S.H., Sanford, E., 2014. The Role of Temperature in Determining Species' Vulnerability to Ocean Acidification: A Case Study Using *Mytilus galloprovincialis*. PLoS ONE 9, e100353. https://doi.org/10.1371/journal.pone.0100353

Lantzsch, H., Hanebuth, T.J.J., Henrich, R., 2010. Sediment recycling and adjustment of deposition during deglacial drowning of a low-accumulation shelf (NW Iberia). Cont. Shelf Res. 30, 1665–1679. https://doi.org/10.1016/j.csr.2010.06.013

Lesser, G.R., Roelvink, J.A., van Kester, J.A.T.M., Stelling, G.S., 2004. Development and validation of a three-dimensional morphological model. Coast. Eng. 51, 883–915. https://doi.org/10.1016/j.coastaleng.2004.07.014

Levitus, S., Antonov, J.I., Boyer, T.P., Stephens, C., 2000. Warming of the world ocean. Sci. 287, 2225–2229. https://doi.org/10.1126/science.287.5461.2225

Liu, M., Tanhua, T., 2019. Characteristics of Water Masses in the Atlantic Ocean based on GLODAPv2 data. Ocean Sci. Discuss. 1–43. https://doi.org/10.5194/os-2018-139

Lopes, C.L., Dias, J.M., 2015. Assessment of flood hazard during extreme sea levels in a tidally dominated lagoon. Nat. Hazards 77, 1345–1364. https://doi.org/10.1007/s11069-015-1659-0

López, J.L., Mosquera, E., Fuentes, J., Marina, A., Vázquez, J., Alvarez, G., 2001. Two-dimensional gel electrophoresis of *Mytilus galloprovincialis*: differences in protein expression between intertidal and cultured mussels. Mar. Ecol. Prog. Ser. 224, 149–156. https://doi.org/10.3354/meps224149

Lopes, C.L., Alves, F.L., Dias, J.M., 2017. Flood risk assessment in a coastal lagoon under present and future scenarios: Ria de Aveiro case study. Nat. Hazards 89, 1307–1325. https://doi.org/10.1007/s11069-017-3025-x

Lourenço, C.R., Zardi, G.I., McQuaid, C.D., Serrão, E.A., Pearson, G.A., Jacinto, R., Nicastro, K.R., 2016. Upwelling areas as climate change refugia for the distribution and genetic diversity of a marine macroalga. J. Biogeogr. 43, 1595–1607. https://doi.org/10.1111/jbi.12744

MacMillan, D.S., Beckley, B.D., Fang, P., 2004. Monitoring the TOPEX and Jason-1 microwave radiometers with GPS and VLBI wet zenith path delays. Mar. Geod. 27, 703–716. https://doi.org/10.1080/01490410490904780

Martínez, B., Viejo, R.M., Carreño, F., Aranda, S.C., 2012. Habitat distribution models for intertidal seaweeds: responses to climatic and non-climatic drivers: Distribution models for intertidal seaweeds in north-western Iberia. J. Biogeogr. 39, 1877–1890. https://doi.org/10.1111/j.1365-2699.2012.02741.x

Martínez, B., Arenas, F., Trilla, A., Viejo, R.M., Carreño, F., 2015. Combining physiological threshold knowledge to species distribution models is key to improving forecasts of the future niche for macroalgae. Glob. Change Biol. 21, 1422–1433.

Mendes, R., Vaz, N., Dias, J.M., 2013. Potential impacts of the mean sea level rise on the hydrodynamics of the Douro river estuary. J. Coast. Res. https://doi.org/10.2112/si65-330.1

Mendes, R., Sousa, M.C., deCastro, M., Gómez-Gesteira, M., Dias, J.M., 2016. New insights into the Western Iberian Buoyant Plume: Interaction between the Douro and Minho River plumes under winter conditions. Prog. Oceanogr. 141, 30–43. https://doi.org/10.1016/j.pocean.2015.11.006

Mesas, A., Tarifeño, E., 2015. Temperaturas letales superiores para el mejillón, *Mytilus galloprovincialis* (Lamarck, 1819), en la costa de Chile central. Lat. Am. J. Aquat. Res. 11.

Míguez, B.M., Pérez, F.F., Souto, C., Fariña-Busto, L., 2001. Flujos residuales de intercambio entre la Ría de Vigo y la plataforma continental. Física Tierra 13, 119–137.

Miranda, P.M.A., Alves, J.M.R., Serra, N., 2013. Climate change and upwelling: response of Iberian upwelling to atmospheric forcing in a regional climate scenario. Climate Dynamics 40, 2813–2824. https://doi.org/DOI 10.1007/s00382-012-1442-9

Navarro, E., Iglesias, J.I.P., Perez camacho, A., Labarta, U., Beiras, R., 1991. The physiological energetics of musselsd (*Mytilus galloprovincialis* Lmk) from different cultivation rafts in the Ria de Arosa (Galicia, N.W. Spain). Aquaqulture 94, 197–212.

Oberle, F.K.J., Storlazzi, C.D., Hanebuth, T.J.J., 2014. Wave-driven sediment mobilization on a storm-controlled continental shelf (Northwest Iberia). J. Mar. Syst. 139, 362–372. https://doi.org/10.1016/j.jmarsys.2014.07.018

Oerder, V., Colas, F., Echevin, V., Codron, F., Tam, J., Belmadani, A., 2015. Peru-Chile upwelling dynamics under climate change. J. Geophys. Res.: Oceans 120, 1152–1172. https://doi.org/10.1002/2014JC010299

Otero, P., Ruiz-Villarreal, M., Peliz, A., 2008. Variability of river plumes off Northwest Iberia in response to wind events. J. Mar. Syst. 72, 238–255. https://doi.org/10.1016/j.jmarsys.2007.05.016

Otero, P., Ruiz-Villarreal, M., Peliz, A., 2009. River plume fronts off NW Iberia from satellite observations and model data. ICES J. Mar. Sci. 66, 1853–186412. https://doi.org/10.1093/icesjms/fsp156

Otero, P., Ruiz-Villarreal, M., García-García, L., González-Nuevo, G., Cabanas, J.M., 2013. Coastal dynamics off Northwest Iberia during a stormy winter period. Ocean Dyn. 63, 115–129. https://doi.org/DOI 10.1007/s10236-012-0585-x

Oyarzún, D., Brierley, C.M., 2019. The future of coastal upwelling in the Humboldt current from model projections. Clim. Dyn. 52, 599–615. https://doi.org/10.1007/s00382-018-4158-7

Pawlowicz, R., Beardsley, B., Lentz, S., 2002. Classical tidal harmonic analysis including error estimates in MATLAB using T_TIDE. Comput. Geosci. 28, 929–937.

Peharda, M., Župan, I., Bavčević, L., Frankić, A., Klanjšček, T., 2007. Growth and condition index of mussel *Mytilus galloprovincialis* in experimental integrated aquaculture. Aquac. Res. 38, 1714–1720. https://doi.org/10.1111/j.1365-2109.2007.01840.x

Peliz, Á., Rosa, T.L., Santos, A.M.P., Pissarra, J.L., 2002. Fronts, jets, and counter-flows in the Western Iberian upwelling system. J. Mar. Syst. 35, 61–77. https://doi.org/10.1016/S0924-7963(02)00076-3

Peliz, Á., 2003. Generation and unstable evolution of a density-driven Eastern Poleward Current: The Iberian Poleward Current. J. Geophys. Res. 108, 3268. https://doi.org/10.1029/2002JC001443

Pérez Camacho, A., Labarta, U., Beiras, R., 1995. Growth of mussels (*Mytilus edulis galloprovincialis*) on cultivation rafts: influence of seed source, cultivation site and phytoplankton availability. Aquaculture 138, 349–362. https://doi.org/10.1016/0044-8486(95)01139-0

Pérez Muñuzuri, V., Fernández Cañamero, M., Gómez Gesteira, J.L., 2009. Evidencias e impactos do cambio climático en Galicia. Consellería de Medio Ambiente e Desenvolvemento Sostible, Santiago de Compostela.

Perkins, S.E., Pitman, A.J., Holbrook, N.J., McAneney, J., 2007. Evaluation of the AR4 climate models' simulated daily maximum temperature, minimum temperature, and precipitation over Australia using probability density functions. J. Clim. 20, 4356–4376. https://doi.org/10.1175/JCLI4253.1

Pires, A.C., Nolasco, R., Rocha, A., Dubert, J., 2013. Assessing future climate change in the Iberian Upwelling System. J. Coast. Res. 1909–1914. https://doi.org/10.2112/SI65-323.1

Pires, A.C., Nolasco, R., Rocha, A., Ramos, C., Dubert, J., 2015. Climate change in the Iberian Upwelling System: a numerical study using GCM downscaling. Clim. Dyn. 1–14.

Pitcher, G.C., Figueiras, F.G., Hickey, B.M., Moita, M.T., 2010. The physical oceanography of upwelling systems and the development of harmful algal blooms. Prog. Oceanogr. 85, 5–32. https://doi.org/10.1016/j.pocean.2010.02.002

Prego, R., Guzmán-Zuñiga, D., Varela, M., deCastro, M., Gómez-Gesteira, M., 2007. Consequences of winter upwelling events on biogeochemical and phytoplankton patterns in a western Galician ria (NW Iberian Peninsula). Estuar. Coast. Shelf Sci. 73, 409–422. https://doi.org/10.1016/j.ecss.2007.02.004

Prego, R., Dale, A.W., deCastro, M., Gómez-Gesteira, M., Taboada, J.J., Montero, P., Villareal, M.R., Pérez-Villar, V., 2001. Hydrography of the Pontevedra Ria: Intra-annual spatial and temporal variability in a Galician coastal system (NW Spain). J. Geophys. Res. 106, 19845–19857. https://doi.org/10.1029/2000JC000775

Queiroga, H., 2003. Wind forcing of crab megalopae recruitment to an estuary (ria de aveiro) in the northern portuguese upwelling system. Invertebr. Reprod. Dev. 43, 47–54. https://doi.org/10.1080/07924259.2003.9652521

Rey, D., Álvarez-Iglesias, P., Araújo, M.F., Bernabeu, A.M., Comas, M., DeCastro, M., Druet, M., Ferreira da Silva, E., Ferrín, A., Gesteira, M., Martins, V., Mohamed, K.J., Rubio, B., Vilas, F., 2014. Chapter 8 The NW Iberian continental shelf. Geol. Soc. Lond. Mem. 41, 91–108. https://doi.org/10.1144/M41.8

Ribeiro, A.C., Peliz, Á., Santos, A.M.P., 2005. A study of the response of chlorophyll-a biomass to a winter upwelling event off Western Iberia using SeaWiFS and in situ data. J. Mar. Syst. 53, 87–107. https://doi.org/10.1016/j.jmarsys.2004.05.031

Roemmich, D., McGowan, J., 1995. Climatic Warming and the Decline of Zooplankton in the California Current. Science 267, 1324–1326. https://doi.org/10.1126/science.267.5202.1324

Rykaczewski, R.R., Dunne, J.P., Sydeman, W.J., Garcia-Reyes, M., Black, B.A., Bograd, S.J., 2015. Poleward displacement of coastal upwelling-favorable winds in the ocean's eastern boundary currents through the 21st century. Geophys. Res. Lett. 42, 6424–6431. https://doi.org/10.1002/2015GL064694

Sánchez-Lazo, C., Martínez-Pita, I., 2012. Effect of temperature on survival, growth and development of *Mytilus galloprovincialis* larvae. Aquac. Res. 43, 1127–1133. https://doi.org/10.1111/j.1365-2109.2011.02916.x

Santos, F., Gomez Gesteira, M., deCastro, M., 2011. Coastal and oceanic SST variability along the western Iberian Peninsula. Cont. Shelf Res. 31, 2012–2017. https://doi.org/10.1016/j.csr.2011.10.005

Santos, F., deCastro, M., Gómez-Gesteira, M., Álvarez, I., 2012. Differences in coastal and oceanic SST warming rates along the Canary upwelling ecosystem from 1982 to 2010. Cont. Shelf Res. 47, 1–6. https://doi.org/10.1016/j.csr.2012.07.023

Seabra, R., Varela, R., Santos, A.M., Gómez-Gesteira, M., Meneghesso, C., Wethey, D.S., Lima, F.P., 2019. Reduced Nearshore Warming Associated with Eastern Boundary Upwelling Systems. Front. Mar. Sci. 6, 104. https://doi.org/10.3389/fmars.2019.00104

Shanks, A.L., Largier, J., Brink, L., Brubaker, J., Hooff, R., 2002. Observations on the distribution of meroplankton during a downwelling event and associated intrusion

of the Chesapeake Bay estuarine plume. J. Plankton Res. 24, 391–416. https://doi.org/10.4319/lo.2002.47.4.1033

Soares, P.M.M., Cardoso, R.M., Miranda, P.M.A., Viterbo, P., Belo-Pereira, M., 2012. Assessment of the ENSEMBLES regional climate models in the representation of precipitation variability and extremes over Portugal. Journal of Geophysical Research-Atmospheres 117. https://doi.org/Artn D07114Doi 10.1029/2011jd016768

Sousa, M.C., Alvarez, I., Vaz, N., Dias, J.M., 2011. Physical forcing of the hydrography of the Ria de Vigo mouth. J. Coast. Res. SI64, 1589–1593.

Sousa, M.C., Vaz, N., Alvarez, I., Dias, J.M., 2013. Effect of Minho estuarine plume on Rias Baixas: numerical modeling approach. J. Coast. Res. 165, 2059–2064. https://doi.org/10.2112/SI65-348.1

Sousa, M.C., Vaz, N., Alvarez, I., Gomez-Gesteira, M., Dias, J.M., 2014a. Modeling the Minho River plume intrusion into the Rias Baixas (NW Iberian Peninsula). Cont. Shelf Res. 85, 30–41. https://doi.org/10.1016/j.csr.2014.06.004

Sousa, M.C., Vaz, N., Alvarez, I., Gomez-Gesteira, M., Dias, J.M., 2014b. Influence of the Minho River plume on the Rias Baixas (NW of the Iberian Peninsula). J. Mar. Syst. 139, 248–260. https://doi.org/10.1016/j.jmarsys.2014.06.012

Sousa, M.C., deCastro, M., Alvarez, I., Gomez-Gesteira, M., Dias, J.M., 2017. Why coastal upwelling is expected to increase along the western Iberian Peninsula over the next century? Sci. Total Environ. 592, 243–251. https://doi.org/10.1016/j.scitotenv.2017.03.046

Sousa, M.C., Ribeiro, A.S., Des, M., Mendes, R., Alvarez, I., Gomez-Gesteira, M., Dias, J.M., 2018. Integrated High-resolution Numerical Model for the NW Iberian Peninsula Coast and Main Estuarine Systems. J. Coast. Res. 85, 66–70. https://doi.org/10.2112/SI85-014.1

Spyrakos, E., González Vilas, L., Torres Palenzuela, J.M., Barton, E.D., 2011. Remote sensing chlorophyll a of optically complex waters (rias Baixas, NW Spain): Application of a regionally specific chlorophyll a algorithm for MERIS full resolution data during an upwelling cycle. Remote Sens. Environ. 115, 2471–2485. https://doi.org/10.1016/j.rse.2011.05.008

Sutherland, J., Walstra, D.J.R., Chesher, T.J., van Rijn, L.C., Southgate, H.N., 2004. Evaluation of coastal area modelling systems at an estuary mouth. Coast. Eng. 51, 119–142. https://doi.org/10.1016/j.coastaleng.2003.12.003

Taboada, J.J., Prego, R., Ruiz-Villarreal, M., Gómez-Gesteira, M., Montero, P., Santos, A.P., Pérez-Villar, V., 1998. Evaluation of the Seasonal Variations in the Residual Circulation in the Ría of Vigo (NW Spain) by Means of a 3D Baroclinic Model taboada et al 1998.pdf. Estuar. Coast. Shelf Sci. 47, 661–670. https://doi.org/10.1006/ecss.1998.0385

Taylor, K.E., Stouffer, R.J., Meehl, G.A., 2012. An Overview of Cmip5 and the Experiment Design. Bulletin of the American Meteorological Society 93, 485–498. https://doi.org/Doi 10.1175/Bams-D-11-00094.1

Tilstone, G.H., Figueiras, F.G., Fraga, F., 1994. Upwelling-downwelling sequences in the generation of red tides in a coastal upwelling system. Mar. Ecol. Prog. Ser. 241–253.

Tomanek, L., 2008. The Importance of Physiological Limits in Determining Biogeographical Range Shifts due to Global Climate Change: The Heat-Shock Response. Physiol. Biochem. Zool. 81, 709–717. https://doi.org/10.1086/590163

Vale, L.M., Dias, J.M., 2011. The effect of tidal regime and river flow on the hydrodynamics and salinity structure of the Lima Estuary: Use of a numerical model to assist on estuary classification. Journal of Coastal Research 1604–1608.

Varela, R.A., Rosón, G., Herrera, J.L., Torres-López, S., Fernández-Romero, A., 2005. A general view of the hydrographic and dynamical patterns of the Rías Baixas adjacent sea area. J. Mar. Syst. 54, 97–113. https://doi.org/10.1016/j.jmarsys.2004.07.006

Varela, R., Álvarez, I., Santos, F., deCastro, M., Gómez-Gesteira, M., 2015. Has upwelling strengthened along worldwide coasts over 1982-2010? Sci. Rep. 5, 10016. https://doi.org/10.1038/srep10016

Varela, R., Lima, F.P., Seabra, R., Meneghesso, C., Gómez-Gesteira, M., 2018. Coastal warming and wind-driven upwelling: A global analysis. Sci. Total Environ. 639, 1501–1511. https://doi.org/10.1016/j.scitotenv.2018.05.273

Vieira, M.E.C., Bordalo, A.A., 2000. The Douro estuary (Portugal): a mesotidal salt wedge. Oceanologica Acta 23, 585–594. https://doi.org/Doi 10.1016/S0399-1784(00)01107-5

Wang, D., Gouhier, T.C., Menge, B.A., Ganguly, A.R., 2015. Intensification and spatial homogenization of coastal upwelling under climate change. Nature 518, 390–394. https://doi.org/10.1038/nature14235

Ware, Daniel.M., Thomson, R.E., 2005. Bottom-Up Ecosystem Trophic Dynamics Determine Fish Production in the Northeast Pacific. Science 308, 1280–1284. https://doi.org/10.1126/science.1109049

Warner, J.C., Geyer, W.R., Lerczak, J.A., 2005. Numerical modeling of an estuary: A comprehensive skill assessment. J. Geophys. Res. 110. https://doi.org/10.1029/2004JC002691

Watterson, I.G., 2008. Calculation of probability density functions for temperature and precipitation change under global warming. Journal of Geophysical Research Atmospheres 113. https://doi.org/10.1029/2007JD009254

Wiens, J.J., 2016. Climate-Related Local Extinctions Are Already Widespread among Plant and Animal Species. PLOS Biol. 14, e2001104. https://doi.org/10.1371/journal.pbio.2001104

Wooster, W.S., Bakun, A., Mclain, D.R., 1976. Seasonal Upwelling Cycle Along Eastern Boundary of North-Atlantic. Journal of Marine Research 34, 131–141.

Xie, X., Li, M., Boicourt, W.C., 2017. Baroclinic Effects on Wind-Driven Lateral Circulation in Chesapeake Bay. J. Phys. Oceanogr. 47, 433–445. https://doi.org/10.1175/JPO-D-15-0233.1

Xiu, P., Chai, F., Curchitser, E.N., Castruccio, F.S., 2018. Future changes in coastal upwelling ecosystems with global warming: The case of the California Current System. Scientific Reports 8. https://doi.org/10.1038/s41598-018-21247-7

Zippay, M.L., Helmuth, B., 2012. Effects of temperature change on mussel, *Mytilus*. Integr. Zool. 7, 312–327. https://doi.org/10.1111/j.1749-4877.2012.00310.x

List of Figures

Chapter 3. Data sources

Chapter 4. Numerical model: DELFT3D-Flow

Chapter 5. Set of publications

Hydrodynamics of river plume intrusion into an adjacent estuary: The Minho River and Ria de Vigo

Fig. 3. (a) Simulated surface salinity difference (ΔS) between stations at the inner part and the southern mouth of the Ria de Vigo (V_i and V_s, respectively in Fig. 1c) from January 7th to February 11th, 2010. (b) The meridional wind component (ms^{-1}) at the shelf (black triangle in Fig. 1b). Meridional wind peaks labelled with P represent those winds with a direction and intensity favorable to Minho River intrusion. (c) Discharges of Minho (black line) and Verdugo-Oitavén (gray line) rivers ($m_3 s^{-1}$). Vertical black lines mark the dates of sampling. Solid lines correspond to the dates when intrusion events were detected and dashed lines to the dates when no intrusion was detected……………………………...66

Fig. 4. (a) Time evolution of the predicted filtered velocity at the middle station of the Ria de Vigo (V_m in Fig. 1c) from January 7th to February 11th, 2010. Red colors indicate water flowing into the ria and blue colors represent water flowing out. The dashed contour line corresponds to 0 ms^{-1}. Vertical lines indicate the days when Minho intrusion was detected using in situ data. (b) As (a) but only for surface layer (0 m). Velocity peaks labelled with P represent events with positive surface velocity…………………………67

Fig. 5. (a) Time evolution of the predicted density at the middle station of the Ria de Vigo (V_m in Fig. 1c) from January 7th to February 11th, 2010. Vertical lines indicate the days when intrusion was detected using in situ data. (b) As (a) but only for surface layer (0 m). Density peaks labelled with P represent those events with an abrupt density decrease in the water column, indicating freshwater input into the estuary………………………….67

Fig. 6. Hydrodynamic behavior of the Ria de Vigo under a freshwater intrusion simulated using Delft3D. Five stages of the intrusion event corresponding to the P5 wind peak (January 20–23, 2010) are shown (rows). Vertical profiles of velocity (left column) and density (middle column) along the main axis of the ria and surface density plots of the estuary (right column) are plotted. The black dashed line represents null horizontal velocities along the main axis of the estuary. The distance is measured in km from the southern mouth of the estuary………………………………………………………..68

Fig. 7. Predicted along axis velocities for the cross-section shown in Fig. 1c (red segment) under (a) upwelling favorable conditions, January 23th to February 1st, 2010 and (b) downwelling favorable conditions with Minho river intrusion, February 2nd to 8th, 2010. Red colors indicate inflowing water and blue colors represent outflowing water. The dashed contour line corresponds to 0 ms^{-1}………………………………………………..69

NW Iberian Peninsula coastal upwelling future weakening: Competition between wind intensification and surface heating

How can ocean warming at the NW Iberian Peninsula affect mussel aquaculture?

The impact of climate change on the geographical distribution of habitat-forming macroalgae in the Rías Baixas

List of Tables

Hydrodynamics of river plume intrusion into an adjacent estuary: The Minho River and Ria de Vigo

NW Iberian Peninsula coastal upwelling future weakening: Competition between wind intensification and surface heating

How can ocean warming at the NW Iberian Peninsula affect mussel aquaculture?

List of publications

Fernández-Nóvoa, D., deCastro, M., **Des, M.**, Costoya, X., Mendes, R., Gómez-Gesteira, M., 2017. Characterization of Iberian turbid plumes by means of synoptic patterns obtained through MODIS imagery. Journal of Sea Research 126, 12–25. https://doi.org/10.1016/j.seares.2017.06.013

Sousa, M.C., Ribeiro, A.S., **Des, M.**, Mendes, R., Alvarez, I., Gomez-Gesteira, M., Dias, J.M., 2018. Integrated High-resolution Numerical Model for the NW Iberian Peninsula Coast and Main Estuarine Systems. Journal of Coastal Research 85, 66–70. https://doi.org/10.2112/SI85-014.1

Des, M., deCastro, M., Sousa, M.C., Dias, J.M., Gómez-Gesteira, M., 2019. Hydrodynamics of river plume intrusion into an adjacent estuary: The Minho River and Ria de Vigo. Journal of Marine Systems 189, 87–97. https://doi.org/10.1016/j.jmarsys.2018.10.003

Sousa, M.C., Ribeiro, A., **Des, M.**, Gomez-Gesteira, M., deCastro, M., Dias, J.M., 2020. NW Iberian Peninsula coastal upwelling future weakening: Competition between wind intensification and surface heating. Science of The Total Environment 703, 134808. https://doi.org/10.1016/j.scitotenv.2019.134808

Des, M., Gómez-Gesteira, M., deCastro, M., Gómez-Gesteira, L., Sousa, M.C., 2020. How can ocean warming at the NW Iberian Peninsula affect mussel aquaculture? Science of The Total Environment 709, 136117. https://doi.org/10.1016/j.scitotenv.2019.136117

Des, M., Martínez, B., deCastro, M., Viejo, R.M., Sousa, M.C., Gómez-Gesteira, M., The impact of climate change on the geographical distribution of habitat-forming macroalgae in the Rías Baixas. in publication process.